THE UNIVERSITY
of EDINBURGH

Multiple air pollutants and their health impacts for both present-day and future scenarios

Sara Fenech

Thesis submitted in fulfilment of the requirements for the degree of

Doctor of Philosophy

School of GeoSciences

The University of Edinburgh

September 2018

Declaration

I declare that this thesis has been composed solely by myself and that it has not been submitted, either in whole or in part, in any previous application for a degree. Except where otherwise acknowledged, the work presented is entirely my own.

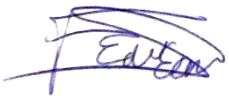

Sara Fenech

September 2018

Abstract

The adverse health impacts of air pollution, both short-term and long-term, have been widely studied in recent years; however there are a number of uncertainties to consider when carrying out health impact assessments. Health effects attributable to exposure to air pollutants are typically estimated using measured or modelled pollutant concentrations which vary both temporally and spatially. The goal of this thesis is to perform health impact assessments using modelled pollutant concentrations for present-day and future. The specific aims are: (i) to study the influence of model horizontal resolution on simulated concentrations of ozone (O_3) and particulate matter less than 2.5 μm in diameter ($PM_{2.5}$) for Europe and the implications for health impact assessments associated with long-term exposure (ii) to model air pollutant concentrations during two air pollution episodes in July 2006 together with the corresponding short-term health impact in the UK (iii) to estimate potential future health burdens associated with long-term pollutant exposure under future UK emission changes for 2050 in the UK.

First, the impact of model horizontal resolution on simulated concentrations of O_3 and $PM_{2.5}$, and on the associated long-term health impacts over Europe is examined, using the HadGEM3–UKCA (UK Chemistry and Aerosol) chemistry–climate model to simulate pollutant concentrations at a coarse (~140 km) and a finer (~50 km) horizontal resolution. The attributable fraction (AF) of total mortality due to long-term exposure to warm season daily maximum 8-hr running mean (MDA8) O_3 and annual-mean $PM_{2.5}$ concentrations is then estimated for each European country using pollutant concentrations simulated at each resolution. Results highlight seasonal variations in simulated O_3 and $PM_{2.5}$ differences between the two model resolutions in Europe. Simulated O_3 concentrations averaged for Europe at the coarse resolution are higher in winter and spring (~10 and ~6 %,

respectively) but lower in summer and autumn (~-1 and ~-4 %, respectively) compared to the finer resolution results. These differences may be partly explained by differences in nitrogen dioxide (NO_2) concentrations simulated at the two resolutions. Compared to O_3, the opposite seasonality in simulated $PM_{2.5}$ differences between the two resolutions is found. In winter and spring, simulated $PM_{2.5}$ concentrations are lower at the coarse compared to the finer resolution (~-8 and ~-6 % averaged for Europe, respectively) but higher in summer and autumn (~29 and ~8 %, respectively). Differences in simulated $PM_{2.5}$ levels are largely related to differences in convective rainfall and boundary layer height between the two resolutions for all seasons. These differences between the two resolutions exhibit clear spatial patterns for both pollutants that vary by season, and exert a strong influence on country to country variations in the estimated AF of mortality for the two resolutions. Results demonstrate that health impact assessments calculated using modelled pollutant concentrations, are sensitive to a change in model resolution with differences in AF of mortality between the countries ranging between ~-5% and ~+3%.

Under climate change, the risk of extreme weather events, such as heatwaves, is likely to increase. Thus the UK health burden associated with short-term exposure to MDA8 O_3 and daily mean $PM_{2.5}$ is examined during two five-day air pollution episodes during a well-known heatwave period in July 2006 (1st - 5th July and 18th – 22nd July) using the UK Met Office air quality model (AQUM) at 12 km horizontal resolution. Both episodes are found to be driven by anticyclonic conditions (mean sea-level pressures ~1020hPa over the UK) with light easterly and south easterly winds and high temperatures that aided pollution build up in the UK. The estimated total mortality burden associated with short-term exposure to O_3 is similar during the each episode with about 70 daily deaths brought forward summed across the UK. The estimated health burden associated with short-term exposure to daily mean $PM_{2.5}$ concentrations differs between the first and second episode resulting in about 43 and 36 daily deaths brought forward, respectively. The

attributable fraction of all-cause (excluding external) mortality for both pollutants differs between UK regions and ranges between 1.6% to 5.2% depending on the pollution levels in each episode; the overall total estimated health burdens are highest in regions with higher population totals. Results show that during these episodes, short-term exposure to MDA8 O_3 and daily mean $PM_{2.5}$ is between 36-38% and 39-56% higher, respectively, than if the pollution levels represented typical seasonal-mean concentrations.

Finally, emission scenarios for the UK following three Intergovernmental Panel on Climate Change (IPCC) Representative Concentration Pathways (RCPs); RCP2.6, RCP6.0 and RCP8.5 are used to simulate future concentrations of O_3, NO_2 and $PM_{2.5}$ for 2050 relative to 2000 using the AQUM air quality model at 12km resolution. The present-day and future AF of mortality associated with long-term exposure to annual mean MDA8 O_3, NO_2 and $PM_{2.5}$ and the corresponding mortality burdens are estimated for each region in the UK. For all three RCPs, simulated annual mean MDA8 O_3 concentrations in 2050 are estimated to increase compared to 2000, due to decreases in nitrogen oxides (NOx) emissions reducing titration of O_3 by NO, and to increases in methane (CH_4) levels across all of the UK. In contrast, annual mean NO_2 concentrations decrease everywhere. This highlights that the whole of the UK is simulated to be in a NO_x-saturated chemical environment. $PM_{2.5}$ concentrations decrease under all RCPs for the 2050s mostly driven by decreases in NO_x and sulphur dioxide (SO_2) emissions affecting secondary inorganic aerosols concentrations. For all pollutants the largest changes are estimated under RCP8.5 while the smallest changes are estimated for RCP6.0 in 2050 as compared to present-day. Consequently, these two RCPs represent the high and low end of the AF and mortality burden difference range relative to present-day for all three pollutants. For all UK regions and all three RCPs, the AF of mortality associated with long-term exposure to O_3 is estimated to increase in 2050 while the AF associated with long-term exposure to NO_2 and $PM_{2.5}$ is estimated to decrease as a result of higher and lower projected pollutant concentrations, respectively. Differences in

the UK-wide mortality burden attributable to long-term exposure to annual mean MDA8 O_3 across the RCPs range from +2,529 to +5,396 additional attributable deaths in 2050 compared to 2000. Long-term exposure to annual mean NO_2 and $PM_{2.5}$ differences in health burdens are between - 9,418 and -15,782 and from -4,524 to -9,481 avoided attributable deaths in 2050 relative to present-day, respectively. These mortality burdens are also sensitive to future population projections.

These results demonstrate that long-term health impact assessments estimated using modelled pollutant concentrations, are sensitive to a change in model resolution across Europe, especially in southern and eastern Europe. In addition, air pollution episodes are shown to have the potential to cause substantial short-term impacts on public health in the UK. Finally the sensitivity of future MDA8 O_3-, NO_2- and $PM_{2.5}$-attributable health burdens in the UK to future emission scenarios as well as population projections is highlighted with implications for informing future emissions control strategies for the UK.

Lay Summary

The three main pollutants in the atmosphere are ozone (O_3), nitrogen dioxide (NO_2) and particulate matter with an aerodynamic diameter less than 2.5 μm ($PM_{2.5}$). These pollutants are linked with various negative health impacts both in the short-term (days or weeks) and in the long-term (year). In order to estimate the health burden associated with these pollutants, the concentrations of these pollutants in the atmosphere needs to be known. A number of measurement sites exist around the world, however such stations are lacking in some areas and thus computer models are required to simulate pollutant concentrations covering a larger area. In doing so, a number of uncertainties are introduced in the health estimates. The main goal of this thesis is to perform health impact assessments using modelled pollutant concentrations for both present-day and future. This goal is divided into three main aims which are: (i) to study the influence of models with different horizontal resolutions on simulated O_3 and $PM_{2.5}$ concentrations in Europe and the associated long-term health impacts (ii) to model air pollutant concentrations during two five-day periods in July 2006 and the associated short-term health impacts in the UK (iii) to estimate the UK future health burdens associated with long-term pollutant exposure following future UK emission changes for 2050 relative to 2000.

First, the influence of model horizontal resolution on simulated concentrations of O_3 and $PM_{2.5}$ is examined over Europe using a model which includes both chemistry and climate at two different model grid sizes; ~140 km (coarse) and ~50 km (finer). Differences in O_3 concentrations between the two model resolutions vary by season, with O_3 concentration averaged for Europe being higher in winter and spring (~10 and ~6%, respectively) but lower in summer and autumn (~-1% and ~-4%, respectively) for the coarse compared to the finer

resolution. In contrast, $PM_{2.5}$ concentrations are lower in winter and spring (~-8% and ~-6% averaged for Europe, respectively) but higher in summer and autumn (~29% and ~8%, respectively). Across Europe, the associated health impacts are estimated to vary between the two resolutions by up to ±5% of the total mortality.

Under climate change, extreme weather events such as heatwaves are likely to increase. These in turn influence the amount of air pollution in the atmosphere and may contribute to air pollution episodes; days during which the levels of air pollution are high. In the second part of this thesis the health impacts during two five-day air pollution episodes in July 2006 are estimated. During both episodes about 70 daily deaths brought forward are associated with short-term exposure to O_3. For $PM_{2.5}$, about 43 and 36 daily deaths brought forward are estimated during the first and second episode, respectively. Results suggest that during these episodes, the health burdens associated with exposure to O_3 and $PM_{2.5}$ across the UK regions are between 36-38% and 39-56% higher, respectively than if no air pollution episode occurred.

Finally, the future burdens are estimated for three different emission scenarios in 2050 relative to 2000. It is estimated that under all three scenarios the simulate O_3 concentrations across the UK will increase in 2050 relative to 2000. However $PM_{2.5}$ and NO_2 concentrations are estimated to decrease. This in turn results in a UK-wide O_3-related mortality burden ranging between 2,529 and 5,396 additional attributable deaths (depending on the scenario) for future compared to present-day. In contrast, the mortality burden due to long-term NO_2 exposure ranges between 9,418 and 15,782 avoided attributable deaths while the $PM_{2.5}$-related mortality burden ranges between 4,524 and 9,481 avoided attributable deaths for 2050 relative to 2000. These mortality burdens are also found to be sensitive to future population projections.

Results presented in this thesis therefore highlight the sensitivity of simulated pollutant concentrations and the associated health impacts to model horizontal resolution in Europe. In addition, air pollution episodes are shown to have the potential to cause health impacts that are up to double those that would have occurred in the absence of an air pollution episode in the UK. Finally, health burdens associated with O_3, NO_2 and $PM_{2.5}$ in the UK are suggested to be sensitive to future emission scenarios as well as future population projections.

Acknowledgements

A huge thank you to my supervisor in Edinburgh, Ruth, who has been there throughout this journey providing endless support on a daily basis both academically and on a personal level especially during the final weeks. Your advice and suggestions have taught me so much. Thanks for believing in me and for pushing me to give my very best. I will truly miss our lunch and coffee break chats in Edinburgh. Thanks also to my supervisors at Public Health England, Clare Heaviside, Helen Macintyre and Sotiris Vardoulakis for hosting me at Chilton, for your guidance with health related research, constant feedback and support. Last but not least, thanks also to Fiona O'Connor who has been instrumental in this thesis by providing exceptional scientific feedback on the work presented in this thesis and by making sure every statement I made was robust.

To the scientists who have inspired me over the course of the PhD through their own outstanding research and/or any suggests they made for my thesis, I thank you. In particular I would like to thank scientists at the Met Office, Paul Agnew and Lucy Neal who have provided invaluable guidance for the past four years and the people who have read parts of this thesis; Paula, Michael, Emma, Declan, Ian, Claudia and Jamie.

There have been many people over the past four years both family and friends, close and far who have helped me get through the rollercoaster of emotions which a PhD brings with it. A huge thanks to the Sacred Heart Parish Church, Ana, Bashka, Anne, Peter and Sophie for providing a family environment away from home, my friends back in Malta; Liz, Oriana and Ioni for always finding the time to meet up whenever I visited and to my friends in Crew especially Rosa, Pedro and my flatmate Paula for the daily coffee and lunch breaks, dinners and yoga sessions. To the one who has been there from the very first day, Jamie. It's been wonderful sharing this journey with you. Thank you for making working till

late and on weekends fun, for listening to my crazy ideas, for making me laugh so much, for calling me out on wasting time on insignificant things and for being there during the toughest of times but most of all for the wonderful memories we've shared. I treasure our friendship greatly.

I would have not arrived where I am today if it wasn't for the never-ending love and support of my family; Mum, Dad, Emma, Ian, Corinne and Mark. Thank you for never doubting I could arrive this far and for constantly encouraging me along the way. And finally, Andrew. No words are enough to describe my gratitude for sticking around over the long distance for so long and during such hard times. Thank you for using up all your free time to come see me (all 17 times of them), for putting up with horrible skype connections and still making me laugh after a day's work, for helping me be grateful for the opportunity of this PhD, but most importantly, for making me happy. This thesis is for us.

Contents

List of Figures

List of Tables

“A clean environment is a human right like any other.

It is therefore part of our responsibility

toward others to ensure that the

world we pass on is as healthy,

if not healthier, than we found it.”

- Dalai Lama

Taken from https://www.fhi.no/en/op/hin/miljo/air-pollution-in-norway---public-he/ last accessed 10th September 2018

Chapter 1 Introduction

Air pollution, both globally and regionally, is closely linked with adverse health effects which vary across different timescales. This introductory chapter is initiated with the motivation of this thesis (Section 1.1). The fundamentals of atmospheric chemistry are described next (Section 1.2) followed by a brief discussion of how atmospheric chemistry is represented in models (Section 1.3). In the second part of this chapter the fundamentals of human health are described (Section 1.4). Following this, the methods for conducting health impact assessments and associated uncertainties are presented (Section 1.5). In the subsequent three sections, the impact of: model horizontal resolution (Section 1.6), air pollution episodes (Section 1.7) and future emission scenarios (Section 1.8) on simulated pollutant concentrations and associated heath impacts are discussed. This chapter ends with an outline of the research questions presented in this thesis (Section 1.9).

1.1 Motivation

Globally, air pollution from both outdoor and indoor sources represents the single largest environmental risk to health (World Health Organization (WHO), 2016). Results from the Global Burden of Disease (GBD) study suggest that diseases from all forms of pollution are responsible for about 9 million premature deaths in 2015

which accounts for 16% of total global mortality (GBD, 2015). This includes diseases from total air pollution, total water pollution, occupational pollution (e.g. carcinogens and particulates), soil, heavy metals and chemicals and lead. Pollution is estimated to be responsible for more deaths than (a) tobacco smoking (7 million), (b) a high-sodium diet (4.1 million), (c) obesity (4.0 million), (d) alcohol (2.3 million), (e) road accidents (1.4 million), or (f) child and maternal malnutrition (1.4 million). In addition pollution is also responsible for three times as many deaths as AIDS, tuberculosis, and malaria combined and for almost 15 times as many deaths as war and all forms of violence (GBD, 2015). The only two risk factors that result in more deaths than air pollution are dietary risk factors (all combined) (12.1 million) and hypertension (10.7 million). However, it is estimated that approximately 2.5 % of deaths due to hypertension are attributable to lead. Another study conducted by WHO estimates that, in 2012 unhealthy environments were responsible for 12.6 million deaths worldwide which accounts for 23% of total global mortality. Thus both the GBD (9 million) and WHO (12.6 million) studies suggest that pollution is a major cause of disease, disability and premature death. The difference between the two estimates is mainly due to differing definitions of environment which are broader and encompass a larger set of risk factors within the WHO study.

Of the estimated 9 million deaths from all forms of pollution in the GBD study, 4.2 million and 0.3 million are linked with ambient particulate and ambient ozone, respectively. In addition 2.9 million are associated with household air pollution as a result of indoor smoke from cooking and heating homes with biomass, kerosene fuels and coals (WHO, 2018). On the other hand WHO suggests that 3.0 million and 4.3 million related deaths in 2012 are due to ambient particulate and household air, respectively. The differences between the GBD and WHO estimates can be linked with different approaches used to quantify exposure-outcome associations. The GBD study uses the integrated exposure-response curve as evidence for non-communicable diseases (Burnett, 2014). In contrast, WHO use relative risks for

certain non-communicable diseases based on evidence from epidemiological studies. However for both studies total air pollution, both indoor and outdoor, constitutes the majority of the global estimated deaths from all forms of pollution. Thus in this study we focus on air pollution, in particular, outdoor air pollution. Indoor air pollution is not considered in this study as this is mostly a concern in households with smoke from cooking which is not typical of households in Europe and the UK.

Air pollution is linked to different sectors which include transport, energy, waste management, urban planning and agriculture (WHO, 2018). Several policies within these sectors have aided the improvement of the air quality. For example the use of clean technologies which reduce industrial smokestack emissions, ensuring access to affordable clean household energy alternatives for cooking, heating and lighting and increased use of low-emissions fuels and renewable power sources (WHO, 2018). In an attempt to further reduce air pollution, global guidance on limits and thresholds for key air pollutant that pose a health risk have been issued (WHO, 2006). These guidelines apply worldwide and are based on current scientific evidence for key air pollutants that contribute the greatest burden to human health: ozone (O_3), nitrogen dioxide (NO_2) and particulate matter with an aerodynamic diameter less than 2.5 µm ($PM_{2..5}$) (WHO, 2016). For this reason the work presented in this thesis is focused on these three air pollutants. In the next few paragraphs the evidence from epidemiological studies showing adverse health effects associated with exposure to O_3, NO_2 and/or $PM_{2.5}$ is discussed.

Epidemiological evidence on the health effects of air pollution is focused on all-cause or cause-specific, mortality and morbidity that can take place both in the short-term and long-term (WHO, 2013a). Gaseous pollutants such as O_3 and NO_2 cause adverse health impacts through oxidation processes (Section 1.2.1) (Jerrett *et al.*, 2009; WHO, 2013b; COMEAP(Committee on the Medical Effects of Air

Pollutants), 2015b; Crouse *et al.*, 2015; RCP, 2016) while $PM_{2.5}$-related health effects occur as small particles are inhaled (Brook et al., 2010; COMEAP, 2010; Krewski et al., 2009; RCP, 2016). The association of adverse health effects depends on the time-scale of the exposure to the air pollutant. A selection of adverse health effects associated with both long-term and short-term O_3 and $PM_{2.5}$ exposure are illustrated in Fig. 1.1.

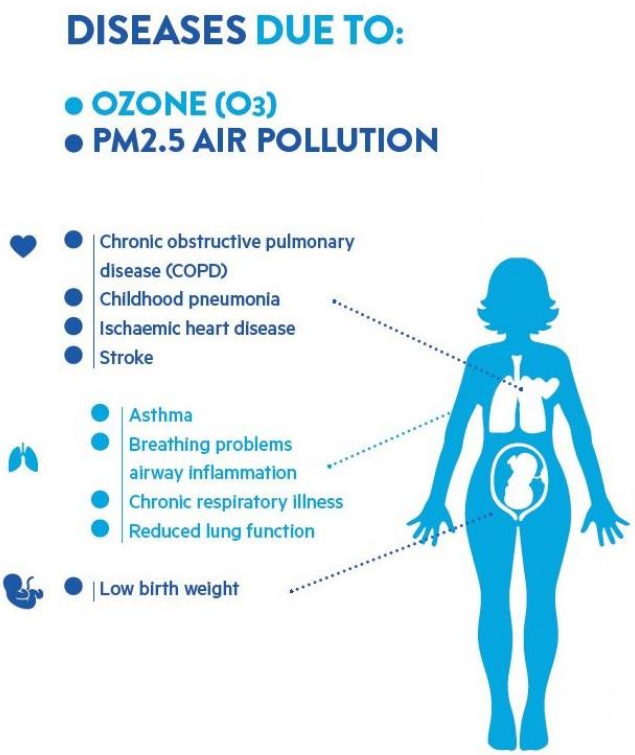

Figure 1.1: Health effects associated with short-term and long-term exposure to O_3 and $PM_{2.5}$ adapted from www.ccacoalition.org, last accessed 3rd September, 2018

In the short-term, exposure to high levels of O_3 may cause irritation to eyes and nose, inflammation of the airways, increase risk of exacerbations of asthma symptoms in adults and children (Guarnieri and Balmes, 2014), increased hospital admissions for cardiovascular diseases and respiratory diseases (WHO, 2013a), premature birth (Ha et al., 2014; RCP, 2016) and all-cause, cardiovascular and respiratory mortality (WHO, 2013a). On the other hand, evidence showing the adverse health impacts due to long-term exposure to O_3 is limited (Atkinson et al., 2016). In particular, long-term exposure to O_3 is only linked to respiratory mortality (Jerrett et al., 2009a; Turner et al., 2015).

Health effects associated with short-term exposure to NO_2 include increased hospital admissions for respiratory diseases (WHO, 2013a) and increased risk of exacerbations of asthma in both children and adults (Guarnieri and Balmes, 2014). Long-term exposure to NO_2 is associated with new-onset (incidence) asthma in both children and adults (Guarnieri and Balmes, 2014), suppression of lung function growth in children (RCP, 2016), mortality from lung cancer and respiratory diseases (Crouse et al., 2015), mortality associated with ischaemic heart disease (IHD) (Krewski et al., 2009) and all-cause mortality (COMEAP, 2015a).

Short-term exposure to $PM_{2.5}$ is also associated with exacerbation of asthma in both children and adults (Guarnieri and Balmes, 2014), adverse birth outcomes (Ha et al., 2014), increase in hospital admissions from cardiovascular diseases and respiratory diseases (WHO, 2013a) as well as all-cause and cardiovascular mortality and morbidity (Brook et al., 2010; RCP, 2016). Long-term exposure to $PM_{2.5}$ is associated with adverse effects such as new-onset asthma in adults and diabetes (RCP, 2016), the developing and aging brain (RCP, 2016), all–cause mortality (COMEAP, 2010; Crouse et al., 2015; Krewski et al., 2009) as well as cause-specific mortality such as cardiovascular mortality (Brook et al., 2010; Krewski et al., 2009; RCP, 2016), mortality from Chronic Obstructive Pulmonary Disease (COPD) (WHO, 2013a), lung cancer, and IHD (Krewski et al., 2009).

The latest GBD study estimates that 4.2 million deaths (95% Confidence Interval (CI): 3.7 million to 4.8 million) from all-cause mortality in 2015 occurred as a result of long-term exposure to ambient $PM_{2.5}$ concentrations, a 20% increase compared to 1990 while ambient O_3 is estimated to cause 254,000 (95% CI: 97,000 to 422,000) deaths from chronic obstructive pulmonary disease in the same year (Cohen et al., 2017).

Air quality in Europe between 2000 and 2015 has improved due to the implementation of various air quality policies (European Environment Agency (EEA), 2017). These policies set by the European Union (EU) as well as the World Health Organization (WHO) implement limits and targets to reduce concentrations of harmful air pollutants such as O_3, NO_2 and $PM_{2.5}$ amongst others (described in Section 1.4.1). However, a large portion of European populations are still exposed to air pollution levels that exceed European standards as well as the WHO Air Quality Guideline (AQGs) (see section 1.4.1). Up to 85% and 98% of the urban population in the 28 EU member countries (EU-28) are thought to be exposed to $PM_{2.5}$ and O_3 concentrations above the WHO AQGs, respectively (EEA, 2017). For Europe, the health impacts attributable to short-term exposure to O_3 and long-term exposure to NO_2 in 2014 are estimated at 14,400 and 78,000 premature deaths, respectively (over 41 countries) (EEA, 2017). The estimated health impacts associated with long-term exposure to $PM_{2.5}$ in the same period and across 41 European countries is estimated at approximately 428, 000 premature deaths (EEA, 2017). Of these estimates, the O_3, NO_2 and $PM_{2.5}$ related health impacts for the UK are 590, 14,050 and 37,600, premature deaths, respectively in the same time period (EEA, 2017). The all-cause mortality burden associated with long-term exposure to anthropogenic $PM_{2.5}$ in the UK is also estimated by COMEAP (2010) and totals 28,861 attributable deaths based on pollutant levels in 2008. The UK's Department for Environment Food and Rural Affairs (Defra) estimate that NO_2 is linked to 23,500 attributable deaths annually in the UK based on pollutant levels in 2013 (Defra,

2015). The combined impact associated with exposure to both NO_2 and $PM_{2.5}$ is estimated at 40,000 deaths annually (COMEAP, 2015a).

The method used for conducting health impact assessments is mostly consistent between different studies. However, less consistency is found in the terminology used to quantify various measures of mortality between the different studies. In the paragraph above, mortality estimates from the EEA for the UK differ from those suggested by COMEAP. These differences are mostly due to different exposure-response relationships used by the different studies. In this thesis the terminology used for long-term exposure in Chapters 3 and 5 is 'attributable deaths' following Gowers et al. (2014) whereas for short-term exposure in Chapter 4 the terminology used is 'deaths brought forward' following Macintyre et al. (2014).

In this thesis both long-term and short-term health impacts of air pollution are examined for Europe and the UK using simulated pollutant concentrations of O_3, NO_2 and $PM_{2.5}$ for both present-day and future. In the next section the fundamentals of atmospheric chemistry are described, followed by a brief explanation of how air pollutants are represented in models.

1.2 Fundamentals of atmospheric chemistry

As discussed in section 1.1, O_3, NO_2 and $PM_{2.5}$ are identified as the key air pollutants having adverse effects on health across the globe and thus their concentrations and health impacts are the focus of this thesis. In this section the fundamental processes that determine the concentrations for these three major air pollutants are described. To begin with, the fundamental chemistry of O_3 and NO_2 is described in Section 1.2.1 followed by that of $PM_{2.5}$ in Section 1.2.2.

1.2.1 Nitrogen Dioxide (NO_2), Ozone (O_3) and its precursors

1.2.1.1 Production of NO_2 and O_3

In the following section a discussion of O_3 that is formed or lost in the troposphere (~0 to 8-18 km altitude depending on the latitude and season; Jacob 1999) through reactions that are relevant for controlling surface O_3 levels is presented. O_3 is not directly emitted but is formed in the atmosphere through a series of chemical reactions involving nitrogen oxides (NO_x = NO and NO_2), together with other precursors: carbon monoxide (CO), methane (CH_4), and other non-methane volatile organic compounds (NMVOCs) of both natural and anthropogenic origin. The major anthropogenic sources of NO_x for the EU-28 in 2015 are illustrated in Fig. 1.2 with 39% of the emissions associated with road transport and 19% from energy production (EEA, 2017).

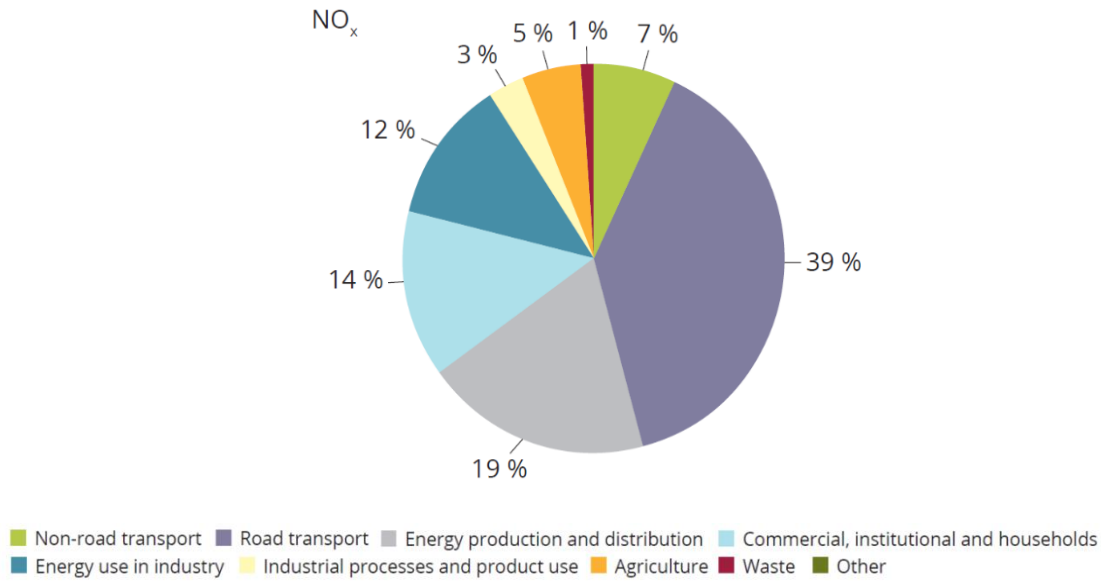

Figure 1.2: Contribution to EU-28 emissions from main source sectors in 2015 of NO_x taken from (EEA, 2017)

O_3 production occurs by hydroxyl radical (OH) oxidation of CO, CH_4 and non-methane hydrocarbons (NMHC) in the presence of NO_x (Monks et al., 2015). Generally the timescales of these reactions are very short (~ seconds to tens of minutes) (Seinfeld and Pandis, 2006). The production of O_3 relies on the oxidation of NO by the peroxy radical (HO_2) (producing NO_2; Reaction R1.1) followed by photolysis (reaction with a photon) of NO_2 (Reaction R1.2) and the subsequent association of the ground electronic state oxygen atom $O(^3P)$ with O_2 following Reaction R1.3, where M is an inert third body (Monks et al., 2015).

$$NO + HO_2 \rightarrow NO_2 + OH \quad \text{(R1.1)}$$

$$NO_2 + h\nu \rightarrow NO + O\,(^3P) \quad \text{(R1.2)}$$

$$O\ (^3P) + O_2 + M \rightarrow\ O_3 + M \qquad \text{(R1.3)}$$

With the addition of carbon monoxide (CO) (R1.4), methane (CH_4) or volatile organic compounds (VOCs), net O_3 production occurs as additional HO_2 from Reaction R1.4 initiates the production of O_3 through R1.1 and the subsequent reactions 1.2 and 1.3.

$$CO + OH \underset{O_2}{\rightarrow}\ CO_2 +\ HO_2 \qquad \text{(R1.4)}$$

Summing up Reactions 1.1 to 1.4, the net O_3 production can be described by Reaction R1.5 below.

$$CO + 2O_2 +\ h\nu\ \rightarrow\ CO_2 +\ O_3 \qquad \text{(R1.5)}$$

The production (Section 1.2.1.1) and loss (Section 1.2.1.2) of surface O_3 is shown schematically in Fig. 1.3.

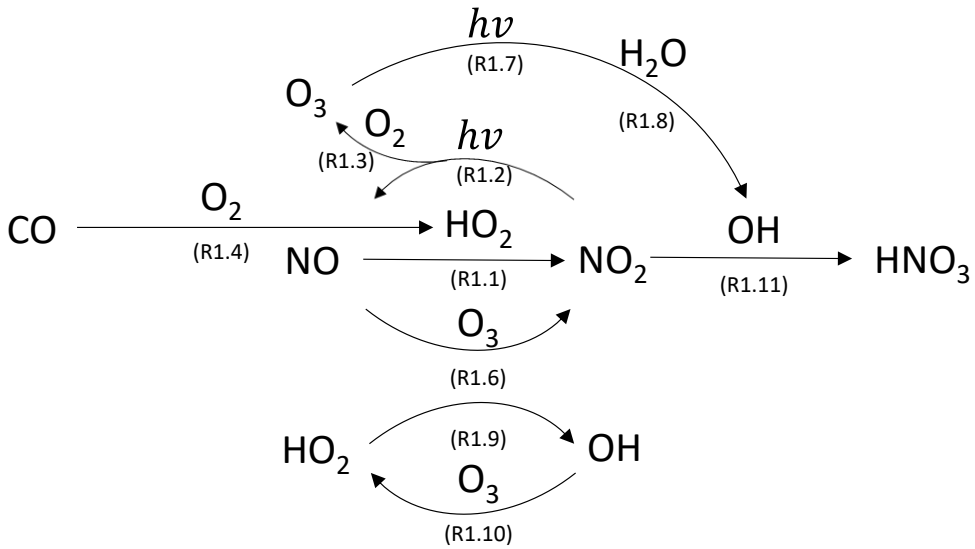

Figure 1.3: Schematic of the production and loss of O_3 and NO_2 concentrations in the troposphere based on the reactions described in this section and based on Jacob (1999) (Numbers in brackets indicate the reaction numbers as used in this section.)

1.2.1.2 Loss of NO_2 and O_3

Apart from Reaction R1.1, production of NO_2 can also occur through Reaction R1.6 where O_3 is depleted through its reaction with NO (Reaction R1.6) (Fig. 1.3).

$$NO + O_3 \rightarrow NO_2 + O_2 \qquad \text{(R1.6)}$$

Reactions R1.2, R1.3 and R1.6 form a null cycle whereby NO_2, NO, O and O_3 are in photochemical equilibrium. The net effect on production or loss of O_3 highly depends on the amount of NO_x present in the atmosphere. Downwind, in low emission regions, NO_x is the catalyst that produces O_3 (Reactions R1.1, R1.2 and R1.3), whilst in urban regions with high NO levels, R1.6 dominates leading to lower O_3 levels. This is referred to as the 'NO_x titration effect' whereby NO_2 constitutes a major part of NO_x (Monks et al., 2009).

The main loss of O_3 occurs through its photolysis (Reaction R1.7) followed by the interaction with water vapour (Reaction R1.8) (Fig. 1.3). Photolysis at wavelengths shorter than ~310 nm yields an O atom in the excited singlet state (O(1D)) which is very reactive (Reaction R1.7) (Monks et al. 2015)

. $$O_3 + h\nu \rightarrow O_2 + O(^1D) \qquad \text{(R1.7)}$$

This O atom then reacts with water vapour producing OH radicals as presented by Reaction R1.8.

$$O(^1D) + H_2O \rightarrow 2OH \qquad \text{(R1.8)}$$

At low levels of NO_x, O_3 is also lost by its reaction with HO_2 and OH radicals resulting in OH and HO_2, respectively (Reactions R1.9 and R1.10).

$$O_3 + HO_2 \rightarrow OH + 2O_2 \qquad \text{(R1.9)}$$

$$O_3 + OH \rightarrow HO_2 + O_2 \qquad \text{(R1.10)}$$

O_3 is also additionally lost through dry deposition to the surface for example onto leaf stomata (Jacob, 1999). The non-linearity of the O_3-VOC-NO_x system and O_3 chemical regime is illustrated in Fig. 1.4 (Monks et al., 2015). Regions having low O_3 levels in the top left (A) and bottom right corners (C)) are generally referred to as the VOC-limited and NO_x-limited regimes. In region A, low levels of O_3 occur in the presence of high levels of NO_x and low levels of VOCs (i.e. a region of NO_x saturation also referred to as VOC-limited). In these regions Reaction R1.6 dominates and O_3 loss, by titration of O_3 by NO, occurs. On the other hand Region C is referred to as a region of VOC saturation or a NO_x-limited region. In Region C, OH is limited due to substantial oxidation by high VOC levels. In the presence of low NO_x, HO_2 levels are also reduced. Therefore with low levels of NO_x and HO_2, Reaction R1.1 is limited and hence so is O_3 formation. Efficient conversion of NO to NO_2 occurs in the rest of the figure resulting in net O_3 production which increases with increasing VOC and NO_x emissions (Region B and Reactions R1.1 to R1.3).

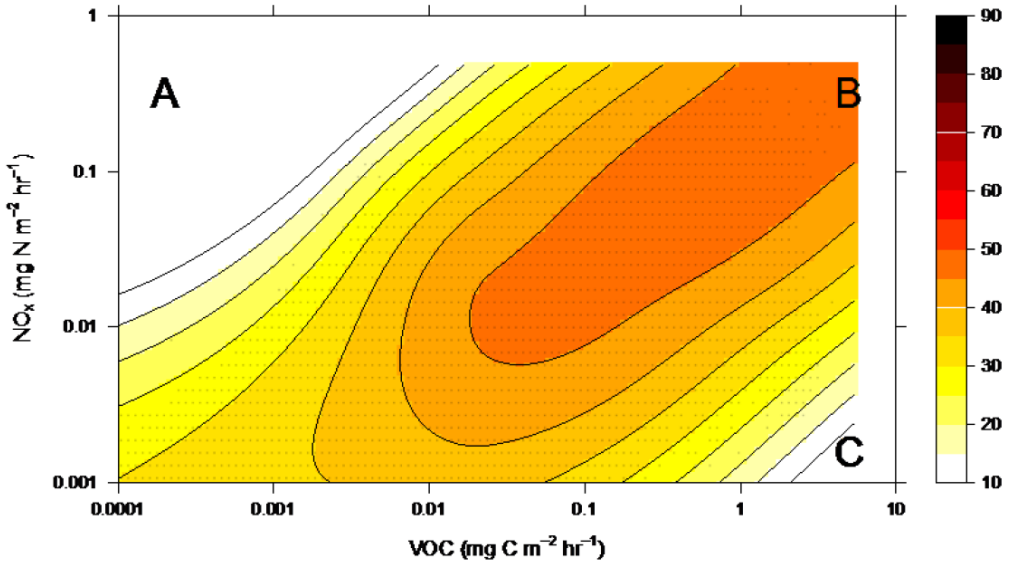

Figure 1.4: O_3 mixing ratios (ppb) as a function of VOC and NO_x emissions simulated using the UKCA model (described in Section 2.1) taken from Monks et al. (2015)

The main sink of NO_2 is the oxidation to nitric acid (HNO_3) during daytime which is a very soluble component and is thus removed by wet deposition in rainfall (Reaction R1.11). A portion of HNO_3 is also removed by dry deposition.

$$NO_2 + OH + M \rightarrow HNO_3 + M \qquad \text{(R1.11)}$$

where *M* is an inert third body.

The lifetime of NO_2 is short and ranges from several hours to a few days (Jacob, 1999). O_3 has a longer lifetime of the order of several weeks (Young et al., 2013), thus enabling transport of O_3 over intercontinental scales.

1.2.2 Particulate Matter (PM)

An aerosol is defined as solid or liquid particles suspended in the gaseous medium (Jacob, 1999). However, common usage (as is the case for this thesis) refers to the aerosol as the particulate component only. Aerosols consist of a complex mixture of organic and inorganic substances, and vary in size from a few nanometers (nm) to tens of micrometers (μm) in diameter. Aerosols can be emitted directly as particles (primary aerosol) or formed in the atmosphere by gas-to-particle conversion processes (secondary inorganic (SIA) and organic aerosol (SOA)).

Once airborne, particles can form and change in their composition and size through a number of processes, namely: clustering of gas molecules termed nucleation (or aitken mode), condensation of a gaseous precursor, coagulation whereby particles collide following random motions and stick together and scavenging through incorporation into cloud droplets. These processes are described in more detail below. Nucleation and gas-to-particle conversion are examples of secondary aerosol formation processes. Particles are removed from the atmosphere through two main mechanisms: deposition at the Earth's surface (dry deposition) and precipitation (wet deposition). Tropospheric aerosols vary widely in composition and concentration over the Earth and residence times of particles in the troposphere vary from a few days to a few weeks (Seinfeld and Pandis, 2006).

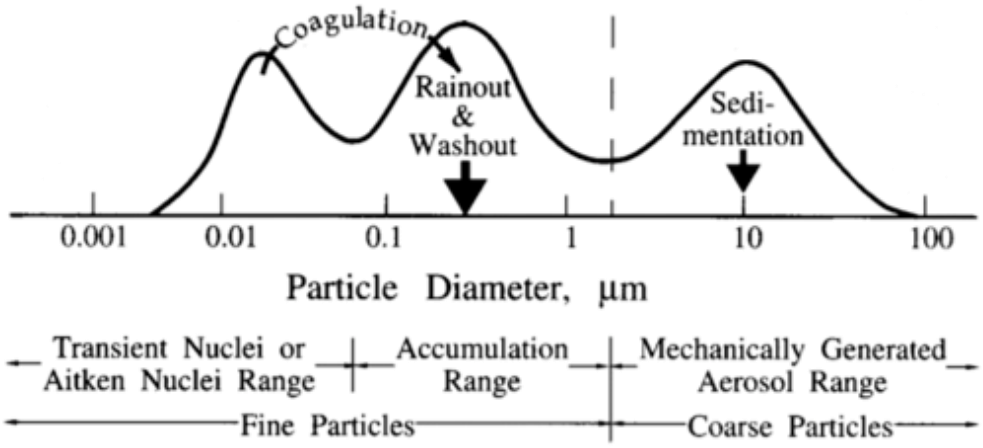

Figure 1.5: Schematic of the distribution of particle surface area of an atmospheric aerosol indicating principal modes, particle formation and removal mechanisms (adapted from Seinfeld and Pandis (1998))

Atmospheric aerosols vary in size, with particles less than 2.5 µm in diameter ($PM_{2.5}$) typically referred to as "fine" and those greater than 2.5 µm in diameter as "coarse". Fine particles are generally divided into two modes: the nucleation and the accumulation mode as illustrated in Fig. 1.5. Particles in the nucleation mode are small in size (ranging from ~ 0.005 to 0.1 µm in diameter) and thus rarely account for more than a few percent of the total mass of airborne particles. These particles are formed from condensation of hot vapours during combustion processes and from the nucleation of atmospheric gaseous species (e.g. sulphur and nitrogen oxides). Particles in the accumulation mode (ranging from ~ 0.1 to 2.5 µm in diameter) account for most of the aerosol surface area as well as a substantial part of the aerosol mass in the troposphere (Fig 1.5). Particles in this mode are generated through the coagulation of particles in the nucleation mode and from condensation of vapours onto existing particles, causing them to grow in size. Coarse mode particles (> 2.5 µm in diameter) are generally formed by mechanical processes and typically consists of anthropogenic and natural dust

particles and sea spray. Particles in the nucleation mode quickly coagulate and grow larger due to condensation of vapour species and coarse particles are removed from the atmosphere in a relatively short time due to a sufficiently large sedimentation velocity, therefore particles in the accumulation mode have a considerable longer atmospheric residence time (Seinfeld and Pandis, 2006).

1.2.2.1 $PM_{2.5}$ chemical composition and sources

$PM_{2.5}$ is made up of a number of chemical species or components. These include sulphate (SO_4^{2-}), sodium (Na^+), ammonium (NH_4^+), elemental carbon (EC), nitrate (NO_3^-), organic carbon (OC), sea salt and mineral dust. An example of the chemical composition of $PM_{2.5}$ at a central background site in Birmingham in the UK between May 2004 and May 2005 is shown in Fig. 1.6.

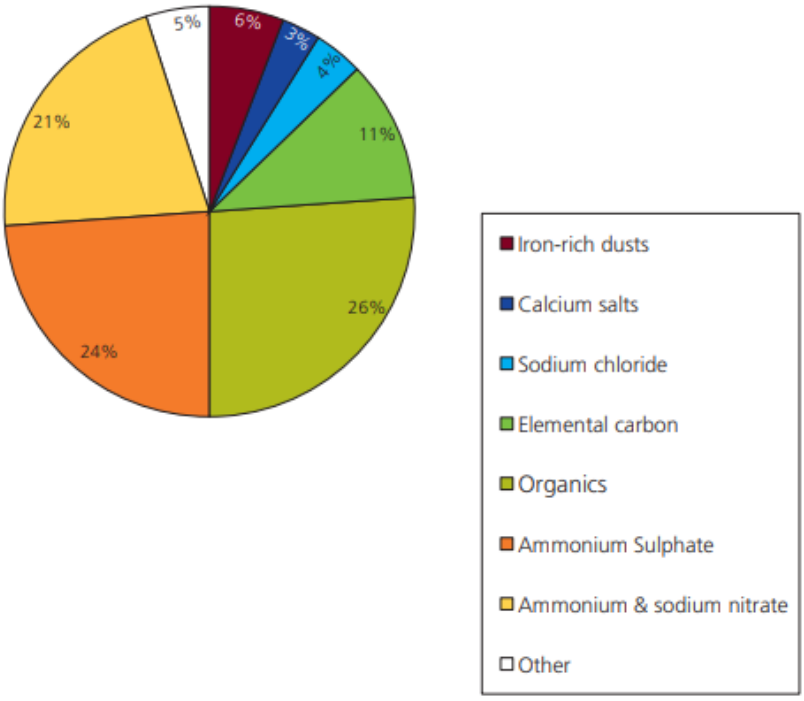

Figure 1.6: Chemical composition contributing to total $PM_{2.5}$ at a central urban background site in Birmingham UK adapted from (Yin and Harrison, 2008)

Primary pollutants have both natural and anthropogenic sources. Natural sources of primary $PM_{2.5}$ include ash from volcanic activity, mineral dust, sea salt and forest fires. The different sectors contributing to total anthropogenic primary $PM_{2.5}$ emissions in the EU-28 in 2015 are illustrated in Fig. 1.7 with the commercial, institutional and households fuel combustion sector being the largest contributor

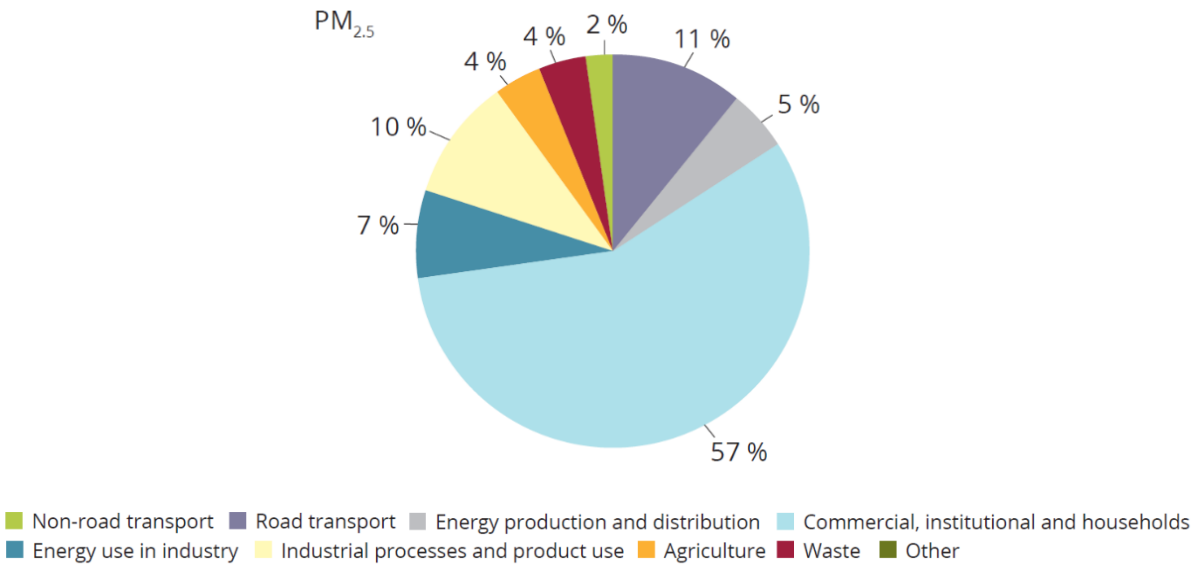

Figure 1.7: Contribution to EU-28 emissions from main source sectors in 2015 of $PM_{2.5}$ taken from (EEA, 2017)

(57%) followed by road transport (11%) (Fig. 1.7).

As discussed in Section 1.2.2, secondary inorganic particles can be formed from nucleation of new particles and gas-to-particle conversion through the oxidation of primary gases such NO_2 and sulphur dioxide (SO_2) into nitric acid (HNO_3 - gas) (Reaction R1.11) and sulphuric acid (H_2SO_4 - liquid), respectively. (Reaction R1.12 to R1.14; Jacob 1999), respectively. SO_2 is oxidised by OH to produce H_2SO_4 following Reactions R1.12 to R1.14 below:

$$SO_2 + OH + M \rightarrow HSO_3 + M \quad \text{(R1.12)}$$

$$HSO_3 + O_2 \rightarrow SO_3 + HO_2 \quad \text{(R1.13)}$$

$$SO_3 + H_2O + M \rightarrow H_2SO_4 + M \quad \text{(R1.14)}$$

Ammonia (NH_3) gas is emitted mostly from the agricultural sector (94%; EEA (2017)) and on reaction with HNO_3 and H_2SO_4 forms ammonium nitrate (Reaction R1.15) and ammonium sulphate (Reaction R1.16) but more readily reacts with the sulphate aerosol due to its lower vapour pressure.

$$NH_{3(g)} + HNO_{3(g)} \leftrightarrow NH_4NO_{3(s)} \quad \text{(R1.15)}$$

$$2NH_{3(g)} + H_2SO_{4(aq)} \leftrightarrow (NH_4)_2SO_{4(s)} \quad \text{(R1.16)}$$

Secondary organic aerosol formation mainly occurs through the oxidation of VOCs. This formation can be highly complex involving biogenic, anthropogenic and biomass burning VOC species.

1.2.2.2 Toxicity of PM

There are different theories about what determines the toxicity of particles. Amongst these are: the size of the particles, the number of particles, the chemical composition, and age. One of the main theories is the "ultrafine hypothesis" (Seaton et al., 1995) which suggests that the number of particles is the driving factor as opposed to the mass of the particles. This is because fine particles which dominate the particle number distribution (but not the particle mass distribution), have a high surface area (Fig. 1.5). Evidence that some individual $PM_{2.5}$ components (e.g. elemental carbon) are more toxic than others is also found (e.g. Peng et al.

2008; Levy et al., 2012). However this is still a growing area of research and robust evidence on the differential toxicity of various components of the PM mixture is still lacking (WHO, 2013b). The next section presents how the atmospheric composition is simulated by models (Section 1.3).

1.3 Modelling atmospheric chemistry

Models are typically used to simulate the gaseous pollutants and aerosols described in Sections 1.2.1 and 1.2.2. All atmospheric models which simulate chemical species within the atmosphere include the main processes controlling them; emissions, transport, chemistry and deposition (Fig. 1.8).

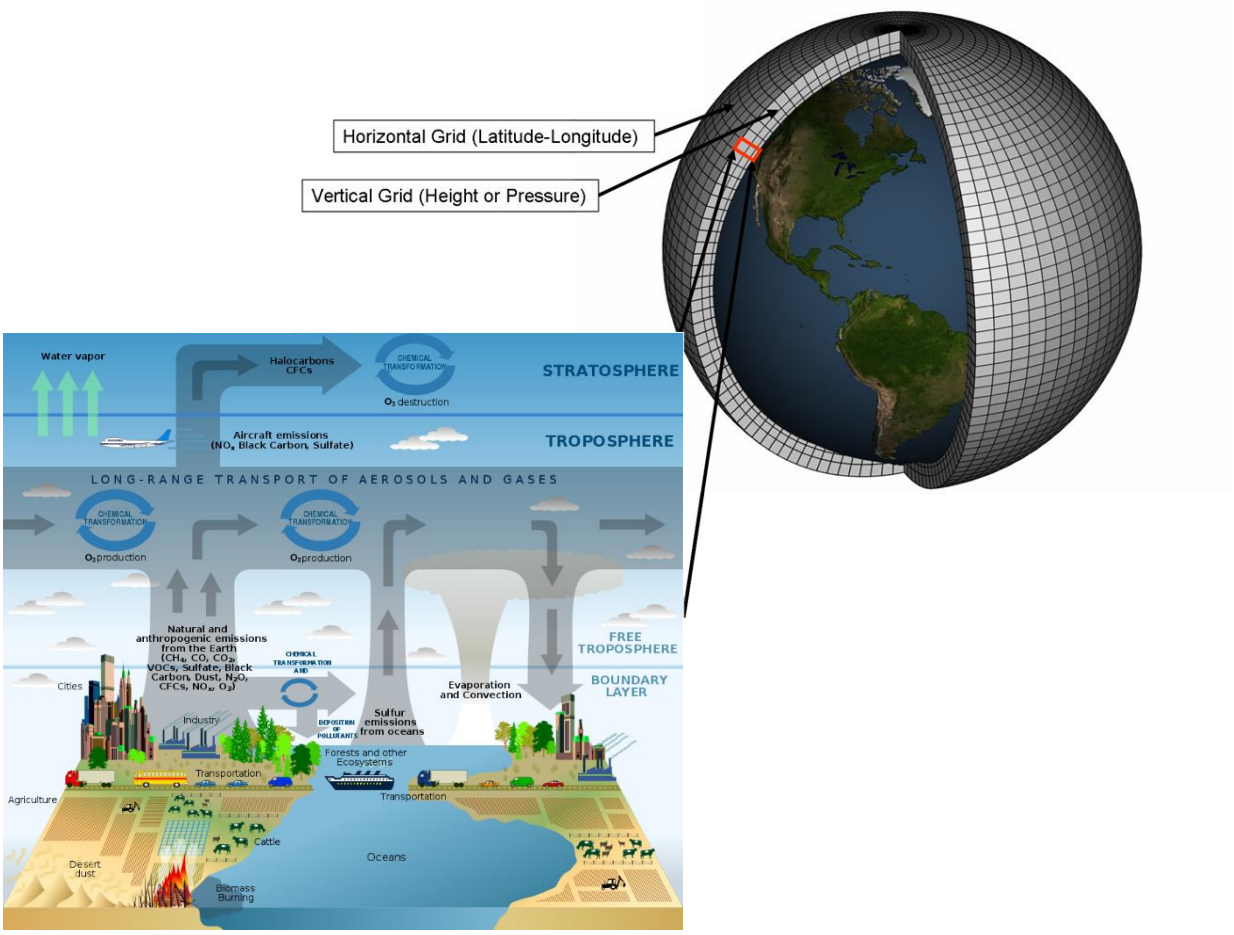

Figure 1.8: Schematic of the simulated atmospheric composition in models adapted from Mahoney et al. (2003)

Three-dimensional models that describe these processes are called chemical transport models (CTMs). These models do not simulate the atmospheric dynamics but rather use meteorological reanalyses fields as input to enable for example the chemical transformation and transport of chemical species as illustrated in Fig. 1.8. On the other hand, chemistry–climate models (CCMs) represent atmospheric chemistry processes but are coupled to a general circulation model (GCM) therefore allowing for interactions between the physical dynamics (represented by a set of equations describing fluid flow hence transport and radiative transfer) and chemistry to influence the model's radiation scheme (Young et al., 2018). Chemistry-climate models can either simulate the climate with weather representative of an average period, referred to as 'free-running' (as used in chapters 3), or they can be constrained by using meteorological reanalyses to simulate a particular meteorological year, referred to as 'nudged' or using model forecast fields (chapter 4 and 5). Apart from a different representation of the meteorology, chemistry-climate models can have different horizontal or vertical resolutions, spatial extent and also different complexity of the chemistry included. Differences in horizontal resolutions can influence the ability of a CTM or CCM to represent an urban environment. For example at a global resolution (Section 1.6) urban NO_x emissions may be diluted over a large grid cell. This may result in lower O_3 levels than simulated with a higher resolution model to less of an impact of the loss of O_3 through titration with NO following R1.6 under high NO_x levels (Section 1.2.1.2). Differences in resolution may also therefore potentially impact the O_3 chemical regime described in Section 1.2.1.2.

Throughout this thesis a chemistry-climate model which is based on the Met Office Unified Model (MetUM; Brown et al., 2012) is used to simulate pollutant concentrations. Chemistry-climate models are chosen over chemistry-transport models to be able to analyse how the model represents various atmospheric dynamics at different model set ups for example: at different model resolutions, air

pollution episodes and for future air pollution estimations. Further details on the research aims of this thesis are presented in Section 1.9.

In chapter 3, two chemistry-climate configurations of the HadGEM3-UKCA (Hadley Centre Global Environmental Model version 3 (HadGEM3, Hewitt et al., 2011) – United Kingdom Chemistry and Aerosol model (UKCA, Morgenstern et al., 2009; O'Connor et al., 2014)) are used; a global configuration with a horizontal resolution of ~140 km and a regional resolution with a horizontal resolution of ~50 km. A more detailed description of the models and model set-up used in Chapter 3 is presented in Section 2.1. In chapters 4 and 5 the UK air quality model also based on the MetUM – the Air Quality in the Unified Model (AQUM; Savage et al., 2013) is used having a horizontal resolution of 12 km. Further details on the AQUM and its set-up are described in Section 2.2. Model simulations for present-day used in this thesis are compared to meteorological and chemical observations which are described in Section 2.3.

Having described the fundamentals of atmospheric chemistry (Section 1.2) and how air pollutants are represented by CCMs in this thesis (Section 1.3), the next section considers the fundamentals of human health in relation to air pollutant exposure (Section 1.4).

1.4 Fundamentals of human health

Air pollution related health effects (Section 1.1) are determined by toxicological, clinical and epidemiological studies. Evidence from such studies is used to implement air quality policies and set air quality guidelines and limits. In this section the UK air quality objectives together with the European obligations for the protection of human health are first described in Section 1.4.1 including a brief

overview of the UK Daily Air Quality Index (DAQI). In this thesis evidence linking air pollution to adverse health effects derived from epidemiological studies is used and these study types are described next in Section 1.4.2. The terminology of exposure response relationships and risk estimates as obtained from epidemiological studies are then discussed in Section 1.4.3 followed by a description of the risk estimates used in this thesis in Section 1.4.4.

1.4.1 Regulatory standards for air pollutants in the EU and UK for the protection of human health

The European Union (EU) developed and adopted a series of directives on air quality and set air quality limits and target values for the major air pollutants most detrimental to health (Section 1.1) which are set out in the European 2008 Ambient Air Quality Directive (2008/50/EC). Each member state is then responsible to implement and achieve the limits and targets set by the EU that relate to short term (e.g. daily) and long-term (e.g. annual-mean) limits. Table 1.1 lists the UK air quality objective together with the European directive limit and target values for O_3, NO_2 and $PM_{2.5}$ for the protection of human health. The UK objective for O_3 is set for an 8-hour mean concentration of 100 μg m^{-3} not to be exceeded more than 10 times a year. The EU target for O_3 varies from that of the UK; EU O_3 concentrations are not to exceed 120 μg m^{-3} by more than 25 times a year averaged over 3 years. Hourly mean NO_2 concentrations in the EU and the UK are not to exceed 200 μg m^{-3} more than 18 times a year and with an annual mean limit of 40 μg m^{-3}. The UK objective and target value for $PM_{2.5}$ is an annual mean concentration not to exceed 25 μg m^{-3} for 2010 and maintained thereafter. A reduction of 15% in annual mean $PM_{2.5}$ concentrations in urban areas is also set as a target to be reached between 2010 and 2020 by the UK in an effort to reduce $PM_{2.5}$ exposure.

While the above mentioned EU targets have aided the improvement of air quality in Europe and the UK, some pollutant concentrations across Europe are still above the EU limits (EEA 2017). Figure 1.9 illustrates observed concentrations of maximum daily 8-hour O_3 mean, annual mean NO_2 and annul mean $PM_{2.5}$ across European monitoring stations in 2015 with orange and red colours indicating concentrations above the set EU limits (Table 1.1).

Table 1.1: National air quality objectives and European Directive limit and target values for the protection of human health taken from https://uk-air.defra.gov.uk/air-pollution/uk-eu-limits last accessed on 10th September 2018.

Pollutant	Applies	Objective	Concentration measured as [10]	Date to be achieved by (and maintained thereafter)	European Obligations	Date to be achieved (by and maintained thereafter)
Ozone	UK	100 µg/m³ not to be exceeded more than 10 times a year	8 hour mean	31 December 2005	Target of 120 µg/m³ not to be exceeded by more than 25 times a year averaged over 3 years	31 December 2010
Nitrogen dioxide	UK	200 µg/m³ not to be exceeded more than 18 times a year	1 hour mean	31 December 2005	200 µg/m³ not to be exceeded more than 18 times a year	1 January 2010
	UK	40 µg/m³	annual mean	31 December 2005	40 µg/m³	1 January 2010
Particles ($PM_{2.5}$) Exposure Reduction	UK (except Scotland)	25 µg/m³	annual mean	2020	Target value - 25 µg/m³	2010
	Scotland	10 µg/m³		31 December 2020	Limit value - 25 µg/m³	1 January 2015
	UK urban areas	Target of 15% reduction in concentrations at urban background		Between 2010 and 2020	Target of 20% reduction in concentrations at urban background.	Between 2010 and 2020

All measured concentrations of daily maximum 8-hour mean O_3 in the UK are within the EU and UK limit in 2015 however, O_3 concentrations are above 120 µg m^{-3} for most stations in Europe in the same period (Fig. 1.9a). Measured annual mean NO_2 concentrations are mostly within the EU limit but concentrations higher than 40 µg m^{-3} can be noted in cities such as London, and pollution hotspots like the Netherlands (Fig. 1.9b). $PM_{2.5}$ concentrations across Europe are only higher than the limit value for 6% of all reporting stations occurring mostly in urban areas in southern and eastern Europe (Fig. 1.9c; EEA, 2017).

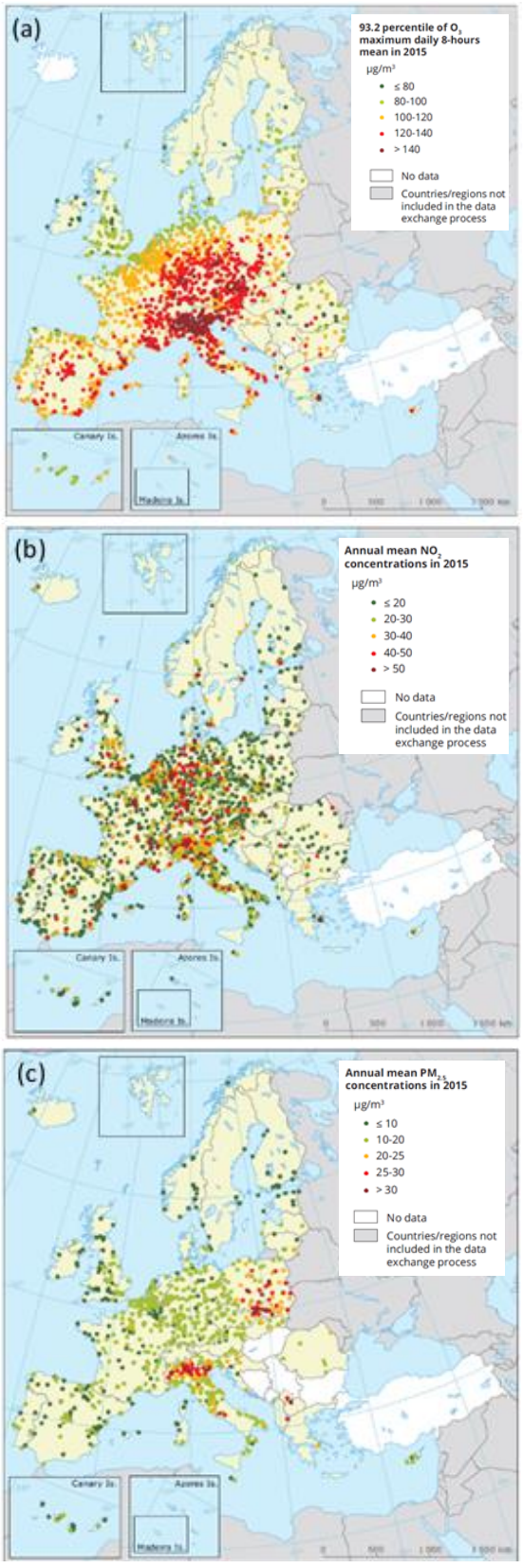

Figure 1.9: Observed concentrations of (a) O_3, (b) NO_2 and (c) $PM_{2.5}$ in 2015 (EEA, 2017)

The daily air quality index (DAQI) is another UK air quality guideline intended to inform the public on the levels of air pollution (Defra, 2013b). The system uses indexes 1 to 10 which are divided into four bands: Low (1-3), Moderate (4-6), High (7-9) and Very High (10) (Fig. 1.10). This index is calculated from the highest concentrations of five pollutants: O_3, NO_2, SO_2, $PM_{2.5}$ and PM_{10}. The concentrations of 8-hour mean O_3, hourly mean NO_2 and daily mean $PM_{2.5}$ within each band are illustrated in Fig. 1.10. A high value of the DAQI is recorded when a high value is reached for any of the five individual pollutants. The DAQI is used in Chapter 4 to determine the days during which moderate to high levels of air pollution occurred in 2006.

Ozone

Based on the running 8-hourly mean.

Index	1	2	3	4	5	6	7	8	9	10
Band	Low	Low	Low	Moderate	Moderate	Moderate	High	High	High	Very High
μgm^{-3}	0-33	34-66	67-100	101-120	121-140	141-160	161-187	188-213	214-240	241 or more

Nitrogen Dioxide

Based on the hourly mean concentration.

Index	1	2	3	4	5	6	7	8	9	10
Band	Low	Low	Low	Moderate	Moderate	Moderate	High	High	High	Very High
μgm^{-3}	0-67	68-134	135-200	201-267	268-334	335-400	401-467	468-534	535-600	601 or more

$PM_{2.5}$ Particles

Based on the daily mean concentration for historical data, latest 24 hour running mean for the current day.

Index	1	2	3	4	5	6	7	8	9	10
Band	Low	Low	Low	Moderate	Moderate	Moderate	High	High	High	Very High
μgm^{-3}	0-11	12-23	24-35	36-41	42-47	48-53	54-58	59-64	65-70	71 or more

Figure 1.10: Concentrations of 8-hour running mean O_3, hourly mean NO_2 and daily mean $PM_{2.5}$ within each band of the daily air quality index (DAQI) **(Defra, 2013b)**

1.4.2 Air pollution epidemiological study types

Numerous epidemiological studies have been conducted to estimate the link between short-term (acute) and long-term (chronic) exposure to air pollution in different populations to a range of health outcomes. Acute effects, such as asthma and all-cause or cause-specific mortality can be short-term and due to time-varying exposures (Section 1.1). On the other hand, chronic or long-term effects are due to

long-developing effects of exposure for example lung cancer, cardiopulmonary diseases and mortality (Section 1.1). Typically epidemiological studies use statistical modelling to quantify the relationship between the pollutant concentration which the population is exposed to and the health outcome (e.g. cause-specific disease or mortality). This is referred to as the concentration-response function (CRF) which is then used to derive the relative risk (RR). The RR is the ratio of the health outcome occurring in the exposed population to the health outcome occurring in the unexposed population (AQEG, 2012). These terms are described in more detail in Section 1.4.3.

Epidemiological studies often report results as an increase in the risk of an adverse health outcome (such as incidence of a disease or death) associated with a certain increment of air pollution. For example, a RR of increased mortality per 10 $\mu g\ m^{-3}$ increase in $PM_{2.5}$ (or any other pollutant) (Gowers et al. 2014). For each RR a 95% confidence interval is also typically provided.

No single epidemiologic study design is best for all applications and thus the choice of an optimal design depends on the research question as well as the availability of data. Each study design targets specific types of effects, outcomes, and exposure sources, and the choice of the optimal design depends on how efficient it is to detect the effect of exposure. This in turn depends on the size of the study and the variability of the exposure. In this thesis CRFs from two main epidemiological study types are used: cohort studies (used in Chapter 3 and 5) and time series studies (used in Chapter 4).

In a cohort study a group of people are followed over a long period of time during which information about risk factors (such as air pollution concentrations) are collected (e.g. Jerrett et al., 2009 and Krewski et al., 2009). Therefore cohort studies represent the combined acute and chronic i.e. short and long-term effect. The occurrence of a health outcome (e.g. respiratory mortality) in people exposed

to the risk factor (e.g. O_3 concentrations) is then compared to the health outcome in people that are not exposed; the RR.

Time-series studies on the other hand analyse the association between daily changes in pollution and daily counts of outcome and are therefore ideal to analyse short-term or acute effects (e.g. Atkinson et al., 2014). For these types of studies individual-level variables like smoking and body mass index are typically not controlled as these factors are not likely to change considerably from day to day. However other variables that vary daily and influence both air pollution and health (e.g. weather) can be accounted for; these are termed confounders. These statistical models are often referred to as single pollutant models. Some studies additionally account for the effect of one pollutant on another, referred to as multi-pollutant models.

In addition some studies summarise findings of other epidemiological studies (e.g. cohort or time-series studies), called meta-analysis studies. This type of study makes use of data from all available epidemiological studies that have addressed the same research questions (e.g. analysing the all-cause mortality effects of long-term exposure to $PM_{2.5}$) and similar study designs (e.g. time series studies) (e.g. Atkinson et al., 2015, 2016). A combined statistical analysis is then conducted and a single summary result is produced. In Chapter 4, CRFs and RRs from a meta-analysis of time-series studies are used.

Details on the RRs and CRFs derived from epidemiological studies are given in the next section (Section 1.4.3).

1.4.3 Exposure response relationships (CRFs) and relative risks (RR)

As briefly mentioned in Section 1.4.2, exposure-response relationships or concentration-response functions (CRFs) and relative risks (RRs) are derived from the different epidemiological studies. The magnitude of the RR or CRF depends on the time-scale of the exposure (i.e. long-term or short-term exposure) and on the health outcome being studied (e.g. cause-specific mortality). In addition, the CRF only holds for the range of pollutant concentrations measured in the epidemiological study, as information on the association between the health outcome and the RR outside the recorded pollutant concentration range would not be available. This may in turn depend on the measurement period e.g. warm season (April-September in the northern hemisphere) or whole year. Therefore, CRFs are often associated with a threshold. This is the lowest pollutant concentration recorded in the respective epidemiological study. Another restriction of the CRF is that the health outcome could be associated with people of a certain age for example aged 30 or over.

The curve of the CRF can have different shapes. For example they can be linear (e.g. Jerrett et al., 2009) or non-linear, which can both be used for long-term and short-term O_3, NO_2 and $PM_{2.5}$ health impacts. Examples of non-linear CRFs include the commonly used log-linear function (e.g. Cohen et al., 2004; Ostro, 2004), the power function (e.g. Pope et al., 2011), and the integrated exposure response (IER) function (Burnett et al., 2014; Cohen et al., 2017). The latter is only used to estimate cause-specific mortality associated with long-term exposure to $PM_{2.5}$.

The integrated exposure-response function combines epidemiological evidence for outdoor air pollution, second-hand smoke, household air pollution and active smoking to estimate the level of disease risk (e.g. stroke) at different $PM_{2.5}$ levels (Burnett et al. 2014). Thus, the same measure is used to estimate the risk of for example heart disease from $PM_{2.5}$ due to outdoor air pollution as that of second-hand smoke or household air pollution. The IER function was also developed to allow for nonlinear patterns for the relationship between $PM_{2.5}$ concentrations and the corresponding diseases causes. The model was fit to the RR estimates from publishes cohort studies. Many major epidemiological studies conducted to estimate the association between long-term exposure to $PM_{2.5}$ and health outcomes have been based in the US, and have only reported relative risks across the $PM_{2.5}$ concentration range from ~ 5 to 30 μg m^{-3} (e.g. Krewski et al, 2009). Thus these studies do not provide knowledge on the association of long-term exposure to $PM_{2.5}$ with mortality at high ambient exposures common in cities and other areas in Asia where annual average exposures can reach higher levels compared to other regions of the world (~ 100 μg m^{-3} in Asia). For this reason the IER function has been developed to estimate the RR of cause-specific mortality associated with long-term $PM_{2.5}$ exposure over the entire range of ambient annual mean $PM_{2.5}$ concentrations across the globe. Burnett et al. (2014) have presented IER function that accounts for changes in the shape of the CRF at high $PM_{2.5}$ concentrations to represent the relative risk of IHD mortality. More recently, Cohen et al. (2017) have developed further IER functions related to long-term $PM_{2.5}$ exposure for IHD, cerebrovascular disease, lung cancer, COPD, and lower respiratory infections (LRI) using risk estimates from meta-analysis studies on ambient air pollution, household air pollution, and second-hand smoke exposure and active smoking (Burnett et al., 2014; Shin et al., 2016). The epidemiological studies, CRFs, RRs and threshold used in this thesis are described next in Section 1.4.4.

1.4.4 Epidemiological studies, risk estimates and thresholds used in this thesis

In this thesis, both long-term (Chapters 3 and 5) and short-term (Chapter 4) exposures to air pollutant concentrations are estimated using the CRFs listed in Table 1.2. In Chapter 3 and 5 the health burden associated with long-term exposure to O_3 and $PM_{2.5}$ is estimated using risk estimates from Jerrett et al. (2009) and Turner et al. (2015) for O_3-related respiratory mortality and Hoek et al. (2013) for $PM_{2.5}$-related all-cause mortality.

The risk estimates for long-term exposure to O_3 from both Jerrett et al. (2009) and Turner et al. (2015) are based on data from the American Cancer Society Cancer Prevention Study II (ACS CPS-II) cohort, but with different study population sizes and follow up times. More importantly, the O_3 exposure metric used in the studies is different; in Jerrett et al. (2009), the summer or warm season average (April-September) daily maximum 1-hour O_3 concentration was used, and in Turner et al. (2015) the annual average daily maximum 8-hour (MDA8) O_3 concentration was used. In this thesis, the CRF suggested by the Health Risks of Air pollution in Europe report (HRAPIE) (WHO, 2013a) is used. This is based on findings by Jerrett et al. (2009) but re-scaled from 1-hour means to 8-hour means using a ratio of 0.72 (Gryparis et al., 2004; WHO, 2013a). The value recommended by HRAPIE for the CRF for the effects of long-term O_3 exposure on respiratory mortality used in Chapter 3 is 1.014 (95% Confidence Interval (CI) = 1.005, 1.024) per 10 μg m^{-3} increase in daily maximum 8-hour running mean (MDA8) O_3 during the warm season (April-September in the northern hemisphere) with a threshold of 70 μg m^{-3} (Table 1.2). In Chapter 5 the CRF used to estimate the effects of long-term O_3 exposure on respiratory mortality is 1.06 (95% Confidence Interval (CI) = 1.04,1.08) per 10 μg m^{-3} increase in annual mean MDA8 O_3 concentrations with a threshold of 53.4 μg m^{-3}

(Table 1.2). Annual-mean based metrics are used in Chapter 5 to match the time period of available baseline mortality data. The CRF from Turner et al. (2015) used in Chapter 5 is also used in Chapter 3 as a sensitivity study.

The long-term $PM_{2.5}$-related CRF associated with all-cause mortality used in this thesis (Chapter 3 and 5) is based on a meta-analysis of all cohort studies published before January 2013 which included thirteen different studies conducted in the adult population of North America and Europe (Hoek et al., 2013). For estimating the health impact of long-term exposure to $PM_{2.5}$ on all-cause excluding external (i.e. environmental events and circumstances as the cause of injury, poisoning and other adverse effects; ICD 10 codes V01-Y98) mortality (in Chapter 3 and 5), a CRF of 1.062 (95% CI = 1.040, 1.083) per 10 μg m^{-3} increase in annual average concentrations (with no threshold; Table 1.2) is used.

In addition, in chapter 5, long-term exposure to NO_2 is related to mortality using a CRF derived from a systematic review and meta-analysis of cohort studies linking long-term average concentrations of NO_2 with all-cause mortality (COMEAP, 2015a). For estimating the long-term NO_2 exposure for all-cause (excluding external) mortality, a CRF of 1.025 (95% CI = 1.01,1.04) per 10 μg m^{-3} increase in annual mean NO_2 concentrations (with no threshold) is used (Table 1.2). Evidence suggesting a threshold associated with long-term exposure to $PM_{2.5}$ and NO_2 is lacking (COMEAP, 2015a; WHO, 2013a). Thus in this thesis no threshold is included when estimating the long-term health burden associated with these two pollutants (Table 1.2). Long-term exposures to pollutant concentrations in Chapter 3 and 5 exclude people younger than 30 years.

Table 1.2 **Health impact assessment details used for health calculations in chapters 3-5. Numbers in brackets indicate the 95% confidence interval of uncertainties associated with the concentrations-response function (CRF). Warm season MDA8 O_3 is the daily maximum 8-hr running mean O_3 averaged between April and September. Long-term exposures hold for population 30 years and older while the short-term exposures hold for all ages.**

	Chapter 3		**Chapter 4**		**Chapter 5**		
Pollutant	**O_3**	**$PM_{2.5}$**	**O_3**	**$PM_{2.5}$**	**O_3**	**NO_2**	**$PM_{2.5}$**
Exposure	Long-term	Long-term	Short-term	Short-term	Long-term	Long-term	Long-term
Metric	Warm season MDA8 O_3	Annual mean $PM_{2.5}$	MDA8 O_3	Daily mean $PM_{2.5}$	Annual mean MDA8 O_3	Annual mean NO_2	Annual mean $PM_{2.5}$
Concentration-response coeff.	1.014 (1.005,1.024)	1.062 (1.04,1.083)	1.0034 (1.0012,1.0056)	1.0104 (1.0052,1.0156)	1.06 (1.04,1.08)	1.025 (1.01,1.04)	1.062 (1.04,1.083)
	WHO (2013a)	WHO (2013a)	COMEAP (2015b)	Atkinson et al. (2014)	Turner et al. (2015)	COMEAP (2015a)	WHO (2013a)
Threshold ($\mu g\ m^{-3}$)	70	/	/	/	53.4	/	/

To estimate the health burden associated with short-term exposure to O_3 and $PM_{2.5}$ in Chapter 4, CRFs derived from systematic reviews and meta-analysis of time series studies are used ((COMEAP, 2015b) and (Atkinson et al., 2014), respectively) alongside daily exposure estimates. The all-cause mortality associated with short-term exposure to O_3 is estimated using a CRF of 1.0034 (95% CI: 1.0012, 1.0056) per 10 μg m^{-3} increase in MDA8 O_3 , and for short-term exposure to $PM_{2.5}$, a CRF of 1.0104 (95% CI: 1.0052, 1.0156) per 10 μg m^{-3} increase in 24-hr mean $PM_{2.5}$ is used (Table 1.2). Evidence for a threshold below which no adverse effects from short-term exposure to O_3 and $PM_{2.5}$ is limited, therefore the full range of pollutant exposure is used to calculate the health burdens which applies for all ages (COMEAP, 1998, 2015b; Table 1.2).

1.5 Health impact assessments

In Health Impact Assessments (HIAs) the CRFs derived from epidemiological studies (Section 1.4.3) are used to translate estimates of population exposure in terms of air pollutant concentrations into health impact estimates (Briggs et al., 2008). In this section a description of the method used for calculating HIAs by different studies is first presented (Section1.5.1) followed by uncertainties associated with HIAs in Section 1.5.2.

1.5.1 Methods for calculating HIAs (examples from literature)

The global, long-term attributable mortality or health burden due to anthropogenic $PM_{2.5}$ and O_3 concentrations, has been estimated by a number of studies (e.g. Anenberg et al., 2010; Lelieveld et al., 2013; Silva et al., 2013; Li et al., 2015) using the following equations. The attributable mortality due to long-term exposure to the air pollutant is estimated by multiplying the attributable fraction of mortality (AF) by the baseline mortality rate y_0 and the size of the exposed population Pop.

$$Mort = y_0 \times AF \times Pop \quad (1.1)$$

The number of attributable deaths is a metric widely used in the literature and can also be expressed as a rate. However it is important to note that this metric does not simply represent the number of individuals whose length of life has been shortened by air pollution (COMEAP, 2010). For example, long-term exposure to air pollution is understood to be a contributory factor to deaths from respiratory and cardiovascular disease and it is unlikely to be the sole cause of deaths of individuals (Gowers et al., 2014).

The fraction of disease burden attributable to the risk factor, the attributable fraction (AF) of the disease, often expressed as a percentage is defined as:

$$AF = \frac{RR-1}{RR} \quad (1.2)$$

Where a log-linear relationship between the RR and pollutant concentrations as defined by Jerrett et al. (2009) and Krewski et al. (2009) for O_3 and $PM_{2.5}$ health impacts, respectively is used (equation 1.3).

$$RR = \exp(\beta(x - x_0)) \quad (1.3)$$

In equation 1.3, β is the estimated slope of the log-linear relationship between air pollutant concentration and mortality (ie the CRF) and *x* is the population-weighted pollutant concentration with a threshold x_0. Health impact assessments (HIAs) are performed using air pollutant concentration data from monitoring stations, satellites and from chemistry-climate models. For example, the global burden of disease due to ambient air pollution was originally estimated based on measured levels of pollution at ground stations (e.g. Cohen et al., 2004). More recent studies use simulated pollutant concentrations from global and regional atmospheric models (e.g. Cohen et al. 2017; Lelieveld et al. 2015; Lelieveld 2017; Butt et al. 2017; Punger & West 2013; Silva et al. 2016) or global modelling output combined with observations (Evans et al., 2013) as well as satellites (Crouse *et al.*, 2015; Anenberg *et al.*, 2018; Kushta et al., 2018) to estimate exposure to air pollutants.

Lelieveld et al. (2015) also estimate the global burden of disease associated with long-term exposure to O_3 and $PM_{2.5}$ however they implement a different definition for the RR to that in equation 1.3 as the former is based on epidemiological cohort studies in the US and Europe where annual mean $PM_{2.5}$ concentrations are typically below 30 μg m^{-3}. Thus to account for higher $PM_{2.5}$ concentrations typical of countries such as South and East Asia, Lelieveld et al. (2015) and Kushta et al. (2018) use the CRF of Burnett *et al.* (2014) (Section 1.4.3) as described in equation 1.4 below where a and p are factors derived from statistical models to account for large $PM_{2.5}$ concentrations.

$$RR = 1 + a\{1\text{-}exp[\text{-}\beta(X\text{-}Xo)^p]\} \quad (1.4)$$

For COPD attributable to long-term exposure to O_3 Lelieveld et al. (2015) (as well as other studies e.g. Schmidt, 2013; Butt *et al.*, 2016) use the definition of RR by Ostro (2004):

$$RR = \left[\frac{(x+1)}{(x_0+1)}\right]^{\beta} \quad (1.5)$$

Where in this case $x_0$and x are the base case and perturbed population-weighted pollutant concentration, respectively.

Other studies that estimate the global burden of disease, for example Cohen et al. (2017) or global and regional trends (Butt *et al.*, 2017; Kushta et al., 2018), make use of a IER functions (Section 1.4.3) for IHD, COPD, lung cancer, and lower respiratory infections to estimate the relative risk of mortality, RR, for each cause of death using non-linear CRFs spanning the global range of exposure to pollutant concentrations.

In addition statistical tools to perform health impact assessments are also available e.g. the widely used Benefit Mapping and Analysis Program (BenMAP) tool from the US Environmental Protection Agency (USEPA)) (Punger and West, 2013; Thompson et al., 2014). BenMap is a geographic information systems program which combines US census-level population and incidence data at country-level resolution with user-supplied air pollution data (from monitors, satellite or models) to estimate health effects (Abt Associates, 2010). Thus in contrast, in this case all the calculations are conducted by the single package BenMap therefore ensuring coherence at every step of the HIAs.

Short-term HIAs are conducted in a similar was to long-term HIAs however short-term HIAs are conducted daily and the terminology used for the health burden is deaths brought forward. For example Macintyre et al. (2016) estimate the mortality associated with $PM_{2.5}$ episodes across the UK in spring 2014. The total all-cause mortality, Mort associated with short-term exposure to $PM_{2.5}$ summed over each day of the air pollution episode i, is calculated following equation 1.6.

$$Mort = \sum_i^N D_i \times AF_i \quad (1.6)$$

Where D_i is an estimate of the total regional daily baseline mortality. The daily AF of mortality is calculated following equation 1.2 and using the definition of RR given by equation 1.7.

$$RR_i = \exp(\beta x_i) \tag{1.7}$$

Similar to equation 1.3, β is slope of the log-linear relation between concentration and mortality (ie CRF) and x_i is the daily mean population-weighted $PM_{2.5}$ concentration. A similar approach for estimating the short-term O_3 exposure over the UK in July 2006 is implemented by Pope *et al.* (2016).

In this thesis, all health impact assessments are either focused on Europe (Chapter 3) or the UK (Chapter 4 and 5) where $PM_{2.5}$ concentrations generally do not exceed ~30 μg m^{-3} especially in the UK (Fig 1.9 Section 1.4.1) thus a log-linear function is used throughout the thesis. Long-term health impacts are estimated following a similar method to Anenberg et al. (2010) (Chapters 3 and 5) while an approach similar to Macintyre et al. (2016) is implemented for short-term health impacts (Chapter 4).

1.5.2 Uncertainties associated with HIAs

A number of uncertainties are associated with the estimation of mortality burdens attributable to long-term or short-term exposure to air pollution. These include: the use of a CRF derived from an epidemiological study based in one geographical location, uncertainties related to the use of CRFs derived from single-pollutant statistical models, uncertainties associated with population and baseline mortality rates and representativeness of the pollutant exposure estimates or pollutant concentrations derived from modelling or observations.

Quantification of the health burden for one pollutant from single-pollutant statistical models may to some extent include effects attributable to another. Consequently, the recommendations by the HRAPIE project (WHO, 2013a) suggest that for any particular health outcome and exposure period, estimated O_3, NO_2 and $PM_{2.5}$ related health burdens should not be added without acknowledging that this will, in most circumstances lead to some overestimation of results. On the other hand, impacts estimated for one pollutant only are suggested to underestimate the true impact of the pollution mixture, if other pollutants also affect the same health outcome. For example, Williams et al. (2014) demonstrate that the analysis of O_3 and NO_2 separately in epidemiological studies can underestimate the combined effects on the population from exposure to both pollutants.

Having outlined how HIAs are generally conducted together with the associated uncertainties, the next three sections describe three different aspects which can influence air quality and the associated health impacts related to uncertainty of pollutant exposure estimates, and short-term and long-term changes in air pollutant concentrations. These are the impact of model horizontal resolution, the impact of air pollution episodes and the impact of future emissions scenarios on air pollution concentrations and the associated health impacts.

1.6 The impact of model horizontal resolution on pollutant concentrations and the associated health impacts

In this thesis a chemistry-climate model (CCM) is used to simulate pollutant concentrations. CCMs vary in many different aspects (Section 1.3) and in particular, these models can have different horizontal resolutions. Different horizontal resolutions present advantages and disadvantages. Global CCMs have coarse resolutions (~50-100 km in the horizontal) to enable long-term integrations for the

globe. However such coarse resolutions can lead to inaccuracies in the representations of local or urban effects such as high levels of emissions in pollution hotspots (Section 1.3).

Several studies have been conducted to analyse the effect of changing the model horizontal resolution on different pollutant concentrations (e.g. Ridder et al., 2014; Stock et al., 2014; Thompson et al., 2014; Valari and Menut, 2008). However, only a few studies have evaluated the impact of changes in model horizontal resolution on the estimated human health burdens (Punger and West, 2013; Thompson et al., 2014; Li *et al.*, 2015; Kushta et al., 2018). The majority of these studies find that mortality associated with long-term exposure to O_3 is higher, because simulated O_3 concentrations are often larger (section 1.3), when using coarse resolution compared to a finer resolution (Thompson and Selin, 2012; Punger and West, 2013; Thompson et al., 2014). Less agreement between the available studies is found for $PM_{2.5}$-related health estimates. While some studies suggest that the attributable mortality associated with long-term exposure to $PM_{2.5}$ is lower at coarse resolutions larger than 100 km (Li et al., 2015; Punger and West, 2013), another study finds that using horizontal resolutions less than 36 km had negligible effect on changes in $PM_{2.5}$ concentrations and associated health impacts (Thompson et al., 2014). More recently, the uncertainties in ambient $PM_{2.5}$-related mortality in Europe have been analysed in relation to model simulations of $PM_{2.5}$ concentrations at 100 km and 20km (Kushta et al., 2018). Findings of this study also suggest that simulated $PM_{2.5}$ concentrations and corresponding health impacts at the coarse resolution (100 km) are lower compared to estimates at the 20 km resolution for most European countries. Moreover uncertainties of mortality estimates are dominated by the estimated CRFs derived from epidemiological studies rather than the representation of annual mean $PM_{2.5}$ concentrations by air quality models having varying horizontal and vertical resolutions (Kushta et al., 2018). However, the majority of the abovementioned studies have been conducted in the US and similar studies over Europe are limited. Quantifying the impacts of

model resolution on health impacts of O_3 and $PM_{2.5}$ over Europe is therefore the focus of Chapter 3. NO_2 health impacts associated with long-term exposure are not estimated in Chapter 3 due to the relatively coarse model horizontal resolutions (global and regional) used which would not adequately represent NO_2 concentrations typically high in highly populated regions.

1.7 The impact of air pollution episodes on pollutant concentrations and the associated health impacts

Meteorology has a major influence on air quality, through its impact on chemical reaction rates by changes in temperature, on the deposition of $PM_{2.5}$ through changes in precipitation, and on the stagnation of air and long-range transport through changes in wind speed and direction. Under anticyclonic weather conditions with low wind speeds, resulting stable conditions can often create an inversion of the temperature profile, hence trapping pollutants in the shallow boundary layer close to the ground resulting in high levels of air pollutants and producing an air pollution episode (e.g. Pope et al., 2016, Rebetez et al., 2009). In summer these air pollution episodes can also coincide with heatwaves (Solberg *et al.*, 2008; Tong et al., 2010; Schnell and Prather, 2017). In addition, synoptic flows over the UK can lead to transport of polluted air from over Europe (e.g. Francis et al., 2011) or clean air from the Atlantic, depending on the orientation of the prevailing weather system.

Several studies have estimated the impact of short-term exposure to O_3 and PM on human health during air pollution episodes. In particular a number of studies estimate the morality burden associated with all-cause mortality due to air pollution during the European heatwave in August 2003. For example, Stedman (2004) estimate that in England and Wales, 83 and 29 deaths per day occurred due

to short-term exposure to daily maximum 8hr running mean (MDA8) O_3 and 24 hour mean PM_{10} (particulate matter with an aerodynamic diameter less than 10 μm), respectively during the first two weeks in August 2003. This represented an increase of 38 (O_3) and 13 (PM_{10}) deaths per day compared with the previous year. $PM_{2.5}$ air pollution episodes have also been studied. Macintyre et al., (2016) estimate that a spring time air pollution episode in 2014 is associated with ~60 daily deaths brought forward from short-term exposure to $PM_{2.5}$ in the UK and suggest a mortality burden that is 2.0 to 2.7 times that associated with typical urban background levels of $PM_{2.5}$ during the same period. In summer 2006, stagnant weather conditions resulted in high O_3 and $PM_{2.5}$ concentrations across the UK. Using measured pollutant concentrations between June and July 2006, the UK Health Protection Agency (HPA – now Public Health England) estimate 11 and 7 additional daily deaths brought forward in England and Wales associated with increased O_3 and PM_{10} concentrations compared to 2004 (HPA, 2006). Monitoring of $PM_{2.5}$ concentrations only became routine in the UK following the 2008 ambient air quality directive (EU, 2008) and thus due to lack of data the $PM_{2.5}$ health burden has not previously been quantified for this period.

Under climate change extreme events such as heatwaves are likely to be more frequent, more intense, and last longer (IPCC, 2014). This could give rise to increases in the occurrence of air pollution episodes and associated short-term health burdens. However, the frequency of air pollution episodes may also be affected by climate change through changes in the frequency of large-scale blocking episodes which have been shown to decrease in winter and summer over Europe in the 21st century (Masato et al. 2013). However the climate-driven relationship between changes in blocking and stagnation and hence air pollution episodes remains uncertain (Kirtman et al., 2013).

Nonetheless studying the health impacts associated with air pollution episodes for present-day may help quantify the variability of health impacts

associated with such air pollution episodes. Hence, in chapter 4, the estimated mortality burdens associated with short-term exposure to O_3 and $PM_{2.5}$ for two air pollution episodes in July 2006 together with links to the underlying meteorology for the air pollution episodes are presented.

1.8 The impact of future emission scenarios on pollutant concentrations and the associated health impacts

A number of future emission and climate scenarios have been used in previous studies to simulate potential changes in air pollution in the future. The most commonly used future emissions scenarios used in global chemistry-climate modelling studies are issued by the Intergovernmental Panel on Climate Change Fifth Assessment Report (IPCC AR5) and are called Representative Concentration Pathways (RCPs). There are four pathways: RCP8.5, RCP6, RCP4.5 and RCP2.6 where the numbers refer to radiative forcing in Watts per square metre, for each RCP. Each RCP contains a set of estimated emissions of a number of species including CO, NO_x, NMVOC, BC, OC, SO_2, NH_3 and CH_4 up to 2100, based on assumptions about economic activity, energy sources, population growth and other socio-economic factors. The total (anthropogenic, shipping, aircraft and biomass burning) global emissions for O_3 precursors and PM primary and precursors for each RCP are shown in Table 1.3.

Table 1.3: Total global emission for O_3 precursors and aerosols: Tg/(species)/year, except NO_x emissions expressed as Tg(NO_2)/year Lamarque et al., 2011).

		2000	2010	2020	2040	2060	2080	2100
CO	RCP2.6	1067.2	1028.8	982.5	878.1	779.2	663.7	607.8
	RCP4.5	1069.0	1061.8	1002.3	953.1	778.5	558.0	477.3
	RCP6	1068.8	1048.8	1028.3	1049.7	996.1	873.0	792.2
	RCP8.5	1069.4	1029.6	1052.0	951.2	841.1	757.2	690.3
NO_x	RCP2.6	125.3	128.8	120.0	98.4	89.4	67.8	52.5
	RCP4.5	125.5	124.1	117.3	107.0	84.0	62.6	59.3
	RCP6	125.7	124.0	115.6	107.2	93.0	65.5	52.9
	RCP8.5	125.5	129.6	138.3	121.4	104.0	95.2	86.2
NMVOC	RCP2.6	210.5	216.2	212.6	192.0	166.4	138.6	125.5
	RCP4.5	210.8	211.7	196.0	202.3	179.9	150.3	140.0
	RCP6	210.8	213.3	212.0	221.8	214.1	191.8	172.1
	RCP8.5	210.8	214.6	224.4	217.9	201.2	188.6	176.2
BC	RCP2.6	7.8	8.8	8.5	5.7	4.4	3.7	3.4
	RCP4.5	7.8	8.1	7.8	6.8	5.5	4.1	3.9
	RCP6	7.8	8.1	7.7	7.4	6.5	5.1	4.4
	RCP8.5	7.8	7.8	7.5	6.1	5.2	4.7	4.2
OC	RCP2.6	35.9	37.6	37.6	32.3	29.7	26.9	25.3
	RCP4.5	35.9	34.7	30.5	27.9	24.9	20.4	19.4
	RCP6	35.9	37.1	36.8	36.7	35.7	33.3	32.2
	RCP8.5	36.0	34.9	34.1	31.4	28.4	26.4	23.9
NH_3	RCP2.6	48.0	52.7	57.7	64.7	71.1	77.0	81.6
	RCP4.5	48.5	51.3	52.6	56.3	55.8	53.6	52.9
	RCP6	48.6	53.3	52.1	60.8	69.0	73.9	74.9
	RCP8.5	48.6	52.7	58.8	67.8	73.7	77.5	81.6
SO_2	RCP2.6	107.5	107.9	85.6	39.3	27.4	19.5	12.9
	RCP4.5	107.8	111.9	102.9	69.6	41.4	25.5	22.5
	RCP6	107.7	107.4	95.1	83.3	69.8	30.0	21.9
	RCP8.5	107.7	101.5	96.1	65.6	45.4	36.9	25.7

For all RCPs, large decreases in primary and precursor emissions of PM and O_3 are estimated globally following the assumption of more stringent air pollution control measures over time (Table 1.3). However, an exception is ammonia (NH_3, Table 1.3) which increases in nearly all scenarios, and methane (CH_4) which increases for RCP8.5 (~300.2 in 2000 to 887.6 Tg (CH_4)/yr in 2100 under RCP8.5; RCP Database: https://tntcat.iiasa.ac.at/RcpDb last accessed 10th September 2018).

Globally, annual mean O_3 concentrations are projected to decrease by 2050 under most RCPs due to reductions in O_3 anthropogenic precursor emissions especially NO_x. However, under RCP8.5 annual global mean increases in O_3 concentrations are projected as a result of elevated abundance of atmospheric CH_4 (Fiore et al., 2009; Wild et al., 2012).

Previous global scale studies have estimated the impact of future emissions changes on O_3 concentrations for Europe. Under RCP2.6 and RCP 6.0, Wild et al 2012 find reductions in annual mean O_3 concentrations by 2050 due to decreases in O_3 precursors but under RCP8.5 project increases of O_3 concentrations between 2000 and 2050 due to increases in CH_4 concentrations (as above). Other studies over Europe have suggested reductions of O_3 concentrations as a result of reductions O_3 precursor emissions however this signal is not consistent over Europe. O_3 concentrations are found to increase in regions with high NO_x emissions (e.g. the Benelux region and the south of the UK) due to the titration effect of NO on O_3 (R1.6; Section 1.2.1.2) however, overall O_3 concentrations decrease substantially over Europe (Colette *et al.*, 2012; Hedegaard et al., 2013). More recently, Im et al., (2018), suggest an average increase in O_3 concentrations for Europe as a result of reductions in anthropogenic emissions. Over the UK, Heal et al. (2013) used three future scenarios (different to the RCPs) to analyse health burdens of surface ozone for 2030 and find that for the 'worst case' scenario having high O_3 precursor emissions, O_3 concentrations decrease over most of the central England, particularly in urban areas (as a result of high NO_x emissions under this scenario) and increase in rural areas such as much of Scotland.

Globally, $PM_{2.5}$ concentrations driven by emissions changes are generally estimated to decrease under future scenarios due to reduced primary emissions as well as changes in secondary inorganic aerosol emissions. In the Europe, $PM_{2.5}$ concentrations are projected to decrease under RCP4.5 due to reductions in anthropogenic emissions of Sulphur oxides (SO_x) and Black Carbon (BC) (Hedegaard

et al., 2013; Im et al., 2018). In the UK, decreases in $PM_{2.5}$ concentrations are also projected in 2030 due to a 30% reduction in emissions of NO_x, SO_x, VOCs, NH_3 and primary $PM_{2.5}$ (Vieno *et al.*, 2016).

The majority of recent studies focusing on future health burdens associated with long-term exposure to O_3 and/or $PM_{2.5}$ concentrations under the RCPs typically analyse the combined emission and climate change impacts. For example, in a global study, Silva *et al.* (2016) suggest decreases in the respiratory mortality burden associated with long-term exposure to O_3 in Europe for all four RCPs in 2050s relative to 2000s (16,600 to 49,400 annual avoided deaths) driven by decreases in O_3 concentrations across Europe. Amongst the different studies, the overall future health burden is found to depend on projected air pollutant concentrations as well as changes in baseline mortality rates and population projections with the latter intensifying differences between present-day and future estimates (e.g. Silva et al., 2016). Studies looking at the impact of emission changes on air pollutant concentrations and the consequent health impacts in the UK are limited. This is therefore the focus of Chapter 5.

The research aims of this thesis are based on the concepts described in Sections 1.6, 1.7 and 1.8 and are described in further detail in Section 1.9.

1.9 Outline of research aims and chapters

The goal of this thesis is to perform health impact assessments (HIAs) over Europe and the UK using modelled pollutant concentrations for present-day and future. The specific aims are:

(i) to quantify the influence of model horizontal resolution on simulated concentrations of ozone (O_3) and particulate matter less than 2.5 μm in diameter ($PM_{2.5}$) for Europe and the implications for HIAs associated with long-term exposure to these pollutants (Section 1.9.1).

(ii) to assess the variability in air pollutant concentrations of O_3 and $PM_{2.5}$ during two air pollution episodes during a well-known heatwave in July 2006 in the UK together with the corresponding attributable fraction (AF) of mortality and mortality burden associated with short-term exposure to each pollutant (Section 1.9.2). The two 5-day air pollution episodes are chosen based on a DAQI reaching a 'moderate' or 'high' level and high O_3 and $PM_{2.5}$ concentrations occurring concurrently. Further details are presented in Section 4.3.

(iii) to estimate future changes in the AF of mortality and mortality burden associated with long-term exposure to O_3, NO_2 and $PM_{2.5}$ under future UK emission changes for 2050 in the UK (Section 1.9.3).

1.9.1 The influence of model spatial resolution on simulated O_3 and $PM_{2.5}$ for Europe: implications for health impact assessments (Chapter 3).

Aim: How does a change in model resolution effect simulated O_3 and $PM_{2.5}$ concentrations over Europe and the corresponding long-term health impacts?

In Chapter 3, one of the key uncertainties, model horizontal resolution, associated with HIA is investigated. The impact of horizontal resolution on simulated concentrations of O_3 and $PM_{2.5}$ in Europe is examined using a chemistry–climate model (CCM) at two different horizontal resolutions: (i) a global (~ 140 km) and (ii) a regional (~40 km) resolution. These simulated pollutant concentrations are then used to estimate the attributable fraction (AF) of mortality associated with long-term exposure to summer mean (April-September) daily maximum 8hr running mean (MDA8) O_3 and annual mean $PM_{2.5}$ for both resolutions at the European country level to analyse the corresponding influence of a change in horizontal resolution on O_3 and $PM_{2.5}$ related health impacts.

1.9.2 Mortality associated with O_3 and $PM_{2.5}$ air pollution episodes in the UK in 2006 (Chapter 4).

Aim: How do air pollution episodes with high levels of O_3 and $PM_{2.5}$ in 2006 impact the short-term exposure to these two pollutants in the UK?

In Chapter 4, the impact of air pollution episodes on the UK health burden in July 2006 is examined. The Met Office air quality model (AQUM) at a 12 km horizontal

resolution is used to simulate O_3 and $PM_{2.5}$ concentrations during two five-day air pollution episodes in July 2006 (1st - 5th July and 18th – 22nd July) across the UK. The episode days are selected based on days when the Daily Air Quality Index (DAQI) was 'moderate' to 'high' (Section 1.4.1) and with high levels of O_3 and $PM_{2.5}$ occurring concurrently. Firstly, the driving meteorological factors contributing to high levels of simulated O_3 and $PM_{2.5}$ are examined and compared to observations. Next, the AF of all-cause mortality and the mortality burdens associated with short-term exposure to MDA8 O_3 and daily mean $PM_{2.5}$ during each episode in 2006 are estimated for each region in England, Scotland and Wales.

1.9.3 Future mortality related health burdens associated with RCP emission scenarios for 2050 for the UK (Chapter 5).

Aim: How are simulated air pollutant concentrations of O_3, NO_2 and $PM_{2.5}$ and associated long-term health impacts in the UK projected to change in the future due to UK emission changes in 2050 under the RCP scenarios?

In Chapter 5, the impacts of changes in future emissions on the UK health burden are examined. Pollutant concentrations of O_3, NO_2 and $PM_{2.5}$ for 2050 (future) are simulated using the Met Office air quality model- AQUM (as used in Chapter 4) following three emission scenarios that range the whole span of the RCPs. For this reason the two extreme scenarios : IPCC RCP2.6 and RCP8.5 are chosen. A middle scenario is also chosen, RCP6.0. The other RCP scenario in between RCP2.6 and RCP85, RCP4.5 was not included in this thesis as the emission files for 2050 regridded at 12 km for this scenario were not readily available. Simulated pollutant concentrations for 2050 following the different RCPs are compared to simulated pollutant concentrations for 2000 (present-day). The present-day and future AF of

mortality associated with long-term exposure to annual mean MDA8 O_3, NO_2 and $PM_{2.5}$ and the corresponding mortality burdens are calculated for each region in the UK. In addition the sensitivity of future health burdens to two different population scenarios is analysed.

In the next chapters, the main methods used for this thesis are described in Chapter 2 followed by results corresponding to the three research aims discussed above in Chapters 3, 4 and 5. A summary of results followed by the main conclusions of this thesis are presented in Chapter 6 which includes uncertainties and limitations of this research and ideas for future work.

Chapter 2 Methods

The overall aim of this thesis is to simulate pollutant concentrations for both present-day and future and to examine the corresponding health impacts (Section 1.9). This is achieved by using a climate model coupled to a chemistry and aerosol model referred to as a chemistry-climate model (section 1.3) using different configurations listed in Table 2.1. Configurations used in Chapter 3 are described in more detail in Section 2.1 and configurations used in Chapters 4 and 5 are described in more detail in Section 2.2. The measurements used for evaluating the different configurations are described in Section 2.3 followed by a description of the methodology used to calculate the health impacts for the respective chapters in Section 2.4.

Table 2.1: Modelling system comparison of the major components between the global, regional (HadGEM3-UKCA) and the UK national-scale (AQUM) configurations of the Met Office Unified Model (MetUM)

	Global	**Regional**	**AQUM**
Horizontal Resolution	1.875° × 1.25° (~140 × 140 km)	0.44° × 0.44° (~50 × 50 km)	0.11° × 0.11° (~12 × 12 km)
Domain Extent	Global	Most of Europe and N. Africa	UK and nearby Western Europe
Vertical Resolution	63 levels (spanning 41 km)	63 levels (spanning 41 km)	38 levels (spanning 39 km)
Aerosol Scheme	CLASSIC	CLASSIC	CLASSIC
Gas-phase Chemistry	UKCA – ExtTC (89 chemical species)	UKCA – ExtTC (89 chemical species)	UKCA – RAQ (58 chemical species)
Photolysis Scheme	offline 2-D photolysis scheme	offline 2-D photolysis scheme	On-line photolysis scheme Fast-JX
Meteorology	Free-running	Free-running	Global model forecast fields (~17 km)

2.1 The global and regional chemistry-climate models (HadGEM3-UKCA)

In Chapter 3, the two chemistry–climate configurations used are based on the Hadley Centre Global Environmental Model version 3 (HadGEM3, Hewitt *et al.*, 2011), of the Met Office Unified Model (MetUM, Brown et al., 2012). The various components included in the chemistry–climate model used for both configurations are illustrated in Fig. 2.1 and consist of: (i) the Global Atmosphere 3.0 (GA3.0; Walters *et al.*, 2011) and (ii) the Global Land 3.0 (GL3.0; Walters et al., 2011) component of HadGEM3 and (iii) the United Kingdom Chemistry and Aerosol model (UKCA, Morgenstern et al., 2009; O'Connor et al., 2014) (Fig. 2.1). At different model time steps, exchanges occur between the individual components of the chemistry-climate model such as exchanges of meteorology between HadGEM3 and air pollutant concentrations in UKCA resulting in coupling of the different components of the chemistry-climate model.

In the next sections the individual components of the chemistry-climate model are described in more detail starting with a description of the atmospheric and land components of HadGEM3 (Sections 2.1.1 and 2.1.2) followed by a description of the gas phase chemistry included in the UKCA model and aerosol phase chemistry which forms part of the atmospheric component of HadGEM3 (Section 2.1.3 and 2.1.4)

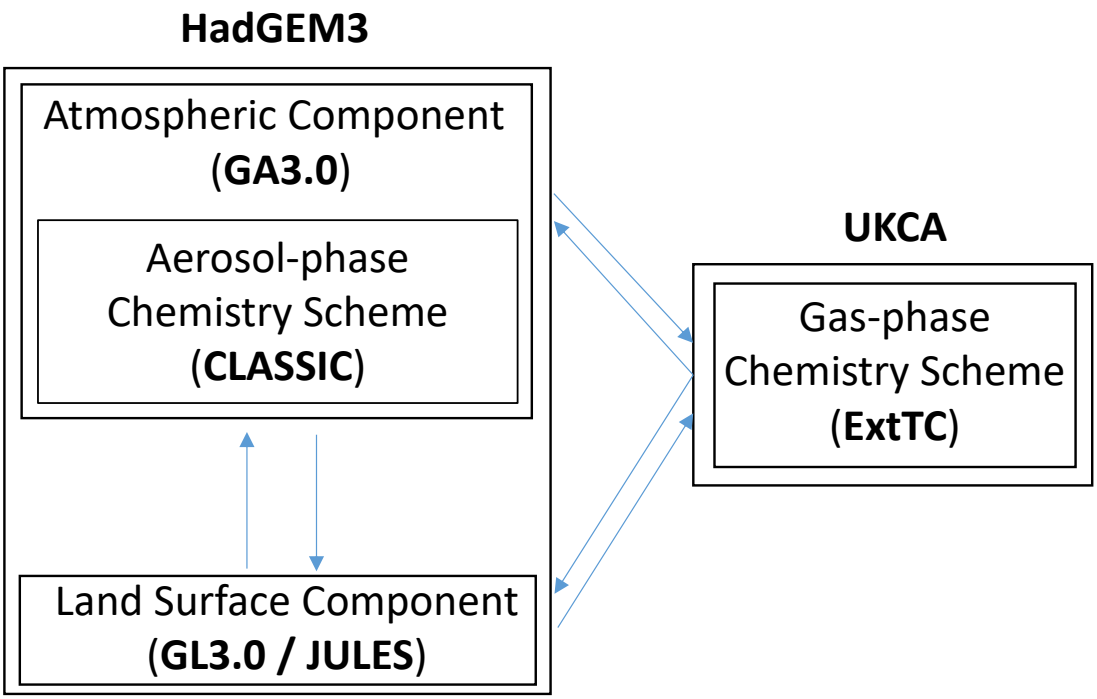

Figure 2.1: **Schematic diagram of the interactions between components of HadGEM3 and UKCA models. Lines indicate how components of the model are coupled to one another, allowing exchange of variables (e.g. composition and dynamical processes).**

2.1.1 The Atmosphere Component (GA3.0) of the climate-model (HadGEM3)

As described previously, the atmospheric component of the chemistry-climate model used in Chapter 3 is the Global Atmosphere 3.0 (GA3.0, Walters et al., 2011) of the HadGEM3 family (Hewitt et al. 2011). In Chapter 3, two configurations having a different horizontal model resolution are used: (i) a global configuration with a horizontal resolution of 1.875° × 1.25° (~ 140 km, Walters et al., 2011) and (ii) a regional configuration with a horizontal resolution of 0.44° × 0.44° (~50 km, Moufouma-Okia and Jones, 2014) and a domain covering most of Europe (Fig. 2.2 blue box; Table 2.1). The global and regional configurations consist of 63 vertical levels from the ground up to an altitude of 41 km (Table 2.1). The mid-point of the

lowest model level for both configurations (which is selected as representative of surface concentrations throughout this thesis) is at 20 m. While this level is considered representative of surface or ground-level concentrations, local orographically driven flows or sharp gradients in mixing depths cannot be represented at this vertical resolution (Fiore et al., 2009). The sensitivity of simulated pollutant concentrations to vertical model resolution within this thesis has not been examined. Kushta et al. (2018) suggest that mortality rates due to long-term exposure to $PM_{2.5}$ differ by only 0.6% due to vertical distribution of $PM_{2.5}$.

Sea surface temperature (SST) and sea ice extent (SIE) fields are prescribed for all simulations performed in Chapter 3 and are used to drive the meteorology. The model is therefore referred to as 'free-running' (Section 1.3; Table 2.1) with lateral boundary conditions (LBCs) from the global resolution (at 6-hourly intervals) driving the regional-scale configuration ensuring that the same processes operate at the two resolutions.

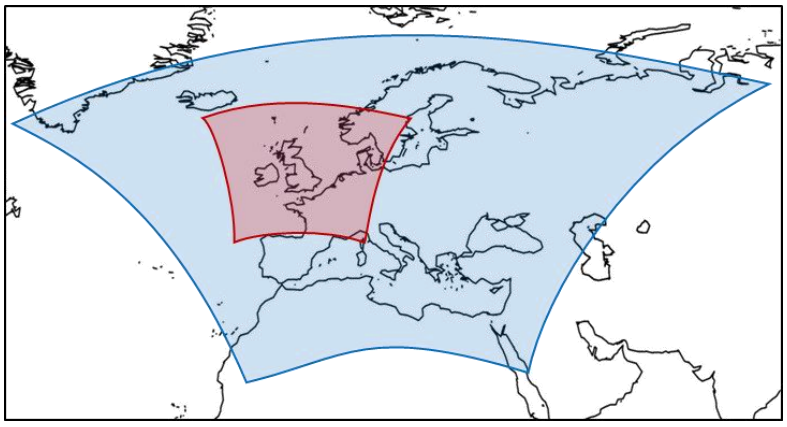

Figure 2.2: **A simplified illustration of the extent of the model domains for the regional configuration, plotted in blue and the UK national-scale configuration (AQUM) in red.**

Within the atmospheric components of the climate model dynamical processes enable interactions with other components of the model such as the land and UKCA components transporting emissions and pollutants (Fig. 2.1). The boundary layer scheme includes parameterisations of turbulent motions and tracer mixing in the atmosphere (Brown et al., 2008; Lock, 2001; Lock et al., 2000). This parameterisation represents mixing over the full depth of the troposphere and not solely within the boundary layer. The convection scheme represents sub-grid scale transport of heat, moisture and momentum associated with cumulus clouds within a grid-box (Gregory and Rowntree, 1990). Large-scale transport of tracers use the MetUM dynamical core (Davies et al., 2005) with advection of tracers following Priestley (1993).

The formation and evolution of precipitation due to grid scale processes is parametrized by the microphysics or large-scale precipitation scheme (Wilson and Ballard, 1999), while small scale precipitation is represented by the convection scheme outlined above. Shortwave and long-wave radiation drive atmospheric processes by supplying energy to the atmosphere. These are parameterized by the radiation scheme (Edwards and Slingo, 1996; Cusack et al., 1999).

The GA3.0 configuration incorporates an interactive aerosol scheme, CLASSIC (COUPLE Large-scale Aerosol Simulator for Studies in Climate, Jones et al. (2001); Bellouin et al. (2011)). The aerosols can influence the atmospheric cloud and radiative properties referred to as aerosol-cloud and aerosol-radiation interactions. CLASSIC is described in further detail in Section 2.1.4.

Gaseous chemistry is simulated by the UKCA (Morgenstern et al., 2009; O'Conner et al., 2014) and described in Section 2.1.3. Coupling between the HadGEM3-GA3.0 and UKCA models allows the inclusion of gases in the dynamical processes described above. These can also feedback onto climate via changes in radiation and cloud properties.

2.1.2 The Land-surface component (GL3.0) of the climate model (HadGEM3)

Different parameters such as heat and moisture as well as exchanges of greenhouse gases and biogenic emissions from vegetation are represented in the atmospheric boundary layer through exchanges of fluxes between the land surface (GL3.0) and the atmosphere (GA3.0; Section 2.1.1). The land-surface component of HadGEM3 uses a land surface model called JULES (Joint UK Land Environment Simulator, (Clark et al., 2011)Best et al., 2011; Clark et al., 2011) which models all processes at the land-surface and in the sub-surface soil. The surface of each land point within JULES is subdivided into five types of vegetation: broadleaf, trees, needleleaf trees, temperate C3 grass, tropical C4 grass and shrubs and four non-vegetated surface types: urban areas, inland water, bare soil and land ice. Within JULES, emissions of biogenic volatile organic compounds (BVOCs) are calculated interactively using the iBVOC emissions model Pacifico et al. (2011). Isoprene emissions throughout this thesis are calculated interactively using this scheme.

2.1.3 Gas-phase chemistry-scheme (ExtTC) within the UKCA model

The concentrations of gas-phase species in the UK Chemistry and Aerosol model (UKCA, Morgenstern et al., 2009; O'Connor et al., 2014) are determined by various atmospheric and chemical processes which include emissions, transport (Section 2.1.1), chemical production, chemical removal and deposition. The chemical production and loss processes that relate to NO_2 and O_3 are described in Section 1.2.1. The chemistry scheme used for both configurations in Chapter 3 is the UKCA Extended Tropospheric Chemistry (UKCA-ExtTC) scheme (Folberth et al., In prep.) which is an extension to the TropIsop chemistry scheme (O'Connor et al., 2014) and

includes 89 chemical species (Table 2.1). The scheme includes 198 reactions with 45 photolysis reactions and includes odd oxygen (O_x), odd nitrogen (NO_y), odd hydrogen (HO_x, $OH+HO_2$), and carbon monoxide (CO). It also includes a number of hydrocarbons such as methane (CH_4), ethane (C_2H_6), propane (C_3H_8) and isoprene (C_5H_8). The UKCA-ExtTC scheme also considers the degradation pathways of C2 and C3 alkenes, C4+ alkanes, terpenes, and aromatic compounds (e.g. benzene). Hydrogen (H_2), CO_2, oxygen (O_2), and nitrogen (N_2) have fixed global concentrations. Photolysis rates are prescribed for the global and regional configurations in Chapter 3 using the (offline) 2-D photolysis scheme (O'Connor et al., 2014). The anthropogenic and biomass burning emissions used in Chapter 3 are described in Section 3.2.1. The wet deposition scheme in UKCA for gas-phase species is parameterized following a scheme originally developed by (Walton et al, 1988). Dry deposition of gaseous species is based on Wesely (1989).

2.1.4 Aerosol-phase scheme within GA3.0 - CLASSIC

The HadGEM3 mass-based aerosol scheme is called CLASSIC and includes a numerical representation of up to eight tropospheric aerosol species: ammonium sulphate and ammonium nitrate aerosols, mineral dust, sea salt, fossil fuel black carbon (FFBC or soot), fossil fuel organic carbon (FFOC), biomass burning aerosols and secondary organic aerosol (SOA) which are illustrated in Fig. 2.3 and described in further detail below. Each species within CLASSIC is associated with a dedicated aerosol scheme, however some aspects are shared. Emissions or chemical production of species which are calculated interactively include: mineral dust (Bellouin et al., 2007; Woodward, 2001), sea salt (Jones et al., 2001), and nitrate aerosols (Bellouin et al., 2011). Emissions for the other species are prescribed. Transported species undergo boundary layer and convective mixing and are removed by dry and wet deposition (Section 1.2.2) and representation of these

processes defers for different species (e.g. wet deposition of FFBC follows Roberts and Jones (2004)).

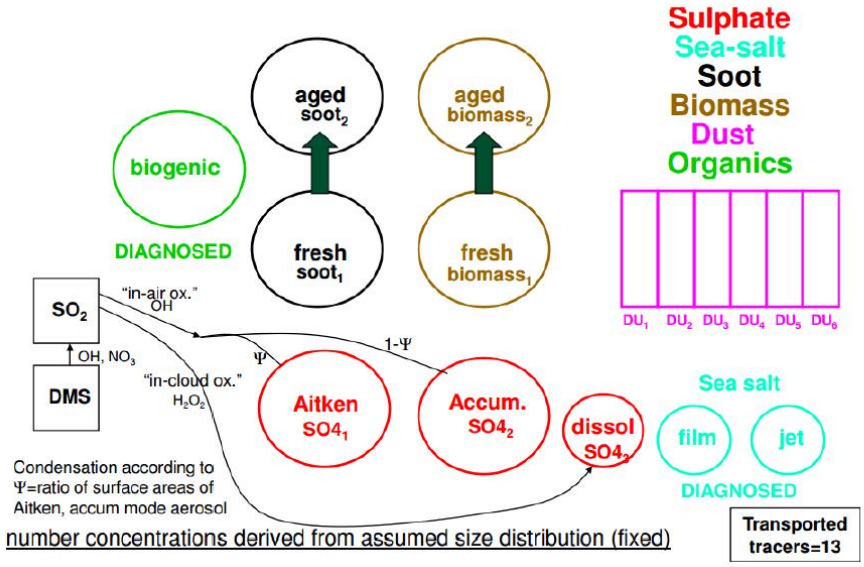

Figure 2.3: A simplified schematic showing tropospheric species included in the CLASSIC aerosol scheme (adapted from (Mann and Carslaw, 2011)

In CLASSIC each aerosol species is generally divided into two modes but for soluble species (e.g. sulphate), another tracer is used to represent the aerosol mass incorporated into cloud water. The two modes are characterized by different size classes: aitken and accumulation mode (Section 1.2.2). For the case of soot and biomass burning aerosol, these two modes are defined as fresh or aged aerosol (Fig. 2.3). Biomass burning includes the sum of biomass burning black carbon and biomass burning organic carbon, which differs from most existing aerosol schemes as they generally simulate both these components independently.

Sea-salt, mineral dust and biogenic aerosol are three species which are treated somewhat differently from the other aerosol species in CLASSIC. Sea-salt aerosols are parameterized as a function of near- surface wind speed over the ocean. However, sea salt is only emitted but not transported in the model version used for this thesis. SOA concentrations are prescribed. Mineral dust is modelled across six size bins (covering radii from 0.0316 μm to 3.16 μm) to incorporate the vast range of size classes of this species (Johnson et al., 2010; Pringle and Mann, 2011; Woodward, 2001) and is transported and deposited through gravitational settling, turbulent mixing and below-cloud scavenging. Ammonium sulphate forms part of the interactive sulphur cycle of HadGEM3 (Jones et al., 2001; Roberts and Jones, 2004) which is not included in the ExtTC (Section 2.1.3) but is included in CLASSIC.

The model has two-way coupling of oxidants between the aerosol and gas phase chemistry schemes such that emissions for SO_2 and DMS are oxidised into the sulphate aerosol (Section 1.2.2.1) by oxidants whose concentrations are calculated using the ExtTC chemistry scheme (Section 2.1.3). The depleted oxidant concentrations are then passed back to the ExtTC scheme to ensure consistency. In the presence of ammonia (NH_3), ammonium sulphate $(NH_4)_2SO_4$ is produced on reaction with sulphuric acid (H_2SO_4) (R.16). Ammonium nitrate is formed through the equilibrium reaction between nitric acid (HNO_3) (formed in reaction R1.11 by reaction with OH; section 1.2.1.2) and NH_3 to form ammonium nitrate (NH_4NO_3) (R1.15). This reaction is highly dependent on the relative humidity and temperature (Bellouin et al., 2011).

Thus nitric acid competes with sulphuric acid for available NH_3 however sulphuric acid is favoured due to its low vapour pressure (Section 1.2.2.1) (Bellouin et al., 2011).

2.2 The UK air quality Model (AQUM)

The UK air quality model - AQUM (Air Quality in the Unified Model) is also based on the MetUM and is used in Chapter 4 and Chapter 5 of this thesis with individual model components linked in a similar way to HadGEM3-UKCA (Fig. 2.1). The development of AQUM builds on the work of the United Kingdom Chemistry and Aerosol (UKCA) project (Morgenstern et al., 2009; O'Connor et al., 2014; Section 2.1.4). A full description of the model can be found in Savage et al. (2013) but is described briefly below. In the next sections the atmospheric component of AQUM is first presented (Section 2.2.1) followed by a description of the gas and aerosol–phase chemistry schemes used in AQUM (Sections 2.2.2 and 2.2.3). A brief description of the LBCs used is given in Section 2.2.4 followed by a brief explanation of the Statistical Post Processing technique (SPPO) used to bias correct AQUM air pollutant concentrations. The emissions used in Chapters 4 and 5 together with the model set-up are described in the respective chapters.

2.2.1 Atmospheric component of AQUM

AQUM has a model horizontal resolution of 0.11° × 0.11° (~ 12 km) covering most of Western Europe (Fig. 2.2) and with a native grid on a rotated-pole coordinate system with the North Pole at latitude 37.5° and longitude at 177.5°. The model vertical resolution has 38 vertical levels reaching 39 km (Table 2.1). Boundary layer mixing within AQUM is parameterized following Lock et al. (2000). Convection is represented with a mass flux scheme and includes downdraughts and momentum transport (Gregory and Rowntree, 1990). Large-scale transport of tracers use the MetUM dynamical core (Davies et al., 2005) with advection of tracers following Priestley (1993). Microphysics from Wilson and Ballard (1999) is employed and

includes ice and snow, rain and graupel. The land surface scheme follows Essery *et al.* (2003). This configuration is used in Chapter 4 and 5.

2.2.2 Gas-phase chemistry in AQUM

The AQUM gas phase chemistry builds on the UKCA tropospheric chemistry scheme (O'Connor et al., 2014) with the inclusion of a new chemistry scheme called the Regional Air Quality (RAQ) scheme. The RAQ scheme includes 58 chemical species, 116 gas phase reactions and 23 photolysis reactions. The on-line photolysis scheme Fast-JX (Neu et al., 2007) is used for AQUM which differs from that used in the global and regional configurations described in Section 2.1.3. The sensitivity of surface O_3 to the choice of photolysis scheme was assessed in previous studies (Neal et al., 2017; O'Connor et al., 2014; Telford et al., 2013).

The RAQ scheme includes the oxidation of both C2-C3 alkenes (e.g. ethane and propene), isoprene and aromatic compounds such as toluene and o-xylene, as well as the formation of organic nitrate. It is adapted from Collins *et al.* (1997) with additional reactions described in Collins *et al.* (1999). Similar to the ExtTC chemistry scheme (section 2.1.3), sulphur chemistry is not included in the RAQ scheme however it is included in the aerosol scheme described in the next section (Section 2.2.3). Removal by wet and dry deposition is considered for 19 and 16 species respectively and is based on Savage et al. (2013).

2.2.3 Aerosols in AQUM - CLASSIC

The aerosol scheme used by AQUM is the same aerosol scheme to that used in the global and regional model configurations described in section 2.1.4 – CLASSIC

containing eight tropospheric aerosol types (Bellouin et al., 2011) with two-way coupling of oxidants between the aerosol and gas phase chemistry schemes (Section 2.1.4).

2.2.4 Lateral boundary conditions

Lateral boundary conditions (LBCs) in AQUM provide a combination of chemistry and aerosol data from GEMS (Global and regional Earth-system Monitoring using Satellite and in-situ data; between 01-05-2006 and 01-01-2008) or MACC (Monitoring Atmospheric Composition and Climate; between 26-12-2005 and 01-05-2006) reanalyses (Flemming et al., 2009). These reanalysis data from GEMS and MACC are used to provide boundary conditions for the composition fields. AQUM initialisation and LBCs for meteorology are from the global MetUM weather forecast fields at a horizontal resolution of ~17 km (Table 2.1).

2.2.5 The Statistical Post Processing Technique (SPPO)

Neal et al. (2014) have developed a bias correction technique, whereby simulated concentrations are related to measurements, referred to as the Statistical Post-Processing for Observations (SPPO, Neal et al., 2014). For bias correction at individual sites the difference between simulated and measured concentrations at AURN (Automatic Urban and Rural Network) sites in the UK (Section 2.3) is calculated, applying a correction technique to smooth out any extreme values. This difference is termed the median residual (equation 2.1).

$$r_{i,t} = 0.5\left(o_{i,t} - m_{i,t}\right) + 0.5\left(median_{j\in S}[o_{j,t} - m_{j,t}]\right) \qquad (2.1)$$

Where $o_{i,t}$ and $m_{i,t}$ are the observed and modelled concentrations at site i and time t. The second term of equation 2.1 includes the median of the difference between observation and modelled concentrations at all sites of the same classification -remote, rural suburban and urban background site types are used. Observational data within the AURN network are only available for a limited number of sites therefore only residuals at these stations can be calculated. Hence, for bias correction across the whole AQUM grid (Fig 2.2), spatial interpolation is performed across the model grid using the Ordinary Kriging technique. The bias corrected pollutant concentrations are then calculated by adding the residual to the raw model field. Further details on the SPPO methodology can be found in Neal et al. (2014). The SPPO technique is applied to the pollutant concentrations quoted in the health section of Chapter 4 (Section 4.5).

2.3 Measurements used for model evaluation

In Chapters 3 and 4 simulated air pollutant concentrations and meteorological fields are compared to observations for model evaluation. The observations used in each of these chapters are described below.

In Chapter 3, modelled seasonal mean O_3 and $PM_{2.5}$ concentrations for 2007 are evaluated using measurement data from the European Monitoring Evaluation Programme (EMEP) network (ebas.nilu.no; last accessed 6th September 2018). All EMEP stations are classified based on a specific distance away from emission sources so as to be representative of larger areas. For example the minimum distance from large pollution sources such as towns and power plant is ~ 50 km (Tørseth et al., 2012; EMEP/CCC, 2001). A sub-set of the available EMEP O_3 measurement sites is chosen with an altitude less than or equal to 200 m above sea level to focus on near-surface comparisons between measurements and simulated

O_3 concentrations (52 sites – Fig. 2.4). As there are fewer measurements of $PM_{2.5}$ for 2007, all available EMEP measurement sites are used for $PM_{2.5}$ evaluation (25 sites – Fig. 2.4).

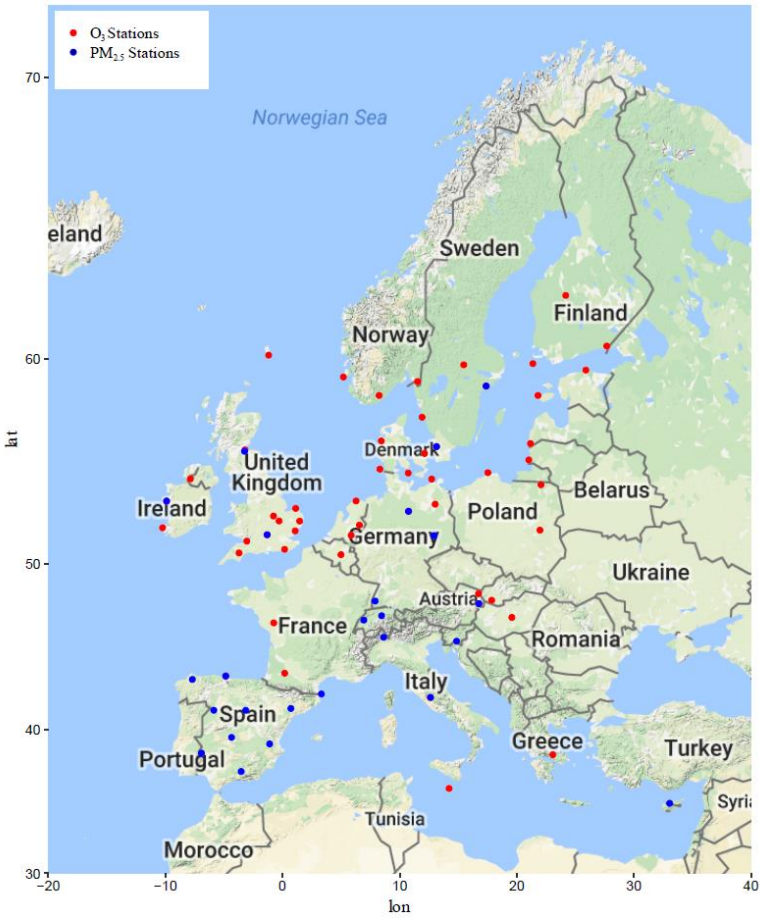

Figure 2.4: EMEP measurement stations with altitude less than or equal to 200 m, used for seasonal mean surface O_3 comparison to modelled concentrations (52 sites – red) and EMEP measurement stations used for seasonal mean $PM_{2.5}$ comparison to modelled concentrations (25 sites - blue)

In Chapter 4, modelled MDA8 O_3 and daily mean $PM_{2.5}$ concentrations for 2006 in the UK are evaluated against measurements from the Automatic Urban and Rural Network (AURN) (https://uk-air.defra.gov.uk/data/data_selector last accessed 6th September 2018). Measurements for $PM_{2.5}$ concentrations for this period are only

available at three sites: London Bloomsbury (urban background), Rochester Stoke (south east UK, rural background) and Harwell (south east UK, rural background). For meteorological fields, wind measurements for 2006 were only recorded at Rochester Stoke, therefore this site is used to show temporal variability in modelled and observed pollutant concentrations and meteorological variables in Sections 4.3 and 4.4.1. Surface temperatures are not recorded for any of the three AURN sites, therefore observed temperatures at the three closest sites to these air pollution measurement sites from the Met Office Integrated Data Archive System (MIDAS) network (MetOffice, 2012) are used (located at St James Park, London, East Malling and Upper Lambourn). Site locations from the AURN and MIDAS networks are illustrated in Fig. 4.3 and Fig. 4.5, respectively.

2.4 Health impact assessments

The method for calculating the health impact assessments associated with exposure to air pollutants for Chapters 3, 4 and 5 is similar in terms of the health metrics calculated but with variations depending on, for example, the temporal scale (i.e. long-term vs. short-term exposure), spatial scale (i.e. at the European country or UK regional level) and concentration-response functions (CRFs) used. The individual health impact assessment details used for Chapter 3, 4 and 5 are shown in Table 1.2 and are described below (Sections 2.4.1 – 2.4.3). Finally, in Section 2.4.4, the method for estimating the 95% confidence interval of differences in the Attributable Fraction (AF) of mortality is presented.

2.4.1 Health impacts associated with long-term exposure to O_3 and $PM_{2.5}$ (Chapter 3)

In Chapter 3, the attributable fraction (AF) of respiratory and all-cause (excluding external) mortality associated with long-term exposure to pollutant concentrations of O_3 and $PM_{2.5}$ is estimated following equations 2.2 to 2.4 analogous to Section 1.5.1 (equations 1.2 and 1.3). These calculations are conducted for pollutant concentrations simulated at both the global and the regional model configurations described in Section 2.1.

$$AF_y = \frac{RR_y - 1}{RR_y} \tag{2.2}$$

where

$$RR_y = \exp(CRF \times x_y) \tag{2.3}$$

and

$$x_y = \frac{\sum_{j \in y} (x_j \times p_j)}{\sum_{j \in y} p_j} \tag{2.4}$$

In equation 2.2, AF_y is the attributable fraction of the baseline mortality associated with long-term exposure to air pollutant concentrations, calculated at the European country level, y. The method for conducting the health impact assessment in Chapter 3 is the same as that used by other studies described in Section 1.5.1 but conducted at the European country level instead of for example the grid cell level (Anenberg et al., 2009). In equations 2.2 and 2.3, RR_y is the relative risk of mortality associated with long-term exposure to warm season (O_3) or annual mean ($PM_{2.5}$) air

pollutant levels for each country. In equation 2.3, *CRF* is the concentration-response function (termed β in equation 1.3; section 1.5.1) and x_y is the population-weighted pollutant concentration also at the country level, y. The effect of a threshold for O_3 is included in equation 2.4 (described below).

The CRF (equation 2.3) varies depending on the air pollutant and the temporal scale at which the health impact assessment is being conducted (Section 1.4.3 and Table 1.2). In Chapter 3 the CRF used for long-term exposure to O_3 is based on recommendations by the HRAPIE (Health Risks of Air Pollution in Europe) project (WHO, 2013; Section 1.4.4). The value recommended by HRAPIE for the CRF (Equation 2.3) for the effects of long-term O_3 exposure on respiratory mortality is 1.014 (95% Confidence Interval (CI) = 1.005, 1.024) per 10 μg m^{-3} increase in daily maximum 8-hour running mean (MDA8) O_3 during the warm season (April-September in the northern hemisphere) with a threshold of 70 μg m^{-3} (Table 1.2). In Chapter 3, the AF of respiratory mortality associated with long-term exposure to O_3 is also estimated based on annual mean O_3 concentrations and CRFs from Turner et al. (2015) of 1.06 (95% CI = 1.04, 1.08) per 10 μg m^{-3} increase in MDA8 O_3 and a threshold of 53.4 μg m^{-3} (The CRF from Turner et al. (2015) is also used in Chapter 5; Section 2.4.3).

For estimating the AF of all-cause (excluding external) mortality associated with long-term exposure to $PM_{2.5}$ (in Chapter 3), HRAPIE (WHO 2013) recommends a CRF of 1.062 (95% CI = 1.040, 1.083) per 10 μg m^{-3} increase in annual average concentrations (with no threshold; Section 1.4.4; Table 1.2). As the CRFs used for O_3 and $PM_{2.5}$ are from the American Cancer Society (ACS) cohort (section 1.4.4), the estimates in Chapter 3 exclude people younger than 30 years.

The population-weighted pollutant concentrations, x_y for Chapters 3 are calculated by first counting the total residential gridded population data for people aged 30 years and over (p, at a resolution of 5 km (GWPv3-Gridded Population of

the World version 3), obtained from the Socioeconomic Data and Applications Centre (SEDAC) (sedac.ciesin.columbia.edu, last accessed 6th September 2018) within each global or regional model grid cell, j (equation 2.4). This population total (p_j) is then multiplied by the pollutant concentration within each grid cell x_j, summed over every grid cell within the country, y, and divided by the total population of the country. For O_3, a threshold of 70 μg m^{-3} is subtracted from the simulated O_3 concentration in each grid cell, j, before multiplication by the population of that grid cell (any negative concentrations are set to zero). When using the CRF from Turner et al. (2015) a threshold of 53.4 μg m^{-3} is subtracted instead.

As the focus of Chapter 3 is the effects of changing resolution on pollutant concentrations, the estimated attributable mortality associated with each pollutant is not estimated (as done in chapters 4 and 5). This is because mortality estimates also depend on the underlying baseline mortality (equation 1.1; Section 1.5.1) which vary for each country in Europe and thus may mask any signal related to the influence of model resolution on pollutant concentrations and corresponding health impacts. In this way, the effect of model resolution on health impacts can be isolated in Chapter 3.

2.4.2 Health impacts associated with short-term exposure to O_3 and $PM_{2.5}$ (Chapter 4)

In chapter 4, mortality burden and the AF of mortality associated with short-term exposure to O_3 and $PM_{2.5}$ are estimated (Section 1.4.4) using pollutant concentrations simulated by the AQUM model described in Section 2.2. The method used is similar to that used to estimate long-term health impacts (Section 2.4.1) with the main difference being the CRF used (Table 1.2) and that the calculation for

short-term health impacts is conducted daily while long-term health impacts are typically calculated seasonally or annually (Section 2.4.1).

The mortality burdens during two five-day air pollution episodes are estimated in Chapter 4. The estimated health burdens attributable to short-term exposure to MDA8 O_3 and daily mean $PM_{2.5}$ in Chapter 4 are calculated following equation 2.5 for each of the nine Government Office Regions (GORs) in England, Scotland and Wales (r) (Fig. 2.5). This is analogous to equation 1.6 (Section 1.5.1):

$$M_r = \sum_{i=1}^{N} BM_{ir} \times AF_{ir} \qquad (2.5)$$

In equation 2.5, M_r is the all-cause (excluding external) mortality associated with short-term exposure to MDA8 O_3 or daily mean $PM_{2.5}$ for each region, r (Fig. 2.5) summed over each day of the air pollution episode, i; N is the total number of days in the air pollution episode, BM_{ir} is the total regional daily (all-cause) mortality (i.e. the total recorded deaths associated with all exposures and causes) and AF_{ir} is the daily attributable fraction associated with short-term exposure to MDA8 O_3 or daily mean $PM_{2.5}$ that is calculated for each region using equation 2.6. In Chapter 4, daily all-cause BM_{ir} for each region was obtained from the Office of the National Statistics for England and Wales (ons.gov.uk, last accessed 6th September 2018) and from the National Records of Scotland (nrscotland.gov.uk).

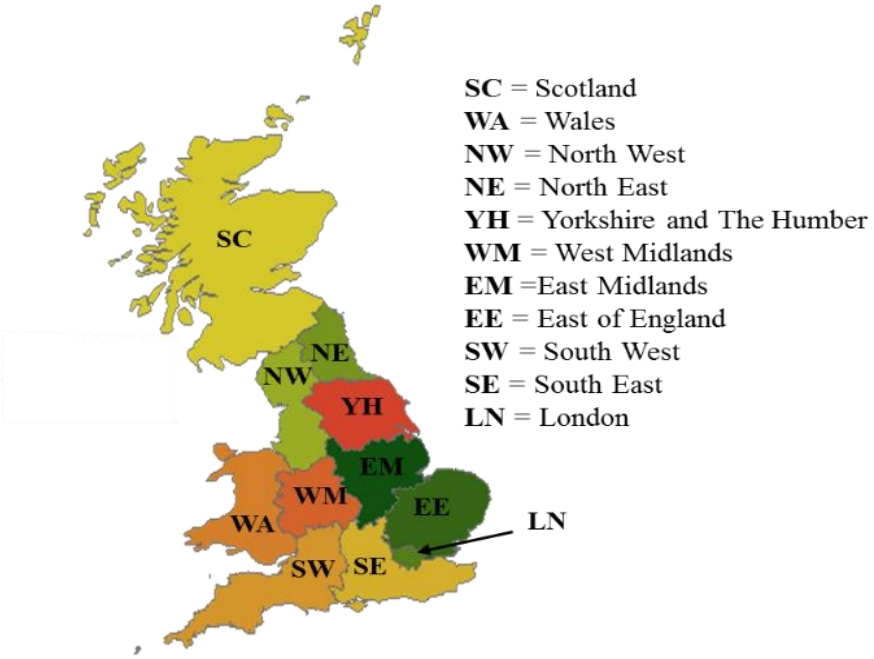

Figure 2.5: Government Office Regions (GOR) for England, Scotland and Wales used in this thesis (Chapter 4 and 5)

The daily (i) AF (AF_{ir}) of mortality is estimated in Chapter 4 following equation 2.6 for each of the nine GORs in England, Scotland and Wales (r) (Fig. 2.5). RR_{ir} in equation 2.7 is the relative risk calculated following equation 1.7 (Section1.5.1), which is analogous to equation 2.3 but calculated per day (i) and for each region (r). In equations 2.7 and 2.8, x_{ir} is the population-weighted pollutant concentration for each region r and each day of the episode i.

$$AF_{ir} = \frac{RR_{ir}-1}{RR_{ir}} \quad (2.6)$$

Where

$$RR_{ir} = \exp(CRF \times x_{ir}) \quad (2.7)$$

and

$$x_{ir} = \frac{\sum_{j \in r} (x_{ij} \times p_{ij})}{\sum_{j \in r} p_j} \quad (2.8)$$

The CRFs used in Chapter 4 for short-term exposure to MDA8 O_3 and daily mean $PM_{2.5}$ are taken from COMEAP (2015) and from a meta-analysis of time series epidemiological studies (Atkinson et al., 2014), respectively (Section 1.4.4, Table 1.2). For health impacts associated with short-term exposure to O_3, a CRF of 1.0034 (95% CI: 1.0012, 1.0056) per 10 μg m^{-3} increase in MDA8 O_3 is used, and for health impacts associated with short-term exposure to $PM_{2.5}$, a CRF of 1.0104 (95% CI: 1.0052, 1.0156) per 10 μg m^{-3} increase in 24-hr mean $PM_{2.5}$ is applied (Table 1.2). Evidence for a threshold below which no adverse effects from short-term exposure to O_3 and $PM_{2.5}$ is limited, therefore the full range of pollutant exposure is used to calculate the health burdens which applies for all ages (COMEAP, 1998, 2015b; Table 1.2).

2.4.3 Health impacts associated with long-term exposure to O_3, NO_2 and $PM_{2.5}$ (Chapter 5)

In Chapter 5, the mortality burdens associated with long-term exposure to annual mean concentrations of MDA8 O_3, NO_2 and $PM_{2.5}$ are estimated for each of the nine GORs in England, Scotland and Wales (r) and for both present-day and future using a similar equation to that used in Chapter 4 (equation 2.5) given by equation 2.9.

$$M_r = BM_r \times AF_r \quad (2.9)$$

Where BM_r is the annual regional baseline respiratory or all-cause mortality data and AF_r is the annual regional AF of respiratory or all-cause mortality depending on the pollutant. Equation 2.9 is also analogous to equation 1.1 (Section 1.5.1) with BM_r (equation 2.9) representing the product of the baseline mortality rate y_0 and the size of the exposed population Pop in equation 1.1.

Baseline mortality data is obtained from the Office of the National Statistics for England and Wales (ons.gov.uk, last accessed 6th September 2018) and from the National Records of Scotland (nrscotland.gov.uk, last accessed 6th September 2018) of which only ages above 30 years were considered. Baseline mortality data is kept at present day levels for both present day and future mortality estimates. To quantify differences in health burdens between the present-day and future, the present-day mortality burden is subtracted from the future mortality burden (ie $M_{r\,Future} - M_{r\,PD}$).

The AF of respiratory (O_3) and all-cause (excluding external) (NO_2 and $PM_{2.5}$) mortality associated with long-term exposure to O_3, NO_2 and $PM_{2.5}$ is estimated for both present-day and future using simulated pollutant concentrations from AQUM (Section 2.2). The method is identical to that described in Section 2.4.1 however health estimates are conducted for each of the nine GORs in England, Scotland and Wales (r) instead of the European country level as given by equations 2.10 to 2.12.

$$AF_r = \frac{RR_r - 1}{RR_r} \tag{2.10}$$

where

$$RR_r = \exp(CRF \times x_r) \tag{2.11}$$

and

$$x_r = \frac{\sum_{j \in r} (x_j \times p_j)}{\sum_{j \in r} p_j} \tag{2.12}$$

The CRF used in equation 2.11 for the effects of long-term O_3 exposure on respiratory mortality is taken from Turner et al. (2015) and is 1.06 (95% Confidence Interval (CI) = 1.04,1.08) per 10 μg m^{-3} increase in annual mean MDA8 O_3 concentrations with a threshold of 53.4 μg m^{-3} (Table 1.2, Section 1.4.4). A different CRF is used for O_3 health effects in Chapter 5 compared to the main analysis in Chapter 3 (and in turn a different pollutant averaging period is used) as mortality data, required to estimate the mortality burden (i.e. equation 2.9), stratified by age and region was only available annually and not by month or season.

The health impacts associated with long-term NO_2 exposure for all-cause (excluding external) mortality, are estimated using the CRF (equation 2.11) suggested by COMEAP (2015) of 1.025 (95% CI = 1.01,1.04) per 10 μg m^{-3} increase in annual mean NO_2 concentrations (with no threshold) (Table 1.2, Section 1.4.4). NO_2 health impacts relating to long-term exposure are not estimated in Chapter 3 due to the relatively coarse model horizontal resolutions (global and regional) used.

The AF of all-cause (excluding external) mortality associated with long-term exposure to $PM_{2.5}$ is estimated using, the same CRF as that used in Chapter 3 (1.062 (95% CI = 1.040,1.083)) per 10 μg m^{-3} increase in annual average concentrations with no threshold) (Section 1.4.4 Table 1.2). The population data used in Chapter 5 for both present day and future estimates in equation 2.12 is also consistent to that used in Chapters 3 and 4. Therefore the changing age structure of the population is not taken into account.

The sensitivity of future health burdens to future population growth projections is also estimated in Chapter 5. This is explained in detail in Chapter 5 (Section 5.2.5).

2.4.4 95% confidence intervals representing uncertainties associated only with the CRF

The 95% confidence intervals (CI) for the estimated AF of mortality associated with pollutant exposure are estimated by repeating the calculation for the AF of mortality (e.g. equation 2.2) using the low and high limit of the 95% CI of the respective CRF (Table 1.2). The equations provided in this section were obtained from Adam Butler (personal communication) of the biomathematics and Statistics Scotland and based on von Storch and Zwiers (1999)

For each of the CRFs used in this thesis, only the 95% CI are quoted in epidemiological studies with no information on the standard error. The latter is required to approximately calculate the 95% CI of the difference in AF of mortality between for example the global and regional estimates (Chapter 3) or between the present-day and future estimated (Chapter 5). The 95% CI of the differences in AF of mortality are therefore estimated by first deriving the standard error for each of the two groups (SE_g; g = group) being compared (e.g. global and regional AF estimates) with the assumption that the means are normally distributed following equation 2.13:

$$SE_g = \frac{(width\ of\ 95\%\ CI)}{3.92} \tag{2.13}$$

The standard error of the differences (SE_d) is then estimated following equation 2.14; with ${SE_1}^2$ and ${SE_2}^2$ representing the standard errors of the two groups being compared each calculated following equation (2.13).

$$SE_d = \sqrt{{SE_1}^2 + {SE_2}^2} \tag{2.14}$$

Equation 2.9 follows from the additivity of variances and relies on the assumption that the means of the two groups are independent. The 95% CI of the differences ($95\%\ CI_d$) is then calculated by first multiplying the SE_d by 1.96 (again under the

assumption that the mean of each group has a normal distribution). This value is then subtracted and added to the mean difference between the two groups (i.e. the mean difference between for example global and regional AF estimates) to get the low and high limits of the 95% CI, respectively following equation 2.15.

$$95\%\ CI_d = (Mean\ diff. - 1.96 * SE_d\ ,\ Mean\ diff. + 1.96 * SE_d\ ) \quad (2.15)$$

In the following chapters, the results associated with the three research aims of this thesis (Section 1.9) are presented.

Chapter 3 The influence of model spatial resolution on simulated ozone and fine particulate matter: implications for health impact assessments

This chapter has been published in the open-access journal Atmospheric Chemistry and Physics (ACP), in collaboration with: Prof Ruth M. Doherty, Dr Clare Heaviside, Dr Sotiris Vardoulakis, Dr Helen Macintyre and Dr Fiona M. O'Connor. This paper is available online from the ACP website (https://www.atmos-chem-phys.net/18/5765/2018/). I set up and conducted all model simulations, did the analysis and wrote the initial draft. My supervisors and other co-authors provided feedback before the manuscript was submitted for publication. The reviewers made further suggestions for improvement which are now included in this chapter. Relevant methods text has been moved to Chapter 2.

Fenech, S., Doherty, R. M., Heaviside, C., Vardoulakis, S., Macintyre, H. L., and O'Connor, F. M.: The influence of model spatial resolution on simulated ozone and fine particulate matter for Europe: implications for health impact assessments, Atmos. Chem. Phys., 18, 5765-5784, https://doi.org/10.5194/acp-18-5765-2018, 2018.

3.1 Introduction

A substantial number of epidemiological studies have derived risk estimates for mortality associated with long-term exposure to ambient fine particulate matter with aerodynamic diameter less than 2.5 µm ($PM_{2.5}$) (Krewski et al., 2009;Brook et al., 2010; WHO, 2013) and also recently, to a lesser extent, for long-term exposure to ozone (O_3) (Jerrett et al., 2009; Forouzanfar et al., 2016; Turner et al., 2016)(see Section 1.1). Differences in risk estimates produced from different epidemiological studies can be due to differences in methodologies, air pollution and health data used including the size and spatial extent of cohort populations. For O_3, these long-term risk estimates are derived from North American studies (Section 1.4.4). In this region O_3 data is typically monitored only during the O_3 season (April-September), hence these derived O_3-risk estimates apply only to the ozone occurring in the warm season part of the year (Section 1.4.4).

Air pollutant exposure estimated from concentrations measured at fixed monitoring stations, is often used to estimate health impacts at the cohort-scale (Section 1.5.1). However, quantifying the adverse health effects of air pollution at the continental-scale requires atmospheric models (with resolutions ranging from ~250 to 50 km) to simulate pollutant spatio-temporal distributions across these scales (e.g. West et al. 2009; Anenberg et al. 2010; Fang et al. 2013; Silva et al. 2013; Lelieveld et al. 2015, Malley et al., 2017) (see Section 1.5.1). Amongst a number of factors, simulated air pollutant concentrations may vary depending on the three-dimensional chemistry model used, its set-up and the model resolution (e.g. Markakis et al. 2015; Schaap et al. 2015; Yu et al. 2016; Neal et al. 2017). Although the same model processes are represented at different model resolutions, simulated pollutant concentrations can vary due to differences in (i) the resolution of emissions, which may have a nonlinear effect on the chemical formation of pollutants, and (ii) the resolution of the driving meteorology (Valari and Menut

2008; Tie et al. 2010; Arunachalam et al. 2011; Colette et al. 2013; Markakis et al. 2015; Schaap et al. 2015).

The impact of model horizontal resolution on simulated O_3 concentrations has been primarily linked to less dilution of emissions when using a finer resolution (Valari and Menut 2008; Tie et al. 2010; Colette et al. 2013; Stock et al. 2014; Schaap et al. 2015) (see Section 1.3 and 1.6). Investigating the impact of increasing model horizontal resolution from 48 km to 6 km on O_3 concentrations in Paris, Valari and Menut (2008) found modelled surface O_3 to be more sensitive to the resolution of input emissions than to meteorology. A number of other studies note the sensitivity of simulated O_3 to simulated nitrogen oxide (NO_x) concentrations that determine the extent of titration of O_3 by nitrogen monoxide (NO) (Stock et al., 2014; Markakis et al., 2015; Schaap et al., 2015) (Section 1.2.1.2). Furthermore, Stock et al. (2014) found the impact of spatial resolution (150km vs. 40km) on simulated O_3 concentrations to vary with season across Europe. In winter, higher NO_x concentrations produced more pronounced titration effects on O_3 at 40 km resolution with a mean bias error (MBE) of 3.2%, leading to lower O_3 concentrations than at 150 km resolution (MBE = 14.4%). In summer, although similar results were found for O_3 concentrations simulated at the coarse (MBE = 29.7%) and fine resolution (MBE = 32.8%) simulated boundary layer height was suggested to be largely responsible for the spatial differences in O_3 concentrations at the two resolutions.

$PM_{2.5}$ concentrations have also been found to be sensitive to the model horizontal resolution (Arunachalam et al. 2011; Punger and West 2013; Markakis et al. 2015; Neal et al. 2017) (Section 1.6). In the US., Punger and West (2013) found population-weighted annual mean $PM_{2.5}$ concentrations to be 6% higher at 36 km compared to 12 km, but 27% lower when simulated at 408 km compared to 12 km. However in this study, statistical averaging was used to estimate pollutant concentrations at the coarsest resolutions, and therefore differences in emissions

and meteorology and their atmospheric processing between the resolutions were not included. In contrast, Li et al. (2015) found annual mean $PM_{2.5}$ concentrations simulated at a resolution of ~ 2.5° in the US to be similar to $PM_{2.5}$ concentrations simulated at a resolution of ~ 0.5° suggesting that the horizontal scales being compared and the methodology for comparison are important. However maximum $PM_{2.5}$ concentrations which occur in highly populated regions were found to be 21% lower at the coarse resolution (Li et al., 2015).

As outlined above, a number of studies have analysed the effect of model resolution on O_3 and $PM_{2.5}$ concentrations but few have looked at the sensitivity of the associated health impacts to model resolution (Punger and West 2013; Thompson et al. 2014; Li et al. 2015; Kushta et al. 2018) (Section 1.6). Punger and West (2013) found mortality associated with long-term exposure to O_3 in the US to be 12% higher at a 36 km resolution compared to the mortality estimate at 12 km, as a result of higher O_3 simulated at the coarser-scale. Thompson et al. (2014) also found that especially in urban areas, the human health impacts associated with differences in O_3 between 2005 and 2014 calculated using a coarse resolution model (36 km) were on average two times greater than those estimated using finer scale resolutions (12 km and 4 km). In addition, Thompson and Selin (2012) found that the estimated avoided O_3-related mortalities between a 2006 base case and a 2018 control policy scenario at a 36 km resolution were higher compared to estimates at the finer resolutions (12 km , 4 km and 2 km) . However, their health estimates at the 36 km resolution fall within the range of values obtained using concentrations simulated at the finer resolutions used.

For $PM_{2.5}$-related health estimates, studies by Punger and West (2013) and Li et al. (2015) (in the US) and Kushta et al. (2018) (in Europe) all suggest that attributable mortality associated with long-term exposure to $PM_{2.5}$ is lower for their coarser resolution simulations (> 100 km) due to lower simulated $PM_{2.5}$ concentrations in densely populated regions compared to the higher resolution

estimates at 12 km and 20 km respectively. However, Thompson et al. (2014) found that using model horizontal resolutions of 36, 12 and 4 km had a negligible effect on changes in $PM_{2.5}$ concentrations and associated health impacts (Section 1.6). This is likely due to the relatively small range of resolutions used by Thompson et al. (2014) compared to these other studies.

The majority of health effect studies relating to the impact of model resolution have been conducted in North America. Hence, similar studies are lacking over Europe. This study is therefore the first to examine the impact of two different model resolutions: a coarse (~ 140 km) and a finer resolution (~ 50 km) on O_3 and $PM_{2.5}$ concentrations, and their subsequent impacts on European-scale human health through long-term exposure to O_3 and $PM_{2.5}$. The sensitivity of health impacts to model resolutions is defined by calculating the attributable fraction (AF) of total mortality which is associated with long-term exposure to O_3 and $PM_{2.5}$ for various European countries, based on simulated concentrations at both resolutions, and expressed as a percentage.

The remainder of this chapter is organised as follows. Section 3.2 describes the modelling framework used for both the coarse and finer simulations and gives an outline of the methods used to calculate the AF of mortality associated with O_3 and $PM_{2.5}$ for various European countries. Section 3.3 presents differences in seasonal mean O_3 and $PM_{2.5}$ concentrations between the two resolutions. In section 3.4, differences in warm season daily maximum 8-hour running mean (MDA8) O_3 concentrations and annual $PM_{2.5}$ concentrations between the two resolutions are first analysed, then differences in country-level population-weighted MDA8 O_3 and annual mean $PM_{2.5}$ concentrations are quantified. Secondly, the country-level AF associated with long-term exposure to MDA8 O_3 and annual mean $PM_{2.5}$ simulated at both resolutions are presented. The conclusions drawn from this chapter are then presented in Section 3.5.

3.2 Methods

3.2.1 Model Description and Experimental Setup

The two chemistry-climate configurations used in this Chapter are based on the Global Atmosphere 3.0 (GA3.0) / Global Land (GL3.0) configuration of the Hadley Centre Global Environmental Model version 3 (HadGEM3, Walters et al., 2011), of the Met Office's Unified Model (MetUM, Brown et al., 2012) (Section 2.1). The global (referred to as coarse in this chapter) configuration has a horizontal resolution of 1.875° × 1.25° (~ 140 km, Walters et al., 2011) while the regional (referred to as finer in this chapter) configuration has a horizontal resolution of 0.44° × 0.44° (~50 km, Moufouma-Okia and Jones, 2014) with a domain covering most of Europe (Chapter 2 Fig. 2.1).

As this chapter focuses on health impacts, the analysis is restricted to European land regions. Gas phase chemistry is simulated within HadGEM3 by a tropospheric configuration of the United Kingdom Chemistry and Aerosol (UKCA) model (Morgenstern et al., 2009; O'Connor et al., 2014). The chemistry scheme used for both configurations is the UKCA Extended Tropospheric Chemistry (UKCA-ExtTC) scheme (Section 2.1.3). The GA3.0/GL3.0 configuration of HadGEM3 (Walters et al., 2011) also includes an interactive aerosol scheme called CLASSIC (Coupled Large-scale Aerosol Simulator for Studies in Climate; Jones et al., 2001;Bellouin et al., 2011) from which $PM_{2.5}$ concentrations are estimated (Section 2.1.4).

The model simulations for both these configurations cover a period of one year and 9 months starting from April 2006, from which the first nine months were discarded as spin-up. The coarse configuration uses monthly mean distributions of

sea surface temperature (SST) and sea ice cover (SIC), derived for the present-day (1995-2005) from transient coupled atmosphere-ocean simulations (Jones et al., 2001) of the HadGEM2-ES model (Collins et al., 2011). Using a simple linear re-gridding algorithm, the SST and SIC climatologies developed for the coarse configuration were downscaled to the finer configuration. The coarse configuration was set to produce lateral boundary conditions (LBCs) at six-hourly intervals which were then used to drive the finer configuration.

A consistent set of baseline emissions have been used for both configurations by using the same source data and then re-gridding to the coarse and finer resolutions of the chemistry-climate model. The surface emissions for chemical species were implemented from emission data at 0.5° by 0.5° resolution developed by Lamarque et al. (2010) for the Fifth Coupled Model Inter-comparison Project (CMIP5) report which include reactive gases and aerosols from anthropogenic and biomass burning sources. Both model configurations are driven by decadal mean present-day emissions from Lamarque et al. (2010), representative of the decade centred on 2000. Biogenic emission of isoprene and monoterpenes are calculated interactively following Pacifico et al. (2011) and the biogenic emissions of methanol and acetone are prescribed, taken from Guenther et al. (1995). A full description of both configurations can be found in Section 2.1.

The two configurations are consistent in terms of driving meteorology and emissions as discussed above, however a change in model resolution also requires changes to model's dynamical time-step (from 20 min; coarse resolution to 12 min; finer resolution) as well as some of the parameters in the model parametrisations schemes that are resolution dependent. In this chapter it is assumed any such differences to be a model resolution effect. To compare pollutant concentrations simulated at the two resolutions, the coarse model results were re-gridded to the finer resolution via bi-linear interpolation and differences between the two configurations were then calculated at each grid box. For consistency, all figures,

tables and values shown in the following sections show differences calculated as coarse minus finer results. All pollutant concentrations used in this Chapter have been extracted at the lowest model level with a mid-point at 20 m. While this level is considered representative of surface or ground-level concentrations, local orographically driven flows or sharp gradients in mixing depths cannot be represented at this vertical resolution (Fiore et al. 2009).

3.2.2 Measurement data

Modelled seasonal mean O_3 and $PM_{2.5}$ concentrations for 2007 are evaluated using measurement data from the European Monitoring Evaluation Programme (EMEP) network (ebas.nilu.no) (Section 2.3). A total of 52 sites from the EMEP network are chosen for comparison between measurements and simulated O_3 concentrations while all 25 available sites are used for $PM_{2.5}$ evaluation (Fig. 2.4). To perform an observation-model comparison, simulated pollutant concentrations are extracted at measurement site locations using bi-linear interpolation.

3.2.3 Health calculations

Annual total mortality estimates associated with long-term exposure to O_3 and $PM_{2.5}$ are frequently calculated by estimating the country-level Attributable Fraction (AF) of mortality, based on concentration-response relationships associated with each pollutant, and then multiplying the AF by the baseline mortality rate (Section 1.5.1). Since the focus of this chapter is the effects of changing resolution on pollutant concentration, absolute values and differences in the AF between the two resolutions are estimated, rather than the estimated mortality associated with each

pollutant, as the latter also depends on underlying baseline mortality rates. In this way the effect of model resolution on health impacts can be isolated. Note that differences in AF will be the same as the differences in mortality between the two resolutions (expressed as a percentage of total mortality), if calculated as described in this section.

For each model resolution, simulated air pollutant concentrations are used to calculate the country-average AF of respiratory or all-cause mortality associated with long-term exposure to O_3 and $PM_{2.5}$, respectively. Specifically, the country-average AF is derived from the country-averaged population-weighted pollutant concentration ($x_{country}$) and CRF (equation 2.2 to 2.4 with y at the country level; Section 2.4.1)

The CRF used to estimate the AF of respiratory mortality associated with long-term exposure to O_3 is that of 1.014 (95% Confidence Interval (CI) = 1.005, 1.024) per 10 μg m^{-3} increase in daily maximum 8-hr running mean (MDA8) O_3 during the warm season (April-September) with a threshold of 70 μg m^{-3} (Table 2.1 and Section 2.4.1) For estimating the health impact of long-term exposure to $PM_{2.5}$ on all-cause (excluding external) mortality, a CRF of 1.062 (95% CI = 1.040, 1.083) per 10 μg m^{-3} increase in annual average concentrations (with no threshold) is used (Table 2.1 and Section 2.4.1). As the CRF values used for O_3 and $PM_{2.5}$ are from the ACS cohort (Section 1.4.4), the estimates in this study exclude people younger than 30 years.

3.3 The impact of model resolution on pollutant concentrations

3.3.1 The impact of model resolution on seasonal mean O_3: comparison with observations

Modelled and observed means and, standard deviations (SD), normalised mean bias (NMB) and percentage differences between the two resolutions for all four seasons at the 52 EMEP site locations (Fig. 2.4) are shown in Table 3.1. Similarly modelled means, SD and percentage differences between the two resolutions are also shown for all model cells within the European domain (discussed in Section 3.3.2). Compared to measurements, mean values simulated by the chemistry-climate model across the 52 station locations are lower in winter (DJF) and higher in summer (JJA) and autumn (SON) with NMB values up to -19%, 27% and 19%, respectively. In spring (MAM), simulated mean O_3 concentrations at the finer resolution are closest to observations (NMB = ~ -4 %), whilst in all other three seasons the simulated values at the coarse resolution are in closer agreement with observations (NMB = ~ -8%, ~24% and ~ 5%, respectively). For all seasons, the SD of seasonal mean O_3 concentrations, simulated at the two resolutions are more similar to each other than to observations. However, the SD across all 52 sites, simulated at the coarse resolution is higher than that simulated at the finer resolution.

Table 3.1: Statistical results comparing seasonal mean O_3 concentrations simulated at the global and finer resolutions to observations from 52 stations within the EMEP network in 2007. Statistical results for all model grid-cells of both resolutions are also shown. Percentage differences between the two model resolutions are calculated as $(O_{3\ global\ resolution} - O_{3\ finer\ resolution})/(O_{3\ global\ resolution})$.

			52 sites		all grid-cells	
Season		**Obs.**	**Model**		**Model**	
			140 km	**50 km**	**140 km**	**50 km**
DJF	Mean (μg m^{-3})	52.8	48.5	42.6	35.1	31.7
	Difference (%)		12.2		9.7	
	NMB (%)		-8.1	-19.2		
	SD (μg m^{-3})	11.0	17.0	16.0	17.3	16.5
MAM	Mean (μg m^{-3})	70.4	80.7	67.9	75.7	71.5
	Difference (%)		15.9		5.5	
	NMB (%)		14.6	-3.6		
	SD (μg m^{-3})	8.9	13.7	12.8	12.9	12.9
JJA	Mean (μg m^{-3})	63.6	78.6	80.8	84.4	85.6
	Difference (%)		-2.8		-1.4	
	NMB (%)		23.7	27.1		
	SD (μg m^{-3})	10.2	16.3	15.1	20.6	20.5
SON	Mean (μg m^{-3})	46.3	48.6	55.0	52.7	54.9
	Difference (%)		-13.2		-4.2	
	NMB (%)		4.9	18.8		
	SD (μg m^{-3})	10.2	15.0	14.2	15.2	14.1

Modelled versus observed seasonal mean O_3 concentrations for each of the 52 EMEP station locations are shown in Fig. 3.1, with arrow lengths indicating the change in concentrations when simulated at the coarse versus finer resolutions. For both resolutions, higher O_3 concentrations are simulated during summer compared to observations as noted above (between 50 to 150 µg m^{-3}; Fig. 3.1). In winter, simulated O_3 concentrations are lower compared to measurements (< 30 µg m^{-3}), and are most similar to observations in spring and autumn in accordance with lower NMB (Table 3.1).

The magnitude of the differences in simulated O_3 concentrations between the two resolutions varies seasonally, with the smallest (coarse-finer) differences in summer (green arrows – Fig. 3.1; -3 % ;Table 3.1) and the largest difference in spring, as noted above (16 % ;Table 3.1). Similar differences in July mean O_3 concentrations between a 150 km and a 40 km resolution were also found by Stock et al. (2014). Over the majority of the stations, during winter and spring, O_3 concentrations simulated at the finer resolution are lower than concentrations simulated at the coarse resolution (downward arrows; Fig. 3.1, positive difference; Table 3.1). In contrast during summer and autumn, O_3 concentrations are higher when simulated at the finer resolution (upward arrows; Fig. 3.1, negative difference; Table 3.1). These results are analysed further at the seasonal level in Fig. S3.1 Section 3.6.

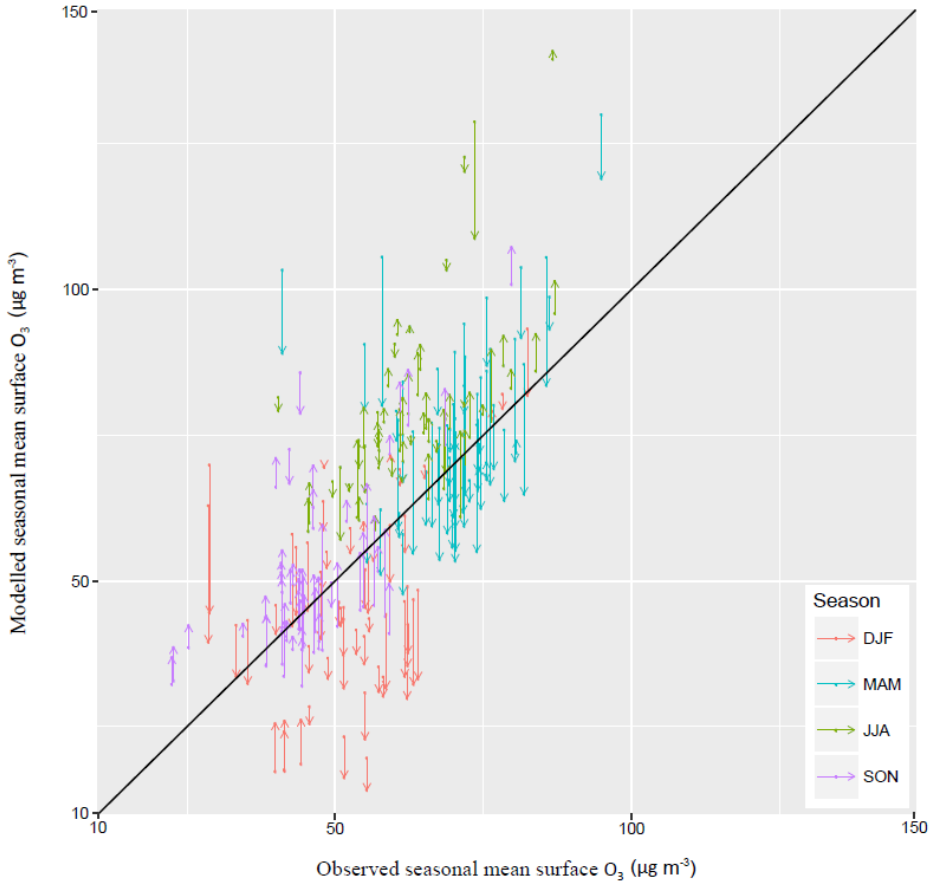

Figure 3.1: Seasonal mean modelled vs observed O_3 for 52 sites across the EMEP network for the year 2007. The arrow tails mark O_3 concentrations at the coarse resolution while the arrow heads represent the corresponding O_3 concentrations at the finer resolution. The 1:1 line shows agreement between observed and simulated O_3.

3.3.2 Impact of resolution on seasonal mean O_3: spatial differences

This section extends the investigation presented in the previous sections to examine the impact of model grid resolution on the spatial distribution of O_3 over the whole of Europe. The seasonal variation in O_3 concentrations simulated at the finer resolution across Europe shows the same features as at the 52 site locations (section 3.3.1), with highest values in spring and summer (> 50 µg m^{-3} and up to 120 µg m^{-3}; Fig. 3.2b and 3.2c, respectively) and lowest values in autumn and winter (<55 µg m^{-3}; Fig. 3.2a and 3.2d). In all seasons, except winter, there is a clear latitudinal gradient with higher O_3 concentrations in southern compared to northern Europe. In winter (Fig. 3.2a), very low O_3 concentrations are simulated across much of Europe (~30 µg m^{-3}).

For most of Europe, in winter and spring, mean O_3 concentrations are generally higher when simulated at the coarse compared to the finer resolution (Fig. 3.2e and 3.2f, 10% and 6% respectively; Table 3.1), in agreement with the findings for the sub-set of 52 locations. However parts of northern Scandinavia and the UK, and parts of south-eastern Europe have lower O_3 concentrations simulated at the coarse resolution in these two seasons. In summer and autumn, O_3 concentrations are slightly lower when simulated at the coarse compared to the finer resolution (-1% and -4% respectively –Table 3.1) as found for the sub-set of locations, except in areas of easternmost Europe (especially in autumn) and parts of Spain and Italy (Fig. 3.2g and 3.2h). The greatest positive differences in simulated O_3 concentrations, i.e. higher values at the coarse resolution, are found in winter, especially in the far south of Europe in Spain (~ 20 µg m^{-3}; Fig. 3.2e). Some of these positive differences are clear around the coastal regions which is likely due to differences in the land/sea mask at the two resolutions, which leads to less deposition over oceanic grid-cells at the coarse resolution and higher simulated O_3 concentrations compared to the same locations that are designated as land at the

finer scale (Coleman et al., 2010). In addition, large negative differences in simulated O_3 concentrations between the two resolutions occur over the Alps, whereby simulated O_3 concentrations are higher at the finer scale (Fig. 3.2e and 3.2h). This is most likely due to the differences in orography at the two resolutions with higher elevations at the finer scale leading to higher O_3 concentrations.

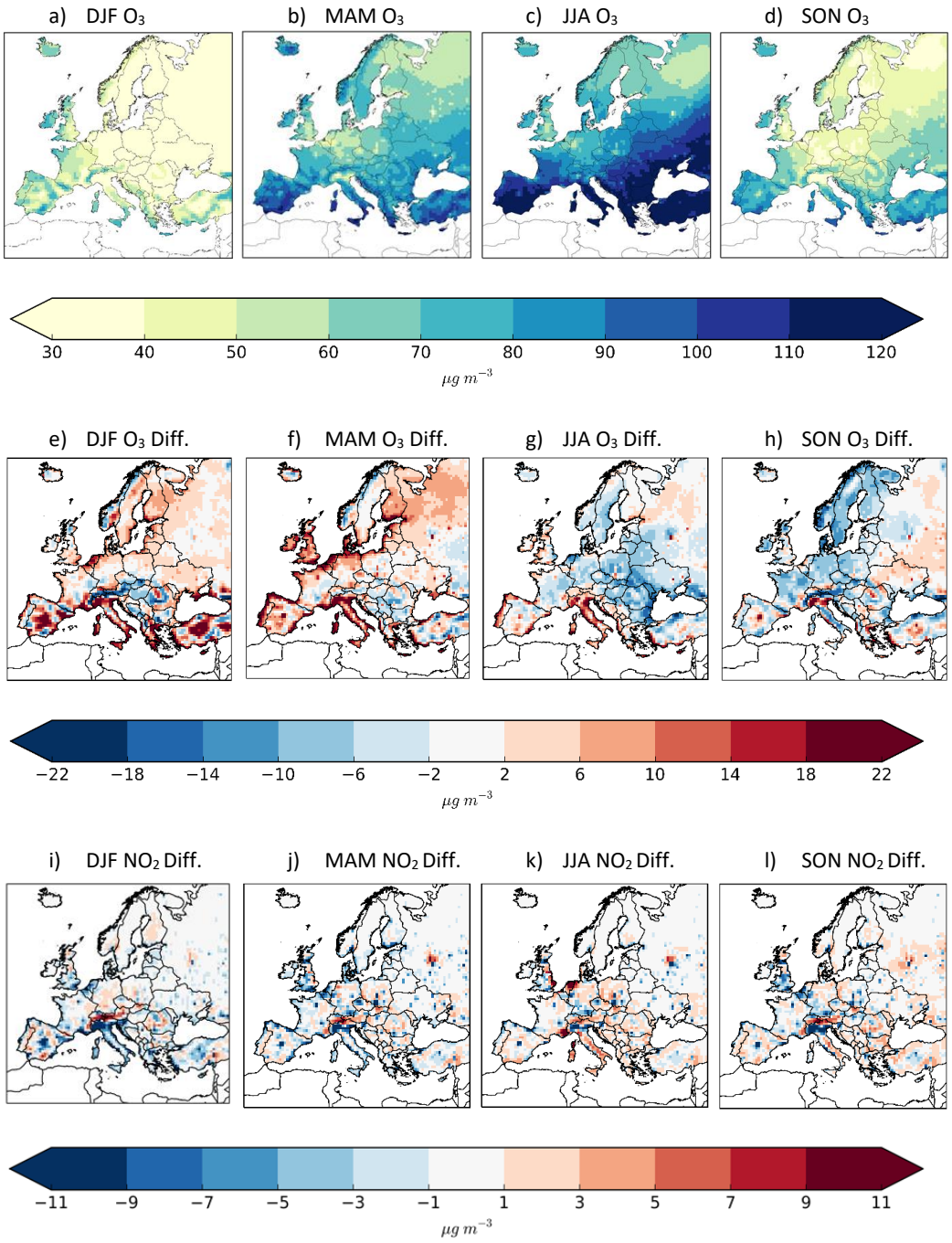

Figure 3.2: Seasonal mean O_3 simulated at the finer resolution (top panel), differences in seasonal mean O_3 between the coarse and finer resolutions ($O_{3\ coarse\ resolution} - O_{3\ finer\ resolution}$) (middle panel) and NO_2 ($NO_{2\ coarse\ resolution} - NO_{2\ finer\ resolution}$) (bottom panel). Blue regions in middle and bottom panels indicate that pollutant concentrations at the coarse resolution are lower (negative difference) while red regions indicate that concentrations are higher (positive difference) than those at the finer resolution.

Differences in simulated seasonal mean NO_2 concentrations at the two resolutions show similar, but less extensive differences and generally inverse patterns as for O_3 concentrations, with some negative differences, i.e. lower NO_2 values in winter and spring (Fig. 3.2i and 3.2j), when simulated at the coarse compared to the finer resolution. In contrast, in summer and autumn, NO_2 concentrations are higher in some regions when simulated at the coarse compared to the finer resolution (e.g. Italy; Fig. 3.2k and 3.2l). An inverse relationship i.e. a positive difference in O_3 concentrations and a negative difference in NO_2 concentrations is most prominent for locations in Spain (all year around) and Italy (winter and spring) and parts of the Benelux region (southern UK and Netherlands; all year around). This inverse relationship is driven by lower NO_x concentrations at the coarse resolution which lead to less O_3 titration by NO compared to the finer resolution (Fig. 3.2i). This in turn results in higher simulated seasonal mean O_3 concentrations at the coarse resolution compared to the finer resolution (Fig. 3.2e).

The planetary boundary layer (PBL) height is a key meteorological variable that affects the vertical transport of pollutants from the surface into the free troposphere from where they can then undergo strong horizontal transport. Thus the impact of changing model resolution on PBL height and how this impacts O_3 and NO_2 concentrations is also investigated. Spatial differences in PBL height between the two resolutions are shown in Fig. 3.3. In all seasons, over most of western and central Europe and especially in summer, the PBL height is generally lower when simulated at the coarse resolution (negative differences up to 275m; Fig. 3.3c). In winter and spring (Fig. 3.3a and 3.3b), this lower height corresponds to generally higher O_3 concentrations but also lower NO_2 concentrations simulated at the coarse resolution, over the same region and vice versa in summer and autumn (Fig. 3.3c and 3.3d). If a shallower PBL is the main driver of pollutant trapping producing higher O_3 levels, then we would also expect NO_2 concentrations to be higher with a lower PBL height at the coarse resolution, but their frequent inverse relationship

suggest a stronger role for chemistry rather than PBL effects. However, these chemical and physical processes cannot be clearly separated.

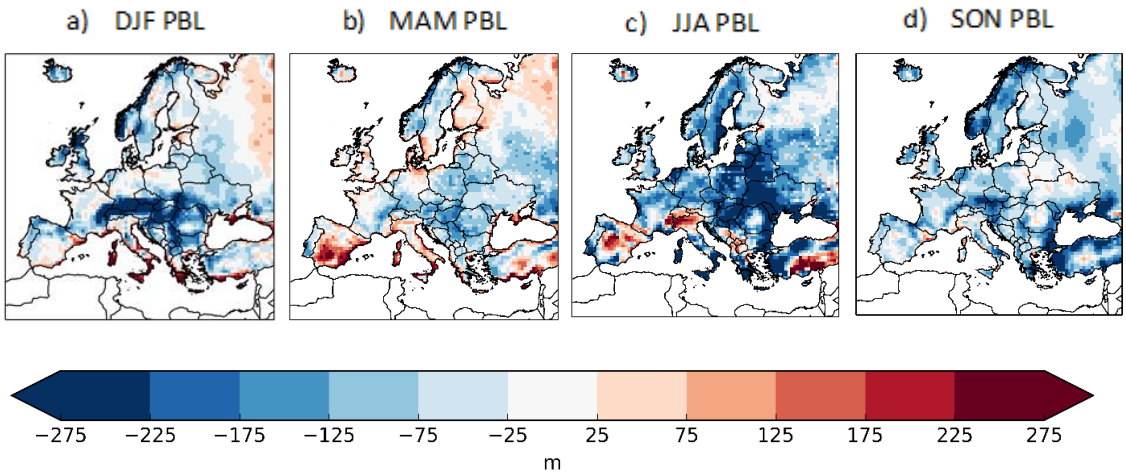

Figure 3.3: Difference between global and regional seasonal mean boundary layer height (PBL $_{coarse\ resolution}$ – PBL $_{finer\ resolution}$) for a) DJF b) MAM c) JJA and d) SON for 2007

In summary, a seasonal variation in simulated O_3 differences between the two resolutions is found. Simulated O_3 concentrations at the coarse resolution are higher in winter and spring and lower in summer and autumn compared to the finer resolution. NO_2 concentrations are lower at the coarse compared to the finer resolution in a number of locations and correspond to higher O_3 concentrations at the coarse resolution as a result of reduced titration with lower NO_x levels. Orography also plays an important role in some coastal locations, leading to an overestimation of O_3 concentrations. The PBL height differs between the two resolutions especially during summer, with the finer resolution resulting in a deeper boundary layer. However, it is not possible to separate chemistry and mixing effects on simulated O_3 concentrations.

3.3.3 The impact of resolution on seasonal mean $PM_{2.5}$ – comparison with observations

Simulated seasonal mean $PM_{2.5}$ concentrations are compared to available EMEP observations at 25 sites (Table 3.2). Mean values for the observations are fairly similar across all seasons, with values in summer and autumn being slightly lower. $PM_{2.5}$ concentrations simulated at both the coarse and finer resolutions are lower in winter and higher in summer compared to measurements. In addition, mean $PM_{2.5}$ concentrations simulated at the finer resolution are higher than those simulated at the coarse resolution except in summer. The coarse resolution simulates $PM_{2.5}$ levels with the smallest bias during spring (NMB = -0.2%). In contrast, $PM_{2.5}$ concentrations simulated at the finer resolution during spring have a large positive bias (NMB = 31%). Similarly in autumn NMB values are larger for $PM_{2.5}$ concentrations simulated at the finer resolution. The largest bias for both resolutions occurs in summer with the coarse resolution resulting in a NMB of 70%. Using, a similar finer configuration, Neal et al. (2017) found a year-round small positive bias in simulated $PM_{2.5}$ concentrations averaged over a five year period (2001-2005) at two UK locations. The SD of $PM_{2.5}$ concentrations across the 25 sites is fairly similar between model results and measurements except in winter, when simulated SD values are lower at both resolutions compared to measurements and in autumn, when the SD at the finer resolution is higher compared to measurements.

Modelled versus measured $PM_{2.5}$ concentrations across the 25 individual EMEP stations highlight the low simulated $PM_{2.5}$ concentrations in winter (Fig. S3.2; Section 3.6). Large variations in $PM_{2.5}$ levels between the two resolutions are prominent in spring (-31%; Table 3.2). Smaller $PM_{2.5}$ concentrations simulated at the coarse resolution in winter, spring and autumn are apparent (upward arrows; Fig. S3.6, negative differences; Table 3.2).

Table 3.2: Statistical results comparing seasonal mean $PM_{2.5}$ concentrations simulated at the global and finer resolutions to observations from 25 stations within the EMEP network in 2007. Statistical results for all model grid-cells of both resolutions are also shown. Percentage differences between the two model resolutions are calculated as ($PM_{2.5 global\ resolution} - PM_{2.5\ finer\ resolution}$)/($PM_{2.5\ global\ resolution}$).

Season		**25 sites**			**All grid-cells**	
		Obs.	**Model**		**Model**	
			140 km	**50 km**	**140 km**	**50 km**
DJF	Mean (μg m^{-3})	12.1	8.3	9.5	5.1	5.5
	Difference (%)		-14.5		-7.8	
	NMB (%)		-31.0	-21.3		
	SD (μg m^{-3})	9.2	2.5	3.1	3.1	3.7
MAM	Mean (μg m^{-3})	12.6	12.4	16.2	9.0	9.5
	Difference (%)		-30.6		-5.5	
	NMB (%)		-0.2	31.1		
	SD (μg m^{-3})	5.1	2.6	5.4	4.9	6.2
JJA	Mean (μg m^{-3})	10.6	18.0	14.9	11.9	8.4
	Difference (%)		17.2		29.4	
	NMB (%)		70.0	40.1		
	SD (μg m^{-3})	4.0	5.4	6.4	7.0	6.2
SON	Mean (μg m^{-3})	11.0	10.7	13.2	12.3	11.3
	Difference (%)		-23.4		8.1	
	NMB (%)		-2.4	22.0		
	SD (μg m^{-3})	4.8	4.1	10.3	7.0	6.7

3.3.4 Impact of resolution on seasonal mean $PM_{2.5}$: spatial differences

Spatial distributions of $PM_{2.5}$ concentrations, simulated at the finer resolution as well as differences between the two resolutions over the whole European domain are illustrated in Fig. 3.4. Over the whole domain, $PM_{2.5}$ concentrations simulated at the finer resolution are lowest in winter (Fig. 3.4a) and highest in spring (Fig. 3.4b). As for O_3, there is clear latitudinal gradient with higher $PM_{2.5}$ levels in southern Europe in all seasons. Differences in seasonal mean $PM_{2.5}$ concentrations, between the coarse and fine resolutions, vary seasonally across the European domain with the smallest differences occurring during winter (± 3 μg m^{-3}; Fig. 3.4e, -8% ; Table 3.2) in agreement with the findings for the 25 EMEP stations described above (section 3.3.3). This suggests that at low $PM_{2.5}$ concentrations (~ 8 μg m^{-3}) in winter, model results do not differ greatly when increasing the model resolution from 150 km to 50 km. In spring, $PM_{2.5}$ concentrations simulated at the coarse are lower than at the finer resolution over large parts of central and western Europe but are slightly higher in easternmost parts of Europe (negative differences ~-10 μg m^{-3} Fig. 4f; -6% Table 3.2), as found at the 25 EMEP station locations. The opposite result occurs in summer with generally higher $PM_{2.5}$ concentrations simulated at the coarser resolution (positive differences ~ 10 μg m^{-3} Fig. 4g; 29% Table 3.2). In autumn, the differences in $PM_{2.5}$ concentrations at the two resolutions exhibit a marked east-west contrast, with lower values at the coarse resolution in western Europe (where the EMEP stations are generally located; Fig. 2.4) and higher values at the coarse resolution in eastern Europe (Fig. 3.4h). While $PM_{2.5}$ concentrations at the 25 EMEP site locations are on average lower when simulated at the coarse resolution (-23%), over all grid-cells, $PM_{2.5}$ concentrations are higher at the coarse resolution (8%). This highlights issues with representivity of the EMEP network

across Europe, with much fewer EMEP measurement stations for $PM_{2.5}$ in eastern Europe.

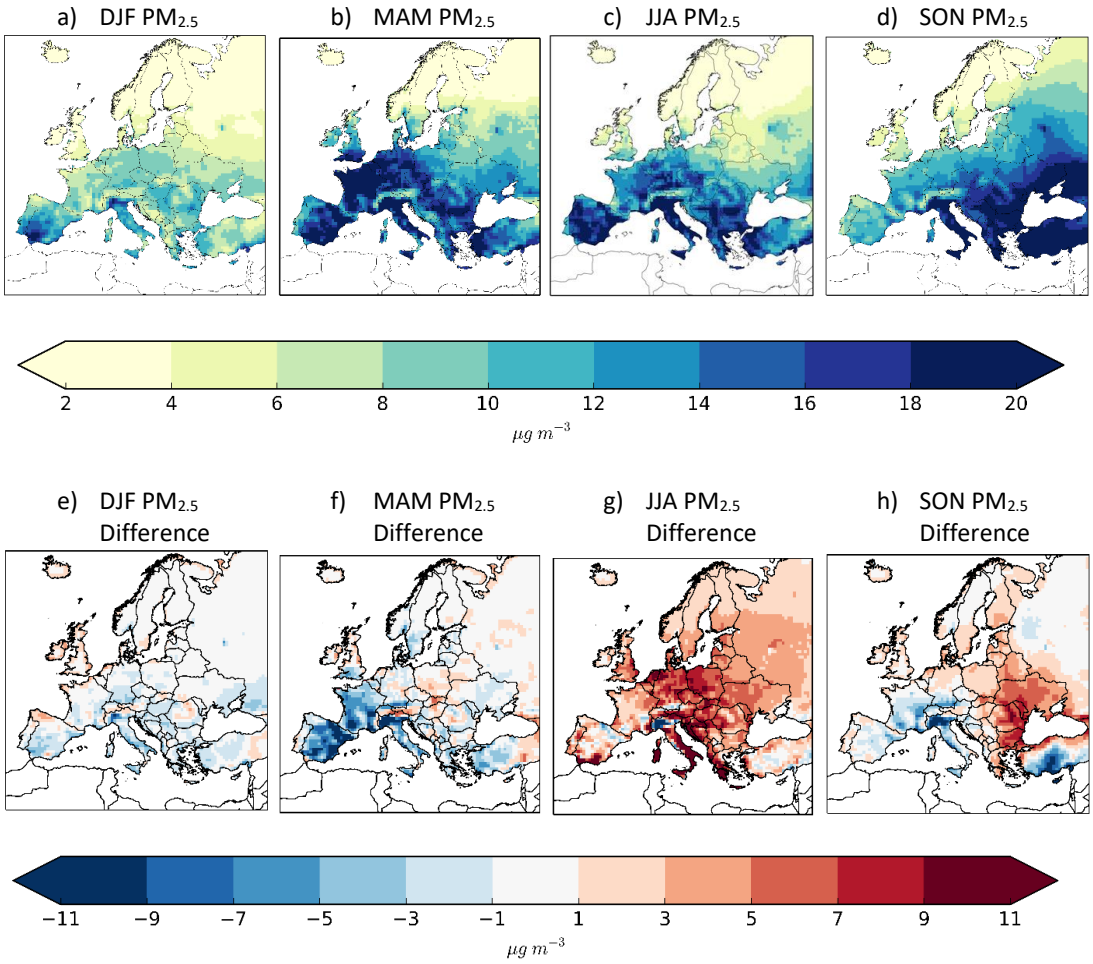

Figure 3.4: Seasonal mean $PM_{2.5}$ simulate at the finer resolution (top panel) and differences between seasonal mean $PM_{2.5}$ at the coarse and finer resolution in 2007 ($PM_{2.5\ coarse\ resolution} - PM_{2.5\ finer\ resolution}$) (bottom panel).

The seasonality in $PM_{2.5}$ differences, brought about by a change in model horizontal resolution, can be partly explained by differences in PBL height between the two resolutions, as outlined in section 3.3.2. In particular, the deeper boundary layer in summer simulated at the finer resolution may lead to greater vertical lofting from the surface, producing lower $PM_{2.5}$ levels compared to that simulated at the coarse resolution. In addition, differences in simulated precipitation (especially smaller-scale convective precipitation) between the two resolutions may be important, through its influence as the dominant mechanism in UKCA for removal of aerosols through wet deposition (O'Connor et al., 2014). Spatial patterns of convective precipitation differences between the two resolutions are shown in Fig. 3.5. In winter and spring, convective rainfall is higher at the coarse compared to the fine resolution (Fig. 3.5a and 3.5b). Thus removal of $PM_{2.5}$ through wet deposition is greater, producing lower $PM_{2.5}$ concentrations at the coarser resolution (Fig. 3.4e and 3.4f). The opposite holds in summer and autumn as the convective rainfall is lower at the coarse compared to the finer resolution (Fig. 3.5c and 3.5d) therefore resulting in higher $PM_{2.5}$ concentrations simulated at the coarse resolution (Fig. 3.4g and 3.4h).

Overall, a large seasonal variation in simulated $PM_{2.5}$ concentrations between the two resolutions is also found, with typically lower levels simulated in winter and spring at the coarse compared to the finer resolution and the opposite result in summer and autumn. Hence, the seasonality of differences in simulated $PM_{2.5}$ concentrations between the two model resolutions is generally the inverse of that found for O_3 in Section 3.3.2. We find that these seasonal differences can be largely explained by meteorological effects: PBL height differences, especially in summer, and by differences in convective rainfall between the two resolutions.

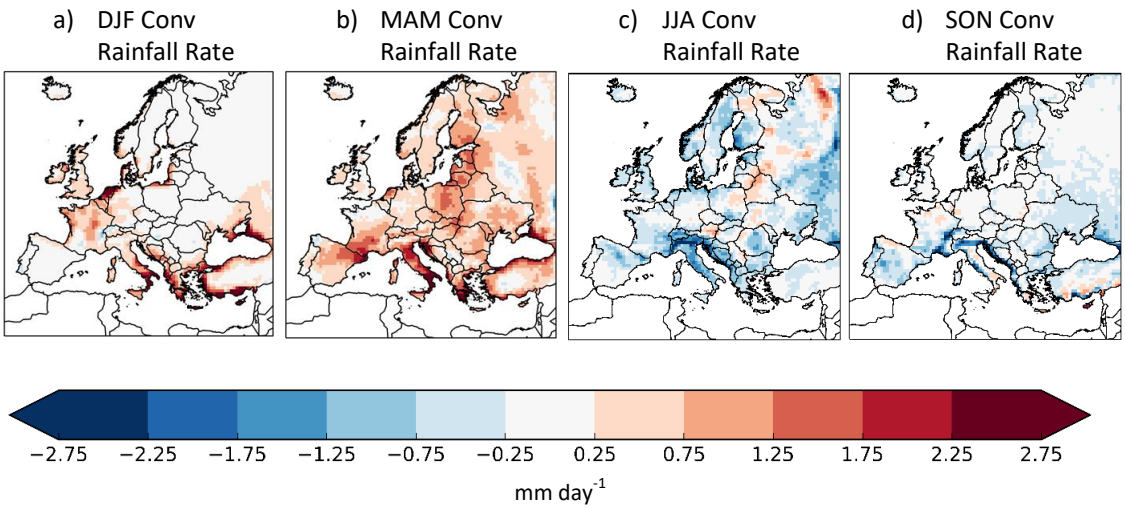

Figure 3.5: Difference between coarse and finer seasonal mean convective rainfall rate (mm day^{-1}) for a) DJF b) MAM c) JJA and d) SON for 2007

3.4 Sensitivity of health impact estimates to model resolution

In this section the impact of differences in O_3 and $PM_{2.5}$ concentrations simulated at the two resolutions on health impact estimations across Europe is examined at the country level. For this analysis warm season daily maximum 8-hour running mean (MDA8) O_3 (above 70 μg m^{-3}) and annual-average $PM_{2.5}$ concentrations are used. To estimate health impacts, air pollution concentrations (with an averaging period consistent with that used in epidemiological studies) are combined with population estimates and CRFs (Section 2.4.1).

3.4.1 Warm season MDA8 O_3 and annual-average $PM_{2.5}$ concentrations

Statistics for warm season MDA8 O_3 and annual $PM_{2.5}$ concentrations compared between EMEP measurements and model results at the two resolutions are provided in Table 3.3. Mean simulated MDA8 O_3 levels in the warm season at the 52 EMEP locations for both resolutions, are higher compared to observations (NMB = 11% and 9 %; Table 3.3), in agreement with findings for summer and autumn mean O_3 levels (c.f., Table 3.3, Table 3.1). The SD is also higher for both resolutions compared to observations. However, in contrast with summer mean O_3 levels, mean simulated MDA8 O_3 concentrations are 0.8% higher at the coarse compared to the finer resolution at the 52 EMEP site locations (Table 3.3). Simulated annual mean $PM_{2.5}$ concentrations are also higher compared to observations at the 25 locations (NMB =~10-20%; Table 3.3) with concentrations being 8.7% lower at the coarse compared to the finer resolution. This represents the net effect of seasonality in NMB shown in Table 3.2.

Table 3.3: Warm season (April-September) mean of daily maximum 8-hour running mean O_3 concentrations (MDA8 O_3) and annual mean $PM_{2.5}$ concentrations at the coarse and finer resolutions compared to observations from 52 and 25 stations within the EMEP network, respectively.

Season		**Obs.**	**140 km**	**50 km**
MDA8 O_3 (Apr - Sept)	Mean (μg m^{-3})	86.3	95.6	94.8
	Difference (%)		0.8	
	NMB (%)		10.9	8.9
	SD (μg m^{-3})	9.2	14.7	14.2
$PM_{2.5}$ (Annual)	Mean (μg m^{-3})	11.4	12.6	13.7
	Difference (%)		-8.7	
	NMB (%)		10.5	20.2
	SD (μg m^{-3})	5.1	2.8	5.0

Differences in warm season MDA8 O_3 and annual mean $PM_{2.5}$ concentrations, simulated at the coarse and finer resolution, are shown in Fig. 3.6. The spatial distribution of differences in warm season MDA8 O_3 between the two resolutions (Fig. 3.6a) is most similar to the distribution of differences in summer mean O_3 concentrations (Fig. 3.2g). Differences in MDA8 O_3 concentrations range from ~ -7 μg m^{-3} in Northeast Europe to ~ +20 μg m^{-3} in Southern Europe, UK and Ireland (Fig. 3.6a). It is noted that if a different time-averaging period was chosen e.g., annual as opposed to warm season, the spatial patterns of MDA8 O_3 differences would alter considerably due to the seasonal variation displayed in Fig. 3.2.

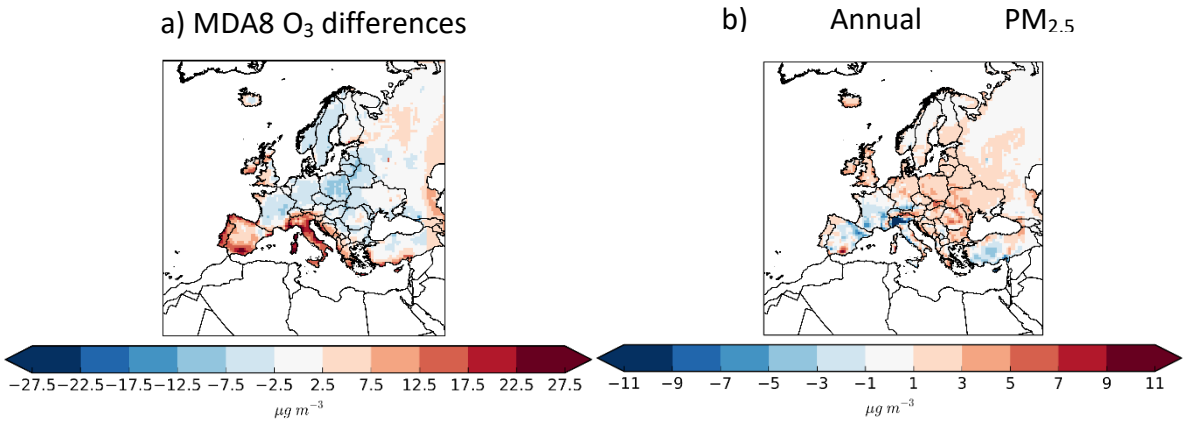

Figure 3.6: Differences in a) warm season (April-September) mean of daily maximum 8-hour running mean O_3 (concentrations above 70 µg m^{-3}) and b) annual mean $PM_{2.5}$ between the coarse and finer resolution (coarse – finer).

The spatial distribution of differences in annual mean $PM_{2.5}$ concentrations between the two resolutions (Fig. 3.6b) are most similar to the spatial distribution of differences in spring and especially autumn mean $PM_{2.5}$ concentrations notably with an east-west gradient (Fig. 3.4f and h). Differences in $PM_{2.5}$ concentrations between the two resolutions range from ~ -8 µg m^{-3} in the southwestern part of Europe and Cyprus to ~ +4 µg m^{-3} in north and eastern Europe (Fig. 3.6b).

3.4.2 Effect of applying population-weighting to MDA8 O_3 and annual $PM_{2.5}$ concentrations

The warm season MDA8 O_3 concentrations and annual mean $PM_{2.5}$ concentrations, simulated at both resolutions, were weighted by population totals for each country to produce country average population-weighted concentrations (Section 2.4.1). Figure 3.7a shows the impact of the two resolutions on country-average warm season average MDA8 O_3 and the corresponding population-weighted MDA8 O_3 concentrations. Similarly differences in annual mean $PM_{2.5}$ concentrations between

the two resolutions for non-population-weighted and population-weighted concentrations are shown in Fig. 3.7b.

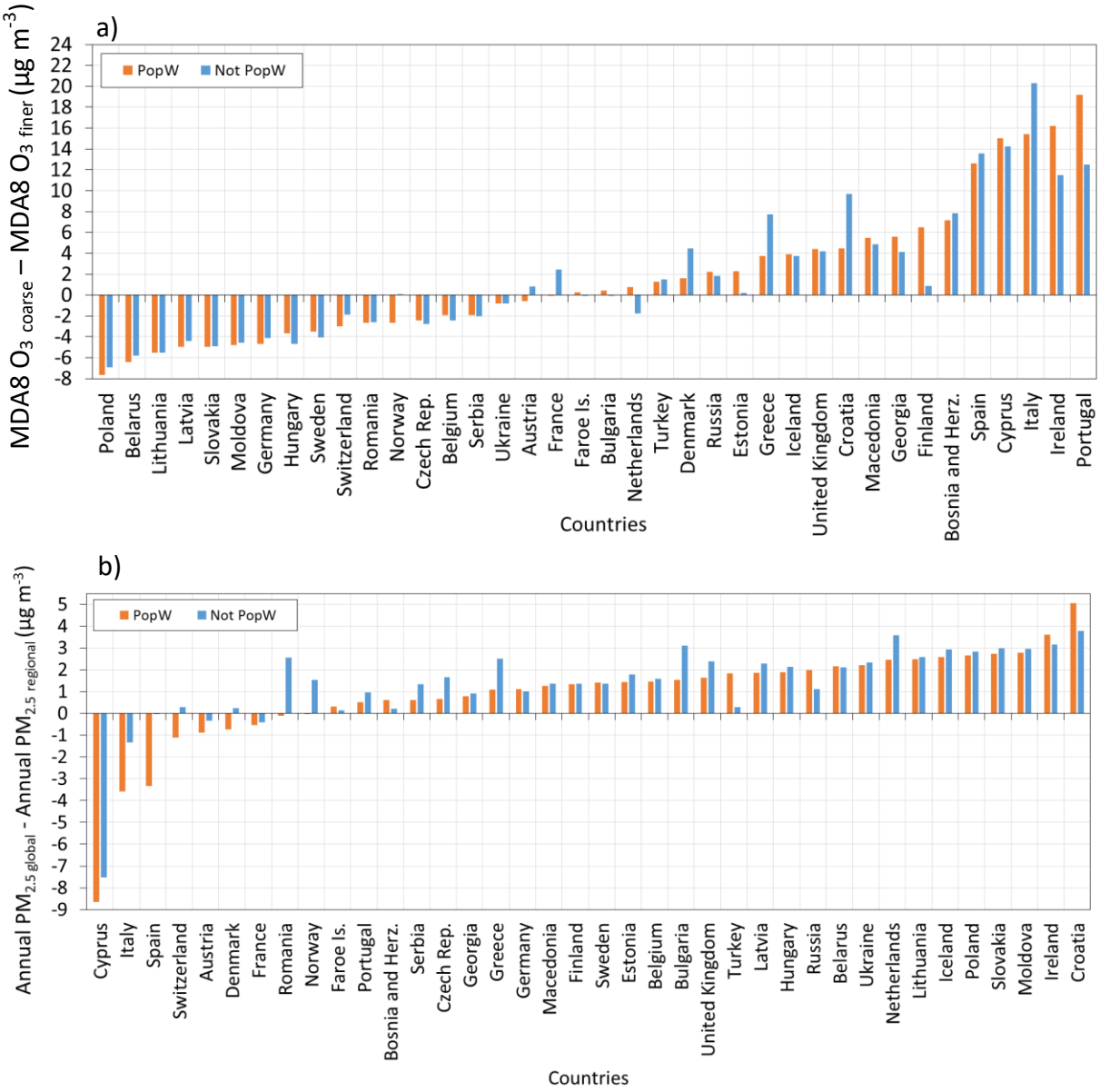

Figure 3.7: a) Differences between warm season mean daily maximum 8-hour running mean (MDA8) O_3 concentrations simulated at the two resolutions (coarse – finer) for population-weighted (PopW) concentrations (orange bars) and concentrations with no population-weighting (Not PopW; blue bars) b) same holds for annual mean $PM_{2.5}$ concentrations. Countries are ordered by differences in PopW pollutant concentrations between the two resolutions.

Population-weighting of pollutant concentrations has different impacts across the European countries (Fig. 3.7a and 3.7b). In many countries, differences in population-weighted pollutant concentrations between the two resolutions are enhanced (i.e. larger positive or more negative differences) relative to non-population-weighted pollutant concentrations. However, in some countries population-weighting may reduce the positive or negative difference between the two resolutions. Several cases are examined below.

For warm season MDA8 O_3 concentrations, the largest negative differences, implying lower MDA8 O_3 levels using coarse compared to the finer resolution results, occur in eastern Europe (Fig. 3.6a). Hence, the largest negative differences in non-population-weighted and population-weighted MDA8 O_3 concentrations are found in eastern European countries (Fig. 3.7a). The difference between the two resolutions is greatest when population-weighting is applied. This is generally due to slightly lower population-weighted MDA8 O_3 concentrations compared to MDA8 O_3 concentrations derived from the coarse resolution results (Fig. 3.8).

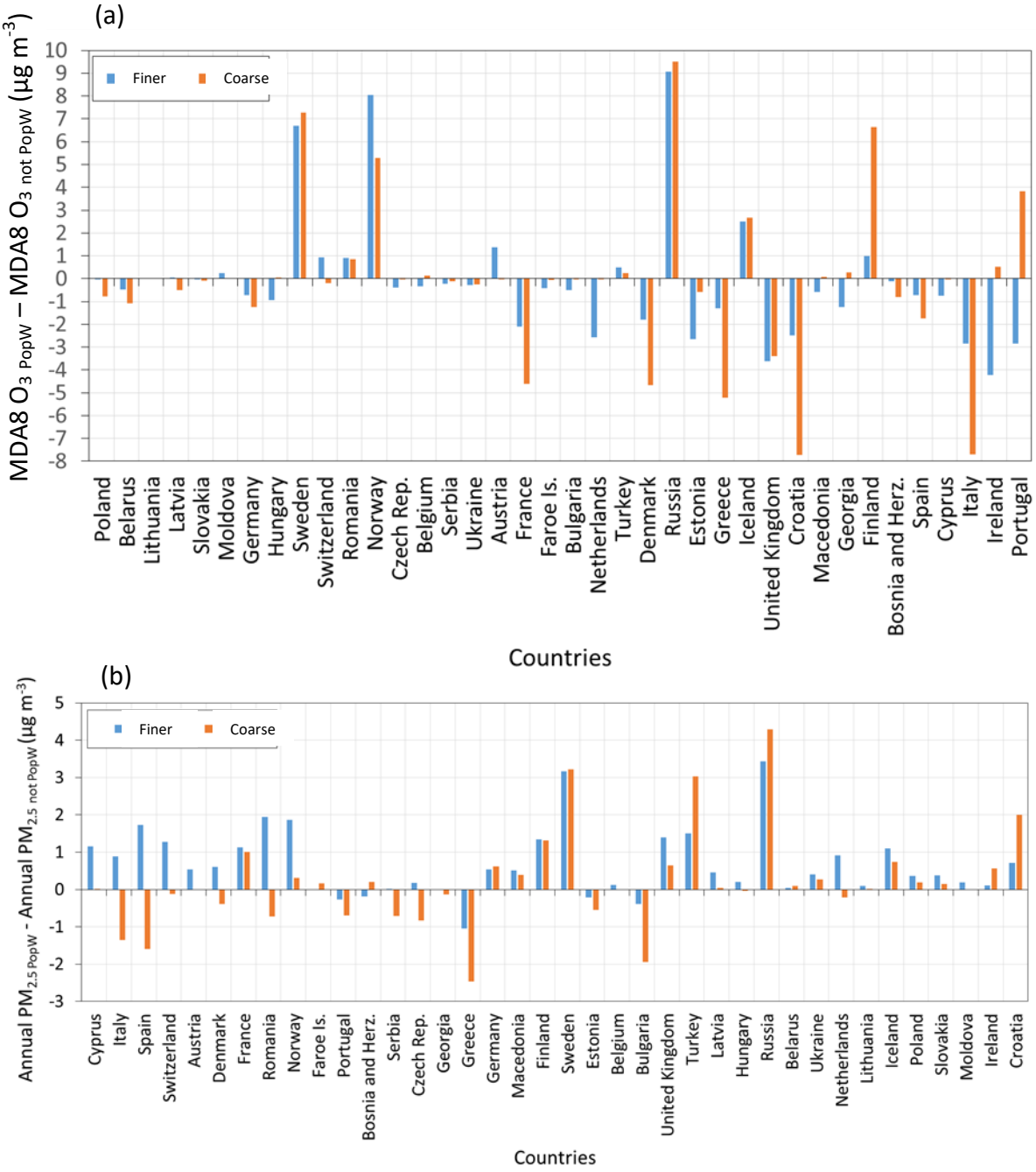

Figure 3.8: a) Difference between MDA8 O_3 concentrations with and without population-weighting as simulated by the coarse (orange bars) and finer (blue bars) resolutions b) same holds for annual mean $PM_{2.5}$ concentrations.

In the Netherlands warm season non-population-weighted MDA8 O_3 is also lower when derived from coarse compared to finer resolution results (negative difference; Fig. 3.6a, 3.7a). However population-weighted MDA8 O_3 concentrations are higher when derived from the coarse resolution results (Fig. 3.7a). This is caused by lower MDA8 O_3 concentrations simulated at the finer resolution when applying population-weighting (Fig. 3.8a). This suggests that in populated regions, MDA8 O_3 concentrations simulated at the finer resolution are lower which might be linked to higher NO_2 concentrations.

Warm season MDA8 O_3 show the largest positive differences, with higher values simulated at the coarse resolution, for southern Europe and the UK/Ireland (Fig 3.6a). Thus, the largest positive differences for non-population-weighted and population-weighted MDA8 O_3 concentrations occurs in south European countries (Fig. 3.7a). Population–weighed MDA8 O_3 concentrations in Portugal are higher compared to MDA8 O_3 concentrations at the coarse but lower at the finer resolution (Fig. 3.8a). This suggests that, at the coarse resolution, areas with high levels of O_3 are co-located with high population densities whilst at the finer resolution areas with lower levels of O_3 are co-located with high population densities.

Annual-average $PM_{2.5}$ concentrations show the largest negative differences, with higher values simulated at the finer resolution, in parts of western Europe (Fig. 3.6b). Hence, the largest negative non-population-weighted and population-weighted annual mean $PM_{2.5}$ concentrations are found for Cyprus, Italy and Spain (Fig. 3.7b). Conversely, higher annual-average $PM_{2.5}$ levels are simulated at the coarse resolution in eastern and northern Europe (Fig. 3.6b), hence larger positive non-population-weighted and population-weighted annual mean $PM_{2.5}$ concentrations occur for countries in eastern Europe and northern Europe (Fig. 3.7b).

In Cyprus, population-weighted annual mean $PM_{2.5}$ concentrations simulated at the fine resolution are higher compared to concentrations with no population-weighting, due to denser populations being co-located with areas of higher $PM_{2.5}$ levels (Fig. 3.8b). In Croatia, population-weighted annual mean $PM_{2.5}$ concentrations simulated at the coarse resolution are greater than $PM_{2.5}$ concentrations with no population-weighted, again due to denser populations in regions of high concentrations but in this case when simulated at the coarse resolution (Fig. 3.8b). In a few countries (e.g. Switzerland), differences in population-weighted annual mean $PM_{2.5}$ concentrations between the two resolutions have an opposite sign to differences between concentration with no population-weighting (Fig. 3.7b). This indicates that annual mean $PM_{2.5}$ concentrations simulated at the finer resolution are high in densely populated regions but are low in these same regions at the coarse resolution.

It would be insightful to examine these population-weighted results in relation to model-observation biases in densely populated areas. However, as outlined in Section 2.3, the available sites in the EMEP database are urban background stations which are required to be representative of a wide are and away from industrial areas (EMEP/CCC,2001). Nonetheless it is noted that in southern Europe, simulated summer mean MDA8 O_3 concentrations at the finer resolution are closer to observations than concentrations simulated at the coarse resolution. No consistent result is found for model biases in simulated annual mean $PM_{2.5}$ concentrations with respect to observations for the two model resolutions.

3.4.3 Attributable fraction of mortality associated with long-term exposure to O_3

The Attributable Fraction (AF) associated with long-term exposure to MDA8 O_3, expressed as a percentage of total respiratory mortality and simulated at both resolutions, is calculated for each country (Fig. 3.9a), using the population-weighted warm season MDA8 O_3 concentrations (Fig. 3.9a) as discussed in Section 3.2.3 and 2.4.1. For both resolutions, the estimated AF is shown for each country, with the 95% confidence interval (95% CI) representing uncertainties associated only with the CRF used (shown in grey). For all the countries considered, irrespective of the model resolution used, the AF of total respiratory mortality ranges from 1% (95% CI 0% to 2%) in Finland to 11 % (95% CI 4% to 18%) in Cyprus (Fig. 3.9a).

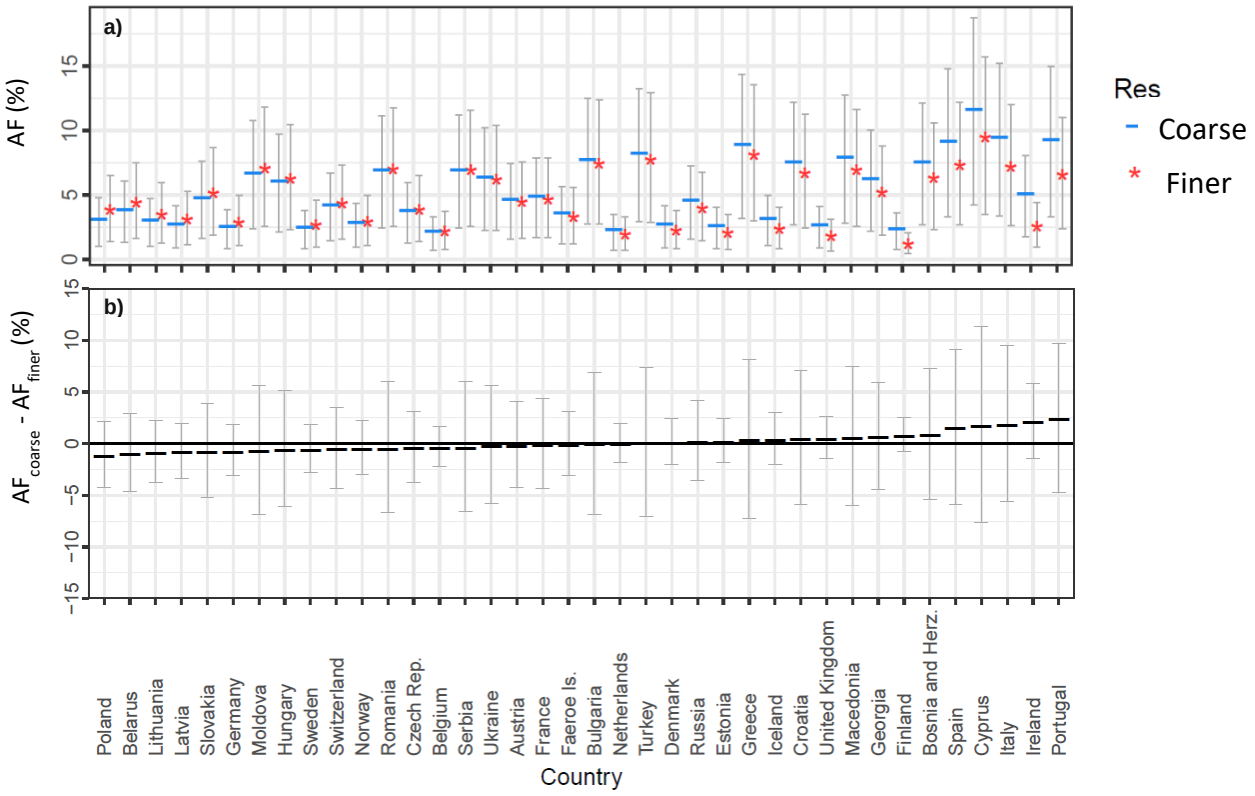

Figure 3.9: a) AF associated with long term exposure to daily maximum 8-hour running mean O_3 for each model resolution expressed as a percentage b) Differences in AF between the two resolutions expressed as a percentage for each European country (AF_{coarse} – AF_{finer}). Grey lines show the 95% CI which represents uncertainties associated only with the concentration-response function used.

Differences in AF between the countries are solely attributed to differences in population-weighted MDA8 O_3 concentrations. Thus, countries with the highest population-weighted concentrations also have the highest AF. Similarly countries with the highest differences in population-weighted MDA8 O_3 concentrations between the two resolutions also have the largest differences in AF between the coarse and finer resolution. If the AF was calculated for each model grid-cell rather than at the country level, the differences in AF for the two pollutants would have identical spatial distributions to the differences in warm season MDA8 O_3 and annual-mean $PM_{2.5}$ concentrations depicted in Fig. 3.6, as the AF is only dependent on the pollutant concentration and the CRF (which is constant across all countries).

The differences in country level AF associated with long-term exposure to warm season MDA8 O_3, simulated at the two resolutions, are shown in Fig. 3.9b. These values highlight the sensitivity of respiratory mortality attributable to long-term exposure to O_3 to a change in model resolution. For most of northern and eastern Europe, the AF at the coarse resolution is lower than that at the finer resolution (negative differences; Fig. 3.9b) as for differences in population-weighted warm season MDA8 O_3 concentrations in the same countries (Fig. 3.7a). In contrast, the AF at the coarse resolution is higher than that at the finer resolution for countries in southern Europe (positive differences, Fig. 3.9b). Differences in AF range from -0.9% (95% CI -0.3% to -1.5%) in Poland to +2.6% (95% CI 1.0% to 4.1%) in Portugal (Fig. 3.9b) which directly correspond to the countries having the lowest and highest difference in population-weighted MDA8 O_3 concentration respectively (Fig. 3.7a; Note, although the differences in AF between the two resolution appear low, these are percentages of total respiratory mortality). In Poland and Portugal the estimated AF at the finer resolution is 1.4 times and 0.7 times that estimated at the coarse resolution. For approximately half of the European countries, the AF is higher for the coarse resolution compared to the finer resolution and vice versa.

When considering the uncertainty associated with the concentration-response function used, the 95% CI for the AF of respiratory mortality associated with long term exposure to MDA8 O_3 at the two resolutions overlap over the majority of the countries (Fig. 3.9a). Hence, the sign of the difference in AF between the two model resolutions can be altered (Fig. 3.9b). This suggests that the uncertainty associated with the 95% CI associated with the CRF is crucial to HIAs. Kushta et al. (2018) suggest that the uncertainties in ambient $PM_{2.5}$-related mortalities in Europe are mostly associated with the CRFs rather than the representation of annual mean $PM_{2.5}$ concentrations by air quality models having varying horizontal resolutions. For this reason only uncertainties associated with the CRF used are included in this thesis.

For US averaged mortality estimates, Punger and West (2013) show that mortality estimates related to warm season long-term O_3 exposure, calculated using the O_3 concentrations at 36 km, were higher (by 12%) than estimates calculated at the 12 km resolution. Resolution was also found to play and important role in determining health benefits associated with differences in O_3 between 2005 and 2014 in the US (Thompson et al. 2014). In particular, in urban areas, Thompson et al. (2014) estimate that the benefits calculated using coarse resolution results were on average two times greater than estimates calculated using the finer scale results. Both the studies mentioned are conducted in the US and use a different concentration response function and thus a definitive comparison between these studies and estimates presented in this chapter over Europe is not possible.

Since, seasonal differences in simulated O_3 with resolution are considerable, the AF associated with long-term exposure to O_3 was also calculated based on annual-mean (as opposed to summer-mean) O_3 concentrations based on recommendations by Turner et al. (2015). Turner et al (2015) suggest a higher concentration response function of 1.06 (95% CI: 1.04 to 1.08) per 10 μg m^{-3} and a slight lower MDA8 O_3 threshold of 53.4 μg m^{-3} compared to values used in in this

chapter for summer-mean MDA8 O_3. Using the values from Turner et al. (2015) the differences in AF are found to be of the same sign for the majority of the countries and the rankings across countries are largely similar. This similarity occurs because the difference in annual-mean MDA8 O_3 concentrations between the two resolutions shows generally similar spatial patterns to the differences in warm season MDA8 O_3 concentrations (not shown). However the ranges when using annual-mean O_3 concentrations and recommendations from Turner et al. (2015) are larger: -2.3% to +12.0%, compared to AF ranges given above for MDA8 O_3. From further sensitivity analyses it is found that these greater AF ranges can be attributed to the use of a higher concentration-response function (by a factor of approximately 4) rather than differences in annual-mean compared to summer-mean concentrations.

3.4.4 Attributable Fraction associated with long-term exposure to $PM_{2.5}$

The fraction of all-cause (excluding external) mortality attributable to long-term exposure to $PM_{2.5}$, is shown as percentages for each country in Fig. 3.10a. The AF for all countries, irrespective of the resolution used, ranges from 2% (95% CI 1% to 3%) in Iceland to 15% (95% CI 10% to 19%) in Cyprus (Fig. 3.10a). Differences in AF between the two resolutions are shown in Fig. 3.10b. Since the variability in AF differences across the countries is caused by variability in population-weighted annual mean $PM_{2.5}$ differences, Cyprus and countries in parts of western Europe have the largest negative difference in percentage AF (Fig.3.10b). In contrast, countries in eastern and northern Europe have the largest positive difference in percentage AF (Fig. 3.10b). These differences range from -4.7% (95% CI -6.1% to -3.2%) in Cyprus to 2.8% (95% CI 1.9% to 3.7%) in Croatia. For Cyprus and Croatia, using the finer resolution results in an estimated AF that is 1.5 and 0.7 times that

estimated using the coarse resolution. Over most countries, annual mean population-weighted $PM_{2.5}$ concentrations are higher (positive difference; Fig. 3.8b) for the coarse compared to the finer resolution, thus resulting in a higher AF when using the coarse resolution results.

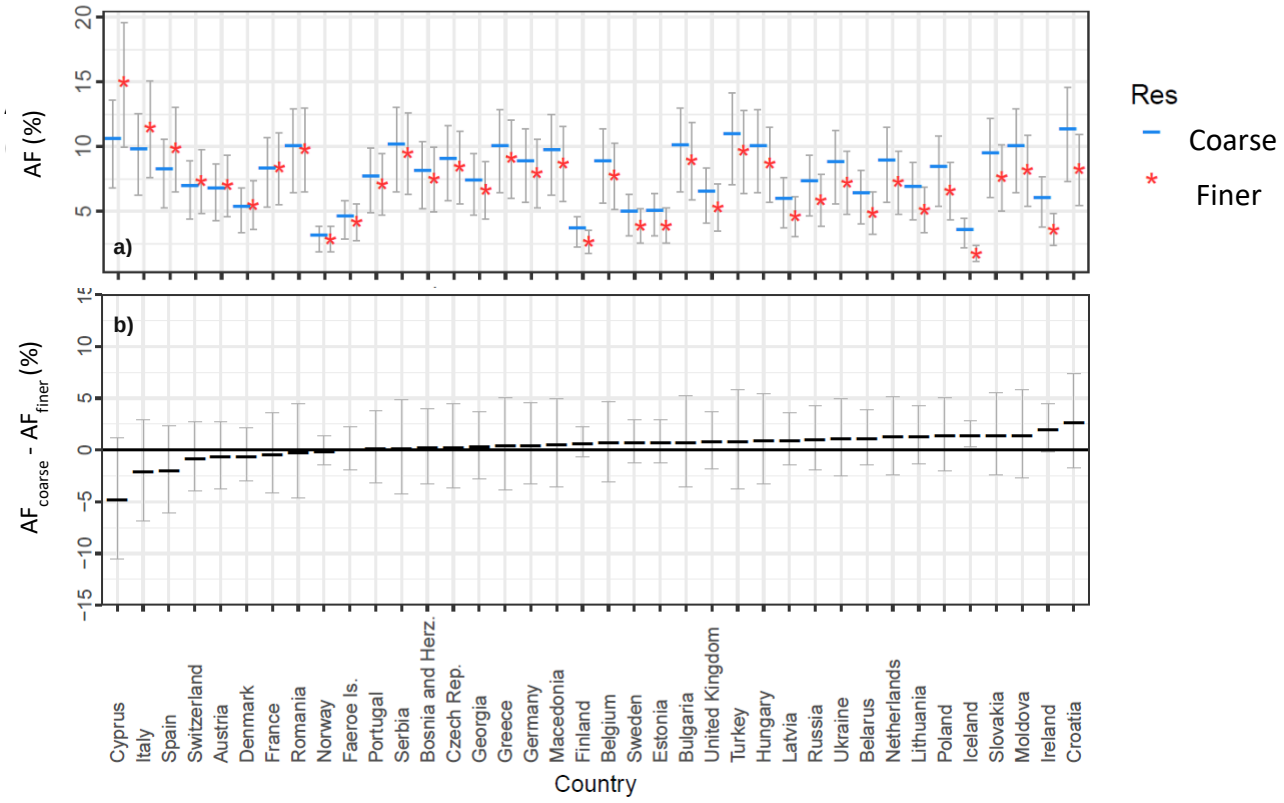

Figure 3.10: a) AF associated with long-term exposure to $PM_{2.5}$ for each model resolution expressed as a percentage b) Differences in AF between the two resolutions expressed as a percentage for each European country (AF_{coarse} – AF_{finer}). Grey lines show the 95 % CI which represents uncertainties associated only with the concentration-response function used.

Note, similar to O_3, the uncertainty associated with the CRF associated with long-term exposure to $PM_{2.5}$ can alter the sign of the difference of the AF of all-cause (excluding external) mortality between the two model resolutions across all

countries (Fig. 3.10b); again highlighting the strong influence of the 95% CI associated with the CRF.

The impact of using a low-concentration threshold is also examined. A threshold of 5.8 μg m^{-3} (suggested by Burnett et al. (2014) which is derived from Lim et al. (2012)) is applied to annual mean $PM_{2.5}$ concentrations. Differences in AF estimates associated with long-term exposure to population-weighted $PM_{2.5}$ concentrations range from -4.8% to +2.1% (as compared to -4.7% to +2.8% above when no threshold is applied). The spatial distribution of these estimates remains unchanged and only slight changes in country rankings occur. Hence, the impact of applying a low concentrations threshold in this study for Europe is small.

Results in this chapter are consistent with other studies, but not all, that examine the impact of model resolution on health estimates associated with long-term exposure to $PM_{2.5}$. Using concentrations simulated at the 36 km resolution, Punger and West (2013) find that the US national health estimate is higher (11%) than the estimate at 12 km resolution. Li et al. (2015) show that averaged over the U.S., a coarse grid resolution (~ 200 km) results in a health estimate that is lower (8%) than the estimated based on the fine scale model results (~ 50 km), in contrast to results in this chapter averaged across Europe. In contrast, Thompson et al. (2014) find that health benefits associated with changes in $PM_{2.5}$ concentrations between 2005 and 2014 in the US, were not sensitive to resolution. Both Punger and West (2013) and Li et al. (2015) find that differences in $PM_{2.5}$ are mainly attributable to primary anthropogenic PM, while Thompson et al. (2014) attribute the greatest differences (between 36 km and 4 km resolutions) to secondary PM. However, in this chapter no substantial differences in $PM_{2.5}$ components between the two resolutions were found. In a recent study focusing on uncertainties in estimates of mortality attributable to ambient $PM_{2.5}$ in Europe, Kushta et al. (2018) suggest that using model concentrations at a 20 km resolution results in health

estimates which are ~2.4% higher across Europe compared to estimates derived at the 100 km resolution.

In summary, results suggest that differences in AF health estimates between coarse and finer resolutions vary across the different European countries with clear differences between southern and eastern Europe for exposure to warm season MDA8 O_3 and west-east differences for exposure to annual-average $PM_{2.5}$ due to the dependence of AF on populated weighted MDA8 O_3 and annual $PM_{2.5}$ concentrations. For differences in AF attributable to long-term exposure to summer mean MDA8 O_3 and annual mean $PM_{2.5}$ concentrations, the uncertainty associated with the CRF used can alter the sign of the difference of AF between the two model resolutions (Fig. 3.9b and 3.10b). Using the CRF in Jerrett et al. (2009), Thompson et al. (2014) find that the avoided mortalities due to difference in ozone concentrations between 2005 and 2014 at a 36 km model resolution are within the 95% uncertainty range associated with the concentration-response function used compared to estimates at a resolution of 12 km and 4 km. These authors also find avoided mortalities associated with long-term effects of $PM_{2.5}$ exposure at 36 km to fall within estimates at the 12 km and 4 km resolution for three different concentration-response function. Thus results are in agreement for summer mean O_3 but less for annual mean $PM_{2.5}$.

3.5 Conclusions

Chemistry-climate model simulations were performed at two resolutions: a coarse resolution (~ 140 km) and a finer resolution (~ 50 km) over Europe to quantify the impact of horizontal model resolution on simulated O_3 and $PM_{2.5}$ concentrations by season; and on the associated Attributable Fraction (AF) of mortality due to long-term exposure to these two pollutants. Simulated O_3 concentrations are lower in

winter and higher in summer and autumn compared to measurements at both model resolutions. Results show a seasonal influence in the mean O_3 differences between the two resolutions. Simulated O_3 concentrations averaged across Europe at the coarse resolution are higher in winter and spring (10% and 6%, respectively), and lower in summer and autumn (-1% and -4%, respectively) compared to the finer resolution. In contrast during winter and spring, NO_2 concentrations are lower in some areas at the coarse compared to the finer configuration, whilst in summer and autumn, there are more locations where NO_2 concentrations are higher at the coarse resolution. The lower O_3 concentrations simulated at the finer compared to the coarse resolution can be partly explained by these higher NO_2 levels that enhance titration of O_3 at this finer resolution. The PBL height also differs between the two resolutions and may also account for differences in O_3 concentrations; however, it is not possible to clearly separate the effects of chemistry and mixing on simulated O_3.

Differences in $PM_{2.5}$ concentrations simulated at the two resolutions also vary seasonally. Modelled $PM_{2.5}$ concentrations are lower in winter and higher in summer compared to measurements at both resolutions. Simulated seasonal mean $PM_{2.5}$ concentrations averaged across Europe during winter and spring are lower at the coarse compared to the finer resolution (-8% and -6%, respectively) but higher in summer and autumn (29% and 8%, respectively). This seasonality in Europe-average differences in $PM_{2.5}$ concentrations is opposite to that found for differences in O_3 concentrations between the two resolutions. Differences in $PM_{2.5}$ concentrations simulated at the two resolutions are also influenced by PBL height, especially in summer when a deeper boundary layer at the finer resolution leads to greater lofting and lower $PM_{2.5}$ concentrations. Furthermore, in all seasons, the differences in $PM_{2.5}$ levels between the two resolutions are closely related to differences in the convective rainfall rate. In winter and spring, the convective rainfall at the coarse resolution is higher than that at the finer resolution thus

resulting in lower $PM_{2.5}$ concentrations. The opposite result holds in summer and autumn.

Results show that differences in warm season mean MDA8 O_3 concentrations between the two resolutions are similar to summer mean differences in simulated O_3 concentrations, with spatial patterns of differences reveal clear and important contrasts. Warm season MDA8 O_3 levels are higher in most of southern Europe as well as the UK and Ireland, but lower in other areas of northern as well as eastern Europe when simulated at the coarse resolution compared to the finer resolution. On the other hand, annual average $PM_{2.5}$ concentrations are higher across most of northern and eastern Europe but lower over parts of southwest Europe at the coarse compared to the finer resolution.

Weighting the pollutant concentrations at both resolutions with the population within each country, results in some added differences between concentrations at the two resolutions which also vary across the countries. In many countries, weighting by population enhances either positive or negative differences in warm season MDA8 O_3 or annual mean $PM_{2.5}$ concentrations between the two resolution, which suggests that high levels of pollutant concentrations coincide with high population density at one resolution but low pollutant concentrations are co-located with high population density at the other resolution. Population-weighting pollutant concentrations also reduces differences between coarse and finer resolution results in some countries.

The AF of respiratory mortality associated with long-term exposure to warm season MDA8 O_3 and annual mean $PM_{2.5}$ is also sensitive to resolution as is it is solely driven by the simulated population-weighted pollutant concentrations. For the AF associated with long-term exposure to O_3, countries in northern as well as eastern Europe have lower AF values at the coarse compared to the finer resolution whilst the opposite result occurs for other countries in southern Europe and Ireland.

For the AF associated with long-term exposure to $PM_{2.5}$, a few countries in southwestern Europe and Cyprus have lower AF values for $PM_{2.5}$ concentrations simulated at the coarse resolution whilst more countries especially in eastern and northern Europe show a higher AF when using $PM_{2.5}$ concentrations simulated at the coarse resolution.

Overall, differences in the country-average AF associated with long term exposure to MDA8 O_3 range between -0.9 % and +2.6 % while differences in the AF associated with long-term exposure to annual mean $PM_{2.5}$ range from -4.7% to +2.8 % of the total baseline mortality. This result emphasizes the importance of model horizontal resolution when conducting country specific health impact studies. However, differences in the AF of mortality between the two resolutions for both pollutants are strongly influenced by the 95% CI associated with the respective CRF used. In addition, these ranges in AF associated with long-term exposure to annual mean $PM_{2.5}$ were largely unaltered with the application of a low-concentration threshold for $PM_{2.5}$.

The calculation for O_3 health impacts only considers warm-season MDA8 O_3 impacts however these may differ to annual MDA8 O_3 impacts because of seasonal differences in simulated O_3 with resolution highlighted in this study. When using annual-mean MDA8 O_3 concentrations alongside a recommended concentration-response function and threshold suggested by Turner et al. (2015) the difference in AF between the two resolutions is considerably larger than estimates in this chapter using summer-mean MDA8 O_3 concentrations. This is driven by the higher concentration-response function (by a factor of approximately 4) quoted in Turner et al. (2015) compared to that suggested by HRAPIE for summer mean MDA8 O_3 concentrations (WHO, 2013). In addition, the same concentration-response function is applied to all populations and assumed that for $PM_{2.5}$-related health impacts, all $PM_{2.5}$ components have the same impact on mortality.

The pollutant concentrations used in this study have been extracted at the lowest model level with a mid-point at 20 m. The sensitivity of simulated pollutant concentrations to vertical model resolution has not been examined. Future research focusing on the sensitivity of AF changes to different averaging periods or seasons would be beneficial. In addition, the use of concentration-response functions that are derived from European cohort data would be useful, although such data are limited. Nonetheless this study provides one of the first insights as to how air pollution related health impacts over Europe are influenced by the model resolution used to simulate pollutant concentrations.

3.6 Supplementary material

This supporting information provides some additional text and figures showing a more in depth analyses on seasonal differences in O_3 concentrations between the coarse and finer resolution for the individual measurement sites (Fig. S3.1). An additional figure showing the seasonal mean differences in $PM_{2.5}$ concentrations as described in the main text is also included (Fig. S3.2).

An analyses on how the seasonality in O_3 concentrations simulated at the two resolutions varies seasonally and also geographically at the country level is conducted (Fig. S3.1). In winter, O_3 concentrations at southerly locations in Greece and Italy (Fig. S3.1 red box) show the largest differences between the two resolutions, with an overestimate of ~ 50 μg m^{-3} at the coarse resolution compared to EMEP measurements. In contrast to the majority of the sites during winter, simulated O_3 concentrations at the finer resolution are higher compared to the coarse resolution for several locations in Austria, Hungary and Slovakia (red circle). Similar to winter, O_3 concentrations at the same locations in Italy are also largely overestimated by both model resolutions in summer (~50 μg m^{-3}, Fig. S3.1c). In autumn, the largest overestimates of low O_3 concentrations at the finer resolution occur at northern European locations in the Netherlands and Belgium (Fig. S3.1d - red box).

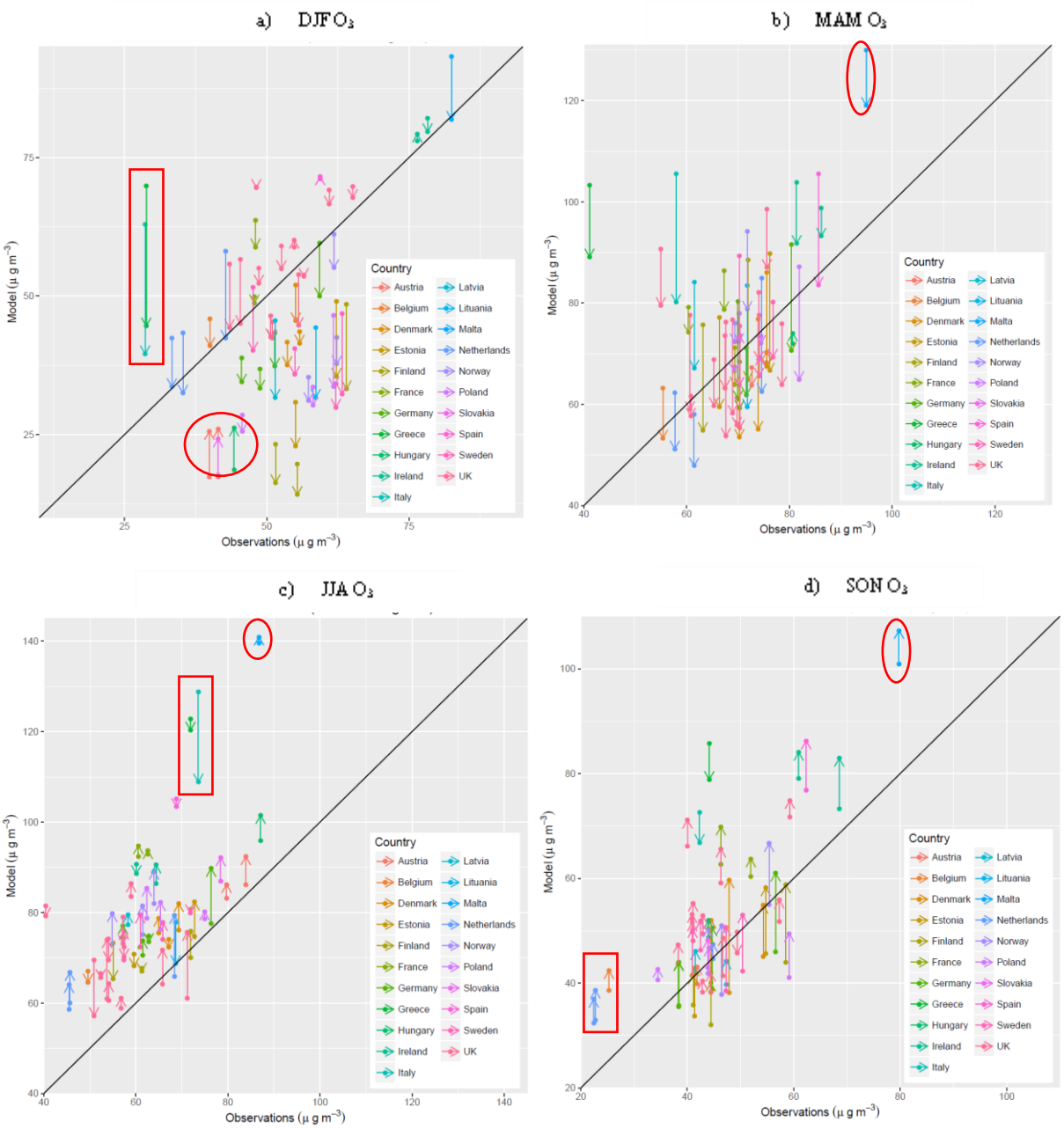

Figure S 3.1: Modelled versus observed seasonal mean O_3 for a) DJF b) MAM c) JJA d) SON 2007 over a subset of 52 sites across the EMEP network as shown in Fig. 3.1. The arrow tails mark O_3 concentrations at the coarse resolution while the arrow heads represent the corresponding O_3 concentrations at the finer resolution.

In spring, summer and autumn, O_3 concentrations simulated at both resolutions in Malta are much higher compared to measurements (~ 40 μgm^{-3}; Fig. S3.1b, c and d -red circle). This is due to the fact that at both resolutions, the grid box covering the Maltese Islands is represented as ocean and not land. Deposition

of O_3 is typically less over the sea than compared to over land, potentially leading to an overestimation in simulated O_3 concentration compared to measurements at this location.

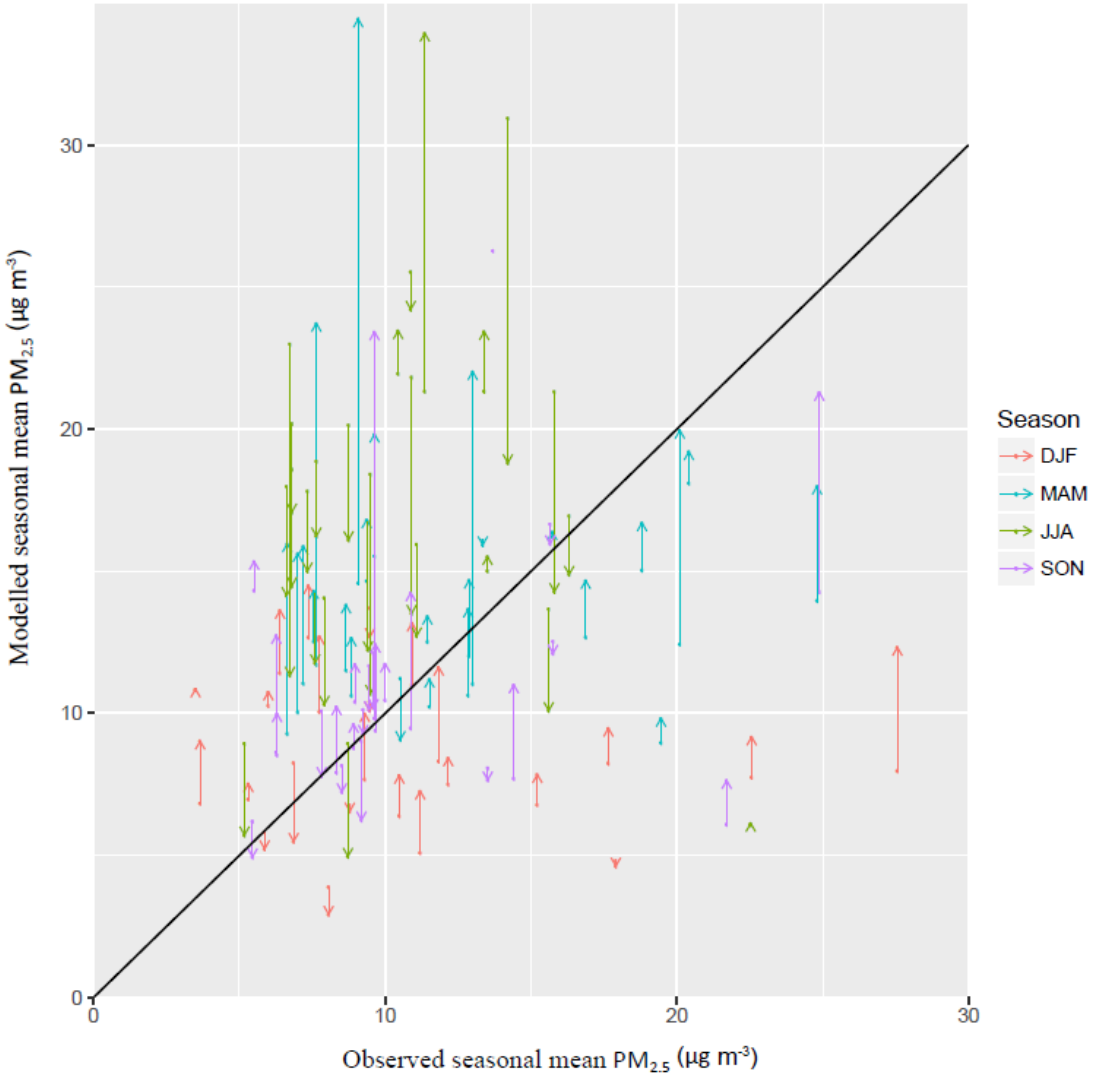

Figure S 3.2: Seasonal mean modelled vs observed $PM_{2.5}$ for 25 sites across the EMEP network for the year 2007. The arrow tails mark $PM_{2.5}$ concentrations at the coarse resolution while the arrow heads represent the corresponding $PM_{2.5}$ concentrations at the finer resolution. The 1:1 line shows agreement between observed and simulated $PM_{2.5}$.

Chapter 4 Mortality associated with O_3 and $PM_{2.5}$ air pollution episodes in the UK in 2006

This chapter is in the review process in the journal Atmospheric Environment, in collaboration with: Prof Ruth M. Doherty, Dr Clare Heaviside, Dr Helen Macintyre, Dr Fiona M. O'Connor, Dr Sotiris Vardoulakis, Dr Lucy Neal and Dr Paul Agnew. I set up and conducted all model simulations, did the analysis and wrote the initial draft. Dr Lucy Neal and Dr Paul Agnew performed the Statistical Post-Processing Technique (SPPO) on simulated concentrations presented in this chapter. My supervisors and other co-authors provided feedback before the manuscript was submitted for publication. Relevant methods text has been moved to Chapter 2.

4.1 Introduction

Air pollution has been identified as one of the top global mortality risk factors by the 2015 Global Burden of Disease (GBD, 2016). Short-term exposure to ozone (O_3) and particulate matter with an aerodynamic diameter less than 2.5 μm ($PM_{2.5}$) has been linked to negative effects on lung function (Chen et al., 2015), increased hospital admissions and mortality (Bell et al., 2005; Ito et al., 2005; Levy et al., 2005; Bell et al., 2006; Atkinson *et al.*, 2014; COMEAP, 2015b; Di *et al.*, 2017) (see Section 1.1).

O_3 is a secondary pollutant which is not directly emitted into the atmosphere but is produced through chemical reactions of precursor emissions, while $PM_{2.5}$ can be directly emitted or formed in the atmosphere via chemical processes. Meteorology is a key factor in determining concentrations of O_3 and $PM_{2.5}$, through its impact on chemical reaction rates via temperature, deposition of pollutants, boundary layer depth, stagnation of air and long-range transport. In the northern mid-latitudes and over the UK, the highest O_3 concentrations typically occur in spring and summer (e.g. Anderson et al., 1996; Derwent et al., 1998; Monks, 2000), while the highest $PM_{2.5}$ levels occur most often in spring, autumn and winter (e.g. AQEG, 2012; Harrison et al., 2012a; Harrison et al., 2012b). However, in anticyclonic weather conditions with low wind speeds, high levels of these two pollutants may occur concurrently (Fischer et al., 2004; Stedman, 2004) and in summer may also be associated with heatwaves (Solberg *et al.*, 2008; Tong et al., 2010; Schnell and Prather, 2017) (see Section 1.7). Analysing the mechanisms responsible for the O_3 build-up over South East England during the August 2003 heatwave using the Community Multiscale Air Quality (CMAQ) model, Francis et al. (2011) found that convergence of westerly and easterly flows over the UK led to trapping of transported O_3 from mainland Europe, thus leading to increased O_3 levels. Using surface and satellite observations, Pope et al. (2016) also found that in the summer period (April-September 2006), anticyclonic conditions with low wind speeds and easterly flows significantly enhanced O_3 concentrations over the UK relative to summer-time average values and further show that the UK Met Office regional air quality model (AQUM) successfully reproduces UK increased O_3 concentrations under such synoptic conditions for this period.

Several studies have examined the impact of short-term exposure to O_3 and particulate matter (PM) on human health during air pollution episodes. Rooney et al. (1998) estimated that 619 extra deaths occurred during the heatwave between July and August 1995 in England and Wales relative to the expected number of deaths based on the 31-day moving average for that period of which 62% of the

excess mortality was attributable to concurrent increases in air pollution. During the first two weeks of August 2003, a major heatwave occurred across much of Europe with temperatures in the UK reaching a record of 38.5 °C associated with a persistent high pressure system over Europe (Johnson et al., 2005; Lee et al., 2006; Solberg et al., 2008; Vieno et al., 2010). Between the 4th and 13th August 2003, an excess of 2,139 deaths above the 1998-2002 average baseline mortality for that period was estimated in England and Wales (16% increase, Johnson et al., 2005). For the first two weeks in August 2003 in England and Wales, an estimated 83 and 29 deaths per day were associated with short-term exposure to daily maximum 8hr running mean (MDA8) O_3 and 24 hour mean PM_{10} (particulate matter with an aerodynamic diameter less than 10 μm), respectively (Stedman, 2004), assuming a 0.6% (O_3) and 0.5% (PM_{10}) increase in mortality for a 10 μg m^{-3} increase in each pollutant (COMEAP, 1998). This represented an increase of 38 (O_3) and 13 (PM_{10}) deaths per day compared with the previous year. Heal et al. (2013) also estimated population burdens attributable to short-term exposure to O_3 in 2003 for all UK regions however, they quote annual values which add up to a total of around 11,500 deaths brought forward. In the Netherlands, between the 31st July and 13th August 2003, Garssen et al. (2005) estimated an excess of around 500 deaths compared to the baseline mortality of an average summer. Also in the Netherlands, Fischer et al. (2004) estimated that between June and August 2003, 15 and 16 daily deaths brought forward were associated with short-term exposure to O_3 and PM_{10}, respectively. Compared to the O_3 and PM_{10}-related deaths brought forward between June and August 2000, approximately 4 and 2 additional daily deaths were brought forward in 2003. The concentration response functions used by Fischer et al. (2004) were of 0.5% and 1.3% increase in mortality for a 10 μg m^{-3} increase in 8hr mean O_3 and weekly mean PM_{10} (Hoek et al., 2000).

In a recent study over the UK, a spring time air pollution episode in 2014 (totalling 10 days) was associated with ~ 60 daily deaths brought forward from short-term exposure to $PM_{2.5}$ when assuming a 1.04% increase in mortality for a 10

µg m^{-3} increase in 24-hour mean $PM_{2.5}$ (Macintyre et al., 2016). Using observed $PM_{2.5}$ levels from other years, it was estimated that the mortality burden was 2.0 to 2.7 times that associated with typical urban background levels of $PM_{2.5}$ at this time of year (Macintyre et al., 2016). As evident from above, differences in health estimates between these previous studies are mainly due to differences in the concentration response function used, as well as the magnitude of pollutant concentrations and the baseline mortality estimates (which vary for each country and from year to year). The method for calculating the excess deaths is also not consistent between the studies and thus a direct comparison between the different studies is not possible.

Under climate change, the risk of heatwaves in the future will likely increase. In the absence of air quality abatement measures, this could give rise to increases in the occurrence of air pollution episodes and UK health burdens associated with short-term exposure to O_3 and $PM_{2.5}$. However, the frequency of air pollution episodes will likely also be affected by climate change through changes in the frequency of large-scale blocking episodes which have been shown to decrease in winter and summer over Europe in the 21st century (Masato et al., 2013).

In this chapter, the focus is on air pollution episodes during a well-known heatwave in summer 2006 during which stagnant weather conditions resulted in high O_3 and $PM_{2.5}$ concentrations across the UK. To identify these episodes, the Daily Air Quality Index (DAQI) (Section 1.4.1) which gives information on the air pollution levels in the UK and provides recommended actions and health advice is used (Defra, 2013b). The index ranges from 'low' (1) to 'very high' (10) and is divided into four bands ('low', 'moderate', 'high' and 'very high'). The DAQI is determined by the highest concentrations of any of the following five pollutants: nitrogen dioxide (NO_2), sulphur dioxide (SO_2), O_3, PM_{10} and $PM_{2.5}$ (uk-air.defra.gov.uk). For this study, episodes were defined based on when the DAQI

reached 'moderate' to 'high' values in the majority of the England regions, Scotland and Wales.

Between the 16th and 28th of July 2006, there was a 4% increase in baseline all-cause mortality (~ 680 excess deaths, Office for National Statistics, 2006) which was lower than that observed in August 2003 (16% increase). During July 2006, elevated temperatures were associated with persistent anticyclonic conditions that favoured the advection of dry air masses over most of northern Europe and the UK (Rebetez et al., 2009). The then UK Health Protection Agency (HPA) used measurements of pollution from fixed site monitors to estimate that between June and July 2006, 11 and 7 additional daily deaths brought forward in England and Wales were associated with increased O_3 and PM_{10} concentrations compared to 2004 (assuming a 0.3% and 0.75% increase in deaths brought forward for a 10 μg m^{-3} increase in O_3 and $PM_{10,}$ respectively) (HPA, 2006). Monitoring of $PM_{2.5}$ concentrations only became routine in the UK since 2008/9 following the 2008 ambient air quality directive (EU, 2008) and thus due to lack of measurement data, the $PM_{2.5}$ health burden has not previously been quantified for this period.

This chapter presents new estimates of health burdens associated with short-term exposure to MDA8 O_3 and daily mean $PM_{2.5}$ for two air pollution episodes in July 2006 using detailed spatio-temporal air pollution modelling for the UK and links to the underlying meteorology for the air pollution episodes in this period. Pollutant concentrations are simulated using the UK Met Office's air quality model (AQUM) at 12 km horizontal grid resolution. The impact on all-cause mortality was calculated both at a national level, also for the nine Government Office Regions (GOR) in England, and for Scotland and Wales (Fig. 2.5; Section 2.3).

The chapter is organised as follows: Section 4.2 describes the modelling framework used to simulate the O_3 and $PM_{2.5}$ pollutant concentrations and the methods used to calculate the health burdens associated with short-term exposure

to MDA8 O_3 and daily mean $PM_{2.5}$ for each region. Section 4.3 presents the observed long-term daily time series of MDA8 O_3 and daily mean $PM_{2.5}$ concentrations for multiple years which are used to identify the air pollution episodes. For both July 2006 episodes the local temporal variability of simulated pollutant concentrations and meteorological drivers of the air pollution episodes are first analysed in Section 4.4.1, then the spatial variability of MDA8 O_3 and daily mean $PM_{2.5}$ concentrations across the UK is analysed in Section 4.4.2. The health impact assessments for the July 2006 air pollution episodes are then presented in Section 4.5 followed by conclusions in Section 4.6.

4.2 Methods

4.2.1 Air Quality in the Unified Model - AQUM

The model used in this chapter is the air quality model AQUM (Air Quality in the Unified Model) which is a limited–area model configuration based on the UK Met Office Unified Model (MetUM, Brown et al., 2012) described in detail in Section 2.2. AQUM has a horizontal resolution of 0.11° × 0.11° (~ 12 km, Savage et al., 2013) with a domain covering the UK and parts of Western Europe. The model has 38 vertical levels from the ground surface up to 39 km (with the lowest model level centred at 20 m). The model includes an interactive aerosol scheme CLASSIC (Coupled Large-scale Aerosol Simulator for Studies in Climate, (Bellouin et al., 2013, 2011; Jones et al., 2001)), which simulates ammonium sulphate and nitrate, fossil-fuel organic carbon (FFOC), mineral dust, soot and biomass burning (BB) aerosol interactively. Biogenic secondary organic aerosols are prescribed from a climatology (Bellouin et al., 2011) and sea salt is calculated over sea points only and does not contribute to PM concentrations over land (Section 2.1.4 and Section 2.2.3). Gas-

phase chemistry is simulated within AQUM by the United Kingdom Chemistry and Aerosol (UKCA) model (Morgenstern et al., 2009; O'Connor et al., 2014). The chemistry scheme used is the Regional Air Quality (RAQ) chemistry scheme, which has 58 chemical species, 116 gas phase reactions and 23 photolysis reactions (Section 2.2.2). Lateral boundary conditions for chemistry and aerosols are derived from the GEMS (Global and regional Earth-system Monitoring using Satellite and in-situ data) and MACC (Monitoring Atmospheric Composition and Climate) global reanalyses fields (Flemming et al., 2009) whilst meteorology is obtained from the UK Met Office Unified Model (MetUM) forecast fields (Section 2.2.4).

Model simulations are performed for the year 2006 (allowing for model spin up) from which hourly pollutant concentrations during the chosen episodes are then extracted, and from which the MDA8 O_3 and daily mean $PM_{2.5}$ are calculated. A statistical post-processing bias correction technique (SPPO) (Section 2.2.5) is applied to correct O_3 and $PM_{2.5}$ simulated concentrations. As outlined above, all simulated O_3 and $PM_{2.5}$ concentrations shown in this study are taken from the lowest model vertical level having a midpoint at 20 m. Bi-linear interpolation is used to extract simulated O_3 and $PM_{2.5}$ concentrations at measurement sites for observation-model comparison. The SPPO technique is applied to the pollutant concentrations quoted in Section 4.4.1 and in the health section of this chapter (Section 4.5) while pollutant concentrations shown in Section 4.4.2 are not bias corrected to enable comparison with the simulated meteorological fields. It is noted that the bias corrected concentrations should agree well with observations as these stations are likely used in the SPPO bias correction process.

4.2.2 Measurement data

Modelled MDA8 O_3 and daily mean $PM_{2.5}$ concentrations for 2006 are evaluated against measurements from the Automatic Urban and Rural Network (AURN) while observed temperatures are evaluated against measurements from the Met Office Integrated Data Archive System (MIDAS) network (Section 2.3). Details on the sites used for model evaluation can be found in Section 2.3. Site locations from the AURN and MIDAS networks are illustrated in Fig. 4.3 and Fig. 4.5, respectively.

4.2.3 Heath impact assessment

Estimated attributable fraction of mortality and mortality burden associated with short-term exposure to MDA8 O_3 and daily mean $PM_{2.5}$ are calculated for each of the nine GOR for England, and for Scotland and Wales (shown in Fig. 2.5) following equations 2.5 to 2.8 Section 2.4.2.

The CRFs used in this chapter for short-term exposure to MDA8 O_3 is of 0.34 % (95% confidence interval (CI): 0.12%, 0.56%) per 10 μg m^{-3} increase in MDA8 O_3, and for short-term exposure to $PM_{2.5}$-related health impacts a CRF of 1.04 % (CI: 0.52%, 1.56%) per 10 μg m^{-3} increase in 24-hr mean $PM_{2.5}$ is used (Table 1.2; Section 2.4.2) . As limited evidence is available for a threshold below which no adverse effects for short-term exposure to MDA8 O_3 and daily mean $PM_{2.5}$ exist, no threshold was applied to pollutant concentrations (Section 1.4.4).

To quantify the deaths brought forward associated with air pollution during the episodes the 'typical' air pollution related daily deaths brought forward that would have occurred in the absence of an air pollution episode are first estimated. This is done by replacing the modelled pollutant concentration which varies for

each day of the air pollution episode (x_{ij}) in equation 2.8 with the summer mean pollutant concentration (following the method in Macintyre et al. 2016), which is assumed to be representative of air pollution levels when an episode does not occur. All other variables are left unchanged, therefore when calculating the 'typical' daily deaths, the AF_{ir} for each day is the same, with baseline mortality (BM) still varying daily. The excess deaths are then estimated by subtracting the 'typical' estimated deaths brought forward from the episode estimated deaths brought forward.

4.3 Identification of air pollution episodes from observations

Measured MDA8 O_3 and daily mean $PM_{2.5}$ concentrations from 2005 to 2007 (inclusive) at the Rochester Stoke site (rural background; Section 2.3) are shown in Fig. 4.1. The seasonal profile of MDA8 O_3 concentrations is similar for all three years, with the highest concentrations occurring in the summer months and the lowest in winter (Fig. 4.1a). Superimposed on this seasonal cycle are daily variations in MDA8 O_3. A seasonal cycle is less evident for daily $PM_{2.5}$ concentrations between 2005 and 2007 (Fig. 4.1b), although a background level of 5-10 μg m^{-3} is evident with substantial day-to-day variability. In 2007, $PM_{2.5}$ peak levels are highest in spring and winter, whilst in 2005 and 2006 concentrations show highest peaks in autumn (Fig. 4.1b). The analysis is focused on periods during 2006 using two criteria to define air pollution episodes: a) high MDA8 O_3 and daily mean $PM_{2.5}$ concentrations occurring concurrently and b) a DAQI (Section 1.4.1) reaching a 'moderate' or 'high' level over the majority of the regions across the UK. This resulted in the selection of two 5-day periods from the 1st -5th July 2006 and from the 18th -22nd July 2006, which are described below.

In July 2006, measured MDA8 O_3 concentrations reached 150 μg m^{-3} on 2nd July 2006 at Rochester Stoke (Fig. 4.1a) which are higher compared to adjacent years. Daily mean $PM_{2.5}$ concentrations at the same station also show peaks occurring during July 2006 (up to 26 μg m^{-3} on the 4th July, Fig. 4.1b). Similarly peaks for MDA8 O_3 and daily mean $PM_{2.5}$ concentrations during this same period were noted at the London Bloomsbury and Harwell stations (Fig. S4.1 Section 4.7). $PM_{2.5}$ concentrations of 0 μg m^{-3} in Fig. 4.1b and Fig. S4.1 indicate missing data and not actual concentrations of 0 μg m^{-3}.

Between the 1st and 5th of July 2006 the DAQI reached a 'moderate' or 'high' level in 96% of the regions in England, Scotland and Wales and in 88% of the regions between the 18th and the 22nd of July 2006 (uk-air.defra.gov.uk). This suggests that overall, more extensive high pollutant concentrations occurred in the first episode compared to the second episode. In particular, in the south east region, the DAQI reached a 'high' level during most days of the first episode and a 'moderate' level during most of the second episode. The only day during the second episode that had a higher DAQI across the regions compared to the first episode was the 19th of July when the DAQI reached a 'high' level (8; Section 1.4.1) in three regions (Eastern England, London and West Midlands).

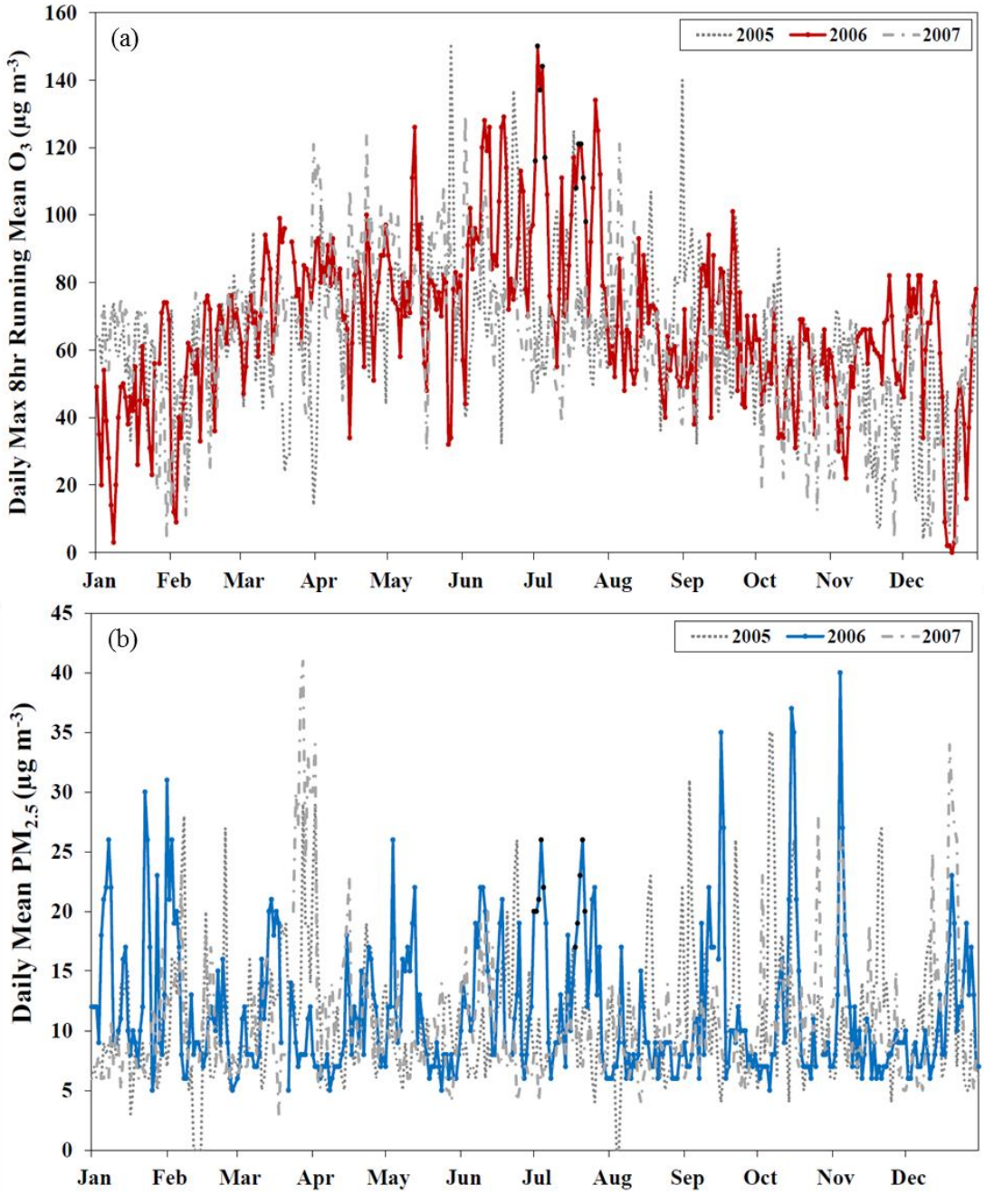

Figure 4.1: (a) Daily maximum 8-hr running mean (MDA8) O_3 and (b) daily mean $PM_{2.5}$ at the Rochester Stoke AURN rural background station from 2005 (dotted), 2006 (red for O_3 and blue for $PM_{2.5}$), and 2007 (dot-dashed). Black points mark the two 5-day air pollution episode days for July 2006 (1^{st}-5^{th} July and 18^{th}-22^{nd} July 2006).

4.4 Meteorological factors contributing to the air pollution episodes

4.4.1 Temporal variability of pollutants and meteorology during the pollution episodes

Simulated (original and bias corrected - as described in Section 4.2.1) and observed MDA8 O_3 and daily mean $PM_{2.5}$ concentrations for July 2006 are shown in Fig. 4.2a for the Rochester Stoke site (rural background). Using the raw model output for both episodes, MDA8 O_3 concentrations are underestimated (mean bias = -10.72 µg m^{-3} and r = 0.67; Table 4.1) while daily mean $PM_{2.5}$ concentrations are overestimated (mean bias of 26.29 µg m^{-3} and r = 0.67; Table 4.1). When applying the SPPO bias correction technique (Section 2.2.5), the temporal variability of MDA8 O_3 and daily mean $PM_{2.5}$ concentrations is largely unaltered with peaks captured well during both episodes (Fig. 4.2a) and with mean bias errors reducing to -2.76 µg m^{-3} (r = 0.89) and 12.03 µg m^{-3} (r = 0.81), respectively (Table 4.1).

Table 4.1: Statistics comparing daily mean model and observed pollutant concentrations and meteorological variables for both original (Raw) and bias corrected (SPPO – Statistical Post-Processing technique) model output averaged over the period 1st -5th July and 18th to 22nd July at Rochester Stoke.

		Bias	R
MDA8 O_3 ($\mu g\ m^{-3}$)	Raw	-10.72	0.67
	SPPO	-2.76	0.89
24-hr mean $PM_{2.5}$ ($\mu g\ m^{-3}$)	Raw	26.29	0.67
	SPPO	12.03	0.81
24-hr mean temperature (°C)	Raw	0.85	0.69
24-hr mean wind direction (°)	Raw	-7.59	0.95
24-hr mean wind speed ($m\ s^{-1}$)	Raw	-0.44	0.85

Figure 4.2b shows simulated and observed daily mean meteorological variables (surface temperature, wind speed and wind direction) during July 2006 at the Rochester Stoke site. Daily variations of temperature, wind direction and wind speed are well captured by the model during both episodes, with r values equal to 0.69, 0.95 and 0.85 respectively (N.B. measured temperatures are taken from St East Malling which is approximately 9 miles from Rochester Stoke). However, the magnitudes of daily mean wind speed is generally underestimated (mean bias = -0.44 m s^{-1}; Table 4.1), while temperature is generally overestimated (mean bias = 0.85 °C; Table 4.1). At Rochester Stoke, wind speeds during both air pollution episodes are generally low (between ~2 and ~ 4 m s^{-1}; Fig. 4.2b) compared to the rest of July, though wind speeds are fairly low throughout this month (not exceeding 7 m s^{-1}; Fig. 4.2b). Compared to the rest of July, daily mean temperatures are higher during the two episodes as well as at the end of the month (ranging from ~20 °C to ~27 °C; Fig. 4.2b). During the first episode, measured and simulated daily mean wind directions ranged from ~ 60° (north east; Fig. 4.2b) to ~ 200° (south west; Fig. 4.2b). In the later July episode wind directions ranged from ~ 60° to ~ 90° for the first two days (north east to east; Fig. 4.2b) and from ~ 140° to ~ 230° for the last three days (south east to south west; Fig. 4.2b). However the prevailing wind during both episodes is from a north easterly and easterly direction.

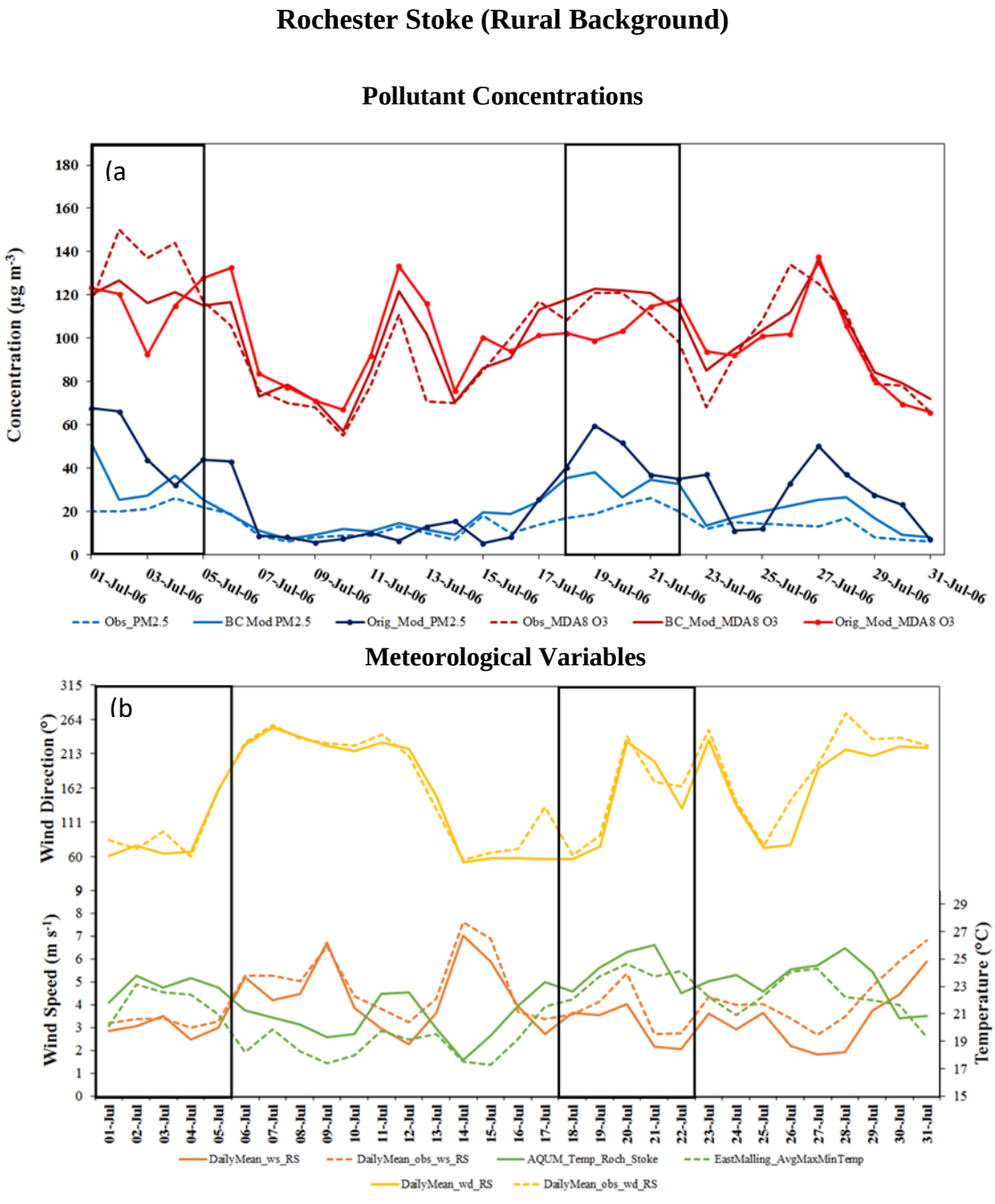

Figure 4.2: Daily time series during July 2006 of modelled (solid lines) and observed (dashed lines) a) $PM_{2.5}$ (blue) and MDA8 O_3 (red) b) wind direction (degrees are taken clockwise starting from the north - yellow), wind speed (orange) and temperature (green) at the rural background AURN station in Rochester Stoke (observed temperatures were obtained from the nearest MIDAS station to Rochester Stoke which is at East Malling.) Black boxes represent the two 5-day air pollution episodes in July 2006 (1^{st}-5^{th} July and 18^{th}-22^{nd} July)). Solid lines with dots indicated the original simulated concentrations while the solid lines with no dots show the bias-corrected concentrations using the SPPO technique.

4.4.2 Spatial variability of O_3 and $PM_{2.5}$ concentrations and meteorology during the pollution episodes across the UK

The spatial distributions of simulated surface MDA8 O_3 and daily mean $PM_{2.5}$ averaged for all of July, and for the two 5-day air pollution episodes are shown in Fig. 4.3 (concentrations shown here are not bias-corrected to enable comparison with meteorology; however spatial patterns for bias-corrected pollutant concentrations are similar (Fig. S4.2 Section 4.7). Simulated MDA8 O_3 concentrations during all three averaging periods generally compare well with observations (to within 15 μg m^{-3}; Fig 4.3a-c). However, simulated MDA8 O_3 concentrations at London Bloomsbury are higher than observed concentrations during the first episode (by ~ 47 μg m^{-3}, Fig. 4.3b). July mean MDA8 O_3 concentrations range between ~ 80 μg m^{-3} in Scotland to ~ 120 μg m^{-3} in south eastern and eastern England (Fig. 4.3a). For the first episode, simulated MDA8 O_3 concentrations are highest in the west of England with concentrations reaching ~ 180 μg m^{-3} in Wales and up to ~ 210 μg m^{-3} in South West England (Fig. 4.3b). Simulated MDA8 O_3 concentrations during the second episode are lower reaching ~ 150 μg m^{-3} in the south of England and also less variable across the UK than for the first episode (Fig. 4.3c) as noted for the DAQI in Section 4.3.

Simulated daily mean $PM_{2.5}$ concentrations during July and the second episode are generally in agreement with observations at Harwell, but are overestimated over the London Bloomsbury and Rochester Stoke locations during the two episodes (Fig 4.3 d-f). Neal et al. (2017) also find an all year round small positive bias in simulated $PM_{2.5}$ concentrations for a 5-year period at two background observational sites. For all three periods shown, higher daily mean $PM_{2.5}$ concentrations are simulated over England and Wales compared to Scotland with a stronger North-South spatial gradient occurring during the air pollution episodes compared to July. Simulated daily mean $PM_{2.5}$ concentrations are highest

during the first episode reaching ~ 45 µg m^{-3} in the west of England (Fig. 4.3e). The spatial pattern of simulated $PM_{2.5}$ concentrations in the second episode differs from that found in the first episode. Simulated daily mean $PM_{2.5}$ concentrations are higher in south east England compared to the west of England for this later episode (~ 45 µg m^{-3} compared to ~ 20 µg $m^{-3,}$ Fig. 4.3f)

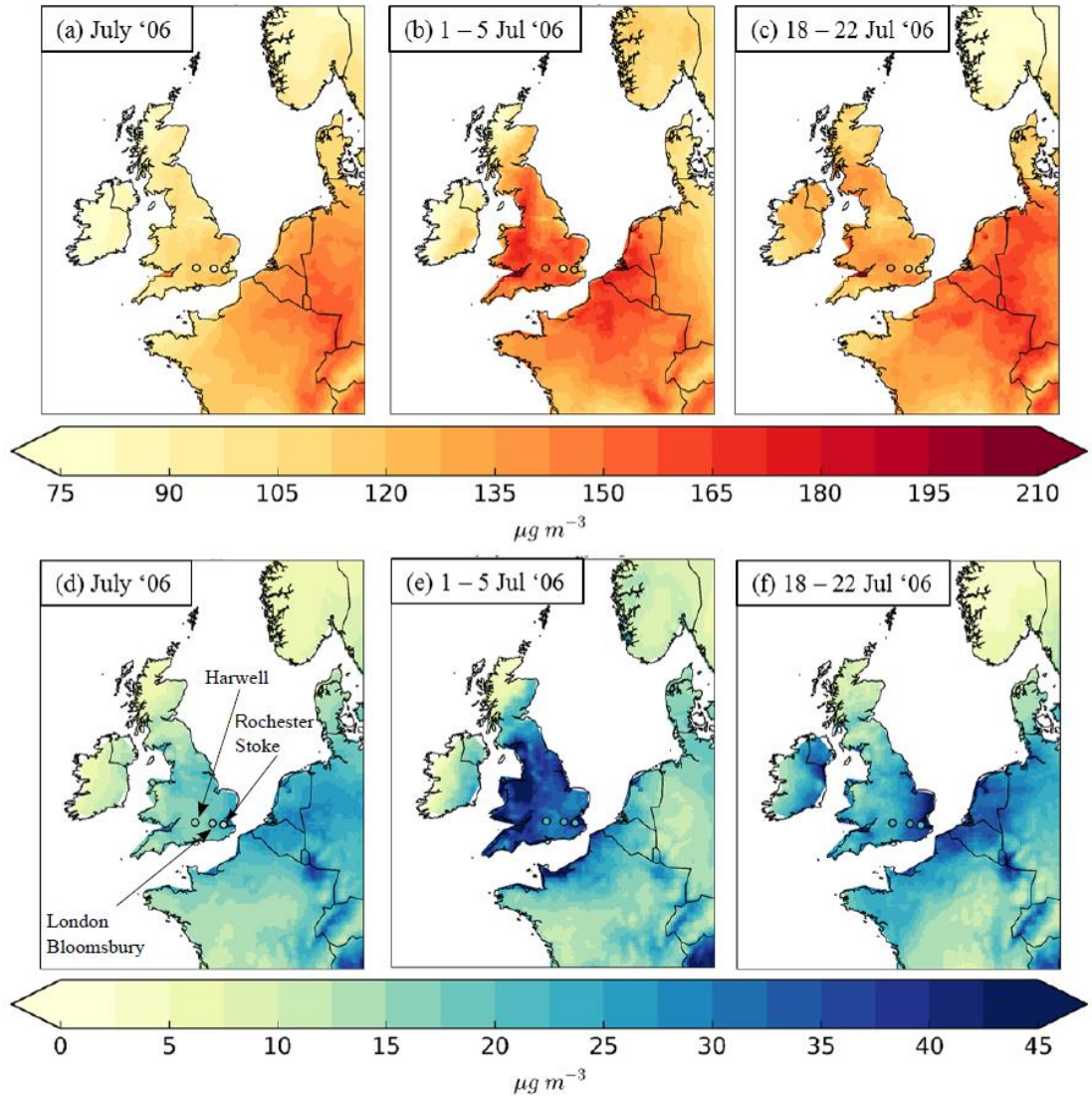

Figure 4.3: Simulated daily maximum 8-hr running mean O_3 concentrations for (a) July mean, (b) 1-5 July mean and (c) 18-22 July 2006 mean and simulated daily mean $PM_{2.5}$ concentrations for the same time periods (d, e and f) (NB concentrations shown here are not bias corrected to enable comparison with meteorology; however spatial patterns are similar (refer to Supplement)). The circles in each plot are coloured with measured data of the respective pollutant at 3 AURN sites - Rochester Stoke, Harwell and London Bloomsbury.

Many factors can contribute to high MDA8 O_3 and daily mean $PM_{2.5}$ concentrations during these two episode periods. First the spatial variations in meteorology (surface wind direction, wind speed, pressure and temperature) within the model domain are presented. Wind direction and wind speeds for all model land grid boxes across the UK are illustrated in Fig 4.4. For July 2006, the simulated prevailing hourly wind direction is from the south west (~55% of the time) with a mean wind speed of 1.6 m s^{-1} (Fig. 4.4a). Simulated mean wind speeds during the two episodes are of similar magnitude to the whole July period. However, the dominant wind direction varies between the two episodes. Over most of the UK easterly and south easterly winds occur during the first episode (~32% and ~22% of the time, respectively; Fig 4.4b), whilst for the later episode south easterly and southerly winds are more prevalent (~52% and ~36% of the time, respectively; Fig 4.4c). Thus light winds bringing air from continental Europe are characteristic of both the episodes in July 2006. Note that the general wind direction across the UK differs slightly from that at the Rochester Stoke location where the prevailing wind direction is north easterly and easterly during both episodes (Section 4.4.1). The different wind direction for Rochester Stoke (Section 4.4.1) might be linked to the

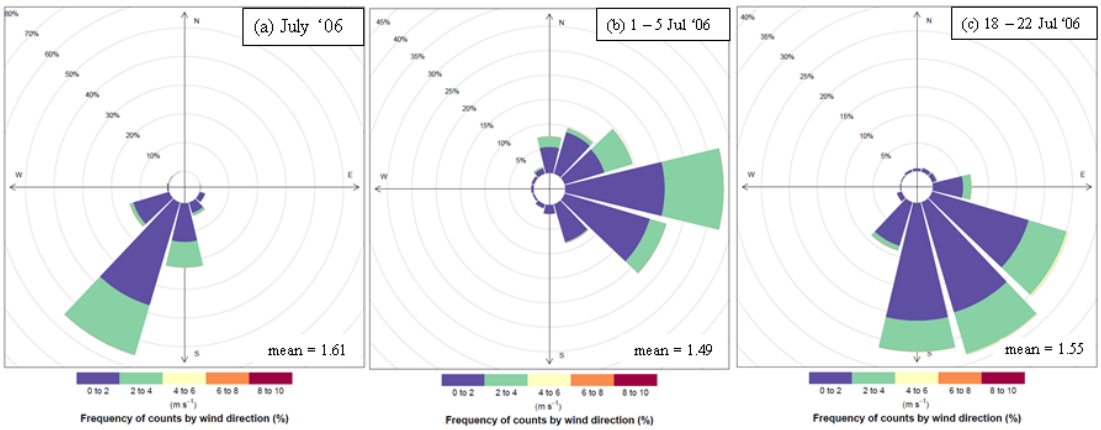

Figure 4.4: Wind roses showing the frequency of hourly wind directions for each land grid box in the UK for (a) July 2006, (b) 1st – 5th July, (c) 18th- 22nd July 2006. Colours indicate the wind speed.

coastal location of this site.

Simulated spatial variations in daily mean surface pressure, wind direction and temperature are shown in Fig. 4.5. In July light winds of a south to south-westerly direction over southern and central England are indicated by the widely spaced simulated pressure contours and wind vectors in Fig. 4.5a and 4.5d, respectively. During this same period, anticyclonic conditions are simulated over northern Europe (> 1020 hPa, Fig. 4.5a). As discussed above, during the first episode, a change in wind direction compared to the July mean can be noted with winds blowing from an easterly and south easterly direction over most of the UK (Fig. 4.5e, Fig 4.4b). Also, higher pressures over central and northern UK (>1019 hPa) occur compared to the July mean with the high pressure centred over Norway and Sweden (Fig. 4.5b). A high pressure system is also characteristic of the second air pollution episode, but in this case is centred over the North Sea (Fig. 4.5c, f.). The high pressure simulated during both episodes leads to light winds and hence favourable stagnant weather conditions for high pollutant concentrations as well as slow transport of pollution from the European continent. Other possible reasons for high pollutant concentrations may include lack of cloud and precipitation, enhancing photolysis as well as reducing wet deposition. Using the same model Pope et al. (2016) also found O_3 concentrations to be high under anticyclonic and south-easterly conditions for the summer (Apr-Sept) 2006. High temperatures are also associated with anticyclonic conditions as discussed in Section 4.4.1. An increase in simulated daily mean surface temperatures during the two episodes compared to the July mean can be clearly seen (Figs. 4.5g-i). Measured daily mean surface temperatures from three MIDAS stations are also shown as coloured circles (Upper Lambourn, St James Park London and East Malling). Good agreement can be seen between modelled and observed July mean temperatures (to within 0.5 °C) at the St James Park station in Greater London. However, over the other two locations, July-mean temperatures are overestimated by the model by about 1°C for the Upper Lambourn and East Malling sites. Simulated July mean temperatures range

from 15°C to 23°C and are highest in south east England (Fig. 4.5g). While the spatial distribution of simulated temperatures during the two episodes is similar to those in July (low temperatures in the north and high temperatures in the south), daily-mean values are generally between 16°C and 24°C for the first episode and range between 19°C and 26°C during the later episode (Fig. 4.5h and 4.5i). These higher temperatures in the central and south eastern England may partly explain the higher simulated MDA8 O_3 concentrations towards the south east of England for the July mean and two episodes as temperature and sunlight promote photochemical formation of O_3 (Fig. 4.5). $PM_{2.5}$ concentrations may also be influenced by temperature (c.f. Fig. 4.3d-f; Fig 4.56g-i). Higher temperatures may lead to increased sulphate aerosol formation due to increased reaction rates; however levels of other secondary components of $PM_{2.5}$ (e.g. nitrate aerosol) may be reduced due to increased partitioning from the aerosol phase into the gas phase (Doherty et al., 2017; Fiore et al., 2012). Overall, anticyclonic conditions of light winds, high temperatures, combined with prevailing easterly and south easterly wind directions contribute to high MDA8 O_3 and daily mean $PM_{2.5}$ levels during the two episodes, likely due to local emissions trapping as well as slow transport of both primary and secondary pollution from the European continent.

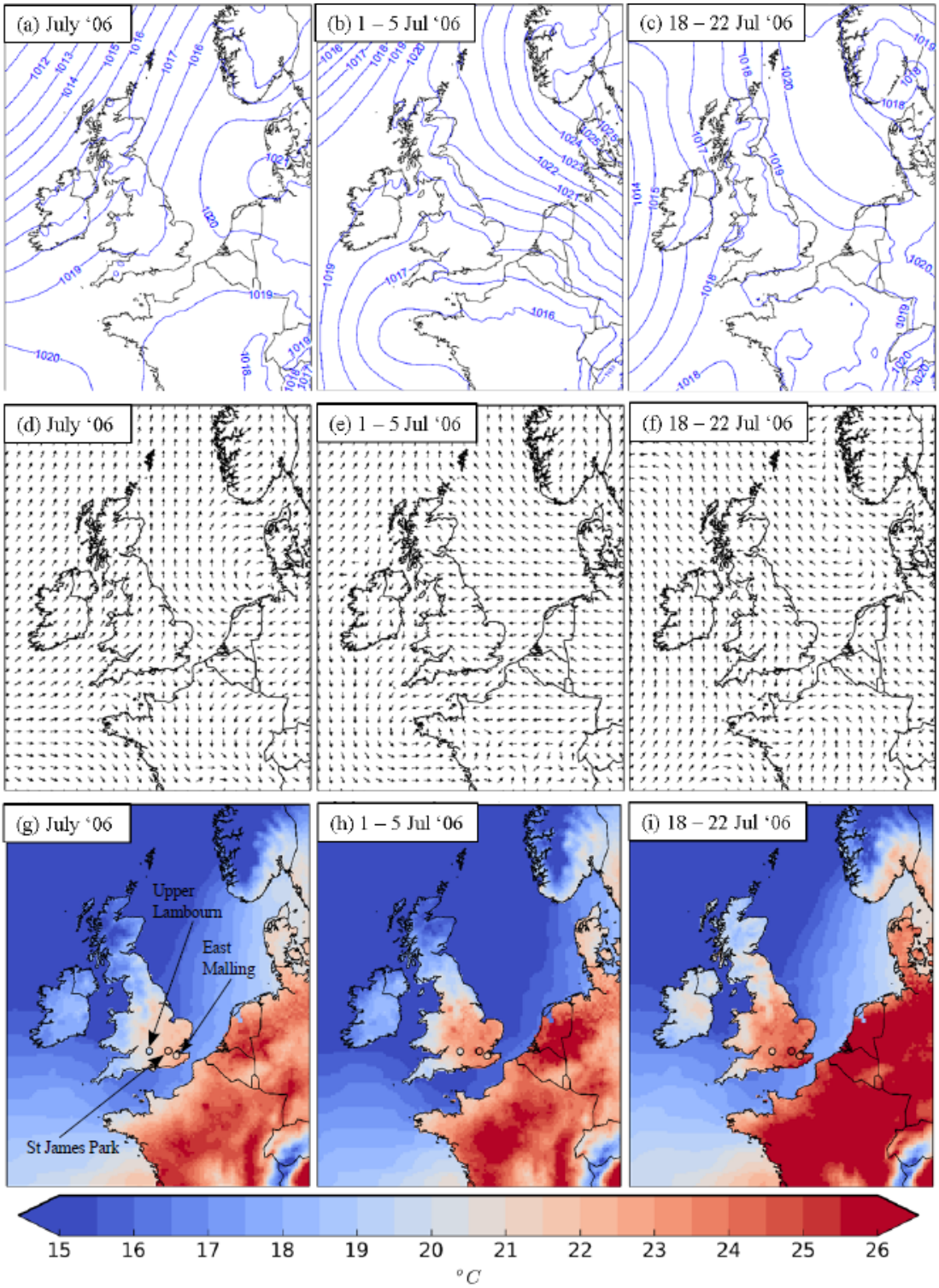

Figure 4.5: Daily mean air pressure at mean sea level (top panel), wind vectors (middle panel) and surface temperature (bottom panel) averaged for all of July (left column), 1st to 5th July (middle column) and 18th to 22nd July (right column). Measured levels of daily mean temperature averaged for the same time periods from three MIDAS stations (St James Park, East Malling and Upper Lambourn) are shown in coloured circles (bottom panel)

4.5 Mortality from short term exposure to O_3 and $PM_{2.5}$

In this section the attributable fraction of mortality and mortality burdens associated with short-term exposure to MDA8 O_3 and daily mean $PM_{2.5}$ concentrations using bias-corrected population-weighted pollutant concentrations for the two episodes in July 2006 are presented (refer to Fig. S4.1) at the national and for each GOR region in England, Scotland and Wales (Section 4.2.3). For each region, the total population and the population-weighted MDA8 O_3 concentrations for the summer (June-July-August, JJA) and for the two episode periods together with the percentage of all-cause mortality and the estimated number of deaths brought forward are shown in Table 4.2. In summer, population-weighted simulated MDA8 O_3 concentrations range from ~75 μg m^{-3} in Scotland to ~ 96 μg m^{-3} in east England (Table 4.2). In contrast, MDA8 O_3 concentrations range from ~ 98 μg m^{-3} to ~ 155 μg m^{-3} in the first episode (for Scotland and South West England, respectively; Table 4.2) and from ~ 112 μg m^{-3} to ~ 147 μg m^{-3} in the second episode (for Scotland and East England, respectively; Table 4.2). These regions having the highest simulated population-weighted bias corrected MDA8 O_3 concentrations are the same regions that have the highest uncorrected pollutant concentrations as discussed in Section 4.4.2. The south west and the east of England regions are also the regions with the highest percentage of all-cause mortality attributed to air pollution (AF) during the first and second episode, respectively (5.16% and 4.87%; refer to Table S4.1 in Section 4.7 for confidence intervals for all the regions) as this value only depends on the population-weighted pollutant concentration which is highest in these regions (refer to equation 2.6 to 2.8 in Section 2.4.2). The AF due to short-term exposure to MDA8 O_3 is higher for the first compared to second episode which again reflects the higher concentrations discussed in Section 4.4.2.

The total health burden associated with short-term exposure to MDA8 O_3 summed over all the regions for the first and second episode is similar: 69 and 70

daily deaths brought forward, respectively (Table 4.2; refer to Table S4.1 for confidence intervals for all the regions). However, as discussed in Section 4.4.2 higher MDA8 O_3 concentrations are simulated during the first compared to the second episode. The calculation to determine the health burden does not depend solely on pollutant concentrations but also depends on the population of the region as well as the baseline mortality. For each region, the all-cause baseline mortality in the second episode is higher compared to that in the earlier episode (by up to 17 daily deaths in the West Midlands) which may be linked to higher temperatures over that period. Therefore differences in baseline mortality between the two episodes appear to balance differences in simulated MDA8 O_3 concentrations when calculating the mortality attributable to short-term exposure to MDA8 O_3 (as described in equation 2.5 Section 2.4.2). The regions with the highest health burden during both air pollution episodes are the North West and South East England (Table 4.2) which is due to a combination of high pollutant concentrations and a larger total population in these two regions (Table 4.2).

Table 4.2: GOR regions for England, Scotland and Wales and their populations together with the regional bias corrected population-weighted daily maximum 8-hour O_3 concentrations for summer (JJA) and averaged between the 1st-5th July and the 18th-22nd July 2006. For each of the episodes the percentage of all-cause mortality and the daily deaths brought forward are also included.

		JJA 2006	1-5 July 2006			18-22 July 2006		
				Daily deaths brought forward			Daily deaths brought forward	
Region	Pop. (1000s)	MDA8 O_3 ($\mu g\ m^{-3}$)	MDA8 O_3 ($\mu g\ m^{-3}$)	Percent of all-cause	Number	MDA8 O_3 ($\mu g\ m^{-3}$)	Percent of all-cause	Number
East Midlands	4356	86.2	137.0	4.57%	5	135.6	4.51%	5
East England	5591	96.3	148.3	4.94%	7	147.1	4.87%	7
London	7237	89.7	136.8	4.58%	7	139.6	4.65%	7
North East	2433	77.4	123.0	4.05%	3	119.6	3.95%	3
North West	6637	77.8	146.6	4.80%	9	125.6	4.26%	9
Scotland	4802	74.7	98.0	3.35%	4	112.1	3.74%	5
South East	8084	94.1	146.5	4.86%	10	144.5	4.81%	10
South West	4930	90.3	155.4	5.16%	7	134.0	4.56%	7
Wales	2811	86.2	152.4	5.09%	4	138.1	4.63%	4
West Midlands	5323	84.0	148.0	4.91%	7	137.2	4.59%	7
Yorkshire and The Humber	4967	78.7	126.5	4.20%	5	119.9	4.03%	5
Total					69			70

The population-weighted daily mean $PM_{2.5}$ concentrations during summer range from 9.4 μg m^{-3} in Scotland to 14.7 μg m^{-3} in east midlands and east England. Higher concentrations occur during the first and second episode with concentrations range from 17 μg m^{-3} to 38 μg m^{-3} (in Scotland and North West; Table 4.3) and from 15.4 μg m^{-3} to 28.5 μg m^{-3} (in Scotland and East England; Table 4.3), for the first and second episodes, respectively. The percentage of attributable all-cause mortality is highest in the North West and East England regions for the first (3.9%) and second episode (2.9%), respectively, again reflecting high $PM_{2.5}$ concentrations in these regions (Table 4.3; refer to Table S4.2 in Section 4.7 for confidence intervals in mortality estimates for all the regions). Due to higher population-weighted $PM_{2.5}$ concentrations during the first episode compared to the later episode, the percentage of attributable all-cause mortality is overall also higher during the first episode. The total number of deaths brought forward attributable to short-term exposure to $PM_{2.5}$ during the first and second episodes are 43 and 36 daily deaths brought forward, respectively (Table 4.3). In this case differences in $PM_{2.5}$ concentrations between the two episodes outweigh differences in baseline mortality when calculating the mortality attributable to short-term exposure to $PM_{2.5}$ thus resulting in a higher number of estimated deaths brought forward in the first compared to the second episode (as described in equation 2.5 Section 2.4.2). The regions having the highest number of deaths brought forward during the first and second episode are again the North West and South East regions, respectively as high $PM_{2.5}$ concentrations and a large population density coincide.

Table 4.3: GOR regions for England, Scotland and Wales and their populations together with the regional bias corrected population-weighted daily mean $PM_{2.5}$ concentrations for summer (JJA) and averaged between the 1st-5th July and the 18th-22nd July 2006. For each of the episodes the percentage of all-cause mortality and the daily deaths brought forward are also included.

		JJA 2006	1-5 July 2006			18-22 July 2006		
				Daily deaths brought forward			Daily deaths brought forward	
Region	Pop. (1000s)	Mean Daily $PM_{2.5}$ ($\mu g\ m^{-3}$)	Mean Daily $PM_{2.5}$ ($\mu g\ m^{-3}$)	Percent of all-cause	Number	Mean Daily $PM_{2.5}$ ($\mu g\ m^{-3}$)	Percent of all-cause	Number
East Midlands	4356	14.7	27.5	2.88%	3	21.9	2.27%	3
East England	5591	14.7	23.2	2.39%	3	28.5	2.92%	4
London	7237	14.6	22.5	2.25%	3	26.8	2.72%	4
North East	2433	13.3	28.2	2.81%	2	19.1	2.02%	1
North West	6637	14.2	38.0	3.91%	7	20.5	2.13%	4
Scotland	4802	9.4	17.0	1.72%	2	15.4	1.63%	2
South East	8084	14.3	24.8	2.50%	5	24.9	2.54%	5
South West	4930	14.3	33.8	3.43%	5	24.9	2.62%	4
Wales	2811	13.3	36.1	3.72%	3	23.2	2.42%	2
West Midlands	5323	14.1	32.4	3.28%	4	20.0	2.04%	3
Yorkshire and The Humber	4967	14.6	30.0	3.11%	4	21.3	2.16%	3
Total					43			36

Using the summer mean (JJA) pollutant concentrations discussed above as 'typical' concentrations that would occur in the absence of an air pollution episode, it is estimated that the mortality burden associated with short-term exposure to MDA8 O_3 in the first and second episode is 38% and 36% higher than the 'typical' summer mean estimate, respectively (Table 4.4; refer to Section 4.2.3). Similarly, it is found that the mortality burden associated with short-term exposure to daily mean $PM_{2.5}$ during the first and second episode is 56% and 39% higher than if the concentrations were more similar to those occurring in the absence of an air pollution episode (Table 4.4; regional estimates for 'typical' concentrations can be found in Tables S4.1 and S4.2; Section 4.7).

Estimated health burdens attributable to exposure to MDA8 O_3 during both episodes are lower than estimates for the first two weeks of August 2003 derived by Stedman (2004) (~70 compared with 88 daily deaths). This difference is due primarily to the use of a concentration response function by Stedman (2004) that is about double that used in this study (0.6% compared with 0.34% for a 10 μg m^{-3} increase in MDA8 O_3) as well as different baseline mortality rates as discussed previously. The $PM_{2.5}$-related estimates presented in this chapter differ from estimates of Macintyre et al. (2016) of approximately 59 daily deaths brought forward from short-term exposure to $PM_{2.5}$ during a total of 10 days across the UK in spring 2014 (compared to 43 and 36 daily deaths brought forward during the first and second episode in this study). The $PM_{2.5}$-related concentration response function used in this chapter and that of Macintyre et al. (2016) is the same, however population-weighted daily mean $PM_{2.5}$ concentrations during the air pollution episode studied in Macintyre et al. (2016) reach a mean concentration of 50 μg m^{-3}, which is approximately 12 μg m^{-3} higher than the highest mean daily population-weighted $PM_{2.5}$ concentrations observed during the first episode in North West England in this study (38 μg m^{-3}, Table 4.3). $PM_{2.5}$ concentrations for both July episodes in this study are unusually high compared to other years (Figure 4.1b for 2005 and 2007) and although slightly lower, are of similar magnitude to

those reported in spring 2014 by Macintyre et al. (2016). Hence the health burden estimated in this chapter for the July 2006 episodes is somewhat comparable to the $PM_{2.5}$-related health burden found by Macintyre et al. (2016) in spring 2014.

Table 4.4: Estimated deaths brought forward from short-term exposure to 'typical' summer time population-weighted MDA8 O_3 and daily mean $PM_{2.5}$ concentrations compared to the population-weighted pollutant concentrations simulated between the 1st-5th July and the 18th-22nd July 2006. Excess deaths brought forward from short-term exposure to MDA8 O_3 and daily mean $PM_{2.5}$ are calculated as a percentage using (((Episode Estimate – Typical Estimate)/Episode Estimate) * 100)

			Pollutant Concentrations ($\mu g\ m^{-3}$)	Daily Deaths Brought Forward		
				Number	Percentage of all-cause	Excess (%)
1-5 July 2006	MDA8 O_3	Episode	138.0	69	4.59	
		Typical *	85.0	43	2.85	38
	$PM_{2.5}$	Episode	28.5	43	2.91	
		Typical *	13.8	19	1.28	56
18-22 July 2006	MDA8 O_3	Episode	132.1	70	4.42	
		Typical *	85.0	45	2.85	36
	$PM_{2.5}$	Episode	22.4	36	2.32	
		Typical *	13.8	22	1.42	39

*** Simulated population-weighted summer mean (JJA) concentrations for 2006 for each region are used as 'typical' concentrations. This is kept constant for each day of the episode.**

4.6 Conclusions

Air pollution episodes are typically driven by stagnant weather conditions. Between the 1st - 5th July and the 18th - 22nd July 2006, persistent anticyclonic conditions with mean sea-level pressures ~ 1020hPa, light winds, high temperatures, and prevailing winds from the East and South East led to high MDA8 O_3 and daily mean $PM_{2.5}$ levels, likely emanating from both local emissions trapping and processing, and slow transport of pollution from continental Europe.

Over the two episodes in July 2006, the estimated total mortality burden associated with short-term exposure to MDA8 O_3 is around 70 daily deaths brought forward summed across the UK. By using summer 2006 (JJA) population-weighted simulated MDA8 O_3 concentrations as 'typical' concentrations during this time of year, the health burden is estimated to be 38% and 36% higher during the first and second episode, respectively compared to the summer average. The estimated health burden associated with short-term exposure to $PM_{2.5}$ varies between the two episodes resulting in 43 and 36 daily deaths brought forward during the first and second episode, respectively. Using $PM_{2.5}$ concentrations representative of the summer average, the health burden is estimated to be 56% and 39% higher than if the pollution levels represented typical season-mean concentrations.

The regions with the highest percentage of all-cause mortality (AF) associated with short-term exposure to MDA8 O_3 and daily mean $PM_{2.5}$ varied between the episodes, as this depends on population-weighted pollutant concentrations. During the first episode in July 2006 the regions with the highest simulated population-weighted MDA8 O_3 and daily mean $PM_{2.5}$ concentrations and thus the highest AF due to exposure to MDA8 O_3 and daily mean $PM_{2.5}$ were the South West and North West regions. During the second air pollution episode, MDA8 O_3 and daily mean $PM_{2.5}$ concentrations were highest in the East of England

resulting in the highest AF in this region. In contrast, the estimate mortality also depends on the baseline mortality and thus for all episodes, regions with the greatest total population which coincided with relatively high pollutant concentrations had the highest mortality estimates (e.g. North West and South East regions).

Results in this chapter show that episodes of high MDA8 O_3 and daily mean $PM_{2.5}$ such as those presented in this study can lead to an increase in deaths brought forward up to double that expected from typical concentrations over the same period.

In this chapter concentration-response functions derived from single pollutant studies are used, and thus relationships between O_3 and/or $PM_{2.5}$ concentrations with health effects are not accounted for. However, the effects of O_3 and those of PM have been shown to be relatively independent (WHO, 2006). Also, in the calculation to estimate the excess deaths during the chosen episodes compared to 'typical' conditions only 'typical' pollutant concentrations are taken into account however, baseline mortality data for the episode dates is left unchanged. Therefore estimates of the impact of the air pollution episode are conservative. Nonetheless, this study provides insights into the health effects of short-term exposure to MDA8 O_3 and daily mean $PM_{2.5}$ during air pollution episodes in July 2006 in the UK as well as the meteorological drivers. Using modelled pollutant concentrations at a 12 km resolution, this study also provides an indication of the regional variability of such impacts which is difficult to achieve with the paucity of observational data.

4.7 Supplementary Material

In this section additional figures and tables representing: measured MDA8 O_3 and daily mean $PM_{2.5}$ concentrations from 2005 to 2007 (inclusive) at the London Bloomsbury and Harwell site (Fig. S4.1), spatial distributions of simulated bias-corrected MDA8 O_3 and daily mean $PM_{2.5}$ concentrations (Fig. S4.2), and tables including the estimated regional daily deaths brought forward during the episodes as well as the associated 95% CI for both pollutants (Table S4.1 and S4.2) are shown.

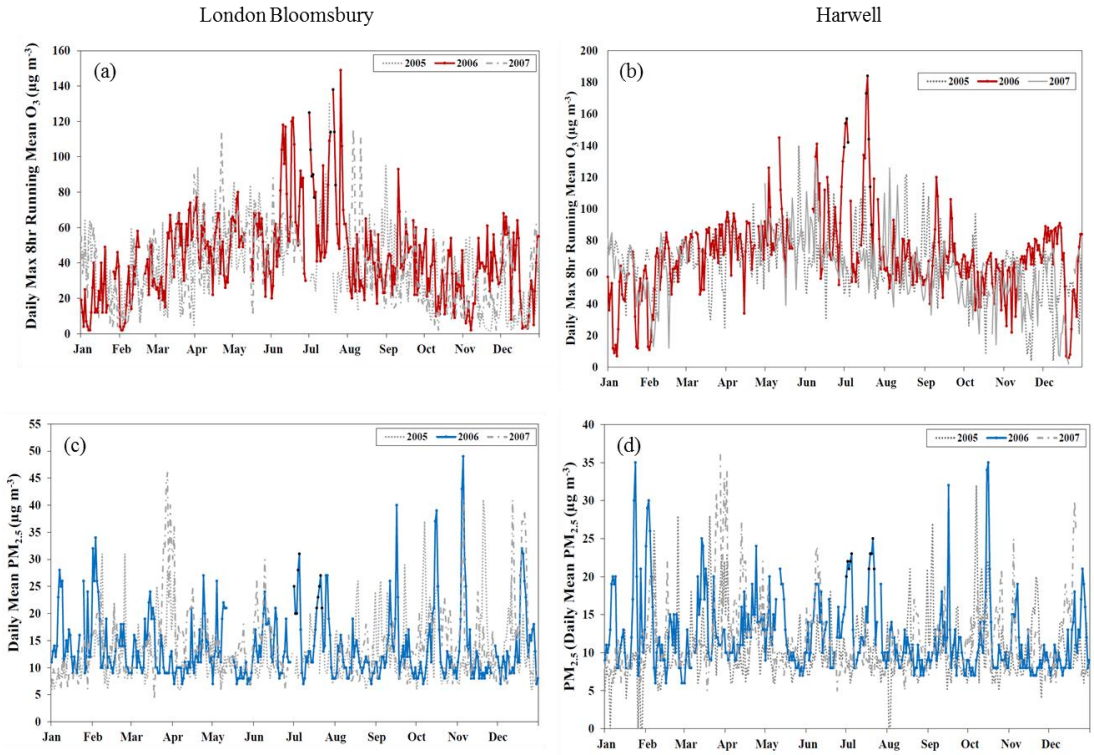

Figure S 4.1: Daily maximum 8-hr running mean (MDA8) O_3 (top panel) and daily mean $PM_{2.5}$ (bottom panel) at (a and c) the London Bloomsbury and (b and d) the Harwell AURN urban and rural background stations from 2005 to 2007 (inclusive). Black points mark the two 5-day air pollution episode days for July 2006.

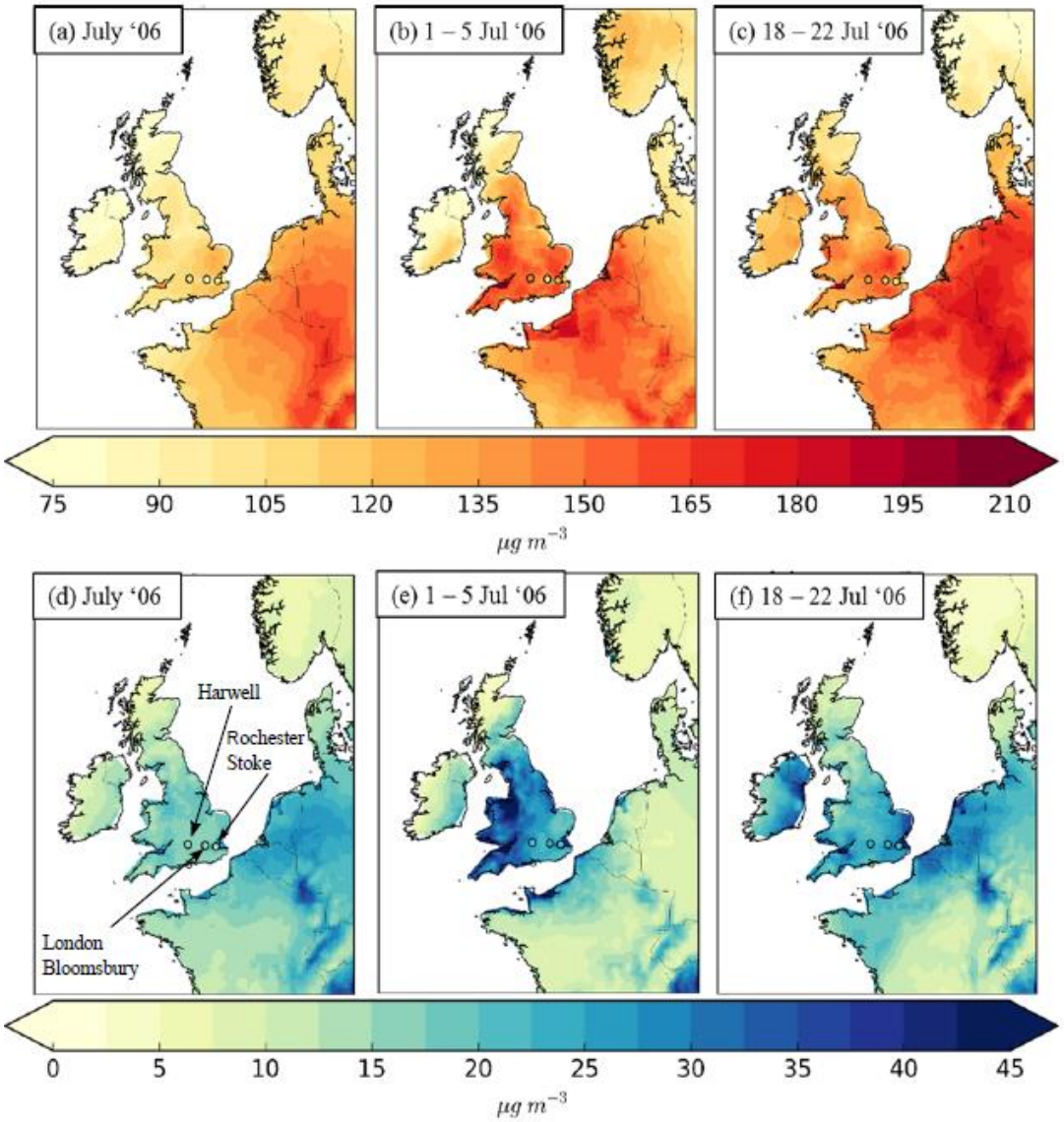

Figure S 4.2: Simulated bias-corrected daily maximum 8-hr running mean O_3 concentrations for (a) July mean, (b) 1-5 July mean and (c) 18-22 July 2006 mean and simulated daily mean $PM_{2.5}$ concentrations for the same time periods (d, e and f). The circles in each plot are coloured with measured data of the respective pollutant at 3 AURN sites - Rochester Stoke, Harwell and London Bloomsbury

Table S 4.1: GOR regions for England, Scotland and Wales and the corresponding 'typical' and episode estimated number of deaths brought forward and percentage of all-cause mortality associated with short-term exposure to MDA8 O_3 for each of the episodes in July 2006 (1st-5th July and the 18th-22nd July). Numbers in brackets represent the 95% confidence interval based on the concentration response function.

	1st -5th July 2006				18th -22nd July 2006			
	Daily deaths brought forward				Daily deaths brought forward			
	Episode		Typical		Episode		Typical	
Region	Number	Percent of all-cause	Number	Percent of all-cause	Number	Percent of all-cause	Number	Percent of all-cause
East Midlands	5	4.57%	3	2.89	5	4.51%	3	2.89
	(2,9)	(1.64,7.41)	(1,5)	(1.03,4.71)	(2,9)	(1.62,7.31)	(1,6)	(1.03,4.71)
East England	7	4.94%	5	3.22	7	4.87%	5	3.22
	(3,11)	(1.77,8.00)	(2,7)	(1.15,5.25)	(3,11)	(1.75,7.89)	(2,8)	(1.15,5.25)
London	7	4.58%	4	3.01	7	4.65%	4	3.01
	(2,11)	(1.64,7.43)	(2,7)	(1.07,4.90)	(2,11)	(1.67,7.54)	(2,7)	(1.07,4.90)
North East	3	4.05%	2	2.60	3	3.95%	2	2.60
	(1,4)	(1.45,6.58)	(1,3)	(0.92,4.24)	(1,5)	(1.41,6.42)	(1,3)	(0.92,4.24)
North West	9	4.80%	5	2.61	9	4.26%	5	2.61
	(3,14)	(1.72,7.78)	(2,8)	(0.93,4.26)	(3,14)	(1.53,6.92)	(2,9)	(0.93,4.26)
Scotland	4	3.35%	3	2.51	5	3.74%	4	2.51
	(2,7)	(1.20,5.46)	(1,5)	(0.89,4.10)	(2,9)	(1.34,6.09)	(1,6)	(0.89,4.10)
South East	10	4.86%	7	3.15	10	4.81%	7	3.15
	(4,17)	(1.74,7.88)	(2,11)	(1.12,5.13)	(4,16)	(1.72,7.79)	(2,11)	(1.12,5.13)
South West	7	5.16%	4	3.02	7	4.56%	4	3.02
	(3,11)	(1.85,8.36)	(1,7)	(1.08,4.93)	(2,11)	(1.64,7.39)	(2,7)	(1.08,4.93)
Wales	4	5.09%	2	2.89	4	4.63%	3	2.89
	(2,7)	(1.83,8.25)	(1,4)	(1.03,4.71)	(2,7)	(1.66,7.51)	(1,5)	(1.03,4.71)
West Midlands	7	4.91%	4	2.81	7	4.59%	4	2.81
	(2,11)	(1.76,7.95)	(1,6)	(1.00,4.59)	(2,11)	(1.65,7.44)	(2,7)	(1.00,4.59)
Yorkshire and The Humber	5	4.20%	3	2.64	5	4.03%	3	2.64
	(2,9)	(1.50,6.83)	(1,6)	(0.94,4.31)	(2,8)	(1.44,6.55)	(1,6)	(0.94,4.31)
Total	69		43		70		45	

Table S 4.2: GOR regions for England, Scotland and Wales and the corresponding 'typical' and episode estimated number of deaths brought forward and percentage of all-cause mortality associated with short-term exposure to daily mean $PM_{2.5}$ for each of the episodes in July 2006 (1^{st}-5^{th} July and the 18^{th}-22^{nd} July). Numbers in brackets represent the 95% confidence interval based on the concentration response function.

	1^{st} -5^{th} July 2006				18^{th} – 22^{nd} July 2006			
	Daily deaths brought forward				Daily deaths brought forward			
	Episode		Typical		Episode		Typical	
Region	Number	Percent of all-cause	Number	Percent of all-cause	Number	Percent of all-cause	Number	Percent of all-cause
East Midlands	3	2.88%	2	1.35	3	2.27%	2	1.52
	(2,5)	(1.45,4.28)	(1,2)	(1.12,1.74)	(1,4)	(1.14,3.38)	(1,3)	(0.76,2.27)
East England	3	2.39%	2	1.36	4	2.92%	2	1.52
	(2,5)	(1.20,3.57)	(2,3)	(1.09,1.78)	(2,6)	(1.47,4.35)	(1,3)	(0.76,2.27)
London	3	2.25%	2	1.36	4	2.72%	2	1.5
	(2,5)	(1.13,3.35)	(2,3)	(1.05,1.81)	(2,6)	(1.37,4.05)	(1,3)	(0.76,2.25)
North East	2	2.81%	1	1.28	1	2.02%	1	1.37
	(1,3)	(1.42,4.17)	(1,1)	(0.93,1.68)	(1,2)	(1.01,3.01)	(1,2)	(0.69,2.05)
North West	7	3.91%	2	1.33	4	2.13%	3	1.47
	(4,11)	(1.98,5.81)	(2,3)	(1.01,1.78)	(2,6)	(1.07,3.18)	(1,4)	(0.74,2.19)
Scotland	2	1.72%	1	0.87	2	1.63%	1	0.98
	(1,3)	(0.86,2.56)	(1,2)	(0.7,1.14)	(1,3)	(0.82,2.44)	(1,2)	(0.49,1.46)
South East	5	2.50%	3	1.34	5	2.54%	3	1.48
	(3,8)	(1.23,3.72)	(2,4)	(1.02,1.79)	(3,8)	(1.28,3.79)	(2,5)	(0.74,2.21)
South West	5	3.43%	2	1.33	4	2.62%	2	1.47
	(2,7)	(1.73,5.10)	(1,2)	(1.01,1.79)	(2,6)	(1.32,3.91)	(1,3)	(0.74,2.20)
Wales	3	3.72%	1	1.24	2	2.42%	1	1.37
	(2,5)	(1.88,5.53)	(1,1)	(0.94,1.67)	(1,3)	(1.22,3.60)	(1,2)	(0.69,2.05)
West Midlands	4	3.28%	2	1.31	3	2.04%	2	1.45
	(2,6)	(1.65,4.88)	(1,2)	(1.02,1.73)	(2,5)	(1.02,3.04)	(1,3)	(0.73,2.17)
Yorkshire and The Humber	4	3.11%	2	1.34	3	2.16%	2	1.51
	(2,6)	(1.57,4.62)	(1,2)	(1.10,1.74)	(1,4)	(1.08,3.21)	(1,3)	(0.76,2.25)
Total	43		19		36		22	

Chapter 5 Future health burdens associated with emission changes in the UK

5.1 Introduction

Present-day long-term exposure to ambient air pollution has been linked with adverse health impacts notably mortality in numerous studies (e.g. Burnett et al., 2014; Jerrett et al., 2009; Krewski et al., 2009; Turner et al., 2015) (Section 1.1). Risk estimates or concentration response functions (CRFs) (section 1.4.3) for mortality associated with long-term exposure to ambient particulate matter less than 2.5 µm in diameter ($PM_{2.5}$) are well established (e.g. Hoek et al., 2013; Krewski et al., 2009). Several studies have quantified the CRFs associated with long-term exposure to ozone (O_3) (Jerrett et al., 2009; Turner et al., 2015) and nitrogen dioxide (NO_2) (Hoek *et al.*, 2013; Faustini et al., 2014; COMEAP, 2015a; Crouse *et al.*, 2015) (see Section 1.1). However for both O_3 and NO_2, long-term effects are still emerging with the majority of studies to date performed over North America (Section 1.1).

Air pollution levels are controlled by emissions, transport, chemical and physical formation and loss processes including deposition which are influenced in turn by meteorology; temperature, precipitation and relative humidity amongst others. Thus future air pollution levels (and in turn future health burdens) can be influenced by a number of factors including changes in emissions of air pollutants (both natural and anthropogenic) and in climate. In this chapter the focus is on the

emissions-driven impacts on air pollutants and the corresponding health burdens. To estimate future ambient air quality, several future scenarios are employed utilising the Intergovernmental Panel on Climate Change (IPCC) Representative Concentration Pathways (RCPs) (van Vuuren et al., 2011b). These are future pathways of global greenhouse gas (GHG) and air pollutants and their precursor emissions as used in the Coupled Model Intercomparison Project Phase 5 (CMIP5) project. They consist of a total of four scenarios that lead to radiative forcing levels from the combined effects of greenhouse gases and aerosols of 2.6 W m^{-2} (van Vuuren et al., 2011a), 4.5 W m^{-2} (Thomson et al., 2011), 6 W m^{-2} (Masui et al., 2011), and 8.5 W m^{-2} (Riahi et al., 2011) by 2100. For all RCPs, large decreases in emissions of particulate matter (PM) and precursors of O_3 especially nitrogen oxides (NO_x), carbon monoxide (CO), sulphur dioxide (SO_2), fossil fuel black carbon (FFBC) and fossil fuel organic carbon (FFOC) are projected globally following the assumption of more stringent air pollution control measures over time (van Vuuren et al., 2011b). An exception is ammonia (NH_3) which increases in nearly all scenarios and methane (CH_4) which increases for RCP8.5. However these are global trends which may vary both spatially and temporally. Note that the assumption of more stringent air pollution measures across the globe is a caveat of the RCPs as these may not represent the true uncertainty in emissions pathways. In addition, it is noted that the RCPs are developed independently and are governed by different assumptions about social, economic and political development.

Several studies have analysed the impact of emission changes on future pollutant concentrations both globally and regionally. For example, for O_3, using a parameterized approach, Wild et al. (2012) suggest annual global mean reductions in O_3 concentrations (~2 ppb) by 2050 under three RCPs due to reductions in O_3 anthropogenic precursor emissions; however under RCP8.5, global O_3 concentrations are estimated to increase (~1.5 ppb) as a result of elevated atmospheric CH_4 concentrations. Using an improved and extended parameterized approach based on Wild et al. (2012), Turnock et al. (2018) suggest increases in

annual mean surface O_3 concentrations across most world regions by 2050 which are mainly driven by regional emissions and changes in global CH_4 abundance that occur under the ECLIPSE (Evaluating the CLimate and Air Quality ImPacts of Short-livEd Pollutants) and the SSPs (Shared Socioeconomic Pathways) emission scenarios.

There have been a number of global scale studies on the impact of future emission changes on O_3 concentrations for Europe. Wild et al. (2012) find reductions in model ensemble mean annual O_3 concentrations in Europe of 4.7 ppb and 2.0 ppb by 2050 under RCP2.6 and RCP6.0, respectively due to decreases in O_3 precursors (as above). On the other hand, O_3 concentrations are found to increase by 0.3 ppb between 2000 and 2050 under RCP8.5 due to increases in CH_4 concentrations. In addition, reductions in regional NO_x emissions are suggested to lead to increases in wintertime O_3 concentrations as a result of the titration effect of NO on O_3 (reaction R1.6; Section 1.2.1.2) for RCP8.5 in Europe despite using results from coarse model resolutions (1° × 1° to 5° × 5°; Wild et al. (2012), that potentially dilute high urban NO_x emissions over large grid-cells (section 3.3.2)). However this study does not represent fully the non-linear chemistry that occurs between the O_3 response and large NO_x emission changes.

For RCP4.5, Hedegaard et al. (2013) suggest O_3 reductions of ~20% for most of the northern hemisphere for 2090 relative to 1990 due to decreases in anthropogenic emissions of NO_x and non-methane volatile organic compounds (NMVOCs). However this signal is not consistent over all of Europe; O_3 concentrations increase in regions with high NO_x levels (e.g. the Benelux region and the south of the UK) again due to the titration effect of NO on O_3 (Hedegaard et al., 2013). As a result of a 30% to 50% reduction in NO_x emissions for 2030, Colette et al. (2012) find increases in O_3 concentrations in regions with high NO_x emissions especially in Northern Europe however, overall O_3 concentrations are found to decrease substantially over Europe. Colette et al. (2012) also show large decreases in NO_2 levels throughout Europe in 2030 due to these NO_x emission reductions. In a

recent multi-model study, Im et al. (2018) suggest an average increase in O_3 concentrations (by up to ~6%) for Europe in response to a 20% reduction of anthropogenic emissions; this study also suggests a larger contribution of non-regional sources for O_3 concentrations in Europe than within region sources.

Future emission changes also typically reduce $PM_{2.5}$ concentrations due to reduced primary emissions as well as changes in secondary inorganic aerosol (Section 1.2.2) that occur through changes in SO_2 and ammona (NH_3) emissions. Sulphate and nitrate aerosols compete for ammonia, such that reductions in SO_2 emissions (which lead to reductions in sulphate concentrations) and increases in NH_3 emissions could increase nitrate aerosol levels (Pye et al., 2009; Section 1.2.2.1). Simulated $PM_{2.5}$ concentrations under RCP4.5 are suggested to decrease across most of the northern hemisphere in the 2090s as a result of reduced anthropogenic emissions of SOx (sulphur oxides) and Black Carbon (BC) (Hedegaard et al., 2013). With a 20% reduction in anthropogenic emissions over Europe, Im et al. (2018) estimate a reduction in $PM_{2.5}$ and NO_2 levels especially over central and eastern Europe with a large contribution from regional sources.

In the UK, Vieno et al. (2016) show decreases in $PM_{2.5}$ concentrations in 2030 as a result of 30% reductions in UK anthropogenic emissions of NMVOC, NO_x, SO_x, primary $PM_{2.5}$ and NH_3. The largest decreases in $PM_{2.5}$ concentrations (~6%) resulted from 30% reductions in NH_3 and primary $PM_{2.5}$ emissions (Vieno et al., 2016). Chemel et al. (2014) also suggest reductions in annual mean $PM_{2.5}$ concentrations of 20-40% in the Midlands for 2020 due to reductions in SO_2, NOx and NMVOCs based on the MEGAPOLI (Megacities: Emissions, urban, regional and Global Atmospheric Pollution and climate effects, and Integrated tools for assessment mitigation) emission scenarios.

Studying the impact of agricultural emissions reductions on $PM_{2.5}$ components and public health, Pozzer et al. (2017) estimate a decrease in global

mortality attributable to $PM_{2.5}$ by about 250 thousand people per year globally due to a 50% reduction in agricultural emissions. This response is associated with non-linear responses in the sulphate-nitrate-ammonia system as described above (Pozzer et al., 2017). However, the majority of recent studies focusing on future health burdens associated with long-term exposure to O_3 and/or $PM_{2.5}$ concentrations under the RCPs typically analyse the combined emission and climate change impacts. Following RCP4.5, the estimated $PM_{2.5}$ and O_3-related global mortality burden is 1.1 ±0.5 and 0.2± 0.1 million avoided deaths per year in 2050, respectively (West et al., 2013). Silva et al. (2016a) suggest decreases in O_3-related respiratory mortality in Europe for all four RCPs for the 2050s relative to the 2000s (16,600 to 49,400 annual avoided deaths) as a result of decreases in O_3 concentrations across Europe. Similarly, due to reduced $PM_{2.5}$ concentrations, future premature mortality associated with long-term exposure to $PM_{2.5}$ is found to decrease in the 2050s for all RCPs in Europe (187,000 to 200,000 annual avoided deaths) (Silva et al., 2016a).

Some studies have focused on the UK future health impacts following different emission scenarios. Using three IPCC Special Report on Emissions Scenarios (SRES; Nakicenovic et al., 2000) and including population projections for 2030, Heal et al. (2013) estimate that, the O_3-health burden increases over the UK by 16-28% compared to that in 2003 (Heal et al., 2013). A recent modelling study for the UK examines air pollutant concentration changes in 2035 and 2050 and health impacts following three UK specific scenarios; a baseline scenario with no climate change mitigation, a nuclear replacement scenario and a low-greenhouse gas scenario (Williams et al., 2018). In all three scenarios, NO_2 concentrations decrease in 2050 due to reductions in NO_x emissions. The subsequent reduction in long-term NO_2- related mortality following the baseline scenario in 2050 is estimated to be ~6.5 (95% CI: 2.7 to 10.2) million life-years gained (Williams et al., 2018) compared to 2011. $PM_{2.5}$ concentrations across the UK are also projected to decrease for this baseline scenario leading to ~17.8 (3.1 to 34.2) million life-years

gained in 2050 compared to 2011 (Williams et al., 2018). Using the AQUM model (Section 2.2), Pannullo et al. (2017) find reductions in NO_2 concentrations for three RCPs across the UK in the 2050s due to reductions in NO_x emission totals of ~31%, 25% and ~57% for RCP2.6, RCP6.0 and RCP8.5. Subsequently, respiratory hospital admissions associated with exposure to NO_2 are estimated to decrease by 1.7% (RCP2.6), 1.4% (RCP6.0) and 2.4%(RCP8.5) (Pannullo et al., 2017).

Future health burdens associated with long-term exposure to air pollution do not solely depend on projected future air pollutant concentrations but also depend on changes in mortality rates and demographic or population changes. Despite projected future reductions in pollutant concentrations, Silva et al. (2016) suggest increases in premature mortality due to increases in total population size in 2050. Another study showed how the impacts of changes in population outweigh the impacts of climate change on heat-related mortality (Marsha et al., 2018). They suggest that while mortality is estimated to increase across both socioeconomic and climate projections, the combined socioeconomic changes (such as population growth, demographic and economic changes) have a larger impact than climate change alone (Marsha et al., 2018). West et al. (2013) also suggest that globally and in Europe, the population growth and baseline mortality rates amongst other demographics exacerbate the health impacts resulting from the RCP scenarios particularly in 2100.

As discussed above, several global and regional studies have analysed the impact of emission changes on future air quality. However, to date no such HIA has been conducted comprehensively using the RCPs for the three pollutants O_3, NO_2 and $PM_{2.5}$ over the UK. The focus of this chapter is on UK primary and precursor emission changes for 2050 based on three RCPs: RCP2.6, RCP6.0 and RCP8.5 and the subsequent impacts on changes in annual means of daily mean 8-hr running mean (MDA8) O_3, NO_2 and $PM_{2.5}$. In addition the effects of long-term exposure associated with each pollutant under each RCP is estimated and the sensitivity of future health burdens to two population scenarios is assessed.

This chapter is organised as follows: the methods are described in Section 5.2, then the impact of future emission projections following the RCPs on simulated annual mean MDA8 O_3, NO_2 and $PM_{2.5}$ concentrations in 2050 across the UK are discussed in Section 5.3.1 and 5.3.2. The corresponding future attributable fraction (AF) of mortality and mortality burdens associated with long-term exposure to annual mean MDA8 O_3, annual mean NO_2 and annual mean $PM_{2.5}$ are next described in Sections 5.4.1, 5.4.2 and 5.4.3, respectively. The sensitivity of estimated mortality burdens associated with each pollutant to future population projections is then presented in Section 5.4.4 followed by a summary and conclusions in Section 5.5.

5.2 Methods

In this section the model used in this chapter is briefly described in Section 5.2.1 followed by a description of the model set-up in Section 5.2.2. The present-day (2000) and future (2050) UK emissions under three RCPs are presented in Section 5.2.3 followed by the method to calculate the health impact assessment in Section 5.2.4. This section ends with a description of future population projections associated with the RCPs in Section 5.2.5.

5.2.1 The UK Air Quality in the Unified Model – AQUM

The Air Quality in the Unified Model (AQUM; Savage et al., 2013) used in this chapter is described in Section 2.2 and therefore only described briefly in this section. In this chapter, air pollutant concentrations for both 2000 (present-day) and 2050 (future) for the UK are simulated using AQUM which is based on the UK

Met Office Unified Model (MetUM; Brown et al., 2012). AQUM has a horizontal resolution of 0.11° × 0.11° (~12 km) with a domain covering the UK and parts of Western Europe (Fig 2.2). The model has 38 vertical levels from the surface up to 39 km. Gas-phase chemistry is simulated within AQUM by a tropospheric configuration of the United Kingdom Chemistry and Aerosol (UKCA) model (Morgenstern et al., 2009; O'Connor et al., 2014) which is described in more detail in Section 2.2.2. The chemistry scheme used is the Regional Air Quality (RAQ) chemistry scheme (Section 2.2.2), which has 58 chemical species, 116 gas phase reactions and 23 photolysis reactions (Savage et al., 2013). The model includes an interactive mass-based aerosol scheme CLASSIC (Coupled Large-scale Aerosol Simulator for Studies in Climate; Bellouin et al., 2013, 2011; Jones et al., 2001) which includes up to eight aerosol species: ammonium sulphate and nitrate, fossil-fuel organic carbon (FFOC), mineral dust, fossil-fuel black carbon (FFBC), biomass burning (BB) aerosol and secondary organic aerosol (SOA). Biogenic secondary organic aerosols are prescribed from a climatology (Bellouin et al., 2011) and sea salt is calculated over sea points only and does not contribute to PM concentrations over land. Within AQUM, sulphate and nitric acid compete for available ammonium to form ammonium nitrate and ammonium sulphate aerosols (Bellouin et al., 2011). A more detailed description of CLASSIC can be found in Section 2.1.4 and Section 2.2.3.

Lateral boundary conditions for chemistry and aerosols are derived from reanalysis fields whilst meteorology is obtained from the UK Met Office Unified Model (MetUM) global forecast fields at a resolution of ~17 km (Section 2.2.4).

5.2.2 Model Set-up

In this chapter a total of four simulations are conducted using the AQUM (Table 5.1): one to derive air pollutant concentrations for 2000 (present-day) and another three simulations to derive air pollutant concentrations following three different

RCPs for 2050 (future). For all these simulations the same meteorology was employed – that of the year 2006 (as used in chapter 4). Present-day and future hourly air pollutant concentrations over England, Scotland and Wales are obtained from the same AQUM configuration used in Chapter 4, and described in Chapter 2, but with different emission fields. For the 2000 simulation, anthropogenic and biomass burning emissions are taken from decadal mean emissions centred on the year 2000 (Lamarque et al., 2011, 2010). These historical emissions were originally created for the 5th Climate Model Intercomparison Program (CMIP5) in support of the IPCC Fifth Assessment Report (AR5) and are used as a starting point for all RCPs. For the future simulations, anthropogenic and biomass burning emissions are obtained from decadal mean emissions centred on 2050 following three IPCC RCPs: RCP2.6 (van Vuuren et al., 2011a), RCP6.0 (Masui et al., 2011) and RCP8.5 (Riahi et al., 2011). Biogenic emissions of isoprene for all simulations are diagnosed from simulations with a fully coupled nested configuration of the MetUM (described in Neal et al., 2017) for future climate under the RCPs for 2000 and 2050 and then prescribed in AQUM with a diurnal cycle imposed. Therefore, although when using AQUM in this chapter the climate is unchanged between 2000 and 2050, the prescribed biogenic isoprene emissions have responded to changes in CO_2 and temperature in 2050 compared to 2000 following Pacifico et al. (2011). All emission changes are discussed in more detail in Section 5.2.3.

The lateral boundary conditions used for future simulations are kept the same as for the present-day and are consistent with those used in Chapter 4 (Section 2.2.4). For all simulations, feedbacks of aerosols and greenhouse gases on the radiation scheme are excluded, thus ensuring the climate is unchanged between the present-day and future simulations. Hence the projected changes in air pollutant concentrations show the influence of anthropogenic, biomass burning and biogenic emission changes only. Greenhouse gases (GHG) are prescribed as concentrations for both present-day and future simulations due to the long lifetime

(>10 years) of CH_4 and other GHG species (carbon dioxide (CO_2) and nitrous oxide (N_2O)).

All simulations (Table 5.1) are conducted for 18 months with the first 6 months discarded as spin-up. Hourly pollutant concentrations taken from the lowest model vertical level (having a midpoint of 20 m) are then extracted, from which the annual mean MDA8 O_3, NO_2 and $PM_{2.5}$ concentrations are calculated.

Table 5.1: Details of the model configuration for the present-day (2000) simulation and each of the future simulations (2050) following RCP2.6, RCP6.0 and RCP8.5.

Simulation Name	**Present-day**	**RCP2.6**	**RCP6.0**	**RCP8.5**
SSTs and SIE (meteorology)	2006	2006	2006	2006
LBCs (meteorology/chemistry/aerosols)	2006	2006	2006	2006
Emissions (Anthropogenic and biomass)	1996-2005	2046-2055 RCP2.6	2046-2055 RCP6.0	2046-2055 RCP8.5
Prescribed GHG concentrations	2000	2050 RCP2.6	2050 RCP6.0	2050 RCP8.5

5.2.3 Present-day and future UK emissions

Emissions totals and percentage differences over the UK between 2000 and 2050 for key O_3 and $PM_{2.5}$ primary and precursor species under each scenario are shown in Fig. 5.1. Most of the emissions over the UK decrease in the future compared to present-day with the greatest reductions occurring for the RCP8.5 (Fig.5.1). For example, nitrogen oxides (NOx) emissions reduce from ~ 1.3 Tg (NO) yr^{-1} in 2000 to ~ 0.5 Tg (NO) yr^{-1} for RCP2.6 and RCP6.0 and ~ 0.3 Tg (NO) yr^{-1} for RCP8.5 in 2050,

corresponding to a reduction of 60%, 58% and 73% (Fig.5.1a). Spatial distributions of NOx emissions for present-day and for differences in future emissions compared to present-day are illustrated in Fig.5.2. For all RCPs, the largest reductions in NOx emissions occur in regions having high present-day emissions (e.g. central and south east England) (Fig. 5.2). Emissions following RCP8.5 exhibit the largest reductions compared to present-day while the smallest reductions are noted for RCP6.0.

Emission changes between 2000 and 2050 for CO, FFOC and FFBC follow a similar pattern to that of NOx with the highest reductions occurring for RCP8.5 and lower reductions for RCP2.6 and RCP6.0 (Fig. 5.1 b-d). SO_2 emissions also decrease in the future in all RCPs. However, reductions in each RCP follow a different pattern, with the highest reductions occurring for RCP2.6 (-92%) and RCP8.5 (-94%) and the lowest reductions occurring for RCP6.0 (-43%; Fig. 5.1e). Ammonia (NH_3) emissions and methane (CH_4) concentrations increase over the UK for certain future scenarios (Fig. 5.1f and g). Ammonia emissions total ~ 0.35 Tg (NH) yr^{-1} in 2000 and increase for all RCPs, with the highest increase occurring for RCP6.0 (29%) followed by RCP2.6 (16%) and RCP8.5 (7%) (Fig. 5.1f). As mentioned in the previous section, CH_4 concentrations are prescribed for all four simulations due to its long lifetime. CH_4 concentrations over the UK are ~1200 µg m^{-3} for present-day, and decrease by 16% in 2050 following RCP2.6 (Fig. 5.1g). In contrast methane concentrations increase following RCP6.0 (8%) and RCP8.5 in 2050 (54%; Fig. 5.1g).

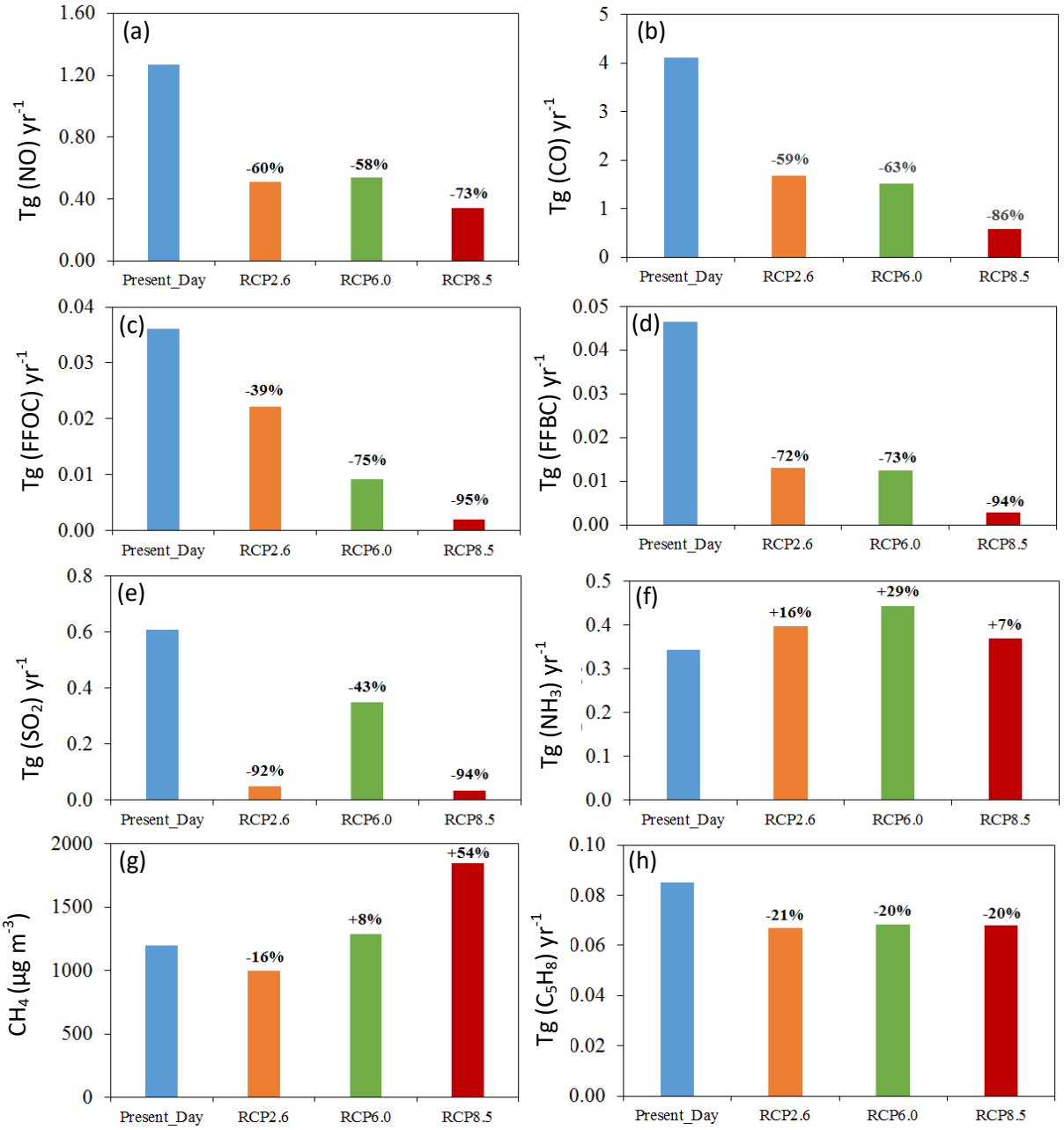

Figure 5.1: Emissions totals and percentage differences over the UK (land only) between 2000 and 2050 for the key O_3 and $PM_{2.5}$ primary and precursor species: (a) nitrogen oxides (NO_x) (b) carbon monoxide (CO), (c) fossil fuel organic carbon (FFOC), (d) fossil fuel black carbon (FFBC), (e) sulphur dioxide (SO_2), (f) ammonia (NH_3), (g) methane (CH_4) (concentrations) and (h) isoprene (C_5H_8) for present-day (blue), RCP2.6 (orange), RCP6.0 (green) and RCP8.5 (red). Percentage differences between future and present-day are shown above each scenario.

Isoprene (C_5H_8) emissions used in this chapter are obtained from a model simulation (section 5.2.2) in which biogenic VOCs emission are calculated interactively responding to changes in carbon dioxide (CO_2) and temperature (Pacifico et al., 2011). These are then prescribed in the UK domain within AQUM. C_5H_8 emissions reduce from ~0.09 Tg (C_5H_8) yr^{-1} for present-day to ~0.07 Tg (C_5H_8) yr^{-1} under all RCPs (~20% reduction; Fig 5.1h). This suggests that the main driver for reductions in isoprene emissions for all future scenarios is CO_2 inhibition of isoprene (high levels of CO_2 suppressing leaf isoprene production)(Arneth et al., 2007) which offset the temperature-driven emission increases, as found by other studies (e.g. Pacifico et al., 2012; Squire et al., 2015) .

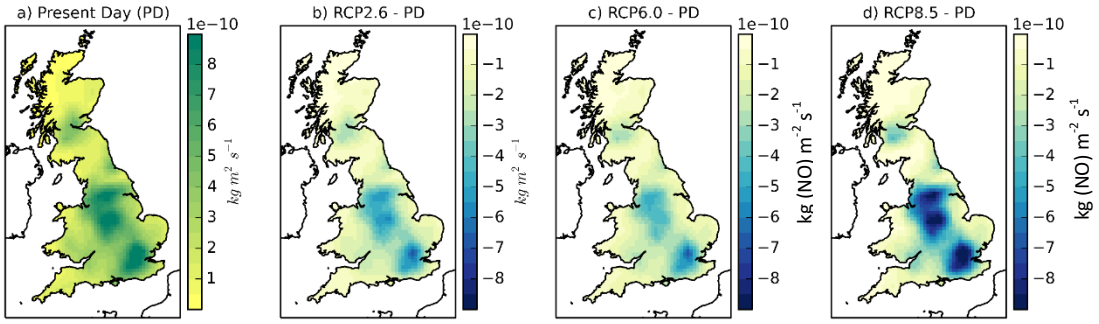

Figure 5.2: Total NOx emissions for (a) present-day (PD - 2000) and (b-d) differences in NOx emissions between present-day and future (2050) under three RCPs

5.2.4 Health impact assessment

The method for calculating the health impact assessment in this chapter is described in detail in Section 2.4. Estimated mortality burdens and attributable fractions of mortality associated with long-term exposure to annual mean concentrations of MDA8 O_3, NO_2 and $PM_{2.5}$ are calculated following equations 2.9 to 2.12 for each of the nine Government Office Regions (GOR) for England, and for Scotland and Wales.

The CRF and any relevant thresholds used for the effect long-term exposure to each pollutant is listed in Table 1.2, described in section 1.4.4 and is briefly mentioned below. The CRF for the effects of long-term O_3 exposure on respiratory mortality is 1.06 (95% Confidence Interval (CI) = 1.04,1.08) per 10 μg m^{-3} increase in annual mean MDA8 O_3 concentrations with a threshold of 53.4 μg m^{-3}. For the effect of long-term NO_2 exposure on all-cause (excluding external) mortality, the CRF used is of 1.025 (95% CI = 1.01,1.04) per 10 μg m^{-3} increase in annual mean NO_2 concentrations with no threshold. The CRF associated with long-term $PM_{2.5}$ exposure on all-cause (excluding external) mortality, is 1.062 (95% CI = 1.040, 1.083) per 10 μg m^{-3} increase in annual average concentration, with no threshold. To quantify differences in mortality burdens between the present-day and future for each region, the present-day mortality estimate is subtracted from the future mortality estimate (ie $M_{r\ Future} - M_{r\ PD}$).

5.2.5 Future population projections associated with the RCPs

In this chapter the sensitivity of future mortality burdens to changes in future population is analysed. To isolate the effect of changes in air pollutant concentrations across the RCPs, the same source for estimates of population growth in the UK is used. This is done by using the future population projections from the Shared Socioeconomic Pathways (SSP) gridded at a resolution of 17 km (Jones and O'Neill, 2017). The SSPs are a set of five different socioeconomic development narratives that describe plausible pathways for the evolution of society over the next century and are intended to provide a range of pathways that can be combined with the RCPs (Riahi et al., 2017). In conjunction with each RCP the population projection following SSP1, or "Sustainability" storyline and SSP5, or "Fossil-fuelled Development" storyline are applied. These two SSPs represent the upper (SSP5) and lower (SSP1) limits of projected population totals for the UK for 2050. Marsha et al. (2018) also use two plausible SSPs in conjunction with two RCPs

to explore the sensitivity of heat-related non-accidental mortality to future changes of demographics, income and climate.

Based on SSP1 and SSP5, the total UK population is estimated to reach 74.7 million and 85.3 million, respectively, in 2050 (a factor of 1.2 and 1.4 greater than present-day totals used in this chapter) (Table 5.2). The UK Office of National Statistics (ONS) projects a total UK population of 72.9 million in mid-2041 based on 2016 data (ONS, 2015), while the Directorate-General of the European Commission (Eurostat) estimates suggest that at the start of 2040 the total UK population will be 75 million (Eurostat, 2017). Hence from the two SSPs used in this Chapter (SSP1 and SSP5), the SSP1 population projections are most similar to these aforementioned regional population projections for 2050. The baseline mortality rates and demographics for the future estimates are kept at present-day rates.

Table 5.2: Present-day and future population (millions of people) showing UK totals (including Northern Ireland) for all ages.

		Total UK Population (million)
Present-day		59.7
Future Scenario	SSP1 (2050)	74.7
	SSP5 (2050)	85.3
	ONS (mid-2041)	72.9
	Eurostat (2040)	75.0

5.3 The impact of changes in future UK emissions on simulated pollutant concentrations

In this section, the influence of changes in future UK emissions (only) on annual mean MDA8 O_3 and annual mean NO_2 concentrations is first discussed (Section 5.3.1). The emissions driven impact on annual mean $PM_{2.5}$ concentrations is then described in Section 5.3.2.

5.3.1 The emissions driven impact on O_3 and NO_2 concentrations in the UK

Simulated annual mean MDA8 O_3 concentrations for 2000 average ~ 77 μg m^{-3} across the UK and range from ~ 62 μg m^{-3} in Central England (West and East Midlands regions) to more than 80 μg m^{-3} in the south west of England as well as in Wales and Scotland (Fig 5.3a). O_3 concentrations increase under all RCPs (2050) compared to present-day (2000) and are on average between ~4 μg m^{-3} and ~9 μg m^{-3} higher depending on the RCP (Fig. 5.3b-d). For all three RCPs the largest increases for 2050 occur in regions where present-day O_3 concentrations are low (Fig. 5.3b-d). The largest increases in O_3 concentrations occur for RCP8.5 where concentrations are more than 12 μg m^{-3} (~+40%) and up to 18 μg m^{-3} (~50%) higher across much of the central and southern regions of England compared to present-day (Fig. 5.3d). For RCP2.6 and RCP6.0 increases in O_3 concentrations are about 6 μg m^{-3} (~25%) compared to present-day in Central England with smaller increases elsewhere (Fig. 5.3b and c).

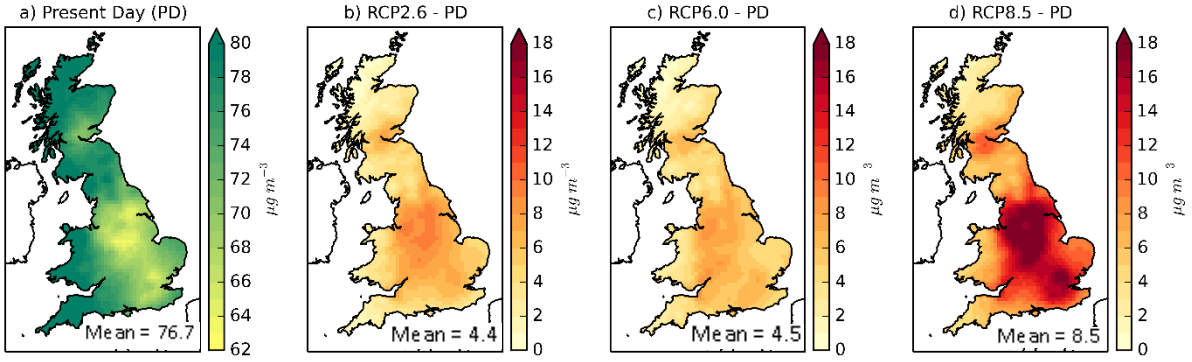

Figure 5.3: Simulated annual mean daily maximum 8-hr running mean (MDA8) O_3 concentrations for (a) present-day (PD - 2000), (b-d) differences in simulated annual mean MDA8 O_3 concentrations between present-day (2000) and future (2050) calculated as MDA8 $O_{3\ future}$ – MDA8 $O_{3\ present\text{-}day}$ for each future scenario. Mean concentrations (μg m^{-3}) are shown at the bottom of each panel.

Changes in O_3 precursor emissions affect the abundance of O_3 concentrations via changes in the availability of atmospheric oxidants (Section 1.2.1). NO_X emissions play a key role in determining surface O_3 concentrations. For all three RCP simulations, UK NO_X emissions decrease in 2050 (by up to 73%; Fig. 5.1 and 5.2 Section 5.2.3) with the largest decreases occurring in regions having high present-day NOx emissions (Fig 5.2), for example central and south eastern England (Fig. 5.2b-d). This results in substantial decreases in annual mean NO_2 concentrations across the UK (Fig. 5.4b-d). Present-day annual mean NO_2 concentrations averaged across the UK are 11.2 μg m^{-3} and range from ~3 μg m^{-3} in most of Scotland to ~ 27 μg m^{-3} in Central and South East England (Fig. 5.4a), with the spatial distribution being approximately the inverse of that for O_3 concentrations (Fig. 5.3a). Annual-mean NO_2 concentrations reduce in the future, with decreases between 6 μg m^{-3} (~-25%) and 12 μg m^{-3} (~-50%) in most of central England for RCP2.6 and RCP6.0 (Fig. 5.4b and c) and higher than 15 μg m^{-3} (~-75%) for RCP8.5 (Fig. 5.4d). Regions showing low present-day O_3 concentrations and high NO_2 concentrations (Fig. 5.3a and 5.4a), also exhibit the greatest increases in O_3 concentrations and the largest decreases in NO_2 concentrations in 2050 relative to

2000 (Fig. 5.3 b-d and Fig. 5.4 f-h). Reductions in NO_2 concentrations are highest for RCP8.5 (Fig. 5.4d) followed by RCP 2.6 (Fig. 5.4b) and RCP6.0 (Fig. 5.4c), consistent with reductions in NO_X emissions (Fig 5.1 and 5.2; Section 5.2.3). The higher O_3 concentrations in the future are likely due to the titration effect of NO on O_3 (equation 1.6; section 1.2.1.2). Thus UK NO_X emission reductions between present-day and future produce increases in O_3 concentrations, suggesting a NO_x saturated environment across all of the UK, but particularly in highly polluted regions, where estimated NO_X emission reductions are highest.

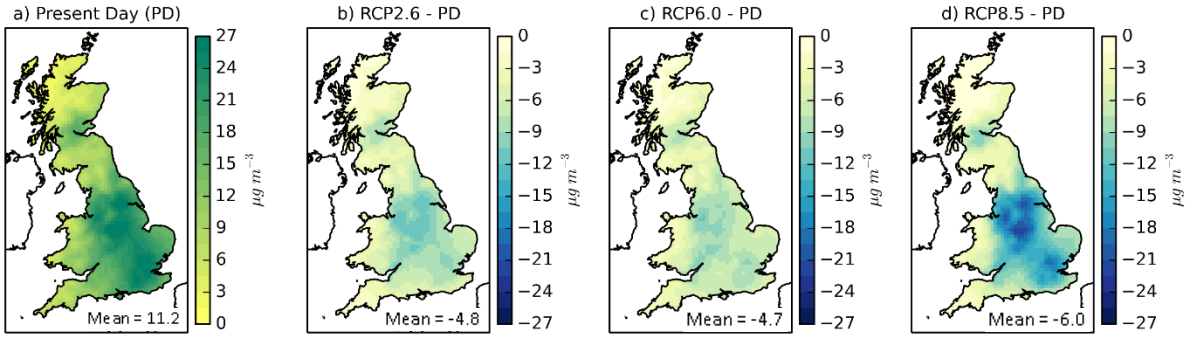

Figure 5.4: Annual mean NO_2 concentrations for (a) present-day (PD - 2000) and (b-d) differences in NO_2 concentrations between present-day and future (2050) under three RCPs. Mean concentrations (μg m^{-3}) are shown at the bottom of each panel.

While annual mean CH_4 concentrations decrease for RCP2.6 (-16%) across the UK, they increase for RCP6.0 (+8%) and RCP8.5 (+54%) (Fig. 5.1; Section 5.2.3). This increase in CH_4 concentrations for RCP6.0 and RCP8.5 between present-day and future which occurs across the UK may aid increases in O_3 concentrations for these two scenarios (Fig. 5.3c and d) but fails to explain increases in annual mean MDA8 O_3 concentrations for RCP2.6 (Fig. 5.3b). Given the long lifetime of CH_4 and the model set-up of this chapter, with lateral boundary conditions kept constant, the contribution to O_3 production in the UK is likely to be small. Nonetheless, the spatial patterns in O_3 differences between present-day and future (Fig. 5.3) are clearly explained by changes in NO_x emissions (Fig. 5.4) as discussed above.

These findings are fairly consistent with previous studies over Europe. A number of global and Europe-wide studies have shown a strong impact of NO_x emission reductions and higher CH_4 levels leading to higher O_3 concentrations in Northern Europe. Hedegaard et al. (2013) find the chemical environment for O_3 production to differ between North-west Europe and elsewhere in Europe. In the Benelux regions and surrounding countries (including the UK), O_3 concentrations were found to increase under RCP4.5 between 1990 and 2090 as a result of NO_x decreases, leading to reduced O_3 titration by NO. However this signal was not consistent across the UK as found in this chapter. Elsewhere in Europe, NO_x emissions reductions under RCP4.5 were found to lead to lower O_3 concentrations (~20%) between 1990 and 2090 (Hedegaard et al. 2013). In another regional European study with different future emission scenarios (Global Energy Assessment scenarios) but which also feature NO_x emission reductions, annual mean O_3 were found to increase across most of north west Europe and the UK in particular Central and south east England (Colette et al. 2012), highlighting North West Europe and the UK as a NO_x saturated environment.

Similar to the work presented in this chapter, a UK-focused report evaluating nine regional models (including AQUM) at 23 measurement sites (rural and urban background), suggests that reducing the total anthropogenic NO_x and VOC emissions by 30% for 2006 across the UK, leads to an increase in annual mean simulated O_3 concentrations ranging between 1.2 and 6.1 μg m^{-3} for all models at all sites (Defra, 2013a). A similar increase in annual mean O_3 concentrations over the UK was also found for a 30% reduction in anthropogenic NO_x and VOC emissions across the UK and Europe. Thus suggesting a greater impact on O_3 concentrations from UK regional emission reductions compared to emission reductions outside the UK.

5.3.2 The emissions driven impact on $PM_{2.5}$ concentrations in the UK

Present-day simulated annual mean $PM_{2.5}$ concentrations averaged across the UK are ~9 µg m^{-3} and range from ~ 4 µg m^{-3} in Scotland to ~ 12 µg m^{-3} in eastern England (Fig. 5.5a). For all RCPs, annual mean $PM_{2.5}$ concentrations decrease compared to present-day with a notable north-south gradient (Fig. 5.5 b-d). Across the UK, the largest reductions in $PM_{2.5}$ concentrations in 2050 relative to 2000 occur under RCP8.5 (Fig. 5.5d). For RCP8.5 and RCP2.6, annual mean $PM_{2.5}$ concentrations are between ~ 1 µg m^{-3} (~-15%) lower in Scotland to ~ 4.5 µg m^{-3} (~-50%) lower in Central and Eastern England compared to present-day (Fig. 5.5 b and d). In 2050, reductions in simulated $PM_{2.5}$ concentrations under RCP6.0 relative to 2000 are smaller than the other two future scenarios with differences ranging from ~ -0.5 µg m^{-3}(~-10%) in Scotland to ~ -2 µg m^{-3}(~ -20%) in eastern England (Fig. 5.5c).

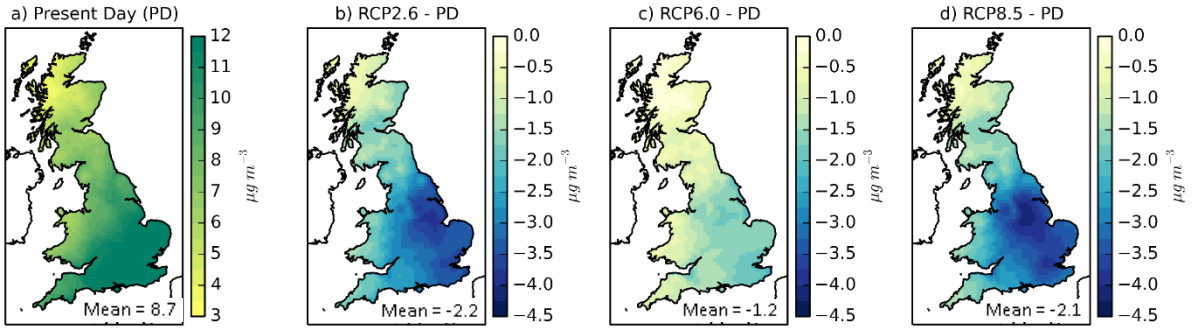

Figure 5.5: Simulated annual mean $PM_{2.5}$ concentrations for (a) present-day (PD – 2000), (b-d) differences in simulated annual mean $PM_{2.5}$ concentrations between present-day and future (2050) calculated as $PM_{2.5\ future} - PM_{2.5\ present\text{-}day}$ for each future scenario. Mean concentrations (µg m^{-3}) are shown at the bottom of each panel.

For both present-day and future simulations, the two major components contributing to $PM_{2.5}$ concentrations are ammonium sulphate concentrations and to a lesser extent, ammonium nitrate concentrations (Fig. 5.6). For present-day ammonium nitrate constitutes 35% of total $PM_{2.5}$ concentrations while ammonium

sulphate constitutes 45% (Fig. 5.6a). For all RCPs, this distribution is modified compared to present-day, with ammonium nitrate increasingly becoming the more dominant constituent of $PM_{2.5}$ concentrations especially under RCP2.6 and RCP8.5 (Fig. 5.6 b-d).

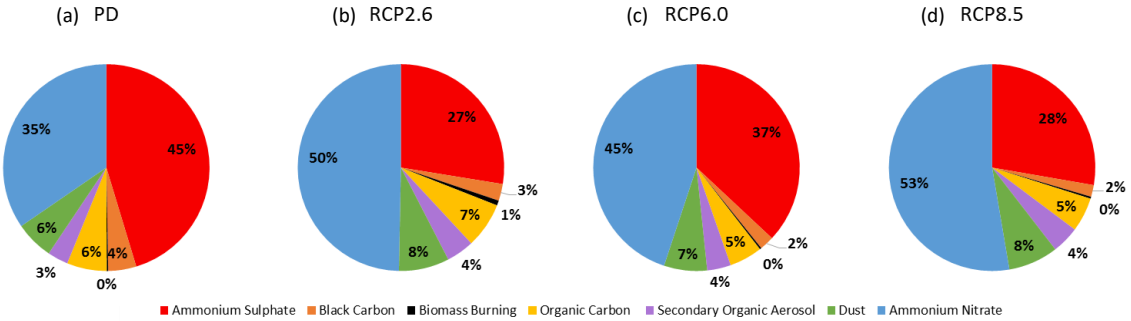

Figure 5.6: The individual components that add up to the total $PM_{2.5}$ concentration as simulated by the AQUM model for (a) present-day (2000) and (b-d) future scenarios following RCP2.6, RCP6.0 and RCP8.5.

The magnitude and spatial distribution of differences in ammonium sulphate concentrations between present-day and future for all three RCP scenarios is similar to that of simulated $PM_{2.5}$ concentrations with reductions ranging from ~ -1 µg m^{-3} in Scotland to ~ -4.5 µg m^{-3} in central and eastern England (Fig. 5.7).

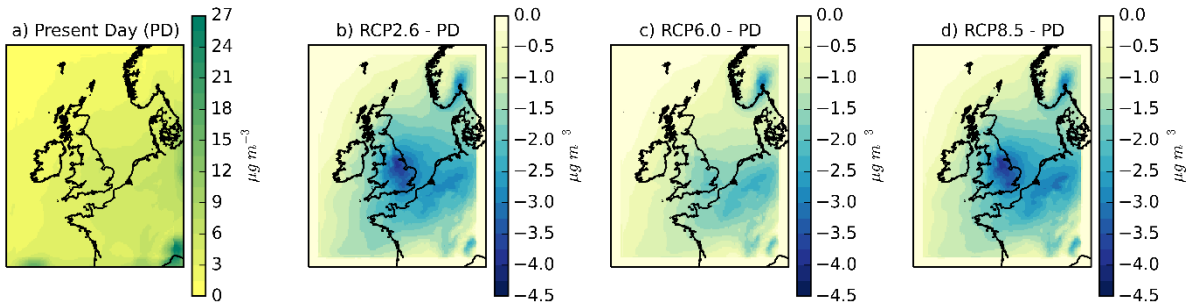

Figure 5.7: Simulated annual mean ammonium sulphate concentrations for (a) present-day (PD), (b-d) differences in simulated annual mean annual mean ammonium sulphate concentrations between present-day (2000) and future (2050) following RCP2.56, RCP6.0 and RCP8.5.

In contrast, simulated ammonium nitrate concentrations over the UK are higher by ~0.25 µg m^{-3} to ~1 µg m^{-3} for all three RCP scenarios compared to present-day (Fig. 5.8). For all future scenarios, UK SO_2 emissions decrease under the RCPs scenarios (Fig. 5.1) leading to a reduction in sulphate aerosol in the future. This reduction in SO_2 emissions in conjunction with increases in ammonia emissions under all three RCPs results in an overall increase in the simulated nitrate aerosols even though NO_x emissions in the UK are projected to decrease in the future.

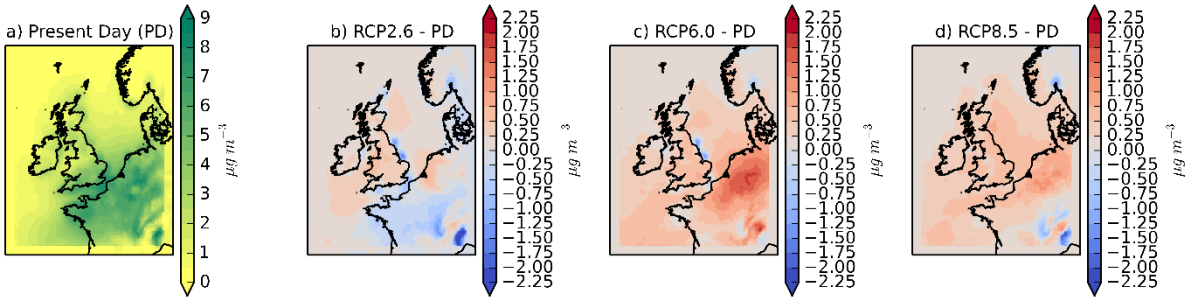

Figure 5.8: Simulated annual mean ammonium nitrate concentrations for (a) present-day (PD), (b-d) differences in simulated annual mean annual mean ammonium nitrate concentrations between present-day (2000) and future (2050) following RCP2.56, RCP6.0 and RCP8.5.

These decreases in $PM_{2.5}$ concentrations in 2050 following the RCPs compared to 2000 are consistent with those of Hedegaard et al. (2013), suggesting that changes in anthropogenic emissions of SO_x and BC following RCP4.5 lead to a decrease in $PM_{2.5}$ concentrations across Europe. Under a European emission reduction scenario for 2020 based on the MEGAPOLI project, Chemel et al. (2014) find annual average $PM_{2.5}$ concentrations reductions > 2 µg m^{-3} over England due to reductions in SO_2, NOx and NMVOCs. Vieno et al. (2016) also suggest that under current legislation (CLE) emissions for 2030, surface annual-average $PM_{2.5}$ concentrations over the UK reduce by up to 2.8 µg m^{-3} compared to 2010. Furthermore, these findings on the impacts of SO_2 emission reductions on the ammonium sulphate and ammonium nitrate balance are similar to those reported in previous studies (e.g. Pye et al., 2009).

5.4 Future mortality burdens due to changes in UK emissions

Using the simulated annual mean MDA8 O_3, NO_2 and $PM_{2.5}$ concentrations discussed in Section 5.3, population-weighted pollutant concentrations are first calculated (equation 2.12) and then the regional attributable fraction (AF) of mortality and mortality burdens associated with long-term exposure to each pollutant are estimated for the present-day (2000) and all three future scenarios (2050) following the methodology described in Section 2.4.3.

5.4.1 Health impacts associated with long-term exposure to annual mean MDA8 O_3

The AF of respiratory mortality associated with long-term exposure to annual mean MDA8 O_3 for both present-day and all three future scenarios is depicted by region in Fig. 5.9a, with the 95% confidence interval (95% CI) representing uncertainties associated only with the concentration-response function (CRF) used. The present-day AF of respiratory mortality in 2000 across the regions ranges from 7.37% (95% CI = 4.98%, 9.71%) in the East Midlands to 14.42% (95% CI = 9.86%, 18.74%) in Wales (Fig. 5.8a). Differences in the AF of respiratory mortality between the different regions solely depend on differences in population-weighted pollutant concentrations (as the CRF is kept constant; equation 2.3 Section 2.4.1). Thus regions with the lowest present-day AF directly correspond to regions with the lowest present-day annual mean MDA8 O_3 concentrations and vice-versa (c.f. Fig. 5.3 and Fig. 5.9). For all three UK future emission scenarios following the RCPs the AF of respiratory mortality associated with long-term exposure to O_3 in 2050 is higher compared to present-day, which is driven by higher pollutant concentrations (c.f. Fig. 5.3 and Fig. 5.9a). Across the regions the AF of respiratory mortality ranges

from 10.96% (95% CI = 7.45%, 14.34%) in East Midlands to 18.81% (95% CI = 12.97%, 24.26%) in Wales following RCP6.0 and RCP8.5, respectively (Fig. 5.9a).

For each region, differences in the AF of respiratory mortality between present-day and the RCPs are illustrated in Fig 5.9b. The largest increases in the AF of respiratory mortality for RCP8.5 are 9.34% (95% CI = 3.74%, 14.94%) in the East Midlands which is due to large increases in annual mean MDA8 O_3 concentrations (Fig. 5.3 Section 5.3.1). In contrast the difference in the AF of respiratory mortality is lowest under RCP2.6 in Wales with a difference of + 2.44% (95% CI = -4.34%, +9.22%) (Fig. 5.9b). As noted in Section 5.3.1 for annual mean MDA8 O_3 concentrations, the largest increases in future AFs occur in regions having the lowest present-day AF, for example the East Midlands (Fig. 5.9a and b).

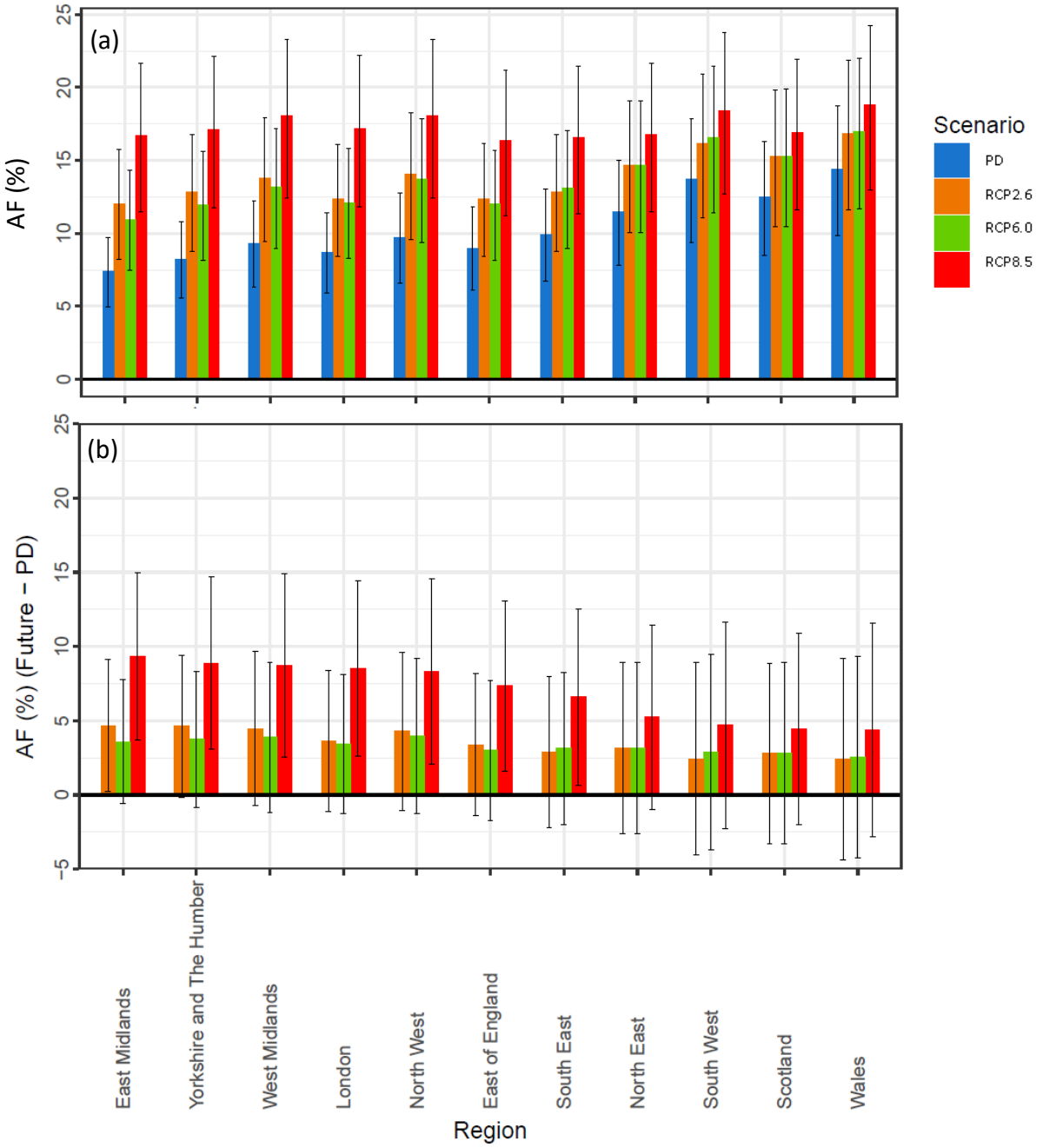

Figure 5.9: (a) Attributable fraction (AF) of respiratory mortality associated with long-term exposure to annual mean MDA8 O_3 for present-day (PD – 2000) and each RCP for 2050 expressed as a percentage of total annual respiratory mortality. (b) Difference in AF between present-day and future expressed as a percentage for each regions in England, Scotland and Wales (AF_{future} – $AF_{present\text{-}day}$). Error bars show the 95% CI which represents uncertainties associated only with the concentrations-response function used. For Figure 5.9b the errors bars are calculated as described in section 2.4.4.

The uncertainty estimates based on the 95% confidence interval of the O_3 concentration-response function are relatively large such that the error bars between present-day and all three future scenarios overlap (Fig. 5.9a). Exceptions are error bars for East Midlands, Yorkshire and the Humber, West Midlands and London between present-day and RCP8.5 which do not overlap (Fig. 5.9a). This suggests a significant difference in the AF of respiratory mortality between present-day and RCP8.5 for these regions. The large uncertainty is further reflected in the confidence intervals of differences between present-day and each future scenario (Fig. 5.9b). For all regions under RCP2.6 and RCP6.0, the lower limit of the 95% confidence interval of the difference is close to zero and in some regions includes both positive and negative AF values (Fig. 5.9b). On the other hand, the uncertainty range of differences between present-day and RCP8.5 only includes positive values for the majority of the regions (Fig. 5.9b).

The regional and total estimated mortality burdens associated with long-term exposure to annual mean MDA8 O_3 are shown in Fig. 5.10a. The estimated total UK-wide present-day (2000) mortality burden reaches a total of 7,705 attributable deaths. Under all RCPs, regions which have high population totals (Table 4.2), such as the North West region, have high estimated mortality burdens in 2050 (Fig. 5.10a). For example under RCP8.5, the North West and South East regions are the regions with the highest estimated mortality burden in 2050 (Fig. 5.10). Under all three RCPs, the future total estimated mortality burden in 2050 is higher than present-day (positive differences, Fig. 5.10b), as a result of higher total AFs of respiratory mortality (Fig 5.9b). Increases in the estimated attributable mortality burden for RCP2.6 and RCP6.0 total 2,710 and 2,529 additional attributable deaths respectively, and reach 5,396 additional attributable deaths for RCP8.5 (Fig. 5.10b).

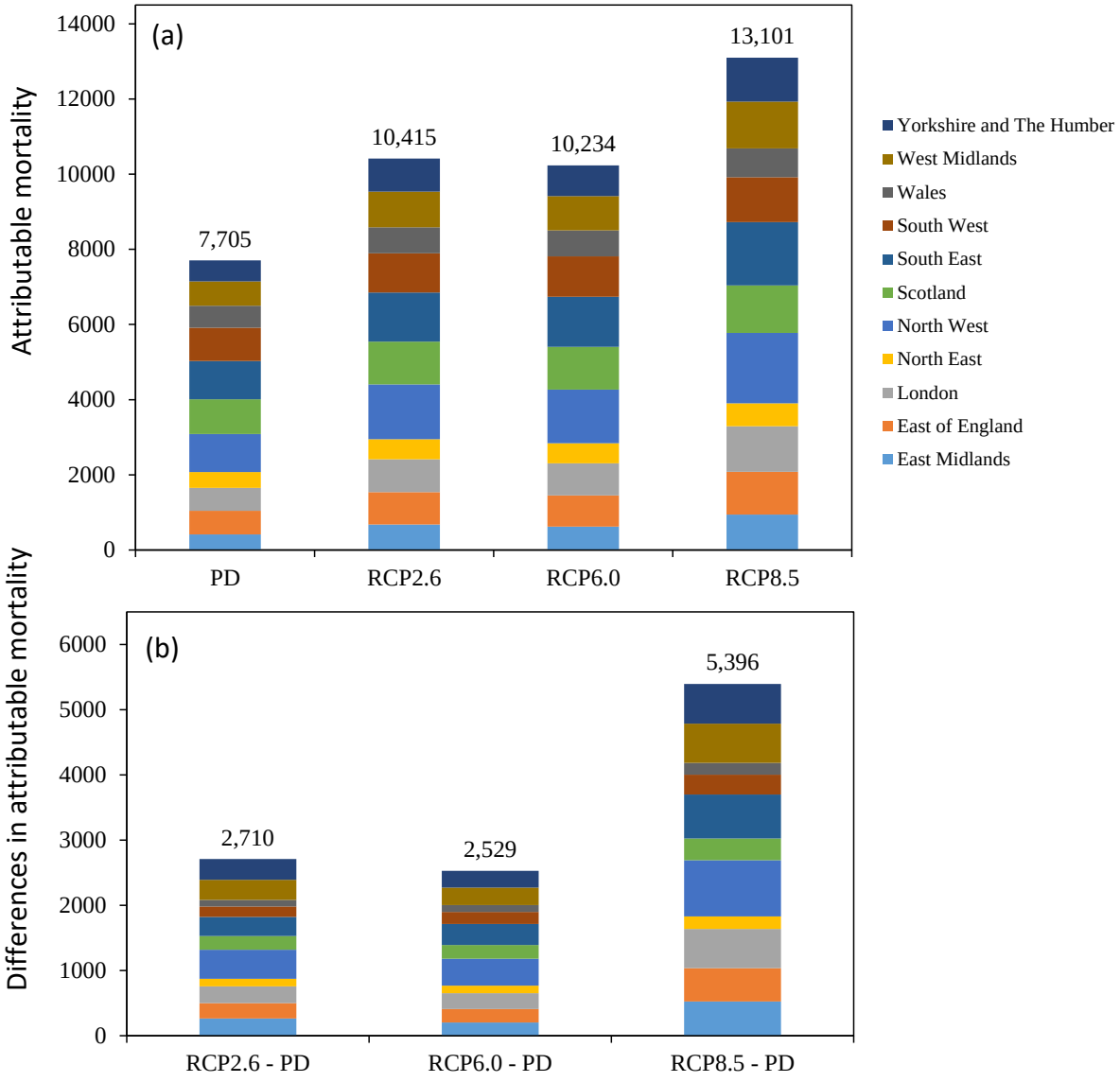

Figure 5.10: (a) UK annual respiratory attributable deaths associated with long-term exposure to annual mean MDA8 O_3 for present-day (PD – 2000), and all three RCPs for 2050. (b) Differences in UK annual attributable deaths between present-day and future under RCP2.6, RCP6.0 and RCP8.5. Colours indicate the annual attributbale deaths for each region in England and Scotland and Wales. N.B. no population projections are included in these future health burdens.

5.4.2 Health impacts associated with long-term exposure to annual mean NO_2

The estimated regional AF of all-cause (excluding external) mortality associated with long-term exposure to annual mean NO_2 for present-day and all three future emission scenarios is illustrated in Fig. 5.11a. The present-day AF of all-cause (excluding external) mortality across the regions ranges from 2.85% (95% CI = 1.15%, 4.52%) in Wales to 6.18% (95% CI = 2.52%, 9.70%) in London (Fig. 5.11a). Across the three future scenarios for 2050, the estimated AF of all-cause (excluding external) mortality ranges from 1.29% (95% CI = 0.52%, 2.05%) in Scotland to 4.31% (95% CI = 1.75%, 6.81%) in London for RCP8.5 and RCP6.0, respectively (Fig. 5.11a).

Corresponding differences in the AF of all-cause (excluding external) mortality between present-day and RCP future scenarios are illustrated in Fig. 5.11b. For all regions, the AF of all-cause (excluding external) mortality estimates are lower in 2050 compared to present-day (Fig. 5.11b) with the smallest reductions estimated for RCP6.0 and the highest reductions estimated for RCP8.5. As the calculation of AF only depends on the population-weighted pollutant concentrations, differences in AF between present-day and each of the future scenarios are consistent with differences in annual mean NO_2 concentrations described in Section 5.3.1 (Fig. 5.4). Differences in the AF of all-cause (excluding external) mortality range from -1.36% (95% CI = -3.59%, +0.87%) in the South West region to -4.06% (95% CI = -7.72%, -0.41%) in East Midlands for RCP2.6 and RCP8.5, respectively (Fig 5.11b).

As noted for the AF of respiratory mortality due to O_3 exposure (section 5.4.1), the error bars based on the 95% confidence interval of the NO_2 concentration-response function are relatively large (Fig. 5.11a). For all regions the 95% confidence interval for each RCP overlaps that of present-day with the least overlap occurring under RCP8.5 (Fig. 5.11a). The 95% confidence intervals of the

difference between present-day and future AF estimates for all RCPs are presented in Fig 5.11 b. Over most regions, the confidence interval includes both positive and negative AF values. However, under RCP8.5 in East Midlands, Yorkshire and the Humber, West Midlands and the North West region, only negative values are included in the 95% confidence interval of differences in the AF of mortality. This suggests significant differences between present-day and future AF estimates under RCP8.5 in these regions which also exhibited significant positive differences in the O_3-related AF estimate (c.f. Fig. 5.7b and Fig. 5.11b).

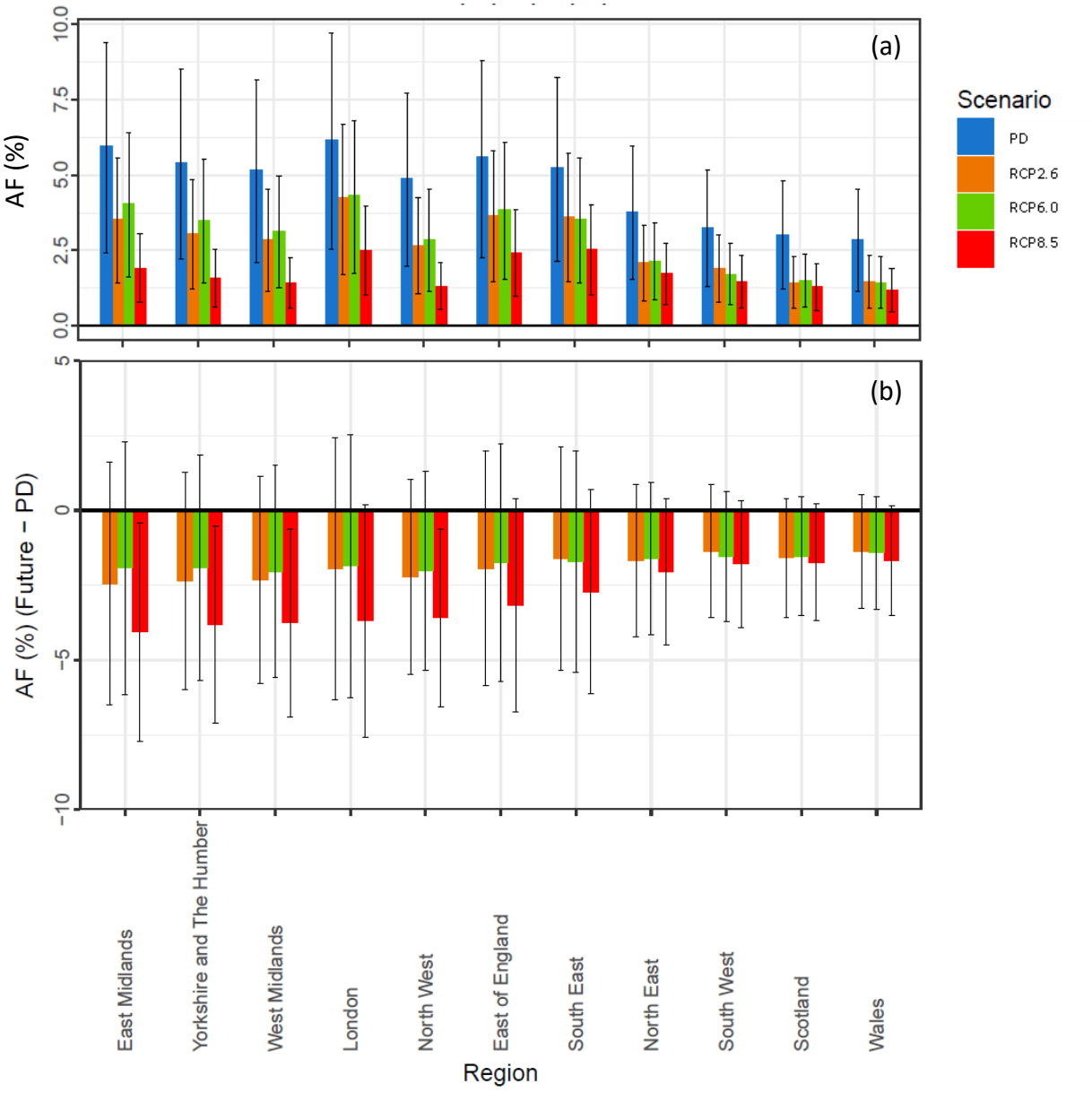

Figure 5.11: (a) Attributable fraction (AF) of all-cause (excluding external) mortality associated with long-term exposure to annual mean NO_2 for present-day (PD) in 2000 and each RCP for 2050 expressed as a percentage of total annual respiratory mortality. (b) Difference in AF between present-day and future expressed as a percentage for each regions in England, Scotland and Wales ($AF_{future} - AF_{present\text{-}day}$). Error bars show the 95% CI which represents uncertainties associated only with the concentrations-response function used. For Figure 5.11b the errors bars are calculated as described in section 2.4.4.

The estimated regional and national mortality burdens associated with long-term exposure to annual mean NO_2 for 2000 and 2050 are illustrated in Fig. 5.12a. The present-day NO_2-related UK mortality burden in 2000, totals 25,278 attributable deaths (Fig. 5.12a). Regions having high present-day population totals (e.g. South East region; Table 4.2) exhibit the highest attributable mortality burden totals. Future estimated mortality burdens for 2050 range from 9,496 to 15,860 attributable deaths for RCP8.5 and RCP6.0, respectively (Fig 5.12a). For all RCP scenarios, the estimated mortality burdens in 2050 are lower compared to present-day; differences in mortality burdens range between 15,782 and 9,418 avoided attributable deaths for RCP6.0 and RCP8.5, respectively (Fig 5.12b). These reductions in estimated mortality burdens are driven by reductions in the estimated AF of mortality which in turn are driven by reductions in population-weighted annual mean NO_2 concentrations. Estimates presented in this section could, to some extent, overlap with the health burden associated with long-term exposure to $PM_{2.5}$ (Section 5.4.3) as the two pollutants are not necessarily independent (COMEAP, 2015a). On the other hand, Williams et al. (2014) demonstrate that the analysis of O_3 and NO_2 separately in epidemiological studies can underestimate the combined effects on the population from exposure to both pollutants.

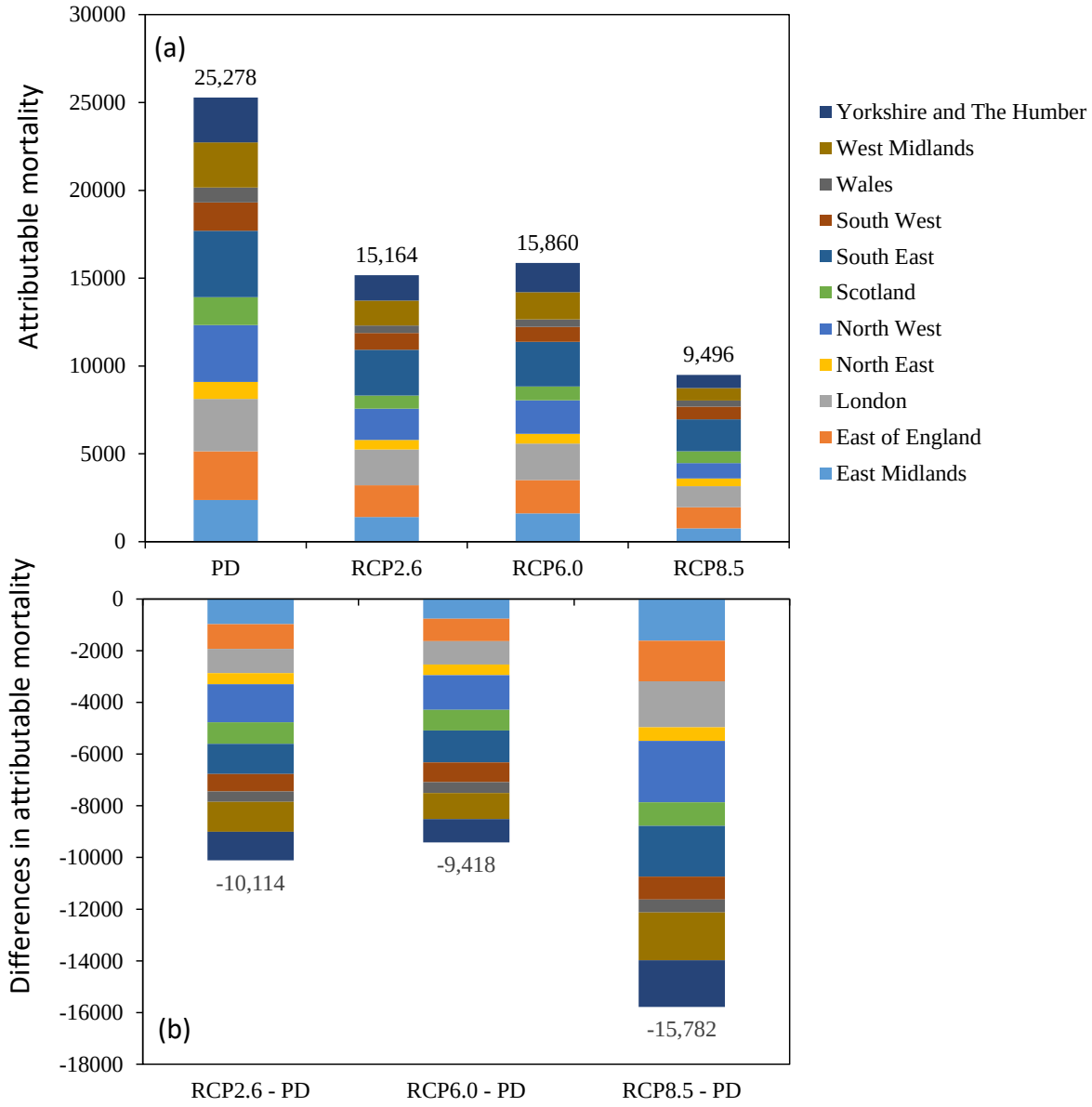

Figure 5.12: (a) UK annual attributable deaths associated with long-term exposrue to annual mean NO_2 for present-day (PD - 2000), and all three RCPs in 2050. (b) Differences in UK annual attributable deaths between present-day and future under RCP2.6, RCP6.0 and RCP8.5. Colours indicate the annual attributable deaths for each region in England and Scotland and Wales. N.B. no population projections are included in these future health burdens.

5.4.3 Health impacts associated with long-term exposure to annual mean $PM_{2.5}$

The AF of all-cause (excluding external) mortality associated with long-term exposure to annual mean $PM_{2.5}$ for present-day and all three future scenarios is depicted in Fig. 5.13a. The present-day AF of all-cause (excluding external) for the year 2000 ranges from 4.01% (95% CI = 2.61%, 5.33%) in Scotland to 7.70% (95% CI = 5.04%, 10.18%) in East England; these regions correspond to those with the lowest and highest present-day $PM_{2.5}$ concentrations, respectively (Fig. 5.5a). For all future RCPs for 2050, the AF of all-cause (excluding external) mortality associated with long-term exposure to annual mean $PM_{2.5}$ is lower than present-day estimates and ranges from 3.06% (95% CI = 1.99%, 4.08%) in Scotland to 6.70% (95% CI = 4.37%, 8.86%) in East England for RCP2.6 and RCP6.0, respectively (Fig. 5.13a).

Differences in the AF associated with long-term exposure to annual mean $PM_{2.5}$ between present-day and each future scenario are illustrated in Fig. 5.13b. Across the UK, the AF of all-cause (excluding external) mortality is lowest under RCP8.5 resulting in a maximum difference of -2.28% (95% CI = -4.86%, +0.30%) in East Midlands (Fig. 5.13b). In contrast, the lowest decreases in the AF of mortality for 2050 relative to 2000 occur for RCP6.0 with differences ranging from -0.43% (95% CI = -2.25%, +1.40%) in Scotland to -1.07% (95% CI = -4.40%, +2.25%) in London. These AF results are in agreement with those for annual mean $PM_{2.5}$ concentrations changes between present-day and future presented in Section 5.3.2 (c.f. Fig. 5.5 and Fig. 5.13b).

The overlap of the 95% confidence intervals between present-day and the three RCPs noted in Sections 5.4.1 and 5.4.2 also holds for the AF of mortality associated with $PM_{2.5}$ exposure (Fig. 5.13a). For all regions, the 95% confidence intervals of differences in the $PM_{2.5}$-related AF of mortality between present-day and all three RCPs include both positive and negative AF levels thus suggesting

$PM_{2.5}$-related differences are not significant (Fig. 5.13b). This contrasts the results for the differences between RCP8.5 and present-day in the estimated AF values associated with O_3 and NO_2 exposure, that appear significant across four regions.

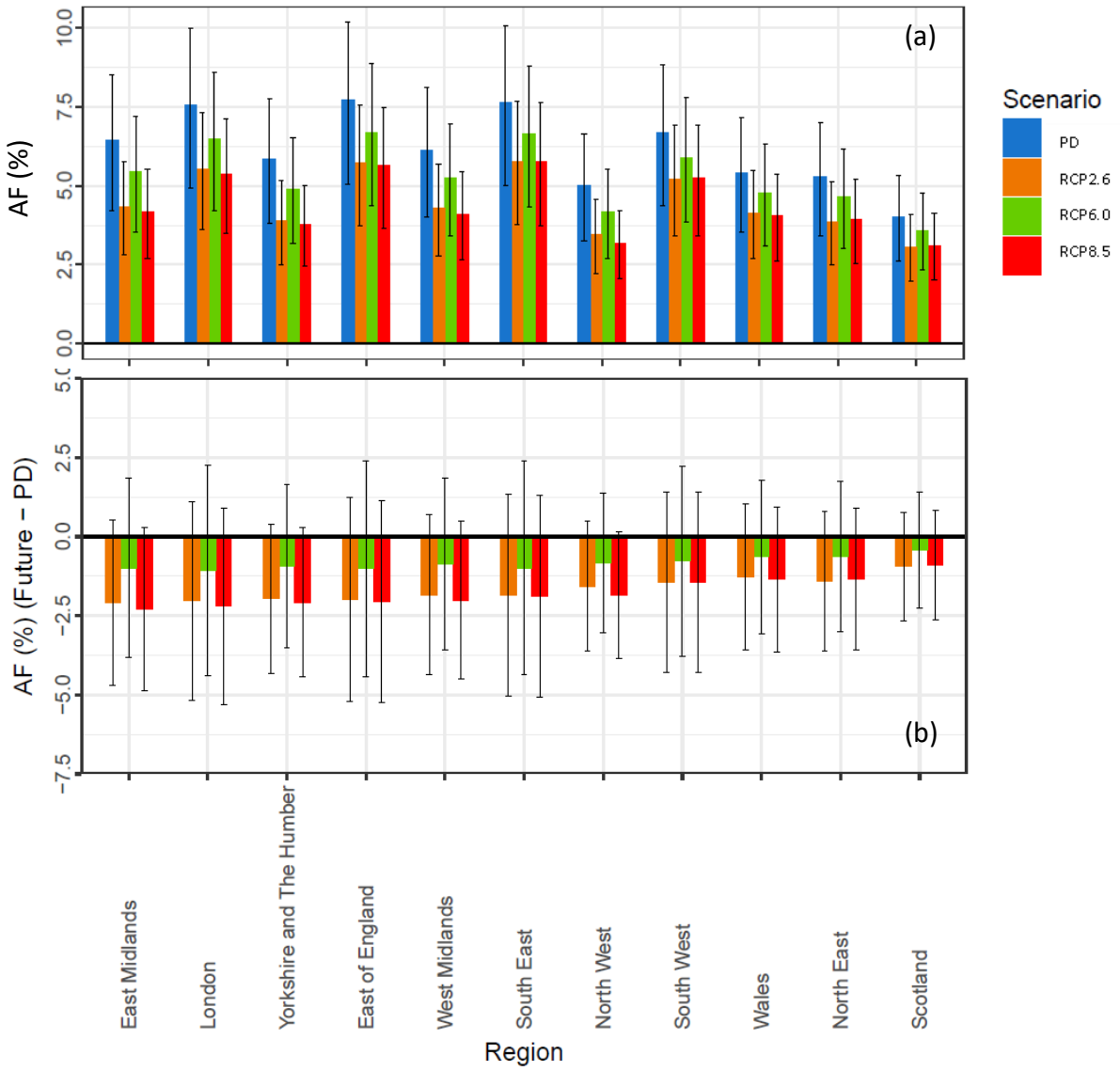

Figure 5.13: (a) Attributable fraction (AF) associated with long-term exposure to annual mean $PM_{2.5}$ for present-day (PD - 2000) and each future RCP for 2050 expressed as a percentage of total annual respiratory mortality. (b) Difference in AF between present-day and future expressed as a percentage for each regions in England, Scotland and Wales ($AF_{future} - AF_{present\text{-}day}$). Error bars show the 95% CI which represents uncertainties associated only with the concentrations-response function used. For Figure 5.13b the errors bars are calculated as described in section 2.4.4.

The estimated regional mortality burdens for present-day (2000) and all three future scenarios (2050) are illustrated in Fig. 5.14a. For present-day, it is estimated that 32,996 attributable deaths are associated with long-term exposure to annual mean $PM_{2.5}$ concentrations. The total UK mortality burdens for each of the future emission scenarios are estimated at 24,034, 28,475 and 23,514 attributable deaths over the UK under RCP2.6, RCP6.0 and RCP8.5 in 2050, respectively (Fig 5.14a). For both present-day and future scenarios the estimated mortality burdens are highest in regions having a combination of a high AF of mortality (Fig 5.13a) and high population totals (Table 4.2). For example, this occurs in the South East, London and East of England regions (Fig 5.14a). Differences in estimated regional mortality burdens between present-day and future scenarios for 2000 and 2050 respectively are shown in Fig. 5.14b. Similar to differences in the AF of mortality, the estimated mortality burden for all RCP scenarios in 2050 are lower compared to present-day estimates (Fig 5.14b). The largest decreases in estimated attributable deaths associated with long-term exposure to $PM_{2.5}$ occur under RCP2.6 and RCP 8.5 (8,962 and 9,481 avoided attributable deaths, respectively) while the smallest decreases occurs under RCP6.0 (4,521 avoided attributable deaths).

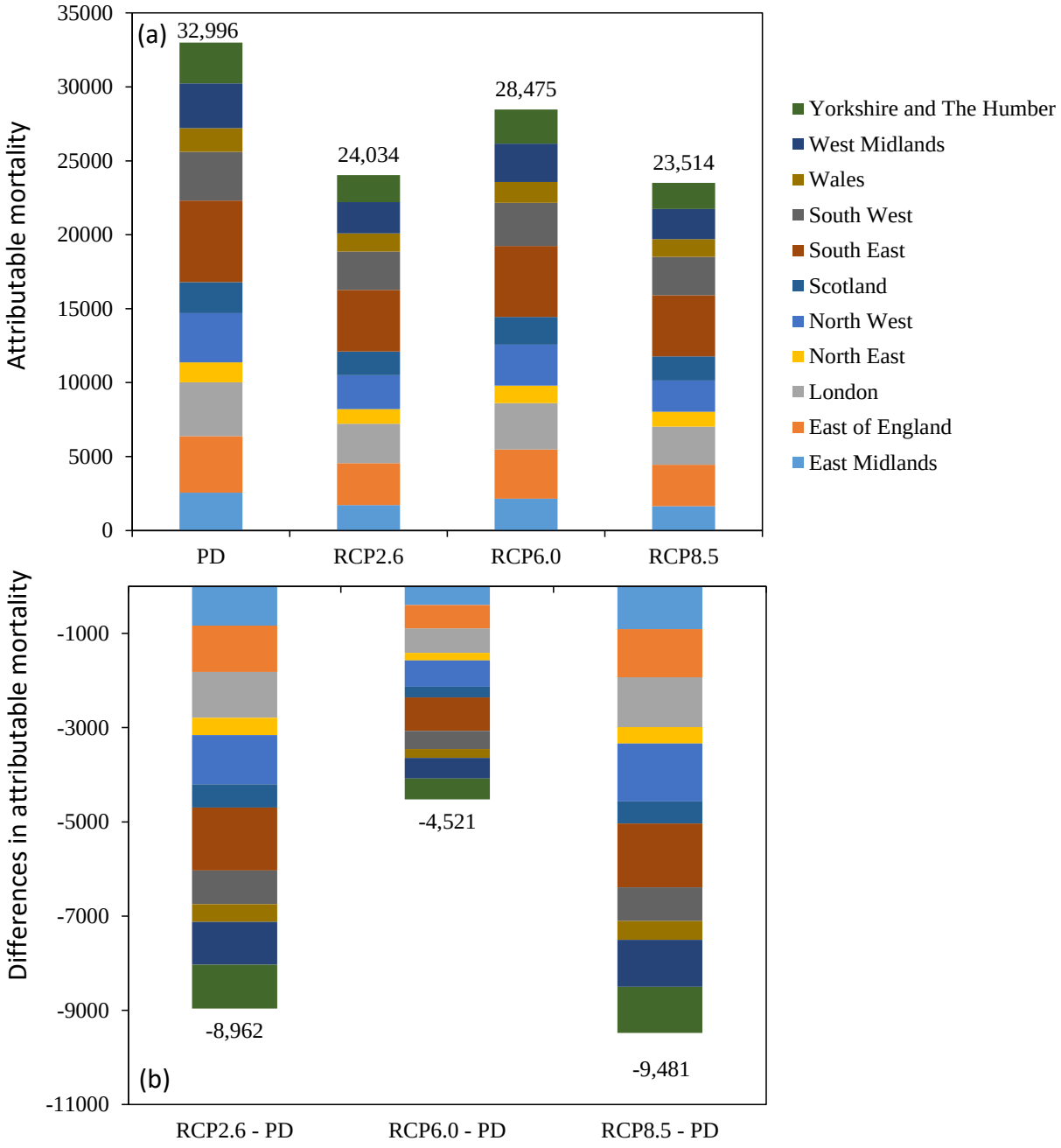

Figure 5.14: (a) UK annual attributable deaths associated with long-term exposure to annual mean $PM_{2.5}$ for present-day (PD - 2000), and all three RCPs for 2050. (b) Differences in UK annual attributbale deaths between present-day and future under RCP2.6, RCP6.0 and RCP8.5. Colours indicate the annual attributable deaths for each region in England and Scotland and Wales. N.B. no population ptojections are included in these future health burdens.

In summary, in section 5.4.1, it is estimated that across all UK regions both the percentage of respiratory mortality (AF) and total mortality burdens associated with long-term exposure to annual mean MDA8 O_3 are higher for all three RCPs in 2050 compared to present-day estimates. In contrast for all RCPs, the mortality burdens associated with long-term exposure to annual mean NO_2 and $PM_{2.5}$ concentrations are lower for 2050 relative to 2000 (Sections 5.4.2 and 5.4.3). These differences are driven by differences in the respective population-weighted pollutant concentrations where annual mean MDA8 O_3 concentrations are higher for future scenarios and annual mean NO_2 and $PM_{2.5}$ concentrations are lower.

Models used to simulate future air pollutant concentrations generally have a coarser (~50km) horizontal resolution and studies typically only quantify impacts at a global or European scale, thus a direct comparison of results in this section with other studies is quantitatively impossible. Instead the direction of changes under different scenarios are compared. In addition, the long-term future O_3 mortality burdens have not yet been quantified for the UK.

Of the studies to date, Heal et al. (2013) estimated the annual mortality associated with short-term exposure to O_3 for the 2030s under future SRES emission scenarios (NOx emission reductions ranging between 20% and 43%), and find overall increases in O_3-related mortality burdens (when including future population projections). However in this study the O_3 concentrations under the different scenarios are not consistently higher over the UK compared to present-day as found in this chapter. This could be associated with larger NO_x reductions (ranging from 58% to 73%) used for the longer timeframe of 2050 in this chapter. Using a similar model set-up to this thesis, but using RCP emissions and climate scenarios (i.e. also including climate change), Pannullo et al. (2017) estimate the respiratory hospital admissions attributable to NO_2 in 2050 and find a reduction of 1.7%, 1.4% and 2.4% in hospital admissions under RCP2.6, RCP6.0 and RCP8.5, respectively in England (relative to average present-day respiratory hospital

admissions per year across England – 613,052). This is to some extent similar to findings in this chapter where reductions in NO_2 concentrations under all RCPs in 2050 lead to reductions in NO_2- related mortality burdens across the UK compared to present-day. Williams et al. (2018) also estimate the health benefits for the UK following emission reductions under three energy consumption scenarios for 2050 (outlined in section 5.1). They suggest a decrease in annual mean NO_2 concentrations as a result of NO_x reductions with a subsequent reduction in NO_2-related mortality burdens in 2050. Annual mean $PM_{2.5}$ concentrations are also estimated to decrease in the future as a result of primary and precursor emission reductions, resulting in lower $PM_{2.5}$-related mortality burdens (Williams et al. 2018). In a broader European context, O_3-related mortality burdens are generally found to reduce in the future under the different RCPs for 2050 with a slight increase for RCP8.5 as a result of increases in methane concentrations (e.g. Silva et al., 2016; West et al., 2013). $PM_{2.5}$ mortality burdens are also generally found to decrease in the future as a result of reductions in primary and precursor emissions (e.g. Pozzer et al., 2017; Silva et al., 2016).

Overall, the findings in this chapter compare well with previous UK-based studies that are based on future emissions reductions, in terms of directions of change in future O_3, NO_2 and $PM_{2.5}$-related mortality burdens. In addition differences in the direction of change between the future O_3-related health burdens that increase in the future in this chapter and that found in different European studies whereby health burdens reduce (West et al. 2013; Silva et al. 2016) (see section 5.1) may be due to the coarser model resolutions used in these studies (section 1.3).

5.4.4 Sensitivity of estimated regional mortality burdens to future population projections under the SSPs

In this section the sensitivity of the future mortality burden estimates in 2050 presented in Sections 5.4.1 – 5.4.3 to future population projections based on two shared socio-economic pathways (SSPs): SSP1 (low UK population total) and SSP5 (high UK population total) is assessed (see Section 5.2.5). These two SPPs are only used to provide future population estimates and do not include any corresponding effects on the emissions types associated with these scenarios. Under these scenarios the population of the UK increases by a factor of 1.2 and 1.4, respectively (Table 5.2 Section 5.2.5). Regional annual baseline mortality rates for the future mortality burdens are assumed to be the same as for present-day.

5.4.4.1 Sensitivity of estimated regional O_3-related mortality burdens to future population projections under the SSPs

Differences in the UK mortality burden or attributable deaths between present-day (2000) estimates (that use present-day population totals) and future estimates for 2050 (including future population projections following the SSP1 and SSP5 scenarios) are presented in Fig. 5.15. Using population projections that follow SSP1, the estimated differences in the UK mortality burden between present-day and future ranges from 4,949 in RCP6.0 to 8,647 in RCP8.5 (Fig. 5.15a), while differences range from 7,985 to 13,661 additional attributable deaths for SSP5 (Fig. 5.15b). For all RCPs under both SSP1 and SSP5 population projections, the differences in estimated mortality burdens between present-day and future are amplified compared to the differences in mortality burdens with static populations levels (c.f. Fig 5.10b and Fig 5.15). Indeed under SSP1, mortality burdens are up to a factor of ~2 greater in 2050 than if no changes in future population totals are taken into account. Future O_3-related mortality burdens are further amplified under SSP5 with results up to a factor of ~3 greater in 2050 than if population totals are kept at

present levels. Under both SSPs, all regions exhibit increases in O_3-related mortality burden following the different RCPs in 2050. In particular, large increases are noted in London especially under RCP8.5 following the SSP5 population scenarios (Yellow box Fig 5.15b)

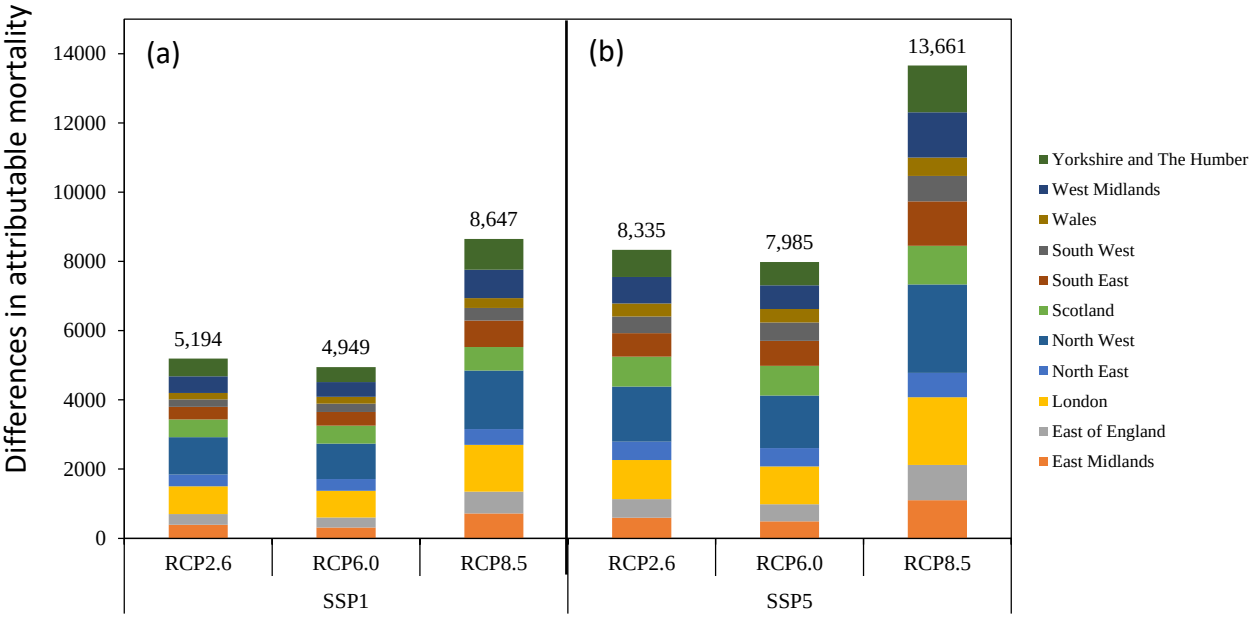

Figure 5.15: Differences in UK annual attributable deaths associated with long-term exposure to annual mean MDA8 O_3 between present-day (PD) for the year 2000 scenario and the future under RCP2.6, RCP6.0 and RCP8.5 emisisosn scenarios including future population projections following (a) SSP1 and (b) SSP5. Colours indicate differences in annual attributable deaths for each region in England and Scotland and Wales.

5.4.4.2 Sensitivity of estimated regional NO_2-related mortality burdens to future population projections under the SSPs

Differences in UK regional mortality burdens associated with long-term exposure to annual mean NO_2 between present-day and future estimates including future population scenarios are shown in Fig. 5.16. Differences in the mortality burden associated with long-term exposure to annual mean NO_2 concentrations range from 5,179 (RCP6.0) to 13,547 (RCP8.5) avoided attributable deaths when using SSP1 and

range from 2,339 (RCP6.0) to 11,877 (RCP8.5) avoided attributable deaths when using SSP5. Including these future SSP population projections the estimated future mortality burdens in 2050 are higher compared to when the present-day population totals are used. Therefore, reductions in the UK mortality burden between present-day and all three future scenarios are diminished (c.f Fig 5.12b and Fig. 5.16). Under SSP1, differences in NO_2-related mortality burdens in 2050 vary from those using present day population totals by up to a factor of 0.9, and under SSP5 by up to a factor of 0.8. For the majority of the regions, the mortality burdens in 2050 are lower compared to present-day when accounting for future population projections (Fig 5.16). The exception is London for SSP1, and especially SSP5, where the future NO_2-related health burden is higher compared to present-day for RCP2.6 and RCP6.0 (yellow box; Fig 5.16). This increase in the NO_2-related mortality burden occurs despite estimated reductions in NO_2 concentrations in this UK region under all three RCPs, thus highlighting the impact of the large estimated increase in the future population for this region for NO_2-related mortality (from 4.5 million people for present-day to 8.3 million people for 2050 in London under SSP5).

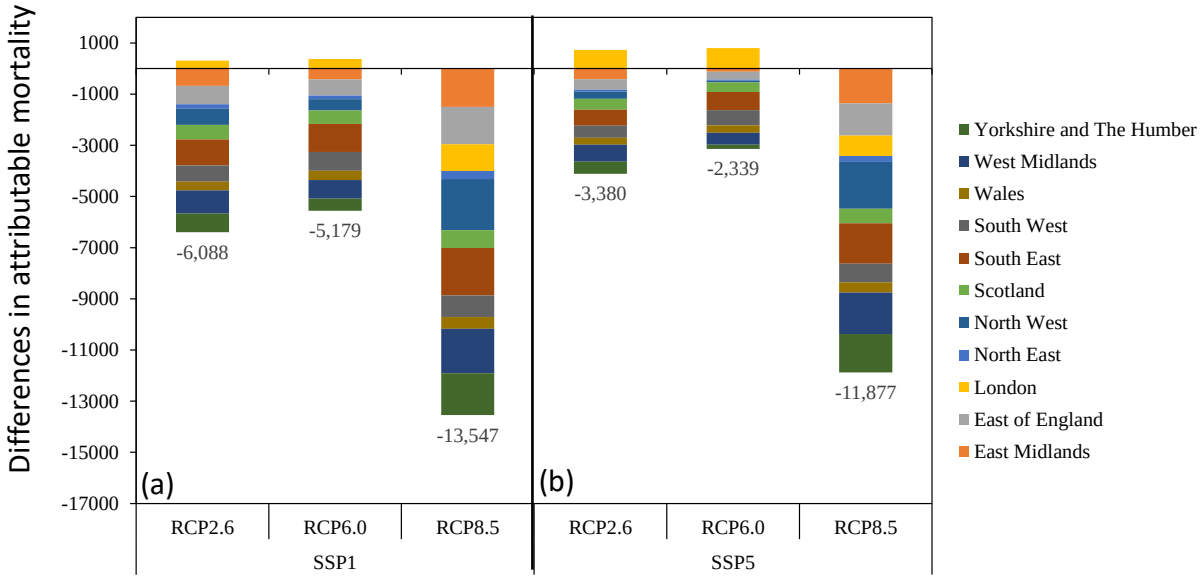

Figure 5.16: Differences in UK annual attributable deaths associated with long-term exposure to annual mean NO_2 between present-day (PD) for 2000 and future under RCP2.6, RCP6.0 and RCP8.5 for 2050 including future population projections following (a) SSP1 and (b) SSP5. Colours indicate differences in annual attributable deaths for each region in England and Scotland and Wales.

5.4.4.3 Sensitivity of estimated regional $PM_{2.5}$-related mortality burdens to future population projections under the SSPs

Differences in attributable deaths between present-day and future estimates including future population projections (SSP1 and SSP5) are illustrated in Fig. 5.17. Applying future projections based on SSP1 it is estimated that the difference in the total UK mortality burden between present-day (2000) and under RCP2.6 and RCP8.5 is 3,533 and 4,259 avoided attributable deaths, respectively (Fig. 5.17a). The magnitude of this reduction in mortality is 0.4 times that estimated using present-day population totals. This indicates that the total UK-wide future mortality burdens are still lower compared to present-day under the RCPs that incorporate population increases in 2050. In contrast it is estimated that the overall mortality burden associated with long-term exposure to $PM_{2.5}$ for RCP6.0 is positive with 2,006 additional attributable deaths (Fig. 5.17a). Without population changes, differences in the $PM_{2.5}$-related mortality burdens between present-day and RCP6.0 estimates in 2050 are smaller than the other two scenarios (Fig 5.14b). Accounting for future population increases under SSP1 and following RCP6.0 in 2050, results in total $PM_{2.5}$-related mortality burdens that are higher compared to present-day estimates.

Considering the individual regions, the overall population increases under SSP1 everywhere, but the difference in mortality burden for the majority of the regions for RCP2.6 and RCP8.5 is still negative (Fig. 5.17a). However, for regions where the population is projected to increase substantially notably London, the impact of increased population leads to an increase in future estimated mortality for all RCPs (yellow box Fig. 5.17a).

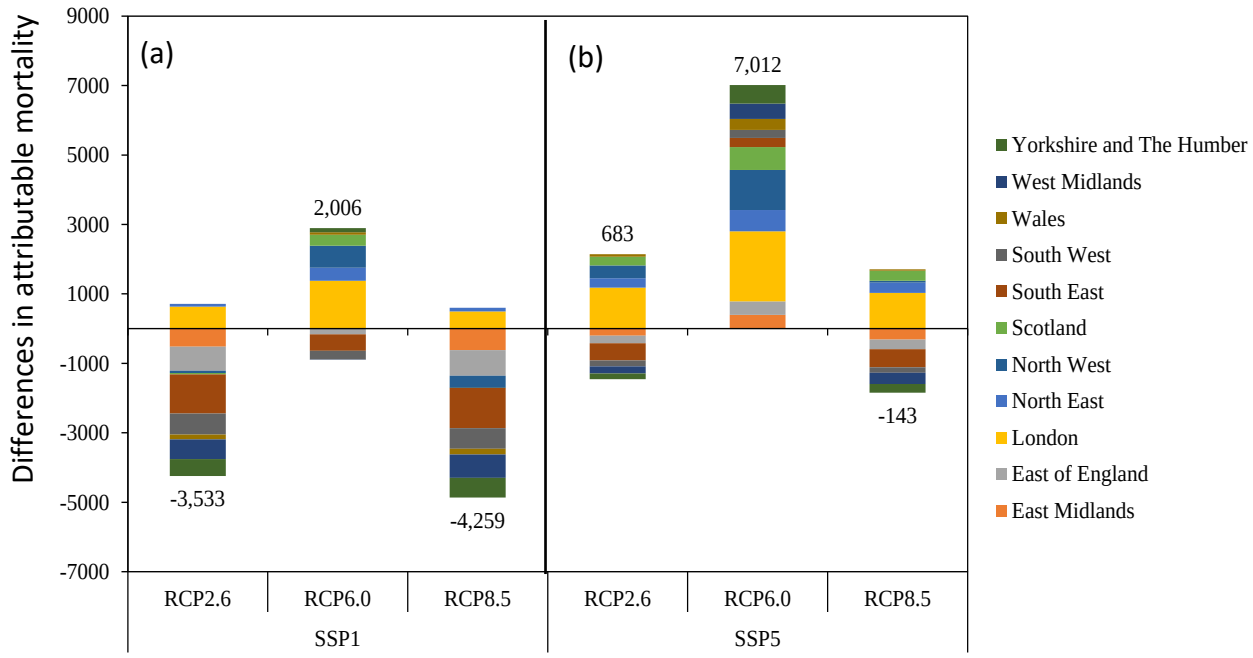

Figure 5.17 Differences in UK annual attributable deaths associated with long-term exposure to annual mean $PM_{2.5}$ between present-day (PD) for 2000 and future under RCP2.6, RCP6.0 and RCP8.5 for 2050 including future population projections following (a) SSP1 and (b) SSP5. Colours indicate differences in annual attributable deaths for each region in England and Scotland and Wales.

As a result of a further increase in total population for SSP5, the estimated future mortality burdens are higher overall compared to present-day for RCP2.6 and RCP6.0 with 683 and 7,012 additional attributable deaths (Fig. 5.17b). In contrast, for the majority of the regions under RCP8.5 with SSP5 population levels for 2050, the $PM_{2.5}$-related UK mortality burden is lower overall compared to present-day with a total of 143 avoided attributable deaths (Fig. 5.17b).

To summarise the results of section 5.4, including the projected population scenarios when estimating future mortality burdens based on the SSP1 and SSP5, results in higher future mortality burdens especially in densely populated regions

such as London. For O_3 whose levels are estimated to increase in the future, the difference in mortality burdens between present-day and future is amplified when incorporating future population scenarios (up to a factor of ~3). However, for NO_2 and $PM_{2.5}$, pollutants that are estimated to decrease under future UK emissions scenarios, including future increases in population may result in a change in sign as well as the magnitude for the total differences in UK mortality burdens between present-day and future. This result is broadly consistent with other studies. For example Silva et al (2016) suggest that future increases in population in 2050 magnify the impact of changes in air pollutant concentrations and find that the future global mortality burden of air pollution for $PM_{2.5}$ can exceed the current burden, even where air pollutant concentrations decrease.

5.5 Conclusions

The influence of changes in UK emissions following three Representative Concentration Pathways (RCPs); RCP2.6, RCP6.0 and RCP8.5 on simulated air pollutant concentrations of O_3, NO_2 and $PM_{2.5}$ over the UK for 2050 relative to 2000 is investigated using an air quality model (AQUM) at a 12 km horizontal resolution. The corresponding changes in attributable fraction (AF) of mortality and mortality burdens associated with long-term exposure to annual mean MDA8 O_3, NO_2 and $PM_{2.5}$ between present-day and future scenarios are estimated for different regions of the UK. In addition the sensitivity of these health estimates to future population projections is also analysed.

Future pollutant levels are driven by changes in precursor and primary aerosol emissions over the UK as well as the underlying chemistry. Under all the three RCPs, O_3 concentrations increase across the entire UK in 2050 compared to 2000 due to substantial decreases in NOx emissions (ranging between -58% and -

73%) leading to less titration of O_3 by NO. Projected increases in CH_4 concentrations for the UK under RCP6.0 and RCP8.5 may also contribute to increases in O_3 concentrations. The increases in O_3 are largest in regions having low present-day O_3 concentrations and reach a maximum (greater than 12 μg m^{-3},~40%) in Central England under RCP8.5. In contrast, under all RCPs, simulated annual mean NO_2 concentrations decrease across the UK with the largest reductions occurring in Central England (~-75%), where O_3 increases are greatest. Overall, this suggests the whole of the UK is simulated in this study as being in a NOx saturated or VOC limited regime (Section 1.2), and highlighting that future emission controls should not only consider NOx emissions reductions.

Annual mean $PM_{2.5}$ concentrations also decrease in 2050 for all RCPs with the highest reductions of ~4.5 μg m^{-3} (~-50%). in Central and eastern England for RCP8.5 (~-50%). This is driven by large reductions in precursor emissions of SO_2 (up to -94% for RCP8.5) which in turn lead to reductions in sulphate aerosol concentrations (a major component of present-day total $PM_{2.5}$); 45% for present-day to 27% under RCP 2.6.

For all regions and under all three RCP emission scenarios, the corresponding AF of respiratory mortality associated with long-term exposure to annual mean MDA8 O_3 is estimated to increase in 2050 while the AF of all-cause (excluding external) mortality associated with long-term exposure to NO_2 and $PM_{2.5}$ is estimated to decrease as a result of higher and lower projected pollutant concentrations, respectively. The future AF of respiratory mortality associated with long-term exposure to MDA8 O_3 is estimated to increase compared to present-day with the largest increase reaching 9.34% (95% CI = 6.50%, 11.93%) in the East Midlands under the RCP8.5 emission scenario. The corresponding total respiratory mortality burden associated with long-term exposure to MDA8 O_3 between the RCPs is estimated to increase by 2,529 (RCP6.0) to 5,396 (RCP8.5) additional attributable deaths in 2050 relative to 2000.

Future AF estimates associated with long-term exposure to annual mean NO_2 are lower compared to present-day with differences ranging between -1.36% (95% CI = -0.55%, -2.14%) in the South West region to -4.06% (95% CI = -1.66%, -6.35%) in East Midlands for RCP2.6 and RCP8.5, respectively. Differences between present-day and future NO_2-related mortality burdens range between 9,418 and 15,782 avoided attributable deaths for RCP6.0 and RCP8.5, respectively.

The AF of mortality associated with long-term exposure to $PM_{2.5}$ concentrations is lower in 2050 for all RCPs compared to present-day, with differences ranging between -2.28% (95% CI = -1.5%, -3.0%) in East Midlands and -0.43% (95% CI = -0.29%, -0.56%) in Scotland for RCP8.5 and RCP6.0, respectively. The UK mortality burden associated with present-day long-term exposure to annual mean $PM_{2.5}$ is estimated at 32,996 attributable deaths. Differences in mortality burdens between present-day and future range from 4,521 to 9,481 avoided attributable deaths for RCP6.0 and RCP8.5, respectively.

Results show that future MDA8 O_3, NO_2 and $PM_{2.5}$-attributable mortality burdens are sensitive to future population scenarios. Population scenarios based on the shared socio-economic pathways (SSPs) are used in this chapter which are compatible with the RCPs. Including future 2050 population scenarios SSP1 and SSP5, whereby the population total for the UK increases by a factor of 1.2 and 1.4, respectively, results in larger positive differences between present-day and future mortality burdens associated with long term exposure to O_3 with a maximum of 13,661 additional attributable deaths for the UK in 2050 for RCP8.5 under the SSP5 population scenario. This value is up to a factor of ~ 3 greater than if population totals are kept at present levels. In contrast the reduction in attributable deaths associated with long-term exposure to NO_2 between present-day and future are diminished, with a maximum difference of 11,877 avoided attributable deaths for the UK when including the SSP5 population scenario and RCP8.5 (up to a factor of ~ 0.9 of estimates with population totals kept at present levels). The impact of

applying future population projections on $PM_{2.5}$-related mortality burdens is similar to the NO_2-related mortality burdens. However, following the SSP5 population scenario, $PM_{2.5}$-related mortality burdens for RCP2.6 and RCP6.0 in 2050 are higher compared to present-day leading to 683 and 7,012 additional attributable deaths, despite simulated reductions in $PM_{2.5}$ concentrations under these future scenarios. Note that, these mortality burdens may be overestimated as the effect of exposure to NO_2 and $PM_{2.5}$ may not be independent.

In terms of uncertainty, the 95% CI representing uncertainties associated with the CRF is quantified for the AF of mortality due to long-term exposure to O_3, NO_2 and $PM_{2.5}$. Results suggest that the uncertainty in the CRF has a substantial impact on the estimates of the AF of mortality for each UK region in terms of their magnitude and direction change, except for four UK regions where significant differences in AF estimates are found between present-day and following RCP 8.5 in 2050. In addition although uncertainties in total population projections are considered, uncertainties associated with the population demographics e.g. aging are not considered. In this Chapter ageing was not considered as gridded population data stratified by age is not currently freely available for future population estimates. Scaling of population totals could have been implemented to account for ageing however results would be highly uncertain. Changes in future baseline mortality rates are also neglected in this Chapter. Nonetheless results in this chapter highlight the sensitivity of annual mean MDA8 O_3, NO_2 and $PM_{2.5}$ concentrations to reducing UK NO_x emissions which in turn drive changes in estimates of UK and regional mortality burdens associated with long-term exposure to these pollutants under three RCPs for 2050 compared to 2000. In addition mortality burdens are also shown to be sensitivity to future population scenarios.

Chapter 6 Conclusions

This chapter presents the main conclusions of this thesis together with the uncertainties and limitations encountered and ideas for future work. First, a brief recollection of the motivation of this thesis and the research questions that have shaped this research is presented.

6.1 Introduction

Air pollution is a major environmental concern with epidemiological evidence linking adverse health impacts to air pollution exposure continuing to strengthen. Results from such epidemiological studies have been extensively used to estimate present-day health burdens due to air pollution exposure both globally and regionally. Chemistry-climate models are often used in global or regional-scale studies to simulate pollutant concentrations. One key uncertainty relates to the influence of different horizontal model resolutions within chemistry-climate models on simulated pollutant concentrations (Section 1.6).

The severity of air pollution events is linked to both emissions and the prevailing weather. Air pollution episodes generally occur under stagnant weather conditions associated with anticyclones (Section 1.7). In summer, such episodes may also be associated with heatwaves. Under a changing climate, while heatwaves

may become more intense and frequent, large-scale blocking episodes may decrease (Section 1.7). Thus studying the subsequent health impacts of air pollution episodes for present-day may shed light on the variability of health impacts associated with air pollution episodes.

In the future, changes in emissions are likely to be highly important for controlling air pollution in many world regions especially in the near-term (Section 1.8). Chemical reactions occurring within the troposphere are often highly non-linear (Sections 1.2.1, 1.2.2), thus research utilising chemistry-climate modelling is useful to estimate future pollutant concentrations under various scenarios which in turn will have implications for public health.

The main three objectives of this thesis are:

(1) To quantify the influence of model horizontal resolution on simulated concentrations of ozone (O_3) and particulate matter less than 2.5 μm in diameter ($PM_{2.5}$) for Europe and the implications for health impact assessments associated with long-term exposure to these pollutants (Chapter 3).

(2) To assess the variability in air pollutant concentrations of O_3 and $PM_{2.5}$ during two air pollution episodes in July 2006 in the UK and estimate the corresponding short-term attributable fraction of mortality and associated mortality burdens (Chapter 4).

(3) To estimate the potential future attributable fraction of mortality and associated mortality burdens in the UK associated with long-term exposure to O_3, NO_2 and $PM_{2.5}$ under future UK emissions for 2050 (Chapter 5).

The rest of this chapter is organised as follows: First, a summary of the impacts of model horizontal resolution on O_3 and $PM_{2.5}$ concentrations and the subsequent long-term health impacts in Europe are presented in Section 6.2. Next, the attributable fraction of mortality and corresponding mortality burdens associated with short-term exposure to O_3 and $PM_{2.5}$ concentrations during two air pollution episodes in July 2006 in the UK are discussed in Section 6.3. Lastly, the future attributable fraction of mortality and mortality burdens related to changes in UK emissions following three Intergovernmental Panel on Climate Change (IPCC) Representative Concentration Pathways (RCPs); RCP2.6, RCP6.0 and RCP8.5 are presented in section 6.4. The main findings of each chapter are also included in point form within a blue text box followed by highlights of each chapter within a green text box at the end of each section. Finally, uncertainties and limitations of this thesis and suggestions for future work are discussed in Sections 6.5 and 6.6.

6.2 The influence of model spatial resolution on simulated O_3 and $PM_{2.5}$ concentrations for Europe: implications for health impact assessments.

In Chapter 3, chemistry-climate model simulations are conducted to examine the influence of model horizontal grid resolution on O_3 and $PM_{2.5}$ concentrations and the associated health impacts in terms of the Attributable Fraction (AF) of mortality (Section 2.4.1). Two simulations are performed using the HadGEM3–UKCA (UK Chemistry and Aerosol) chemistry–climate model (Section 2.1) at two horizontal

resolutions: a global or coarser resolution (~140 km) and a regional or finer resolution (~50 km) to simulate air pollutant concentrations over Europe.

Simulated seasonal mean O_3 concentrations are compared to 52 measurement sites from the European Monitoring and Evaluation Programme (EMEP) network (Section 2.3). Modelled and observed seasonal mean O_3 concentrations averaged across the 52 sites are generally highest in spring and summer and lowest in autumn and winter. Compared to measurements, simulated O_3 concentrations at both resolutions are lower in winter and higher in summer and autumn. In spring, O_3 concentrations simulated at the coarser resolution are higher while concentrations at the finer resolution are lower compared to observations.

A seasonal variation in the mean O_3 differences averaged over Europe between the two model resolutions is found. At the coarse resolution, O_3 concentrations averaged over Europe are higher in winter and spring (~ 10% and ~6%, respectively) but lower in summer and autumn (~-1% and ~-4%, respectively) compared to the finer resolution. Differences in the simulated seasonal mean O_3 concentrations between the two resolutions are closely linked to differences in NO_2 concentrations. At the finer resolution, NO_2 concentrations are higher close to emissions sources and often coinciding with lower O_3 concentrations at these locations. The lower O_3 levels are thus likely due to the titration effect of NO on O_3 (R1.6; Section 1.2.1.2). Differences in seasonal mean planetary boundary layer (PBL) height between the two resolutions may also be linked with differences in seasonal mean O_3 concentrations. However, isolation of the independent impacts of chemistry and mixing on seasonal mean O_3 concentrations is not possible.

Simulated seasonal mean $PM_{2.5}$ concentrations are also compared to available EMEP observations at 25 sites. Observed seasonal mean $PM_{2.5}$ concentrations are highest in winter and spring and lowest in summer and autumn. However simulated seasonal mean $PM_{2.5}$ concentrations averaged across the 25

sites are generally higher in spring and summer and lower in autumn and winter for both resolutions. $PM_{2.5}$ concentrations simulated at both the coarse and finer resolutions are lower in winter and higher in summer compared to measurements. In spring and autumn, $PM_{2.5}$ concentrations simulated at the coarse resolution are lower compared to observations but higher at finer resolution.

Compared to O_3, the opposite seasonality in Europe-average differences in $PM_{2.5}$ concentrations between the two resolutions is found. At the coarse resolution, seasonal mean $PM_{2.5}$ concentrations averaged across Europe are lower in winter and spring (~-8% and ~-6%, respectively) but higher in summer and autumn (~10% and ~6%, respectively). Differences in the seasonal mean PBL height may partly explain differences in seasonal mean $PM_{2.5}$ concentrations. In particular, a deeper PBL height is generally simulated at the finer resolution over Europe in summer which may lead to greater vertical lofting producing lower surface $PM_{2.5}$ concentrations at this resolution compared to the coarser resolution. Furthermore, for all seasons, differences in seasonal mean $PM_{2.5}$ concentrations between the two resolutions are associated with differences in the convective rainfall rate which impact aerosol wet removal rates.

In the second part of Chapter 3, the influence of changing the model horizontal resolution on the estimated health impacts is presented. This is done using warm season (April-September) daily maximum 8-hr running mean (MDA8) O_3 and annual mean $PM_{2.5}$ concentrations as the relevant metrics and averaging periods associated with long-term exposure (Section 1.4.4). For both air pollutants, the spatial patterns of differences between the two model resolutions reveal clear and important contrasts. Using the coarse resolution, warm season MDA8 O_3 levels are shown to be higher in most of southern Europe as well as the UK and Ireland, but lower in other areas of northern and eastern Europe, when compared to the finer resolution. In contrast, annual mean $PM_{2.5}$ concentrations are higher across

most of northern and eastern Europe, but lower over parts of southwest Europe at the coarse compared to the finer resolution.

Finally, the attributable fraction (AF) of respiratory and all-cause (excluding external)mortality associated with long-term exposure to population-weighted warm season MDA8 O_3 and annual mean $PM_{2.5}$ is estimated at both horizontal resolutions for all European countries. The same concentration-response function (CRF; section 1.4.3) is used to estimate health effects at the coarse and finer model resolutions, and thus differences in the O_3 and $PM_{2.5}$-related country specific AF estimates are driven solely by differences in population-weighted pollutant concentrations. Hence the spatial patterns of differences across Europe in the AF of mortality associated with long-term exposure to O_3 and $PM_{2.5}$ between the two resolutions are similar to those outlined above for each pollutant. Across all the European countries, differences in the AF of respiratory mortality associated with long-term exposure to population–weighted warm season MDA8 O_3 range between −0.9 and +2.6% while differences in the AF of all-cause (excluding external) mortality associated with long-term exposure to population–weighted annual mean $PM_{2.5}$ range from −4.7 to +2.8%.

Main findings – Chapter 3

- Seasonal mean O_3 concentrations simulated at the coarse resolution are higher in winter and spring but lower in summer and autumn compared to the finer resolution. An opposite seasonality is found for differences in $PM_{2.5}$ concentrations between the two resolutions.

- The impact of the two resolutions on pollutant concentrations varies spatially, leading to similar spatially varying differences in country-specific AF of mortality associated with long-term exposure to summer mean MDA8 O_3 and annual mean $PM_{2.5}$.

- Across Europe, country-average AF associated with long-term exposure to summer mean MDA8 O_3 range between −0.9% and +2.6% of the total respiratory mortality (largest positive and negative differences in southern and eastern Europe, respectively).

- Differences in AF associated with long-term exposure to annual mean $PM_{2.5}$ range from −4.7% to +2.8% of the total all-cause (excluding external) mortality (largest positive and negative differences in eastern and western Europe, respectively).

Highlights – Chapter 3

- Seasonal variation in simulated O_3 differences between the finer and coarse resolutions.
- Opposite seasonal variation in simulated $PM_{2.5}$ differences between the two resolutions compared to the O_3 differences.
- The corresponding differences in the AF of mortality associated with long-term exposure to O_3 and $PM_{2.5}$ expressed as a percentage range between ~-4% and ~3% between the two resolutions.

6.3 Mortality associated with O_3 and $PM_{2.5}$ air pollution episodes in the UK in 2006.

In Chapter 4 the mortality burden associated with short-term exposure to O_3 and $PM_{2.5}$ during two air pollution episodes in July 2006; 1st-5th July and 18th – 22nd July, are estimated across the UK. The dates selected for the air pollution episodes are based on days when the Daily Air Quality Index (DAQI - and air quality guideline used in the UK; Section 1.4.1) was 'moderate' to 'high' and with high levels of O_3 and $PM_{2.5}$ occurring concurrently. The UK Met Office air quality model (AQUM) at 12 km horizontal resolution is used to simulate pollutant concentrations of O_3 and $PM_{2.5}$ during these two episodes. During both episodes, simulated meteorological variables suggest persistent anticyclonic conditions with mean sea-level pressures ~1020 hPa, light winds (~ 1.5m s^{-1}), high temperatures (~ 16°C to 26°C) and prevailing winds from the east and south east. This leads to high simulated concentrations of MDA8 O_3 (~120-130 µg m^{-3}) and daily mean $PM_{2.5}$ (~20-40 µg m^{-3}),

due to both local emissions trapping under stagnant conditions and slow transport of pollution from continental Europe.

For each episode the daily deaths brought forward associated with short-term exposure to MDA8 O_3 and $PM_{2.5}$ are estimated. For the two episodes in July 2006, the estimated UK total MDA8 O_3-related (all-cause) mortality burden is similar with about 70 total daily deaths brought forward. In contrast the $PM_{2.5}$-related (all-cause) mortality burden differs between the episodes with about 43 and 36 daily deaths brought forward during the first and second episode, respectively. Values across the UK regions, expressed as a percentage of all-cause mortality (AF) due to short-term exposure to O_3 and $PM_{2.5}$, range between 3.4% and 5.2% for the first episode and between 1.6% and 3.9% during the second episode.

For both episodes, the total mortality burdens are estimated to be highest in regions with higher population totals for example the South West and North West regions. However regions having a high AF of mortality associated with short-term exposure to O_3 and $PM_{2.5}$ differ depending on the pollution levels in each episode.

The excess mortality burden associated with the high levels of air pollution during these two five-day air pollution episodes is estimated. This is done by first estimating the 'typical' deaths brought forward that would have occurred if air pollutant concentrations during the air pollution episodes were at levels representative of the summer mean (June-August). The excess deaths are then estimated by subtracting the 'typical' estimated deaths brought forward from the episode estimated deaths brought forward. The MDA8 O_3-mortality burden is estimated to be 38% and 36% higher during the first and second episode, respectively than if 'typical' summer mean concentrations occurred. Using $PM_{2.5}$ concentrations representative of the summer average, the mortality burden during the episodes is estimated to be 56% and 39% higher than if the pollution levels represented 'typical' summer-mean concentrations.

Main findings – Chapter 4

- Simulated meteorological variables between 1st-5th July and the 18th-22nd July 2006 suggest persistent anticyclonic conditions with high temperatures, light winds and easterly to south easterly flow allowing for air pollution build –up.

- For the two episodes, the total (all-cause) mortality burden associated with short-term exposure to MDA8 O_3 is estimated to be ~70 daily deaths brought forward, respectively.

- The estimated health burden associated with short-term exposure to daily mean $PM_{2.5}$ concentrations differs between the first and second episode resulting in about 43 and 36 daily deaths brought forward, respectively.

- The corresponding percentage of all-cause mortality due to short-term exposure to MDA8 O_3 and daily mean $PM_{2.5}$ during these two episodes and across the UK regions, ranges from 3.4% to 5.2% and from 1.6% to 3.9%, respectively.

- During these episodes the short-term exposure to MDA8 O_3 and daily mean $PM_{2.5}$ is between 36-38% and 39-56% higher, respectively, than if the pollution levels represented typical summer-mean concentrations.

Highlights – Chapter 4

- In heatwaves similar to July 2006, high levels of $PM_{2.5}$ and O_3 concentrations are simulated concurrently due to anticyclonic conditions with light easterly and south easterly winds and high temperatures that aid pollution build up.

- Short-term exposure to O_3 is between 36-38% higher during these air pollution episodes compared to typical conditions.

- Short-term exposure to $PM_{2.5}$ is between 39-56% higher during the same time period compared to typical conditions.

6.4 Future health burdens associated with RCP emission scenarios for 2050 for the UK.

In chapter 5, the influence of estimated future UK emissions on simulated pollutant concentrations under three IPCC RCPs; RCP2.6, RCP6.0 and RCP8.5 (Section 1.8) for 2050 (future) relative to 2000 (present-day) is investigated. In this chapter, the AQUM air quality model at 12 km resolution (Section 2.2) is used to simulate present-day and future concentrations of O_3, NO_2 and $PM_{2.5}$. These pollutant concentrations are then used to estimate differences in the attributable fraction (AF) of mortality, and differences in the respiratory (O_3) and all-cause (NO_2 and $PM_{2.5}$) mortality burdens associated with long-term exposure to annual mean concentrations of MDA8 O_3, NO_2 and $PM_{2.5}$ between present-day and future

scenarios for each region in the UK. The sensitivity to future population projections is also analysed.

Simulated future pollutant concentrations are generally driven by changes in primary or precursor emissions as well as the underlying chemistry. Under all three RCPs, annual mean MDA8 O_3 concentrations in 2050 increase across the UK relative to present-day, with increases greater than 12 μg m^{-3} (~+40%) across much of central and southern regions of England for RCP8.5. This is a result of projected decreases in nitrogen oxides (NO_x) emissions ranging between 58% and 73% depending on the RCP across the UK. This leads to less titration of O_3 by NO (R1.6; Section 1.2.1.2) especially in highly polluted regions, and hence higher O_3 levels compared to present-day. Under RCP6.0 and RCP8.5, methane (CH_4) concentrations increase throughout the UK for 2050, which may also contribute to increases in O_3 concentrations. However spatial differences in O_3 concentrations between present-day and future are clearly explained by spatial differences in NO_x emissions. As a result of decreases in NOx emissions, NO_2 concentrations decrease by more than 9 μg m^{-3} (~-75%) across much of central and southern regions of England for RCP8.5. In central and eastern England, annual mean $PM_{2.5}$ concentrations also decrease by at most ~4.5 μg m^{-3} (~-50%) in the future for RCP8.5. This decrease is primarily driven by large reductions in precursor emissions of sulphur dioxide (SO_2; up to -94% for RCP8.5) which affect secondary inorganic aerosol concentrations (Section 1.2.3). These reductions in SO_2 emissions for 2050 in conjunction with projected increases in ammonia emissions (NH_3; up to +29% for RCP6.0) result in an overall change in the simulated composition of $PM_{2.5}$. Simulated present-day $PM_{2.5}$ concentrations consist of 35% ammonium nitrate and 45% ammonium sulphate, whereas in 2050 the major component of $PM_{2.5}$ is ammonium nitrate, ranging from 45% to 53% for RCP6.0 and RCP8.5, respectively compared to ammonium sulphate ranging from 27% (RCP2.6) to 37% (RCP6.0). For all three pollutants, the largest changes between 2050 and present-day are estimated for RCP8.5 while the smallest changes are estimated for RCP2.6 and RCP6.0. Consequently, these two RCPs

represent the high and low end of the AF and mortality burden difference range relative to present-day for all three pollutants.

Under the assumption that the CRF (Section 1.4.3) remains unchanged between present-day and future, differences in the AF of mortality for 2050 relative to present-day are solely dependent on differences in air pollutant concentrations. Thus the AF of respiratory mortality associated with long-term exposure to annual mean MDA8 O_3 is estimated to increase in the future for all regions and under all RCPs (~+2.4% to +9.3%) while the AF of all-cause (excluding external) mortality associated with long-term exposure to NO_2 and $PM_{2.5}$ is estimated to decrease (~-1.4% to -4.1% and ~-0.4% to -2.3%, respectively).

The UK-wide mortality burden due to long-term exposure to O_3 in 2050 is estimated to increase with 2,529 (RCP6.0) to 5,396 (RCP8.5) additional attributable deaths relative to 2000 (depending on the RCP). In contrast, in 2050 the resultant UK-wide mortality burden due to long-term exposure to NO_2 decreases with 9,418 (RCP6.0) to 15,782 (RCP8.5) avoided attributable deaths and for $PM_{2.5}$ decreases with 4,524 (RCP6.0) to 9,481 (RCP8.5) avoided attributable deaths compared to present-day.

Finally, the sensitivity of mortality burdens to two future population scenarios is estimated. This is done by using two future population projections from the Shared Socioeconomic Pathways (SSPs), which can be used in conjunction with the RCPs: SSP1 and SSP5. For both SSPs the UK population is projected to increase by a factor of 1.2 (SSP1) and 1.4 (SSP5). Future estimated mortality burdens are highly sensitive to these population projections. Including population projections in the estimation of health effects augments increases in total UK O_3-mortality burdens between 2050 and 2000 by up to a factor of ~3, but diminishes UK decreases in NO_2-mortality burdens by up to a factor of ~0.9. For $PM_{2.5}$, accounting for future population growth in 2050 following SSP1, results in avoided attributable

deaths compared to 2000 under RCP2.6 and RCP8.5. Similarly following SSP5 and RCP8.5 the mortality burden associated with long-term exposure to $PM_{2.5}$ is lower in 2050 compared to 2000. In contrast, the mortality burden associated with long-term exposure to $PM_{2.5}$ is higher in the future compared to present-day for SSP1 and RCP6.0 and for SSP5 in conjunction with RCP2.6 and RCP6.0. This is due to large increases in population growth under SSP5 which outweigh the impact of lower $PM_{2.5}$ concentrations under these two RCPs in 2050 compared to present-day.

Main findings – Chapter 5

- Simulated annual mean MDA8 O_3 concentrations increase in 2050 relative to 2000 under all RCPs while NO_2 and $PM_{2.5}$ concentrations decrease under all RCPs in 2050 compared to present-day. Increases in O_3 concentrations are largely due to a NO_x saturated regime simulated across all of the UK, whereby large projected NO_x emission reductions result in higher O_3 levels. Decreases in $PM_{2.5}$ concentrations are driven by large reductions in precursor emissions of SO_2.

- The AF of respiratory mortality associated with long-term exposure to MDA8 O_3 is estimated to increase in 2050 compared to 2000 while the AF of all-cause mortality associated with long-term exposure to annual mean concentrations of NO_2 and $PM_{2.5}$ is estimated to decrease for all UK regions and all RCPs.

- Differences in the total UK-wide mortality burden attributable to long-term exposure to annual mean MDA8 O_3, NO_2 and $PM_{2.5}$ between present-day and future are largest for RCP8.5 and lowest for RCP6.0. Across the RCPs these differences in attributable deaths between present-day and future range from +2,529 to +5,396 for O_3, -9,418 to -15,782 for NO_2 and from -4,524 to -9,481 for $PM_{2.5}$ attributable deaths in the future compared to present-day.

- Estimated mortality burdens are sensitive to population growth under SSP1 and SSP5 population scenarios. Across the RCPs, differences in UK O_3-mortality burdens between 2050 and 2000 are magnified by up to a factor of ~3 while differences in NO_2-mortality burdens are diminished by up to a factor of ~0.9. For $PM_{2.5}$, additional UK-wide attributable deaths are estimated in 2050 compared to 2000 under RCP2.6 and RCP6.0 and SSP5 despite a decrease in $PM_{2.5}$ concentrations in 2050.

Highlights – Chapter 5

- All of the UK is simulated to be in a NO_x-saturated chemical environment where large reductions in NO_x emissions result in overall increases in simulated O_3 concentrations.

- For all RCPs, ammonium nitrate increasingly becomes the more dominant constituent of $PM_{2.5}$ concentrations especially under RCP2.6 and RCP8.5 as opposed to present day where ammonium sulphate constitutes 45% of total $PM_{2.5}$ concentrations. This is primarily linked with reductions in SO_2 emissions in conjunction with increases in ammonia emissions under all three RCPs.

- Differences in the UK-wide mortality burden due to long-term exposure to O_3 across the RCPs range from +2,529 to +5,396 additional deaths in 2050 compare to 2000.

- Differences in health burdens from long-term exposure to annual mean NO_2 and $PM_{2.5}$ are between -9,418 and -15,782 and from -4,524 to -9,481 avoided attributable deaths in 2050 relative to present-day respectively.

6.5 Uncertainties and Limitations

In this section the uncertainties and limitations of the work presented in this thesis are discussed. A number of uncertainties in conducting health impact assessments are related to the CRFs used. These are first described below followed by limitations associated with the estimation of the mortality burden during an air pollution episode and the use of present-day baseline mortality data for estimating the future health impact assessment.

In Chapter 3, the influence of model horizontal resolution on the O_3-related long-term health impacts is estimated for warm season (April-September) MDA8 O_3 concentrations, as that is the relevant metric associated with the CRF used (Section 1.4.3). In addition, the sensitivity of differences in the AF of respiratory mortality associated with long-term exposure to annual mean MDA8 O_3 to model horizontal resolution is also studied using a different CRF (Section 1.4.3). However the higher CRF associated with annual mean MDA8 O_3 exposure results in a larger range of differences in the AF of mortality across the countries. This is primarily due to a higher CRF (~ a factor of 4) rather than differences in annual mean O_3 compared to summer mean concentrations. The differences in simulated O_3 concentrations between the coarse (global) and finer (regional) resolution vary with season (Chapter 3), which results in corresponding seasonal differences in estimated AF of respiratory mortality between the two resolutions. However the estimation of differences in the AF of respiratory mortality depends on the available CRF which is associated with a specific averaging period for the pollutant concentrations used. CRFs for O_3 related mortality are only available for the warm season (April to September) or annually thus it is not possible to estimate the range of differences in AF of mortality between the two model resolutions for other seasons or time periods.

In this thesis the CRFs used are derived from a mixture of single and multi-pollutant studies. CRFs from single-pollutant studies (Atkinson et al., 2015; COMEAP, 2015a; Jerrett et al., 2009) do not take into account potential overlaps or interactions in relationships between O_3 and/or NO_2 and/or $PM_{2.5}$ concentrations with health effects. This can lead to an underestimation of the true impact of the pollution mixture, especially if other pollutants also affect the same health outcome (COMEAP, 2015a). For example, Williams et al. (2014) demonstrate that the analysis of O_3 and NO_2 concentrations separately in epidemiological studies can underestimate the combined effects on the population from exposure to both pollutants. On the other hand, the effects of O_3 and PM have been shown to be relatively independent (WHO, 2006). Future work could focus on analysing the combined health impact associated with different air pollutants. For pollutants which are closely related such as $PM_{2.5}$ and NO_2 or O_3 and NO_2, the combined health impact can be examined by using CRFs that account for multiple pollutants. In addition the combined health impact could be more easily implemented for pollutants that are mostly independent such as $PM_{2.5}$ and O_3 by using CRFs derived from single pollutant models and adding the resulting two health burdens. All this is however limited by advancement in epidemiological studies which derive the respective CRFs from single-pollutant and more importantly multi-pollutant studies which are thus far limited.

Some studies suggest differences in CRFs across different population subgroups. The impacts of exposure to air pollution may vary due to variations in vulnerability due to age and pre-existing disease and other factors (National Research Council, 2002). The exposure to air pollution may also vary depending on factors such as place of residence and socioeconomic status. For example people who reside in cities are exposed to higher traffic-related primary emissions (Katsouyanni et al., 2001) while people with a higher education level are often less exposed to high $PM_{2.5}$ concentrations (Krewski et al., 2009). However such effects are not currently included in CRFs. Thus the assumption that the same CRF applies

equally to all European countries (Chapter 3) and all UK regions (Chapters 4 and 5), as well as to all population groups in these regions is also employed in this thesis.

In addition, the CRFs used in this thesis for long-term exposure to O_3 are derived from US based cohort studies (Section 1.4.4). CRFs derived from US based cohorts may not be representative of the relationship between air pollution exposure and health effects in different regions such as Europe or the UK. Nonetheless, the use of CRFs that are derived from European and or UK cohort data would be useful, although such data is limited for Europe in the case of long-term exposure to O_3 (Atkinson et al., 2016).

Another uncertainty in health impact assessments is related to the estimation of a 'typical' mortality burden in Chapter 4. The mortality burden associated with short-term exposure to O_3 and $PM_{2.5}$ during two air pollution episodes is estimated in Chapter 4. To estimate the additional impact that occurred due to high levels of air pollution, the 'typical' mortality burden is estimated for each day of the episode (i.e. the mortality burden due to 'typical' levels of air pollution). In estimating the 'typical' mortality burden, summer mean (June-August) pollutant concentrations are used and are kept constant for all days of the episode while no changes are made to the baseline mortality between the two estimated. Under 'typical' conditions, the baseline mortality is likely to be slightly lower than that occurring during an air pollution episode, and thus may result in an overestimation of the 'typical' mortality burdens (i.e. an underestimation of the additional deaths due to the air pollution episode).

Further uncertainties arise when conducting future health impact assessments. These are associated with future population levels and future baseline mortality. In Chapter 5, when considering the mortality burden associated with different future emissions scenarios, uncertainties that are accounted for are associated with the 95% confidence interval of the CRF, and with future population

projections using the SSP scenarios. However, future population estimates especially extending out to 2050 are highly uncertain for example in terms of changes in population demographics. In addition, for all future mortality burden estimates presented in Chapter 5, the baseline mortality is kept constant, as trends in the mortality rates in the future are highly uncertain. In the UK, since 2011 there has been a decline in mortality rates as life-expectancy has increased (Continuous Mortality Investigation, 2017), however overall evidence to aid the prediction of future mortality rates is limited. Future mortality rates are highly uncertain and may revert to a downward trend, continue fluctuating at present rates or possibly increase (Newton et al., 2017).

6.6 Future Work

In this section, the different areas of potential further research in relation to health impact assessments are outlined. These include the impact of NO_x emission controls (Section 6.6.1), the impact of species-specific CRFs for $PM_{2.5}$ (Section 6.6.2), the impact of different emission sectors (Section 6.6.3), the impacts of emissions from outside Europe and the UK (Section 6.6.4) and the impact of climate change (Section 6.6.5) on pollutant concentrations and the corresponding health impacts.

6.6.1 The influence of model horizontal resolution on future O_3-mortality burdens in Europe

In Chapter 5, simulated O_3 concentrations in 2050 using the AQUM model at a 12 km horizontal resolution for the UK are sensitive to NO_x emission reductions. Results indicate that all of the UK is in a NO_x saturated environment. Therefore

projected reductions in NO_x (up to ~70% in RCP 8.5) lead to increases in O_3 concentrations in 2050 due to the reduction of titration of O_3 by NO. This is an important result pertinent to the development of effective emissions control strategies in the UK. However Chapter 3 indicates that NO_x levels and hence O_3 titration is resolution-dependent. As future health impact assessments at global and continental levels are often conducted using relatively coarse resolution models, the magnitude of this titration effect might be underestimated, or indeed a NO_x limited regime whereby O_3 increases with higher NO_x may be simulated (Fig. 1.4 Section 1.2.1.2). Further research would benefit from quantifying the influence of model resolution on future O_3 concentrations with particular focus on the influence of NO_x emission reductions in different regions.

6.6.2 The toxicity of different air pollutants

Throughout this thesis health impact assessments are conducted for both short-term and long-term exposure to O_3 and $PM_{2.5}$ (Chapter 3 and 4) with the inclusion of long-term exposure to NO_2 in Chapter 5. These pollutants are identified by the World Health Organisation (WHO) as being most detrimental to health based on strong evidence of health effects. Several studies conduct health impact assessments associated with various components of $PM_{2.5}$ however these use the CRFs for total $PM_{2.5}$ to evaluate the composition-specific health impact (Kushta et al., 2018; Li et al., 2015; Punger and West, 2013). Some studies suggest that some individual $PM_{2.5}$ components such as elemental carbon are more toxic than others (Section 1.2.2.2). Future work could attempt to study species-specific health burdens for different $PM_{2.5}$ components by using the same CRFs for total $PM_{2.5}$ and comparing these results to those that account for the different toxicity of $PM_{2.5}$ components by using a species-specific CRFs (e.g. CRF for elemental carbon is given in Peng et al. 2009). However, it is acknowledged that there is limited

epidemiological evidence relating individual $PM_{2.5}$ components to adverse health impacts.

6.6.3 The contribution of individual emissions sectors on pollutant concentrations and the associated UK health burdens

The UK anthropogenic, biomass burning and biogenic emissions from all sectors are considered in combination in Chapter 5 however RCP emissions are divided into different sectors (e.g. the transport sector). On a global scale, Silva et al. (2016) suggest that global reductions of emissions of O_3 precursors from 'Land Transportations', and reduction in $PM_{2.5}$ emissions from the 'Residential and commercial' sectors would be particularly beneficial to public health. In a recent study, Williams et al. (2018) suggest that while total $PM_{2.5}$ concentrations in the UK are projected to decrease (as a result of reductions in exhaust emissions from vehicles and from reductions in the precursors of secondary $PM_{2.5}$), $PM_{2.5}$ from domestic wood burning and the contribution of non-exhaust (e.g. break wear, road wear and tyre wear) emissions from road vehicles are projected to increase. Primary emissions from wood burning contain a human carcinogenic (polycyclic aromatic hydrocarbons) and $PM_{2.5}$ from non-exhaust has also been associated with adverse health effects (Amato et al., 2014). Identifying the most important sectors contributing to changes in future UK air pollutant concentrations following the RCPs or other future emission scenarios can have implications for future emissions control policies. In addition, increases in emissions from certain sectors could result in higher concentrations of more toxic pollutants such as elemental carbon (Section 6.6.2). Thus an additional area of research is to focus on the contribution of individual sector emissions on simulated air pollutant concentrations and the corresponding health impacts following the RCPs or other future emission scenarios.

6.6.4 The impact of local versus non-local emission sources

In this thesis the emissions-driven impact on future pollutant concentrations and the subsequent health impacts are presented for the UK. However changes in emissions from outside the UK and their impact on UK health burdens are not considered. Additional sensitivity studies could be performed to analyse the impact of local versus non local emission sources on UK health impacts. European O_3 concentrations under RCP8.5 are suggested to be influenced by the transport of O_3 from outside Europe (Wild et al., 2012). Im et al. (2018) investigate the response of O_3 concentrations in Europe to a 20% reduction of anthropogenic emissions and suggest a large contribution of non-European sources. However the opposite is found for $PM_{2.5}$ and especially NO_2 levels with a large contribution from local sources as a result of their shorter lifetime (Section 1.2.1 and 1.2.2). Thus the influence of non-local sources on UK health impacts would be an interesting addition to the work presented in Chapter 5.

6.6.5 Climate-driven impacts on future UK health burdens

In this thesis while the emissions-driven impact on pollutant concentrations in the UK for 2050 is estimated, the climate-driven impacts on pollutant concentrations in the UK following the RCPs in 2050 is not studied. In addition the combined climate and emission change effects on UK air quality for 2050 would provide additional insights into projected UK air quality in the future. In addition other time periods could be considered. Estimating the corresponding changes in mortality burdens could aid future policy making in terms of what climate mitigation and /or emission controls are most important. While studies focusing on the climate and/or

emissions change impact on future mortality burdens following the RCPs have been conducted, no similar study using the RCPs for the UK has been conducted. Additional sensitivity studies focusing on future mortality rates and future population projections such as those estimated from Integrated Futures (IF) and as used by Silva et al. (2016) for Europe or from the Office for National Statistics (ONS) for the UK (for future population projections) could also be included in further UK based future health estimates.

6.6.6 Concluding remarks

This thesis performs health impact assessments at different temporal scales using modelled pollutant concentrations from chemistry-climate or air quality models for present-day and future. First the influence of model horizontal resolution on the country-level long-term health impacts for O_3 and $PM_{2.5}$ in Europe are quantified. Next, it is shown that air pollution episodes that occurred in July 2006 have the potential to cause substantial health impacts on short-term O_3 and $PM_{2.5}$ related mortality in the UK that are up to 38% and 56% higher, respectively than those occurring in the absence of an air pollution episode. Finally the emissions-driven impact on future mortality burdens associated with long-term exposure to MDA8 O_3, NO_2 and $PM_{2.5}$ in the UK as well as the sensitivity to future projections is presented with implications for informing future emissions control strategies in the UK. Uncertainties and limitation as well as areas for further research are also presented building on the work presented in this thesis.

References

Abt Associates, I.: Environmental benefits and mapping program (version 4.0). Prepared for US Environmental Protection Agency Office of AirQuality Planning and Standards, 2010.

Amato, F., Cassee, F. R., Denier van der Gon, H. A. C., Gehrig, R., Gustafsson, M., Hafner, W., Harrison, R. M., Jozwicka, M., Kelly, F. J., Moreno, T., Prevot, A. S. H., Schaap, M., Sunyer, J. and Querol, X.: Urban air quality: The challenge of traffic non-exhaust emissions, J. Hazard. Mater., 275, 31–36, doi:10.1016/j.jhazmat.2014.04.053, 2014.

Anderson, H., Ponce de Leon, A., Bland, J., Bower, J. and Strachan, D.: Air pollution and daily mortality in London: 1987-92., Bmj, 312(7032), 665–9, doi:10.1136/bmj.312.7032.665, 1996.

Anenberg, S. C., Horowitz, L. W., Tong, D. Q. and West, J. J.: An estimate of the global burden of anthropogenic ozone and fine particulate matter on premature human mortality using atmospheric modeling, Environ. Health Perspect., 118(9), 1189–1195, doi:10.1289/ehp.0901220, 2010.

Anenberg, S. C., Henze, D. K., Tinney, V., Kinney, P. L., Raich, W., Fann, N., Malley, C., Roman, H., Lamsal, L., Duncan, B., Martin, R. V., van Donkelaar, A., Brauer, M., Doherty, R., Jonson, J. E., Davila, Y., Sudo, K. and Kuylenstierna, J.: Global estimates of the burden of ambient air pollution on asthma, Environ. Health Perspect., 2018.

AQEG: Fine Particulate Matter (PM 2 . 5) in the United Kingdom. [online] Available from: http://uk-air.defra.gov.uk/assets/documents/reports/cat11/1212141150_AQEG_Fine_Particulate_Matter_in_the_UK.pdf, 2012.

Arneth, A., Miller, P. A., Scholze, M., Hickler, T., Schurgers, G., Smith, B. and Prentice, I. C.: CO2 inhibition of global terrestrial isoprene emissions: Potential implications for

atmospheric chemistry, Geophys. Res. Lett., 34(18), 1–5, doi:10.1029/2007GL030615, 2007.

Arunachalam, S., Wang, B., Davis, N., Baek, B. H. and Levy, J. I.: Effect of chemistry-transport model scale and resolution on population exposure to PM2.5 from aircraft emissions during landing and takeoff, Atmos. Environ., 45(19), 3294–3300, doi:10.1016/j.atmosenv.2011.03.029, 2011.

Atkinson, R. W., Kang, S., Anderson, H. R., Mills, I. C. and Walton, H. A.: Epidemiological time series studies of PM2.5 and daily mortality and hospital admissions: A systematic review and meta-analysis, Thorax, 69(7), 660–665, doi:10.1136/thoraxjnl-2013-204492, 2014.

Atkinson, R. W., Mills, I. C., Walton, H. A. and Anderson, H. R.: Fine particle components and health—a systematic review and meta-analysis of epidemiological time series studies of daily mortality and hospital admissions, J. Expo. Sci. Environ. Epidemiol., 25(2), 208–214, doi:10.1038/jes.2014.63, 2015.

Atkinson, R. W., Butland, B. K., Dimitroulopoulou, C., Heal, M. R., Stedman, J. R., Carslaw, N., Jarvis, D., Heaviside, C., Vardoulakis, S., Walton, H. and Anderson, H. R.: Long-term exposure to ambient ozone and mortality: a quantitative systematic review and meta-analysis of evidence from cohort studies., BMJ Open, 6(2), e009493, doi:10.1136/bmjopen-2015-009493, 2016.

Bell, M. L., Dominici, F. and Samet, J. M.: A Meta-analysis of Time-Series Studies of Ozone and Mortality with Comparison to the National Morbidity, Mortality, and Air Pollution Study, Epidemiology, 16(4), 436–445, doi:10.1038/jid.2014.371, 2005.

Bell, M. L., Peng, R. D. and Dominici, F.: The exposure-response curve for ozone and risk of mortality and the adequacy of current ozone regulations, Environ. Health Perspect., 114(4), 532–536, doi:10.1289/ehp.8816, 2006.

Bellouin, N., Rae, J., Jones, A., Johnson, C., Haywood, J. and Boucher, O.: Aerosol forcing in the Climate Model Intercomparison Project (CMIP5) simulations by HadGEM2-ES and the role of ammonium nitrate, J. Geophys. Res. Atmos., 116(20), 1–25, doi:10.1029/2011JD016074, 2011.

Bellouin, N., Mann, G. W., Woodhouse, M. T., Johnson, C., Carslaw, K. S. and Dalvi, M.: Impact of the modal aerosol scheme GLOMAP-mode on aerosol forcing in the hadley centre global environmental model, Atmos. Chem. Phys., 13, 3027–3044, doi:10.5194/acp-13-3027-2013, 2013.

Bellouin, N., Boucher, O., Haywood, J., Johnson, C., Jones, A., Rae, J. and Woodward, S.: Improved representation of aerosols for HadGEM2, Hadley Cent. Tech. note 73, (March), 1–42, 2007.

Briggs, D. J., Sabel, C. E. and Lee, K.: Uncertainty in epidemiology and health risk and impact assessment, Environ. Geochem. Health, 31(2), 189–203, doi:10.1007/s10653-008-9214-5, 2008.

Brook, R. D., Rajagopalan, S., Pope, C. A., Brook, J. R., Bhatnagar, A., Diez-Roux, A. V., Holguin, F., Hong, Y., Luepker, R. V., Mittleman, M. a., Peters, A., Siscovick, D., Smith, S. C., Whitsel, L. and Kaufman, J. D.: Particulate matter air pollution and cardiovascular disease: An update to the scientific statement from the american heart association, Circulation, 121(21), 2331–2378, doi:10.1161/CIR.0b013e3181dbece1, 2010.

Brown, A., Milton, S., Cullen, M., Golding, B., Mitchell, J. and Shelly, A.: Unified modeling and prediction of weather and climate: A 25-year journey, Bull. Am. Meteorol. Soc., 93(12), 1865–1877, doi:10.1175/BAMS-D-12-00018.1, 2012.

Brown, A. R., Beare, R. J., Edwards, J. M., Lock, A. P., Keogh, S. J., Milton, S. F. and Walters, D. N.: Upgrades to the boundary-layer scheme in the met office numerical weather prediction model, Boundary-Layer Meteorol., 128(1), 117–132, doi:10.1007/s10546-

008-9275-0, 2008.

Burnett, R. T., Arden Pope, C., Ezzati, M., Olives, C., Lim, S. S., Mehta, S., Shin, H. H., Singh, G., Hubbell, B., Brauer, M., Ross Anderson, H., Smith, K. R., Balmes, J. R., Bruce, N. G., Kan, H., Laden, F., Prüss-Ustün, A., Turner, M. C., Gapstur, S. M., Diver, W. R. and Cohen, A.: An integrated risk function for estimating the global burden of disease attributable to ambient fine particulate matter exposure, Environ. Health Perspect., 122(4), 397–403, doi:10.1289/ehp.1307049, 2014.

Butt, E. W., Turnock, S. T., Rigby, R., Reddington, C. L., Yoshioka, M., Johnson, J. S., Regayre, L. A., Pringle, K. J., Mann, G. W. and Spracklen, D. V: Global and regional trends in particulate air quality and attributable health burden over the past 50 years, Geophys. Res. Abstr., 19, 2017–3519 [online] Available from: http://meetingorganizer.copernicus.org/EGU2017/EGU2017-3519.pdf, 2017.

Butt, E. W., Rap, A., Schmidt, A., Scott, C. E., Pringle, K. J., Reddington, C. L., Richards, N. A. D., Woodhouse, M. T., Ramirez-Villegas, J., Yang, H., Vakkari, V., Stone, E. A., Rupakheti, M., Praveen, P. S., Van Zyl, P. G., Beukes, J. P., Josipovic, M., Mitchell, E. J. S., Sallu, S. M., Forster, P. M. and Spracklen, D. V.: The impact of residential combustion emissions on atmospheric aerosol, human health, and climate, Atmos. Chem. Phys., 16(2), 873–905, doi:10.5194/acp-16-873-2016, 2016.

Chemel, C., Fisher, B. E. A., Kong, X., Francis, X. V., Sokhi, R. S., Good, N., Collins, W. J. and Folberth, G. A.: Application of chemical transport model CMAQ to policy decisions regarding PM2.5 in the UK, Atmos. Environ., 82, 410–417, doi:10.1016/j.atmosenv.2013.10.001, 2014.

Chen, C. H., Chan, C. C., Chen, B. Y., Cheng, T. J. and Leon Guo, Y.: Effects of particulate air pollution and ozone on lung function in non-asthmatic children, Environ. Res., 137, 40–48, doi:10.1016/j.envres.2014.11.021, 2015.

Clark, D. B., Mercado, L. M., Sitch, S., Jones, C. D., Gedney, N., Best, M. J., Pryor, M.,

Rooney, G. G., Essery, R. L. H., Blyth, E., Boucher, O., Harding, R. J., Huntingford, C. and Cox, P. M.: The Joint UK Land Environment Simulator (JULES), model description – Part 2: Carbon fluxes and vegetation dynamics, Geosci. Model Dev., 4(3), 701–722, doi:10.5194/gmd-4-701-2011, 2011.

Cohen, A. J., Brauer, M., Burnett, R., Anderson, H. R., Frostad, J., Estep, K., Balakrishnan, K., Brunekreef, B., Dandona, L., Dandona, R., Feigin, V., Freedman, G., Hubbell, B., Jobling, A., Kan, H., Knibbs, L., Liu, Y., Martin, R., Morawska, L., Pope, C. A., Shin, H., Straif, K., Shaddick, G., Thomas, M., van Dingenen, R., van Donkelaar, A., Vos, T., Murray, C. J. L. and Forouzanfar, M. H.: Estimates and 25-year trends of the global burden of disease attributable to ambient air pollution: an analysis of data from the Global Burden of Diseases Study 2015, Lancet, 389(10082), 1907–1918, doi:10.1016/S0140-6736(17)30505-6, 2017.

Cohen, A. J., Anderson, H. R., Ostro, B., Pandey, K. D., Krzyzanowski, M., Künzli, N., Gutschmidt, K., Iii, C. A. P., Romieu, I., Samet, J. M. and Smith, K. R.: Urban Air Pollution, in Urban air pollution. In: Comparative quantification of health risks: global and regional burden of disease due to selected major risk factors., edited by M. Ezzati, A. Lopez, A. Rodgers, and C. Murray, pp. 1353–1434, World Health Organization, Geneva., 2004.

Coleman, L., Varghese, S., Tripathi, O. P., Jennings, S. G. and O'Dowd, C. D.: Regional-Scale Ozone Deposition to North-East Atlantic Waters, Adv. Meteorol., 2010, 1–16, doi:10.1155/2010/243701, 2010.

Colette, A., Bessagnet, B., Vautard, R., Szopa, S., Rao, S., Schucht, S., Klimont, Z., Menut, L., Clain, G., Meleux, F., Curci, G. and Rouïl, L.: European atmosphere in 2050, a regional air quality and climate perspective under CMIP5 scenarios, Atmos. Chem. Phys., 13(15), 7451–7471, doi:10.5194/acp-13-7451-2013, 2013.

Colette, A., Granier, C., Hodnebrog, Jakobs, H., Maurizi, A., Nyiri, A., Rao, S., Amann, M.,

Bessagnet, B., D'Angiola, A., Gauss, M., Heyes, C., Klimont, Z., Meleux, F., Memmesheimer, M., Mieville, A., Rouïl, L., Russo, F., Schucht, S., Simpson, D., Stordal, F., Tampieri, F. and Vrac, M.: Future air quality in Europe: A multi-model assessment of projected exposure to ozone, Atmos. Chem. Phys., 12(21), 10613–10630, doi:10.5194/acp-12-10613-2012, 2012.

Collins, W. J., Bellouin, N., Doutriaux-Boucher, M., Gedney, N., Halloran, P., Hinton, T., Hughes, J., Jones, C. D., Joshi, M., Liddicoat, S., Martin, G., O'Connor, F., Rae, J., Senior, C., Sitch, S., Totterdell, I., Wiltshire, A. and Woodward, S.: Development and evaluation of an Earth-system model – HadGEM2, Geosci. Model Dev. Discuss., 4(2), 997–1062, doi:10.5194/gmd-4-1051-2011, 2011.

Collins, W. J., Stevenson, D. S., Johnson, C. E. and Derwent, R. G.: Role of convection in determining the budget of odd hydrogen in the upper troposphere, J. Geophys. Res. Atmos., 104(D21), 26927–26941, doi:10.1029/1999JD900143, 1999.

Collins, W. J., Stevenson, D. S., Johnson, C. E. and Derwent, R. G.: Tropospheric Ozone in a Global-Scale Three-Dimensional LagrangianModel and Its Response to NO X Emission Controls, J. Atmos. Chem., 26(3), 223–274, doi:10.1023/A:1005836531979, 1997.

COMEAP: Interim Statement on Quantifying the Association of Long-Term Average Concentrations of Nitrogen Dioxide and Mortality. [online] Available from: https://www.gov.uk/government/uploads/system/uploads/attachment_data/file/485373/COMEAP_NO2_Mortality_Interim_Statement.pdf, 2015a.

COMEAP: Quantification of Mortality and Hospital Admissions Associated with Ground-level Ozone., 2015b.

COMEAP: Quantification of the Effects of Air Pollution on Health in the United Kingdom, , 1–86, 1998.

COMEAP: The Mortality Effects of Long-Term Exposure to Particulate Air Pollution in the United Kingdom, A Rep. by, 108, doi:ISBN 978-0-85951-685-3, 2010.

Continuous Mortality Investigation: The CMI Mortality Projections Model, London. [online] Available from: https://www.actuaries.org.uk/learn-and-develop/continuous-mortality-investigation/cmi-working-papers/mortality-projections/cmi-working-paper-105, 2017.

Crouse, D. L., Peters, P. A., Hystad, P., Brook, J. R., van Donkelaar, A., Martin, R. V., Villeneuve, P. J., Jerrett, M., Goldberg, M. S., Arden Pope, C., Brauer, M., Brook, R. D., Robichaud, A., Menard, R. and Burnett, R. T.: Ambient PM2.5, O3, and NO2exposures and associations with mortality over 16 years of follow-up in the canadian census health and environment cohort (CanCHEC), Environ. Health Perspect., 123(11), 1180–1186, doi:10.1289/ehp.1409276, 2015.

Cusack, S., Edwards, J. . and Crowther, J. .: Investigating k distibution methods for parameterizing gaseous absorption in the Hadley Centre Climate Model, J. Geo, 104, 2051–2057, 1999.

Davies, T., Cullen, M. J. P., Malcolm, A. J., Mawson, M. H., Staniforth, A., White, A. A. and Wood, N.: A new dynamical core of the Met Office's global and regional modelling of the atmosphere, Q. J. R. Meteorol. Soc., 131(608), 1759–1782, doi:10.1256/qj.04.101, 2005.

Defra: Defra Phase 2 urban model evaluation., 2013a.

Defra: Update on Implementation of the Daily Air Quality Index Information for Data Providers and Publishers., 2013b.

Defra: Valuing impacts on air quality: Updates in valuing changes in emissions of Oxides of Nitrogen (NOx) and concentrations of Nitrogen Dioxide (NO2), , (2), 16 [online] Available from:

https://www.gov.uk/government/uploads/system/uploads/attachment_data/file/460401/air-quality-econanalysis-nitrogen-interim-guidance.pdf, 2015.

Derwent, R. G., Simmonds, P. G., Seuring, S. and Dimmer, C.: Observation and interpretation of the seasonal cycles in the surface concentrations of ozone and carbon monoxide at Mace Head, Ireland from 1990 to 1994, Atmos. Environ., 32(2), 145–157, doi:10.1016/S1352-2310(97)00338-5, 1998.

Di, Q., Dai, L., Wang, Y., Zanobetti, A., Choirat, C., Schwartz, J. D. and Dominici, F.: Association of Short-term Exposure to Air Pollution With Mortality in Older Adults, Jama, 318(24), 2446, doi:10.1001/jama.2017.17923, 2017.

Doherty, R. M., Heal, M. R. and O'Connor, F. M.: Climate Change Impacts on Human Health through its effect on Air Quality, Environ. Heal., 16, 2017.

Edwards, J. M. and Slingo, A.: Studies with a flexible new radiation code. I: Choosing a configuration for a large-scale model, Q. J. R. Meteorol. Soc., 122(531), 689–719, doi:10.1256/smsqj.53106, 1996.

EMEP/CCC: EMEP Manual for Sampling and Analysis, Norwegion Inst. Air Res. [online] Available from: https://www.nilu.no/projects/ccc/manual/index.html (Accessed 14 March 2018), 2001.

Essery, R. L. H., Best, M. J., Betts, R. A., Cox, P. M. and Taylor, C. M.: Explicit Representation of Subgrid Heterogeneity in a GCM Land Surface Scheme, J. Hydrometeorol., 4(3), 530–543, doi:10.1175/1525-7541(2003)004<0530:EROSHI>2.0.CO;2, 2003.

EU: Directive 2008/50/EC of the European Parliament and of the Council of 21 May 2008 on ambient air quality and cleaner air for Europe, Off. J. Eur. Communities, 152, 1–43, doi:http://eur-lex.europa.eu/LexUriServ/LexUriServ.do?uri=OJ:L:2008:152:0001:0044:EN:PDF, 2008.

European Environment Agency (EEA): Air quality in Europe — 2017 report., 2017.

Eurostat: Population Projections, Eurostat, Stat. Off. Eur. Union [online] Available from: http://ec.europa.eu/eurostat/web/population-demography-migration-projections/population-projections-data (Accessed 4 July 2018), 2017.

Evans, J., van Donkelaar, A., Martin, R. V., Burnett, R., Rainham, D. G., Birkett, N. J. and Krewski, D.: Estimates of global mortality attributable to particulate air pollution using satellite imagery, Environ. Res., 120, 33–42, doi:10.1016/j.envres.2012.08.005, 2013.

Fang, Y., Naik, V., Horowitz, L. W. and Mauzerall, D. L.: Air pollution and associated human mortality: The role of air pollutant emissions, climate change and methane concentration increases from the preindustrial period to present, Atmos. Chem. Phys., 13(3), 1377–1394, doi:10.5194/acp-13-1377-2013, 2013.

Faustini, A., Rapp, R. and Forastiere, F.: Nitrogen dioxide and mortality: review and meta-analysis of long-term studies, Eur. Respir. J., 3(44), 744–753, doi:10.1183/09031936.00114713, 2014.

Fiore, A. M., Naik, V., Spracklen, D. V., Steiner, A., Unger, N., Prather, M., Bergmann, D., Cameron-Smith, P. J., Cionni, I., Collins, W. J., Dalsøren, S., Eyring, V., Folberth, G. a., Ginoux, P., Horowitz, L. W., Josse, B., Lamarque, J.-F., MacKenzie, I. a., Nagashima, T., O'Connor, F. M., Righi, M., Rumbold, S. T., Shindell, D. T., Skeie, R. B., Sudo, K., Szopa, S., Takemura, T. and Zeng, G.: Global air quality and climate, Chem. Soc. Rev., 41, 6663, doi:10.1039/c2cs35095e, 2012.

Fiore, A. M., Dentener, F. J., Wild, O., Cuvelier, C., Schultz, M. G., Hess, P., Textor, C., Schulz, M., Doherty, R. M., Horowitz, L. W., MacKenzie, I. A., Sanderson, M. G., Shindell, D. T., Stevenson, D. S., Szopa, S., Van Dingenen, R., Zeng, G., Atherton, C., Bergmann, D., Bey, I., Carmichael, G., Collins, W. J., Duncan, B. N., Faluvegi, G., Folberth, G., Gauss, M., Gong, S., Hauglustaine, D., Holloway, T., Isaksen, I. S. A., Jacob, D. J.,

Jonson, J. E., Kaminski, J. W., Keating, T. J., Lupu, A., Manner, E., Montanaro, V., Park, R. J., Pitari, G., Pringle, K. J., Pyle, J. A., Schroeder, S., Vivanco, M. G., Wind, P., Wojcik, G., Wu, S. and Zuber, A.: Multimodel estimates of intercontinental source-receptor relationships for ozone pollution, J. Geophys. Res. Atmos., 114(4), 1–21, doi:10.1029/2008JD010816, 2009.

Fischer, P. H., Brunekreef, B. and Lebret, E.: Air pollution related deaths during the 2003 heat wave in the Netherlands, Atmos. Environ., 38(8), 1083–1085, doi:10.1016/j.atmosenv.2003.11.010, 2004.

Flemming, J., Inness, a., Flentje, H., Huijnen, V., Moinat, P., Schultz, M. G. and Stein, O.: Coupling global chemistry transport models to ECMWF's integrated forecast system, Geosci. Model Dev. Discuss., 2(2), 763–795, doi:10.5194/gmd-2-253-2009, 2009.

Folberth, G. A., Abraham, N. L., Johnson, C. E., Morgenstern, O., O'Connor, F. M., Pacifico, F., Young, P. A., Collins, W. J. and Pyle, J. a.: Evaluation of the new UKCA climate-composition model. Part III. Extension to Tropospheric Chemistry and Biogeochemical Coupling between Atmosphere and Biosphere, In prep..

Francis, X. V., Chemel, C., Sokhi, R. S., Norton, E. G., Ricketts, H. M. A. and Fisher, B. E. A.: Mechanisms responsible for the build-up of ozone over South East England during the August 2003 heatwave, Atmos. Environ., 45(38), 6880–6890, doi:10.1016/j.atmosenv.2011.04.035, 2011.

Garssen, J., Harmsen, C. and de Beer, J.: The effect of the summer 2003 heat wave on mortality in the Netherlands, Eurosurveillance, 10(165–7), 2005.

GBD: Global, regional, and national comparative risk assessment of 79 behavioural, environmental and occupational, and metabolic risks or clusters of risks, 1990–2015: a systematic analysis for the Global Burden of Disease Study 2015, Lancet, 388(10053), 1659–1724, doi:10.1016/S0140-6736(16)31679-8, 2016.

GBD: Mortality and Causes of Death Collaborators. Global, regional, and national life expectancy, all-cause mortality, and cause-specific mortality for 249 causes of death, 1980–2015: a systematic analysis for the Global Burden of Disease Study 2015. Lancet 2016; 388: 1459–544, 2015.

Gowers, a M., Miller, B. G. and Stedman, J. R.: Estimating Local Mortality Burdens associated with Particulate Air Pollution. [online] Available from: http://www.hpa.org.uk/webc/HPAwebFile/HPAweb_C/1317141074607, 2014.

Gregory, D. and Rowntree, P. R.: A Mass Flux Convection Scheme with Representation of Cloud Ensemble Characteristics and Stability-Dependent Closure, Mon. Weather Rev., 118(7), 1483–1506, doi:10.1175/1520-0493(1990)118<1483:AMFCSW>2.0.CO;2, 1990.

Gryparis, A., Forsberg, B., Katsouyanni, K., Analitis, A., Touloumi, G., Schwartz, J., Samoli, E., Medina, S., Anderson, H. R., Niciu, E. M., Wichmann, H. E., Kriz, B., Kosnik, M., Skorkovsky, J., Vonk, J. M. and Dörtbudak, Z.: Acute effects of ozone on mortality from the "Air Pollution and Health: A European Approach" project, Am. J. Respir. Crit. Care Med., 170(10), 1080–1087, doi:10.1164/rccm.200403-333OC, 2004.

Guarnieri, M. and Balmes, J. R.: Outdoor air pollution and asthma, Lancet, 383(9928), 1581–1592, doi:10.1016/S0140-6736(14)60617-6.Outdoor, 2014.

Guenther, A., Hewitt, C. N., Erickson, D., Fall, R., Geron, C., Graedel, T., Harley, P., Klinger, L., Lerdau, M., McKay, W. A., Pierce, T., Scholes, B., Steinbrecher, R., Tallamraju, R., Taylor, J. and Zimmerman, P.: A global model of natural volatile organic compound emissions, J. Geophys. Res., 100(D5), 8873, doi:10.1029/94JD02950, 1995.

Ha, S., Hu, H., Roussos-ross, D., Haidong, K., Roth, J. and Xu, X.: The effects of air pollution on adverse birth outcomes, , 134, 198–204, doi:10.1016/j.envres.2014.08.002.The,

2014.

Harrison, R. M., Dall'Osto, M., Beddows, D. C. S., Thorpe, A. J., Bloss, W. J., Allan, J. D., Coe, H., Dorsey, J. R., Gallagher, M., Martin, C., Whitehead, J., Williams, P. I., Jones, R. L., Langridge, J. M., Benton, A. K., Ball, S. M., Langford, B., Hewitt, C. N., Davison, B., Martin, D., Petersson, K. F., Henshaw, S. J., White, I. R., Shallcross, D. E., Barlow, J. F., Dunbar, T., Davies, F., Nemitz, E., Phillips, G. J., Helfter, C., Di Marco, C. F. and Smith, S.: Atmospheric chemistry and physics in the atmosphere of a developed megacity (London): An overview of the REPARTEE experiment and its conclusions, Atmos. Chem. Phys., 12(6), 3065–3114, doi:10.5194/acp-12-3065-2012, 2012a.

Harrison, R. M., Laxen, D., Moorcroft, S. and Laxen, K.: Processes affecting concentrations of fine particulate matter (PM2.5) in the UK atmosphere, Atmos. Environ., 46, 115–124, doi:10.1016/j.atmosenv.2011.10.028, 2012b.

Heal, M. R., Heaviside, C., Doherty, R. M., Vieno, M., Stevenson, D. S. and Vardoulakis, S.: Health burdens of surface ozone in the UK for a range of future scenarios, Environ. Int., 61, 36–44, doi:10.1016/j.envint.2013.09.010, 2013.

Hedegaard, G. B., Christensen, J. H. and Brandt, J.: The relative importance of impacts from climate change vs. emissions change on air pollution levels in the 21st century, Atmos. Chem. Phys., 13(7), 3569–3585, doi:10.5194/acp-13-3569-2013, 2013.

Hewitt, H. T., Copsey, D., Culverwell, I. D., Harris, C. M., Hill, R. S. R., Keen, a. B., McLaren, a. J. and Hunke, E. C.: Design and implementation of the infrastructure of HadGEM3: the next-generation Met Office climate modelling system, Geosci. Model Dev., 4(2), 223–253, doi:10.5194/gmd-4-223-2011, 2011.

Hoek, G., Brunekreef, B., Verhoeff, a, van Wijnen, J. and Fischer, P.: Daily mortality and air pollution in The Netherlands., J. Air Waste Manag. Assoc., 50(8), 1380–1389, doi:10.1080/10473289.2000.10464182, 2000.

Hoek, G., Krishnan, R. M., Beelen, R., Peters, A., Ostro, B., Brunekreef, B. and Kaufman, J. D.: Long-term air pollution exposure and cardio- respiratory mortality: a review, Environ. Heal., 12(1), 43, doi:10.1186/1476-069X-12-43, 2013.

HPA: Rapid Evaluation of 2006 Heat Wave: Epidemiological Aspects. [online] Available from: http://www.hpa.org.uk/webc/HPAwebFile/HPAweb_C/1219130165676, 2006.

Im, U., Christensen, J. H., Geels, C., Hansen, K. M., Brandt, J., Solazzo, E., Alyuz, U., Balzarini, A., Baro, R., Bellasio, R., Bianconi, R., Bieser, J., Colette, A., Curci, G., Farrow, A., Flemming, J., Fraser, A., Jimenez-Guerrero, P., Kitwiroon, N., Liu, P., Nopmongcol, U., Palacios-Peña, L., Pirovano, G., Pozzoli, L., Prank, M., Rose, R., Sokhi, R., Tuccella, P., Unal, A., Vivanco, M. G., Yarwood, G., Hogrefe, C. and Galmarini, S.: Influence of anthropogenic emissions and boundary conditions on multi-model simulations of major air pollutants over Europe and North America in the framework of AQMEII3, Atmos. Chem. Phys. Discuss., (March), 1–43, doi:10.5194/acp-2017-1231, 2018.

IPCC: Climate Change 2014 Synthesis Report Summary Chapter for Policymakers., 2014.

Ito, K., De Leon, S. F. and Lippmann, M.: Associations between ozone and daily mortality: Analysis and meta-analysis, Epidemiology, 16(4), 446–457, doi:10.1097/01.ede.0000165821.90114.7f, 2005.

Jacob, D. J.: Introduction to Atmospheric Chemistry, Princeton University Press, Chichester, West Sussex. [online] Available from: http://acmg.seas.harvard.edu/publications/jacobbook/index.html, 1999.

Jerrett, M., Burnett, R. T., Pope, C. A., Ito, K., Thurston, G., Krewski, D., Shi, Y., Calle, E. and Thun, M.: Long-Term Ozone Exposure and Mortality, N. Engl. J. Med., 360(11), 1085–1095, doi:10.1056/NEJMoa0803894, 2009.

Johnson, C. E., Mann, G. W., Bellouin, N., O'Connor, F. M. and Dalvi, M.: Comparison

between UKCA-MODE and CLASSIC aerosol schemes in HadGEM3, Integr. Clim. Program. MOHC Rep. M3.2 to DECC, 23, 2010.

Johnson, H., Kovats, R. S., McGregor, G., Stedman, J., Gibbs, M. and Walton, H.: The impact of the 2003 heat wave on daily mortality in England and Wales and the use of rapid weekly mortality estimates., Eurosurveillance, 10(7), 168–171, doi:10.2807/esm.10.07.00558-en, 2005.

Jones, A., Roberts, D. L., Woodage, M. J. and Johnson, C. E.: Indirect sulphate aerosol forcing in a climate model with an interactive sulphur cycle, J. Geophys. Res., 106, 20293–20310, 2001.

Jones, B. and O'Neill, B. C.: Global Population Projection Grids Based on Shared Socioeconomic Pathways (SSPs), 2010-2100., Socioecon. Data Appl. Cent. [online] Available from: https://doi.org/10.7927/H4RF5S0P (Accessed 3 July 2018), 2017.

Katsouyanni, K., Touloumi, G., Samoli, E., Gryparis, A., Le Tertre, A., Monopolis, Y., Rossi, G., Zmirou, D., Ballester, F., Boumghar, A., Anderson, H. R., Wojtyniak, B., Paldy, A., Braunstein, R., Pekkanen, J., Schindler, C. and Schwartz, J.: Confounding and effect modification in the short-term effects of ambient particles on total mortality: Results from 29 European cities within the APHEA2 project, Epidemiology, 12(5), 521–531, doi:10.1097/00001648-200109000-00011, 2001.

Krewski, D., Jerrett, M., Burnett, R. T., Ma, R. and Hughes, E.: Extended Follow-Up and Spatial Analysis of the American Cancer Society Study Linking Particulate Air Pollution and Mortality, , (June 2009), 2009.

Kushta, J., Pozzer, A. and Lelieveld, J.: Uncertainties in estimates of mortality attributable to ambient PM2.5 in Europe., Environ. Res. Lett., 13(6), 64029, doi:10.1088/1748-9326/aabf29, 2018.

Lamarque, J. F., Kyle, P. P., Meinshausen, M., Riahi, K., Smith, S. J., van Vuuren, D. P.,

Conley, A. J. and Vitt, F.: Global and regional evolution of short-lived radiatively-active gases and aerosols in the Representative Concentration Pathways, Clim. Change, 109(1), 191–212, doi:10.1007/s10584-011-0155-0, 2011.

Lamarque, J. F., Bond, T. C., Eyring, V., Granier, C., Heil, a., Klimont, Z., Lee, D., Liousse, C., Mieville, a., Owen, B., Schultz, M. G., Shindell, D., Smith, S. J., Stehfest, E., Van Aardenne, J., Cooper, O. R., Kainuma, M., Mahowald, N., McConnell, J. R., Naik, V., Riahi, K. and Van Vuuren, D. P.: Historical (1850-2000) gridded anthropogenic and biomass burning emissions of reactive gases and aerosols: Methodology and application, Atmos. Chem. Phys., 10(15), 7017–7039, doi:10.5194/acp-10-7017-2010, 2010.

Lee, J. D., Lewis, A. C., Monks, P. S., Jacob, M., Hamilton, J. F., Hopkins, J. R., Watson, N. M., Saxton, J. E., Ennis, C., Carpenter, L. J., Carslaw, N., Fleming, Z., Bandy, B. J., Oram, D. E., Penkett, S. A., Slemr, J., Norton, E., Rickard, A. R., K Whalley, L., Heard, D. E., Bloss, W. J., Gravestock, T., Smith, S. C., Stanton, J., Pilling, M. J. and Jenkin, M. E.: Ozone photochemistry and elevated isoprene during the UK heatwave of august 2003, Atmos. Environ., 40(39), 7598–7613, doi:10.1016/j.atmosenv.2006.06.057, 2006.

Lelieveld, J.: Clean air in the Anthropocene, Faraday Discuss., 200, 693–703, doi:10.1039/c7fd90032e, 2017.

Lelieveld, J., Evans, J. S., Fnais, M., Giannadaki, D. and Pozzer, A.: The contribution of outdoor air pollution sources to premature mortality on a global scale., Nature, 525, 367–71, doi:10.1038/nature15371, 2015.

Levy, J. I., Chemerynski, S. M. and Sarnat, J. A.: Ozone Exposure and Mortality, Epidemiology, 16(4), 458–468, doi:10.1097/01.ede.0000165820.08301.b3, 2005.

Li, Y., Henze, D. K., Jack, D. and Kinney, P. L.: The influence of air quality model resolution on health impact assessment for fine particulate matter and its components, Air

Qual. Atmos. Heal., 9(1), 51–68, doi:10.1007/s11869-015-0321-z, 2015.

Lim, S. S., Vos, T., Flaxman, A. D., Danaei, G., Shibuya, K., Adair-Rohani, H., Amann, M., Anderson, H. R., Andrews, K. G., Aryee, M., Atkinson, C., Bacchus, L. J., Bahalim, A. N., Balakrishnan, K., Balmes, J., Barker-Collo, S., Baxter, A., Bell, M. L., Blore, J. D., Blyth, F., Bonner, C., Borges, G., Bourne, R., Boussinesq, M., Brauer, M., Brooks, P., Bruce, N. G., Brunekreef, B., Bryan-Hancock, C., Bucello, C., Buchbinder, R., Bull, F., Burnett, R. T., Byers, T. E., Calabria, B., Carapetis, J., Carnahan, E., Chafe, Z., Charlson, F., Chen, H., Chen, J. S., Cheng, A. T. A., Child, J. C., Cohen, A., Colson, K. E., Cowie, B. C., Darby, S., Darling, S., Davis, A., Degenhardt, L., Dentener, F., Des Jarlais, D. C., Devries, K., Dherani, M., Ding, E. L., Dorsey, E. R., Driscoll, T., Edmond, K., Ali, S. E., Engell, R. E., Erwin, P. J., Fahimi, S., Falder, G., Farzadfar, F., Ferrari, A., Finucane, M. M., Flaxman, S., Fowkes, F. G. R., Freedman, G., Freeman, M. K., Gakidou, E., Ghosh, S., Giovannucci, E., Gmel, G., Graham, K., Grainger, R., Grant, B., Gunnell, D., Gutierrez, H. R., Hall, W., Hoek, H. W., Hogan, A., Hosgood, H. D., Hoy, D., Hu, H., Hubbell, B. J., Hutchings, S. J., Ibeanusi, S. E., Jacklyn, G. L., Jasrasaria, R., Jonas, J. B., Kan, H., Kanis, J. A., Kassebaum, N., Kawakami, N., Khang, Y. H., Khatibzadeh, S., Khoo, J. P., Kok, C., et al.: A comparative risk assessment of burden of disease and injury attributable to 67 risk factors and risk factor clusters in 21 regions, 1990-2010: A systematic analysis for the Global Burden of Disease Study 2010, Lancet, 380(9859), 2224–2260, doi:10.1016/S0140-6736(12)61766-8, 2012.

Lock, A. P.: The Numerical Representation of Entrainment in Parameterizations of Boundary Layer Turbulent Mixing, Mon. Weather Rev., 129(5), 1148–1163, doi:10.1175/1520-0493(2001)129<1148:TNROEI>2.0.CO;2, 2001.

Lock, A. P., Brown, A. R., Bush, M. R., Martin, G. M. and Smith, R. N. B.: A New Boundary Layer Mixing Scheme. Part I: Scheme Description and Single-Column Model Tests, Mon. Weather Rev., 128(9), 3187–3199, doi:10.1175/1520-0493(2000)128<3187:ANBLMS>2.0.CO;2, 2000.

Macintyre, H. L., Heaviside, C., Neal, L. S., Agnew, P., Thornes, J. and Vardoulakis, S.: Mortality and emergency hospitalizations associated with atmospheric particulate matter episodes across the UK in spring 2014., Environ. Int., 97(November), 108–116, doi:10.1016/j.envint.2016.07.018, 2016.

Mahoney, J., Asrar, G., Leinen, M. S., Andrews, J., Mary, G., Groat, C., William, H., Lawson, L., Moore, M., Neale, P., Patrinos, A., Schafer, J., Slimak, M. and Watson, H.: Strategic Plan of the U.S. Climate Change Science Program. [online] Available from: papers2://publication/uuid/1BA39553-0B02-4B3D-89B5-5D088B732745, 2003.

Malley, C. S., Henze, D. K., Kuylenstierna, J. C. I., Vallack, H. W., Davila, Y., Anenberg, S. C., Turner, M. C. and Ashmore, M. R.: Updated global estimates of respiratory mortality in adults ≥ 30 years of age attributable to long-term ozone exposure, Environ. Health Perspect., 125(8), 1–9, doi:10.1289/EHP1390, 2017.

Mann, G. and Carslaw, K.: UKCA tutorial, Inst. Clim. Atmos. Sci. Leeds, 2011.

Markakis, K., Valari, M., Perrussel, O., Sanchez, O. and Honore, C.: Climate-forced air-quality modeling at the urban scale: sensitivity to model resolution, emissions and meteorology, Atmos. Chem. Phys., 15(13), 7703–7723, doi:10.5194/acp-15-7703-2015, 2015.

Marsha, A., Sain, S. R., Heaton, M. J., Monaghan, A. J. and Wilhelmi, O. V.: Influences of climatic and population changes on heat-related mortality in Houston, Texas, USA, Clim. Change, 146(3–4), 471–485, doi:10.1007/s10584-016-1775-1, 2018.

Masato, G., Hoskins, B. J. and Woollings, T.: Winter and Summer Northern Hemisphere Blocking in CMIP5 Models, J. Clim., 26(18), 7044–7059, doi:10.1175/JCLI-D-12-00466.1, 2013.

Masui, T., Matsumoto, K., Hijioka, Y., Kinoshita, T., Nozawa, T., Ishiwatari, S., Kato, E., Shukla, P. R., Yamagata, Y. and Kainuma, M.: An emission pathway for stabilization

at 6 Wm-2radiative forcing, Clim. Change, 109(1), 59–76, doi:10.1007/s10584-011-0150-5, 2011.

MetOffice: Met Office Integrated Data Archive System (MIDAS) Land and Marine Surface Stations Data (1853-current), NCAS Br. Atmos. Data Cent. [online] Available from: http://catalogue.ceda.ac.uk/uuid/220a65615218d5c9cc9e4785a3234bd0 (Accessed 12 September 2018), 2012.

Monks, P. S.: A review of the observations and origins of the spring ozone maximum, Atmos. Environ., 34(21), 3545–3561, doi:10.1016/S1352-2310(00)00129-1, 2000.

Monks, P. S., Granier, C., Fuzzi, S., Stohl, a., Williams, M. L., Akimoto, H., Amann, M., Baklanov, a., Baltensperger, U., Bey, I., Blake, N., Blake, R. S., Carslaw, K., Cooper, O. R., Dentener, F., Fowler, D., Fragkou, E., Frost, G. J., Generoso, S., Ginoux, P., Grewe, V., Guenther, a., Hansson, H. C., Henne, S., Hjorth, J., Hofzumahaus, a., Huntrieser, H., Isaksen, I. S. a, Jenkin, M. E., Kaiser, J., Kanakidou, M., Klimont, Z., Kulmala, M., Laj, P., Lawrence, M. G., Lee, J. D., Liousse, C., Maione, M., McFiggans, G., Metzger, a., Mieville, a., Moussiopoulos, N., Orlando, J. J., O'Dowd, C. D., Palmer, P. I., Parrish, D. D., Petzold, a., Platt, U., Pöschl, U., Prévôt, a. S. H., Reeves, C. E., Reimann, S., Rudich, Y., Sellegri, K., Steinbrecher, R., Simpson, D., ten Brink, H., Theloke, J., van der Werf, G. R., Vautard, R., Vestreng, V., Vlachokostas, C. and von Glasow, R.: Atmospheric composition change - global and regional air quality, Atmos. Environ., 43(33), 5268–5350, doi:10.1016/j.atmosenv.2009.08.021, 2009.

Monks, P. S., Archibald, A. T., Colette, A., Cooper, O., Coyle, M., Derwent, R., Fowler, D., Granier, C., Law, K. S., Mills, G. E., Stevenson, D. S., Tarasova, O., Thouret, V., Von Schneidemesser, E., Sommariva, R., Wild, O. and Williams, M. L.: Tropospheric ozone and its precursors from the urban to the global scale from air quality to short-lived climate forcer, Atmos. Chem. Phys., 15(15), 8889–8973, doi:10.5194/acp-15-8889-2015, 2015.

Morgenstern, O., Braesicke, P., O'Connor, F. M., Bushell, A. C., Johnson, C. E., Osprey, S. M. and Pyle, J. A.: Evaluation of the new UKCA climate-composition model – Part 1: The stratosphere, Geosci. Model Dev., 2(1), 43–57, doi:10.5194/gmd-2-43-2009, 2009.

Moufouma-Okia, W. and Jones, R.: Resolution dependence in simulating the African hydroclimate with the HadGEM3-RA regional climate model, Clim. Dyn., 44(3–4), 609–632, doi:10.1007/s00382-014-2322-2, 2014.

Nakicenovic, N., Swart, R., Alcamo, J., Davis, G., Vries, B., Fenhann, J., Gaffin, S., Gregory, K. and Gruebler, A.: IPCC Special Report of Working Group III on Emission Scenarios, Cambridge., 2000.

National Research Council: Exposure and Response, in Estimating The Public Health Benefits Of Proposed Air Pollution Regulations., The National Academies Press, Washington,DC., 2002.

Neal, L. S., Dalvi, M., Folberth, G., McInnes, R. N., Agnew, P., O'Connor, F. M., Savage, N. H. and Tilbee, M.: A description and evaluation of an air quality model nested within global and regional composition-climate models using MetUM, Geosci. Model Dev., 10, 3941–3962, doi:10.5194/gmd-2017-73, 2017.

Neal, L. S., Agnew, P., Moseley, S., Ordóñez, C., Savage, N. H. and Tilbee, M.: Application of a statistical post-processing technique to a gridded, operational, air quality forecast, Atmos. Environ., 98, 385–393, doi:10.1016/j.atmosenv.2014.09.004, 2014.

Neu, J. L., Prather, M. J. and Penner, J. E.: Global atmospheric chemistry: Integrating over fractional cloud cover, J. Geophys. Res. Atmos., 112(11), 1–12, doi:10.1029/2006JD008007, 2007.

Newton, J., Baker, A., Fitzpatrick, J. and Ege, F.: What's happening with mortality rates in England?, Heal. Profile Engl. [online] Available from: https://publichealthmatters.blog.gov.uk/2017/07/20/whats-happening-with-

mortality-rates-in-england/ (Accessed 14 August 2018), 2017.

O'Connor, F. M., Johnson, C. E., Morgenstern, O., Abraham, N. L., Braesicke, P., Dalvi, M., Folberth, G. a., Sanderson, M. G., Telford, P. J., Voulgarakis, A., Young, P. J., Zeng, G., Collins, W. J. and Pyle, J. A.: Evaluation of the new UKCA climate-composition model-Part 2: The troposphere, Geosci. Model Dev., 7, 41–91, doi:10.5194/gmd-7-41-2014, 2014.

Office for National Statistics: Estimated daily mortality during July 2006 in England and Wales. [online] Available from: http://www.thehealthwell.info/node/24860, 2006.

ONS: National Population Projections: 2015-based Statistical Bulletin, , 1–10, 2015.

Ostro, B.: Outdoor air pollution: assessing the environmental burden of disease at national and local levels, Environ. Burd. Dis. Ser., (5), 1–54, doi:ISBN 92 4 159146 3, 2004.

Pacifico, F., Harrison, S. P., Jones, C. D., Arneth, A., Sitch, S., Weedon, G. P., Barkley, M. P., Palmer, P. I., Serça, D., Potosnak, M., Fu, T. M., Goldstein, A., Bai, J. and Schurgers, G.: Evaluation of a photosynthesis-based biogenic isoprene emission scheme in JULES and simulation of isoprene emissions under present-day climate conditions, Atmos. Chem. Phys., 11(9), 4371–4389, doi:10.5194/acp-11-4371-2011, 2011.

Pacifico, F., Folberth, G. A., Jones, C. D., Harrison, S. P. and Collins, W. J.: Sensitivity of biogenic isoprene emissions to past, present, and future environmental conditions and implications for atmospheric chemistry, J. Geophys. Res. Atmos., 117(22), 1–13, doi:10.1029/2012JD018276, 2012.

Pannullo, F., Lee, D., Neal, L., Dalvi, M., Agnew, P., O'Connor, F. M., Mukhopadhyay, S., Sahu, S. and Sarran, C.: Quantifying the impact of current and future concentrations of air pollutants on respiratory disease risk in England, Environ. Heal., 16(1), 29, doi:10.1186/s12940-017-0237-1, 2017.

Pope, C. I., Burnett, R. T., Turner, M. C., Cohen, A., Krewski, D., Jerrett, M., Gapstur, S. M.

and Thun, M. J.: Lung cancer and cardiovascular disease mortality associated with ambient air pollution and cigarette smoke: Shape of the exposure-response relationships, Environ. Health Perspect., 119(11), 1616–1621, doi:10.1289/ehp.1103639, 2011.

Pope, R. J., Butt, E. W., Chipperfield, M. P., Doherty, R. M., Fenech, S., Schmidt, A., Arnold, S. R. and Savage, N. H.: The impact of synoptic weather on UK surface ozone and implications for premature mortality, Environ. Res. Lett., 11(12), doi:10.1088/1748-9326/11/12/124004, 2016.

Pozzer, A., Tsimpidi, A. P., Karydis, V. A., de Meij, A. and Lelieveld, J.: Impact of agricultural emission reductions on fine particulate matter and public health, Atmos. Chem. Phys. Discuss., (May), 1–19, doi:10.5194/acp-2017-390, 2017.

Priestley, A.: A Quasi-Conservative Version of the Semi-Lagrangian Advection Scheme, Am. Meteorol. Soc., 121, 1993.

Pringle, K. and Mann, G.: Comparison of CLASSIC bin dust scheme to UKCA modal dust scheme within the Met Office UM, [online] Available from: http://www.ukca.ac.uk/images/3/3e/Dust_summary_180111.pdf, 2011.

Punger, E. M. and West, J. J.: The effect of grid resolution on estimates of the burden of ozone and fine particulate matter on premature mortality in the United States., Air Qual. Atmos. Health, 6(3), 563–573, doi:10.1007/s11869-013-0197-8, 2013.

Pye, H. O. T., Liao, H., Wu, S., Mickley, L. J., Jacob, D. J., Henze, D. J. and Seinfeld, J. H.: Effect of changes in climate and emissions on future sulfate-nitrate-ammonium aerosol levels in the United States, J. Geophys. Res. Atmos., 114(1), doi:10.1029/2008JD010701, 2009.

RCP: Every breath we take The lifelong impact of air pollution, London., 2016.

Rebetez, M., Dupont, O. and Giroud, M.: An analysis of the July 2006 heatwave extent in

Europe compared to the record year of 2003, Theor. Appl. Climatol., 95(1–2), 1–7, doi:10.1007/s00704-007-0370-9, 2009.

Riahi, K., Rao, S., Krey, V., Cho, C., Chirkov, V., Fischer, G., Kindermann, G., Nakicenovic, N. and Rafaj, P.: RCP 8.5-A scenario of comparatively high greenhouse gas emissions, Clim. Change, 109(1), 33–57, doi:10.1007/s10584-011-0149-y, 2011.

Riahi, K., van Vuuren, D. P., Kriegler, E., Edmonds, J., O'Neill, B. C., Fujimori, S., Bauer, N., Calvin, K., Dellink, R., Fricko, O., Lutz, W., Popp, A., Cuaresma, J. C., KC, S., Leimbach, M., Jiang, L., Kram, T., Rao, S., Emmerling, J., Ebi, K., Hasegawa, T., Havlik, P., Humpenöder, F., Da Silva, L. A., Smith, S., Stehfest, E., Bosetti, V., Eom, J., Gernaat, D., Masui, T., Rogelj, J., Strefler, J., Drouet, L., Krey, V., Luderer, G., Harmsen, M., Takahashi, K., Baumstark, L., Doelman, J. C., Kainuma, M., Klimont, Z., Marangoni, G., Lotze-Campen, H., Obersteiner, M., Tabeau, A. and Tavoni, M.: The Shared Socioeconomic Pathways and their energy, land use, and greenhouse gas emissions implications: An overview, Glob. Environ. Chang., 42, 153–168, doi:10.1016/J.GLOENVCHA.2016.05.009, 2017.

Ridder, K. De, Viaene, P. and Vel, K. Van De: The impact of model resolution on simulated ambient air quality and associated human exposure, Atmósfera, 27(4), 403–410, doi:10.1016/S0187-6236(14)70038-4, 2014.

Roberts, D. L. and Jones, A.: Climate sensitivity to black carbon aerosol from fossil fuel combustion, J. Geophys. Res., 109(D16), D16202, doi:10.1029/2004JD004676, 2004.

Rooney, C., McMichael, a J., Kovats, R. S. and Coleman, M. P.: Excess mortality in England and Wales, and in Greater London, during the 1995 heatwave., J. Epidemiol. Community Health, 52(8), 482–486, doi:10.1136/jech.52.8.482, 1998.

Savage, N. H., Agnew, P., Davis, L. S. and Ordonez, C.: Air quality modelling using the Met Office Unified Model (AQUM OS24-26): model description and initial evaluation, Geosci. Model Dev., 6, 353–372, doi:10.5194/gmd-6-353-2013, 2013.

Schaap, M., Cuvelier, C., Hendriks, C., Bessagnet, B., Baldasano, J. M., Colette, a., Thunis, P., Karam, D., Fagerli, H., Graff, a., Kranenburg, R., Nyiri, a., Pay, M. T., Rouïl, L., Schulz, M., Simpson, D., Stern, R., Terrenoire, E. and Wind, P.: Performance of European chemistry transport models as function of horizontal resolution, Atmos. Environ., 112, 90–105, doi:10.1016/j.atmosenv.2015.04.003, 2015.

Schmidt, A.: Modelling Tropospheric Volcanic Aerosol: From Aerosol Microphysical Processes to Earth System Impacts Doctoral., 2013.

Schnell, J. L. and Prather, M. J.: Co-occurrence of extremes in surface ozone, particulate matter, and temperature over eastern North America, Proc. Natl. Acad. Sci., 114(11), 2854–2859, doi:10.1073/pnas.1614453114, 2017.

Seaton, A., MacNee, W., Donaldson, K. and Godden, D.: Particulate Air Pollution and Acute Health Effects, Lancet, 345, 176–178, 1995.

Seinfeld, J. H. and Pandis, S. N.: Atmospheric Chemistry and Physics From Air Pollution to Climate Change, Second Edi., John Wiley & Sons, New Jersey., 2006.

Seinfeld, J. H. and Pandis, S. N.: Atmospheric Chemistry and Physics From Air Pollution to Climate Change, John Wiley & Sons., 1998.

Shin, H. H., Cohen, A. J., Pope, C. A., Ezzati, M., Lim, S. S., Hubbell, B. J. and Burnett, R. T.: Meta-Analysis Methods to Estimate the Shape and Uncertainty in the Association Between Long-Term Exposure to Ambient Fine Particulate Matter and Cause-Specific Mortality Over the Global Concentration Range, Risk Anal., 36(9), 1813–1825, doi:10.1111/risa.12421, 2016.

Silva, R. A., West, J. J., Zhang, Y., Anenberg, S. C., Lamarque, J.-F., Shindell, D. T., Collins, W. J., Dalsoren, S., Faluvegi, G., Folberth, G., Horowitz, L. W., Nagashima, T., Naik, V., Rumbold, S., Skeie, R., Sudo, K., Takemura, T., Bergmann, D., Cameron-Smith, P., Cionni, I., Doherty, R. M., Eyring, V., Josse, B., MacKenzie, I. a, Plummer, D., Righi,

M., Stevenson, D. S., Strode, S., Szopa, S. and Zeng, G.: Global premature mortality due to anthropogenic outdoor air pollution and the contribution of past climate change, Environ. Res. Lett., 8, 1748–9326, doi:10.1088/1748-9326/8/3/034005, 2013.

Silva, R. A., West, J. J., Lamarque, J. F., Shindell, D. T., Collins, W. J., Dalsoren, S., Faluvegi, G., Folberth, G., Horowitz, L. W., Nagashima, T., Naik, V., Rumbold, S. T., Sudo, K., Takemura, T., Bergmann, D., Cameron-Smith, P., Cionni, I., Doherty, R. M., Eyring, V., Josse, B., MacKenzie, I. A., Plummer, D., Righi, M., Stevenson, D. S., Strode, S., Szopa, S. and Zengast, G.: The effect of future ambient air pollution on human premature mortality to 2100 using output from the ACCMIP model ensemble, Atmos. Chem. Phys., 16(15), 9847–9862, doi:10.5194/acp-16-9847-2016, 2016a.

Silva, R. A., Adelman, Z., Fry, M. M. and West, J. J.: The impact of individual anthropogenic emissions sectors on the global burden of human mortality due to ambient air pollution, Environ. Health Perspect., 124(11), 1776–1784, doi:10.1289/EHP177, 2016b.

Solberg, S., Hov, Søvde, A., Isaksen, I. S. A., Coddeville, P., De Backer, H., Forster, C., Orsolini, Y. and Uhse, K.: European surface ozone in the extreme summer 2003, J. Geophys. Res. Atmos., 113(7), 1–16, doi:10.1029/2007JD009098, 2008.

Squire, O. J., Archibald, A. T., Griffiths, P. T., Jenkin, M. E., Smith, D. and Pyle, J. A.: Influence of isoprene chemical mechanism on modelled changes in tropospheric ozone due to climate and land use over the 21st century, Atmos. Chem. Phys., 15(9), 5123–5143, doi:10.5194/acp-15-5123-2015, 2015.

Stedman, J. R.: The predicted number of air pollution related deaths in the UK during the August 2003 heatwave, Atmos. Environ., 38(8), 1087–1090, doi:10.1016/j.atmosenv.2003.11.011, 2004.

Stock, Z. S., Russo, M. R. and Pyle, J. A.: Representing ozone extremes in European

megacities: the importance of resolution in a global chemistry climate model, Atmos. Chem. Phys., 14, 3899–3912, doi:10.5194/acp-14-3899-2014, 2014.

von Storch, H. and Zwiers, F. .: Statistical Analysis in Climate Research, Cambridge University Press, Cambridge., 1999.

Telford, P. J., Abraham, N. L., Archibald, A. T., Braesicke, P., Dalvi, M., Morgenstern, O., O'Connor, F. M., Richards, N. A. D. and Pyle, J. A.: Implementation of the Fast-JX Photolysis scheme into the UKCA component of the MetUM chemistry climate model, Geosci. Model Dev. Discuss., 5(4), 3217–3260, doi:10.5194/gmdd-5-3217-2012, 2013.

Thompson, T. M. and Selin, N. E.: Influence of air quality model resolution on uncertainty associated with health impacts, Atmos. Chem. Phys., 12(20), 9753–9762, doi:10.5194/acp-12-9753-2012, 2012.

Thompson, T. M., Saari, R. K. and Selin, N. E.: Air quality resolution for health impact assessment: influence of regional characteristics, Atmos. Chem. Phys., 14, 969–978, doi:10.5194/acp-14-969-2014, 2014.

Thomson, A. M., Calvin, K. V., Smith, S. J., Kyle, G. P., Volke, A., Patel, P., Delgado-Arias, S., Bond-Lamberty, B., Wise, M. A., Clarke, L. E. and Edmonds, J. A.: RCP4.5: A pathway for stabilization of radiative forcing by 2100, Clim. Change, 109(1), 77–94, doi:10.1007/s10584-011-0151-4, 2011.

Tie, X., Brasseur, G. and Ying, Z.: Impact of model resolution on chemical ozone formation in Mexico City: application of the WRF-Chem model, Atmos. Chem. Phys., 10(18), 8983–8995, doi:10.5194/acp-10-8983-2010, 2010.

Tong, S., Ren, C. and Becker, N.: Excess deaths during the 2004 heatwave in Brisbane, Australia, Int. J. Biometeorol., 54(4), 393–400, doi:10.1007/s00484-009-0290-8, 2010.

Tørseth, K., Aas, W., Breivik, K., Fjeraa, A. M., Fiebig, M., Hjellbrekke, A. G., Lund Myhre, C., Solberg, S. and Yttri, K. E.: Introduction to the European Monitoring and Evaluation Programme (EMEP) and observed atmospheric composition change during 1972-2009, Atmos. Chem. Phys., 12(12), 5447–5481, doi:10.5194/acp-12-5447-2012, 2012.

Turner, M. C., Jerrett, M., Pope, C. A., Krewski, D., Gapstur, S. M., Diver, W. R., Beckerman, B. S., Marshall, J. D., Su, J., Crouse, D. L. and Burnett, R. T.: Long-Term Ozone Exposure and Mortality in a Large Prospective Study, Am. J. Respir. Crit. Care Med., 193(10), 1134–1142, doi:10.1164/rccm.201508-1633OC, 2015.

Turnock, S. T., Wild, O., Dentener, F. J., Davila, Y., Emmons, L. K., Flemming, J., Folberth, G. A., Henze, D. K., Jonson, J. E., Keating, T. J., Kengo, S., Lin, M., Lund, M., Tilmes, S. and O'Connor, F. M.: The impact of future emission policies on tropospheric ozone using a parameterised approach, Atmos. Chem. Phys., 18(12), 8953–8978, doi:10.5194/acp-18-8953-2018, 2018.

Valari, M. and Menut, L.: Does an Increase in Air Quality Models' Resolution Bring Surface Ozone Concentrations Closer to Reality?, J. Atmos. Ocean. Technol., 25(11), 1955–1968, doi:10.1175/2008JTECHA1123.1, 2008.

Vieno, M., Dore, a. J., Stevenson, D. S., Doherty, R., Heal, M. R., Reis, S., Hallsworth, S., Tarrason, L., Wind, P., Fowler, D., Simpson, D. and Sutton, M. a.: Modelling surface ozone during the 2003 heat-wave in the UK, Atmos. Chem. Phys., 10, 7963–7978, doi:10.5194/acp-10-7963-2010, 2010.

Vieno, M., Heal, M. R., Williams, M. L., Carnell, E. J., Nemitz, E., Stedman, J. R. and Reis, S.: The sensitivities of emissions reductions for the mitigation of UK PM2.52.5, Atmos. Chem. Phys., 16(1), 265–276, doi:10.5194/acp-16-265-2016, 2016a.

Vieno, M., Heal, M. R., Twigg, M. M., MacKenzie, I. A., Braban, C. F., Lingard, J. J. N., Ritchie, S., Beck, R. C., Móring, A., Ots, R., Di Marco, C. F., Nemitz, E., Sutton, M. A. and Reis,

S.: The UK particulate matter air pollution episode of March–April 2014: more than Saharan dust, Environ. Res. Lett., 11(5), 59501, doi:10.1088/1748-9326/11/5/059501, 2016b.

van Vuuren, D. P., Stehfest, E., den Elzen, M. G. J., Kram, T., van Vliet, J., Deetman, S., Isaac, M., Goldewijk, K. K., Hof, A., Beltran, A. M., Oostenrijk, R. and van Ruijven, B.: RCP2.6: Exploring the possibility to keep global mean temperature increase below 2°C, Clim. Change, 109(1), 95–116, doi:10.1007/s10584-011-0152-3, 2011a.

van Vuuren, D. P., Edmonds, J., Kainuma, M., Riahi, K., Thomson, A., Hibbard, K., Hurtt, G. C., Kram, T., Krey, V., Lamarque, J. F., Masui, T., Meinshausen, M., Nakicenovic, N., Smith, S. J. and Rose, S. K.: The representative concentration pathways: An overview, Clim. Change, 109(1), 5–31, doi:10.1007/s10584-011-0148-z, 2011b.

Walters, D. N., Best, M. J., Bushell, A. C., Copsey, D., Edwards, J. M., Falloon, P. D., Harris, C. M., Lock, A. P., Manners, J. C., Morcrette, C. J., Roberts, M. J., Stratton, R. A., Webster, S., Wilkinson, J. M., Willett, M. R., Boutle, I. A., Earnshaw, P. D., Hill, P. G., MacLachlan, C., Martin, G. M., Moufouma-Okia, W., Palmer, M. D., Petch, J. C., Rooney, G. G., Scaife, A. A. and Williams, K. D.: The Met Office Unified Model Global Atmosphere 3.0/3.1 and JULES Global Land 3.0/3.1 configurations, Geosci. Model Dev., 4(4), 919–941, doi:10.5194/gmd-4-919-2011, 2011.

Walton, J. J., Maccracken, M. C. and Ghan, S. J.: A global-scale Lagrangian trace species model of transport, transformation, and removal processes, J. Geophys. Res., 93(D7), 8339–8354, doi:10.1029/JD093iD07p08339, 1988.

Wesely, M. L.: Parameterization of Surface Resistances To Gaseous Dry Deposition in Regional-Scale Numerical Models, Atmos. Environ., 23(6), 1293–1304, 1989.

West, J. J., Smith, S. J., Silva, R. a, Naik, V., Zhang, Y., Adelman, Z., Fry, M. M., Anenberg, S., Horowitz, L. W. and Lamarque, J.-F.: Co-benefits of Global Greenhouse Gas Mitigation for Future Air Quality and Human Health., Nat. Clim. Chang., 3(10), 885–

889, doi:10.1038/NCLIMATE2009, 2013.

West, J. J., Naik, V., Horowitz, L. W. and Fiore, a. M.: Effect of regional precursor emission controls on long-range ozone transport – Part 2: steady-state changes in ozone air quality and impacts on human mortality, Atmos. Chem. Phys. Discuss., 9, 6095–6107, doi:10.5194/acpd-9-7079-2009, 2009.

WHO: Air quality guidelines. Global update 2005. Particulate matter, ozone, nitrogen dioxide and sulfur dioxide, Copenhagen., 2006.

WHO: Ambient Air Pollution: A global assessment of exposure and burden of disease., 2016.

WHO: Ambient (outdoor) air quality and health.Fact sheets.[online] Available from: https://www.who.int/en/news-room/fact-sheets/detail/ambient-(outdoor)-air-quality-and-health, 2018.

WHO: Health Risks of Air Pollution in Europe – HRAPIE project: Recommendations for concentration-response functions for cost-benefit analysis of particulate matter, ozone and nitrogen dioxide. [online] Available from: http://www.euro.who.int/__data/assets/pdf_file/0006/238956/Health_risks_air_pollution_HRAPIE_project.pdf?ua=1, 2013a.

WHO: Review of evidence on health aspects of air pollution – REVIHAAP First results, 2013b.

Wild, O., Fiore, A. M., Shindell, D. T., Doherty, R. M., Collins, W. J., Dentener, F. J., Schultz, M. G., Gong, S., Mackenzie, I. A., Zeng, G., Hess, P., Duncan, B. N., Bergmann, D. J., Szopa, S., Jonson, J. E., Keating, T. J. and Zuber, A.: Modelling future changes in surface ozone: A parameterized approach, Atmos. Chem. Phys., 12(4), 2037–2054, doi:10.5194/acp-12-2037-2012, 2012.

Williams, M. L., Atkinson, R. W., Anderson, H. R. and Kelly, F. J.: Associations between daily mortality in London and combined oxidant capacity, ozone and nitrogen dioxide, Air Qual. Atmos. Heal., 407–414, doi:10.1007/s11869-014-0249-8, 2014.

Williams, M. L., Lott, M. C., Kitwiroon, N., Dajnak, D., Walton, H., Holland, M., Pye, S., Fecht, D., Toledano, M. B. and Beevers, S. D.: The Lancet Countdown on health benefits from the UK Climate Change Act: a modelling study for Great Britain, Lancet Planet. Heal., 2(5), e202–e213, doi:10.1016/S2542-5196(18)30067-6, 2018.

Wilson, D. R. and Ballard, S. P.: A microphysically based precipitation scheme for the UK Meteorological Office Unified Model, Q. J. R. Meteorol. Soc., 125(557), 1607–1636, doi:10.1256/smsqj.55706, 1999.

Woodward, S.: Modeling the atmospheric life cycle and radiative impact of mineral dust in the Hadley Centre climate model, J. Geophys. Res., 106(2000), 18,155-18,166, 2001.

Yin, J. and Harrison, R. M.: Pragmatic mass closure study for PM1.0, PM2.5and PM10at roadside, urban background and rural sites, Atmos. Environ., 42(5), 980–988, doi:10.1016/j.atmosenv.2007.10.005, 2008.

Young, P. J., Archibald, A. T., Bowman, K. W., Lamarque, J.-F., Naik, V., Stevenson, D. S., Tilmes, S., Voulgarakis, A., Wild, O., Bergmann, D., Cameron-Smith, P., Cionni, I., Collins, W. J., Dalsøren, S. B., Doherty, R. M., Eyring, V., Faluvegi, G., Horowitz, L. W., Josse, B., Lee, Y. H., MacKenzie, I. A., Nagashima, T., Plummer, D. A., Righi, M., Rumbold, S. T., Skeie, R. B., Shindell, D. T., Strode, S. A., Sudo, K., Szopa, S. and Zeng, G.: Pre-industrial to end 21st century projections of tropospheric ozone from the Atmospheric Chemistry and Climate Model Intercomparison Project (ACCMIP), Atmos. Chem. Phys., 13(4), 2063–2090, doi:10.5194/acp-13-2063-2013, 2013.

Yu, K., Jacob, D. J., Fisher, J. a., Kim, P. S., Marais, E. a., Miller, C. C., Travis, K. R., Zhu, L., Yantosca, R. M., Sulprizio, M. P., Cohen, R. C., Dibb, J. E., Fried, A., Mikoviny, T., Ryerson, T. B., Wennberg, P. O. and Wisthaler, A.: Sensitivity to grid resolution in

the ability of a chemical transport model to simulate observed oxidant chemistry under high-isoprene conditions, Atmos. Chem. Phys., 16(7), 4369–4378, doi:10.5194/acp-16-4369-2016, 2016.